REPORT NO.
UCB/EERC-91/16
JULY 1991

EARTHQUAKE ENGINEERING RESEARCH CENTER

EVALUATION OF THE SEISMIC PERFORMANCE OF A THIRTY-STORY RC BUILDING

by

JAMES C. ANDERSON
EDUARDO MIRANDA
VITELMO V. BERTERO
KAJIMA PROJECT RESEARCH TEAM

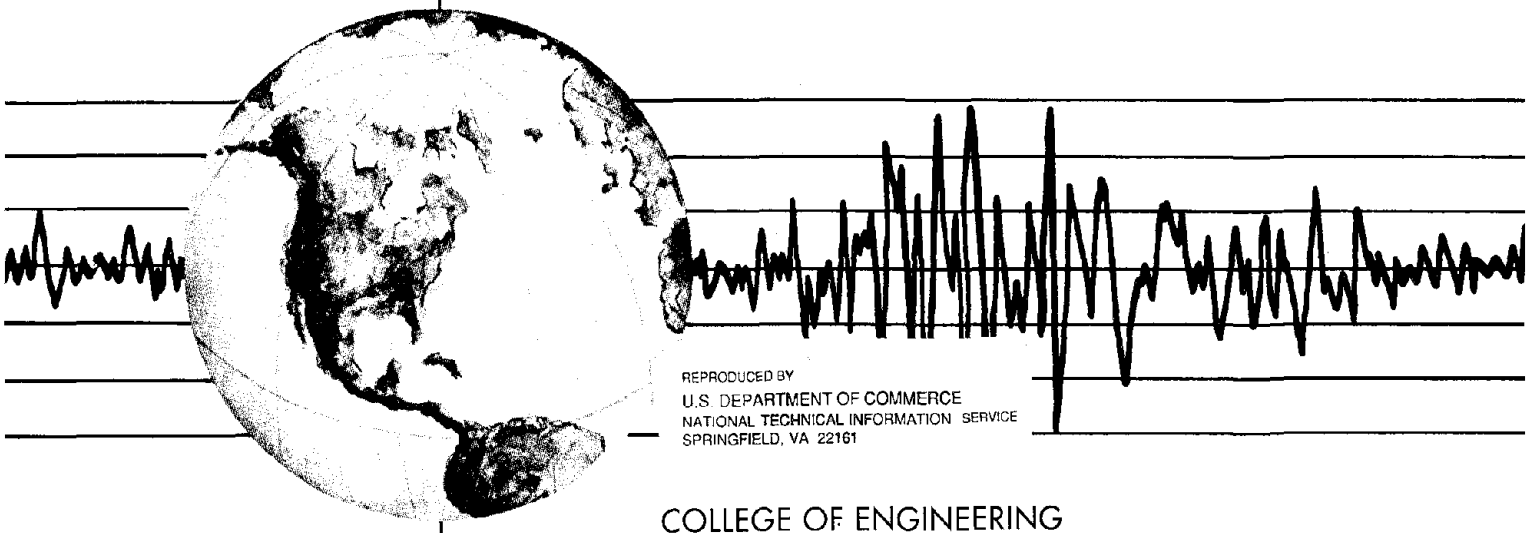

COLLEGE OF ENGINEERING

UNIVERSITY OF CALIFORNIA AT BERKELEY

For sale by the National Technical Information Service, U.S. Department of Commerce, Springfield, Virginia 22161

See back of report for up to date listing of EERC reports.

EVALUATION OF THE SEISMIC PERFORMANCE OF A THIRTY-STORY RC BUILDING

by

James C. Anderson
Eduardo Miranda
Vitelmo V. Bertero
and
The Kajima Project Research Team

Report No. UCB/EERC-91/16
Earthquake Engineering Research Center
College of Engineering
University of California at Berkeley
July 1991

ABSTRACT

This report presents the results of a series of studies conducted to evaluate the seismic performance of a 30-story ductile moment-resistant reinforced concrete frame structure located in Emeryville, California. This building, which is the tallest reinforced concrete building in Northern California, is founded on piles and has a plan which consists of three equally spaced wings which extend outward approximately 112 feet from the central core. At the time of the Loma Prieta earthquake, the building was instrumented with 21 accelerometers deployed throughout the building. In addition, free field recording stations were located on the north and south sides of the building. Inspection of the building following the earthquake did not reveal any significant damage or yielding of the reinforcing steel. In addition to the information obtained from the recorded earthquake response, results from ambient and forced vibration tests that were performed on the building prior to occupancy in 1985 are also available.

The main objectives of these studies are the following: (1) To evaluate the reliability of present system identification techniques for obtaining the building dynamic characteristics from recorded responses; (2) to evaluate the accuracy of current analytical modeling techniques; (3) to evaluate the influence of modeling discretizations on the computed response; (4) to evaluate the validity of current code requirements; (5) to compare current U.S. and Japanese design procedures and requirements for this type of building; and (6) to analyze probable performance under more severe base motions.

In order to achieve these objectives, linear elastic and nonlinear dynamic response analyses

were conducted using both simplified and detailed analytical models. Results are presented in terms of response spectra, time history response comparisons and maximum response envelopes.

Evaluation of the results led to the following main conclusions and recommendations: In the design and analyses of this type of building, there is a need to consider a range (bounds) for the values of the periods as well as to estimate as accurately as possible the period of the soil and the predominant frequency content period of the critical earthquake ground motions. The development of the site design response spectra should contemplate the uncertainties involved in predicting the above different periods, as well as the importance of the higher modes in the response of tall buildings, particularly in the upper stories. Sharp changes in stiffness and strength along the height of the building should be avoided. The building has an overstrength over the design strength of more than 100% (0.17W vs. 0.08 W); the resulting structure system factor R_w is approximately 7.6 rather than 12 as assigned in the UBC. For buildings of this type, the minimum Japanese lateral force requirement would be 2.5 times greater than that of the U.S. There is a need to perform a detailed nonlinear analysis to quantify the local (member) ductility ratio demands.

ACKNOWLEDGEMENTS

This report is based on the results of a series of studies that have been conducted by the authors at the University of California at Berkeley, the University of Southern California in Los Angeles, California, and at Kajima Corporation, Tokyo, Japan. These studies form part of two main research projects. One of these projects, entitled "Implications of Response of Structures to Ground Motions Recorded During the Loma Prieta Earthquake: Evaluation of Structural Response Factors," is supported by a research grant provided by the National Science Foundation (NSF). The other research project, entitled, "Design Guidelines for Ductility and Drift Limits," is supported by a research grant provided by Kajima Corporation and administered by CUREe (California Universities for Research in Earthquake Engineering). Additional support was also provided by the Carpenter/Contractor Cooperative Committee. This financial support is gratefully acknowledged.

The authors are very grateful to the T.Y. Lin International firm in San Francisco, and particularly to T.C. Tai and M. Ketchum of this firm, for providing all the drawings and the needed information regarding the design of the 30-story RC building which has been the main subject of the studies reported herein. The long and fruitful discussions held with Dr. M. Celebi of the U.S. Geological Survey at Menlo Park regarding the instrumentation of the building and the recorded information obtained during the 1989 Loma Prieta earthquake are also greatly appreciated.

The Kajima Research Team included the following: N. Tanaka, N. Inoue, H. Hatamoto, Y. Sunasaka, T. Tsujimoto, S. Orui and T. Fukuda.

TABLE OF CONTENTS

LIST OF TABLES

LIST OF FIGURES

1. INTRODUCTION

1.1 INTRODUCTORY REMARKS

In Reference 1 it is pointed out that most human injury and economic loss due to moderate or severe earthquake ground motions are caused by failures of civil engineering facilities, particularly buildings, many of which presumably were designed and constructed to provide protection against such natural hazards. This has been confirmed dramatically during recent earthquakes around the world (the 1985 Mexico, 1988 Armenia, 1989 Loma Prieta, 1990 Iran, and 1990 Philippines earthquakes). While the threat of severe earthquake ground motions is approximately the same today as it was 100 years ago, the potential for a major earthquake catastrophe has grown alarmingly over this period as a result of an uncontrolled increase in population and urbanization in seismically active regions. For example, in the last century the population of the state of California has grown from 2 million to 30 million. Similarly, the population of the city of Los Angeles has grown from 100,000 at the start of the century to over 15 million today [2]. The two most effective ways to mitigate the destructive effects of earthquakes are the **improvement** of present methods and the **development** of new and better methods of designing, constructing, and maintaining new structures, and of seismic upgrading of existing hazardous facilities.

One of the main steps toward the improvement of the design of new facilities and toward the selection of the most technically and economically efficient strategies and techniques for the seismic upgrading of existing hazardous facilities is the ability to predict in a reliable manner the mechanical (dynamic) behavior of the structures of such facilities when they are subjected to critical combinations of seismic excitations that can occur during their service life.

In an attempt to realize such improvements, it was considered important to find out how reliable the present methods of predicting the seismic behavior of real structures are. This was done by analyzing the performance of instrumented structures whose performances during one or more earthquakes had been recorded. This report summarizes the studies conducted on one such structure: a 30-story reinforced concrete (RC) building.

1.2 OBJECTIVES

The main objectives of these studies are (1) to evaluate the reliability of the analytical models presently available for analyzing the seismic performance of buildings; (2) to estimate through static and dynamic analyses the damage that buildings could suffer under the critical ground motions to which they could be exposed during their service lives; and (3) to assess the implications of the obtained results regarding the reliability of present seismic code regulations for the design of such buildings.

1.3 SCOPE

To achieve the above objectives, the authors and a team of researchers from the Kajima Corporation conducted the following studies which are summarized in this report.

1. **Database Collection**. Structural details and recorded responses of instrumented buildings in the U.S. whose foundations have experienced earthquake ground motions were collected. Two reinforced concrete buildings were selected for detailed study. One is a 30-story Y-shaped building, which will be designated from here on as the "Y Building"; the other is a rectangular 10-story building. This report presents the studies of the Y Building. A second, separate report [3] discusses the results obtained in the studies of the 10-story building.

2. **Description of the Building: Its Design and Instrumentation**. The main mechanical characteristics of the soil-foundation, superstructure, and non-structural elements of the Y Building were studied from available design drawings and are summarized herein. This building is extensively instrumented; the details of the locations of the instruments used were obtained from the U.S. Geological Survey (USGS), and are summarized and discussed in Chapter 2.

3. **Recorded Response During the Loma Prieta Earthquake**. After a brief description of the response recorded during this earthquake, several system identification techniques which were employed to determine the dynamic characteristics (periods and mode shapes) of the Y Building are described. These dynamic characteristics are then compared with those obtained previously using ambient and forced vibration techniques. Special emphasis is placed on identifying and evaluating the importance of torsion, soil-structure interaction, and rocking motion in the overall response of the building. The results of these studies are presented in Chapter 3.

4. **Seismic Response Analyses in the Linear Elastic Range of Behavior**. Several types of linear elastic studies were conducted. A simplified model of the building, consisting of a two-dimensional shear simulation with only one degree of freedom per floor, was used first. The second type of model, consisting of detailed three-dimensional finite element models, was used extensively for prediction of behavior under seismically equivalent static lateral forces, spectral analysis, and time-history analyses. Results of these analyses are presented in Chapter 4.

5. **Estimation of Strength and Deformation Capacities of the Building**. An attempt has been made to estimate these capacities. The Kajima team, using a simplified 3-D nonlinear model consisting of five shearing elements and three bending-shearing elements linked through rigid floor slabs, made an estimate of the strength and deformation capacities. The results of these analyses are presented in Chapter 5. The authors are conducting approximate 3-D nonlinear analyses using simplified models and plan to carry out a more detailed 3-D analysis when the 3-D program Drain-Building is released. Results of these analyses will be published in a separate report.

6. **Evaluation of Results**. To assess the implications of the results obtained in the above studies regarding the present state of the art and practice of predicting seismic responses of buildings in the U.S. and Japan, the results obtained in the analyses of the recorded behavior are compared with those based on mathematical models developed according to the state of the knowledge. Predicted and recorded behavior are also compared with present U.S. and Japanese code requirements. These comparisons and evaluations are presented in Chapter 5, as well as in the conclusions offered in Chapter 6.

7. **Conclusions and Recommendations**. The main conclusions drawn from the above studies are summarized. Recommendations for future research needs for improved evaluation of seismic performance of structures and of earthquake resistant design are put forward.

1.4 COLLECTION OF STRUCTURAL DETAILS AND RECORDED RESPONSES

Structural plans and recorded earthquake responses were collected from 26 instrumented buildings in California. Of these buildings, eight have experienced the 1971 San Fernando

earthquake, fifteen have experienced the 1987 Whittier Narrows earthquake and four have experienced the 1989 Loma Prieta earthquake. The following lateral force resisting systems were identified in the database: nine buildings were reinforced concrete moment frames, seven were reinforced concrete shear walls, one was a reinforced concrete/shear wall frame, five were steel moment frames, three were steel perimeter frames and one was a reinforced concrete frame with prestressed beams. The distribution of framing systems in the data base is shown in the pie chart of Fig. 1.1. The heights of the buildings in the database range from four stories to forty-two stories. The distribution of building heights in the database is shown in the bar graph of Fig. 1.2. Information on the buildings including height, framing system and recorded peak accelerations is summarized in Table 1.1.

Table 1.1 Instrumented building response database

Building	Height	Framing System	Recorded Accelerations in g.	
SAN FERNANDO 1971				
1. Hotel	20	Reinforced Concrete Frame	Base 11th 20th	0.195 Lost 0.175
2. Financial Building	12	Reinforced Concrete Frame	Base 7th Roof	0.230 0.262 0.277
3. Hotel	7	Reinforced Concrete Frame	Base 4th Roof	0.25 0.25 0.40
4. Hotel	7	Reinforced Concrete Frame	Base 4th Roof	0.147 0.261 0.426
5. Office Building	16	Steel Perimeter Frame	Base 9th Roof	0.153 0.180 0.231
6. Office Building	14	Steel Moment Frame	Base 8th Roof	0.137 0.207 0.180
7. Financial Building	14	Shear Walls	Base 6th Roof	0.260 0.390 0.395
8. Office Building	42	Steel Moment Frame	Base 19th Roof	0.14 0.21 Lost
WHITTIER NARROWS 1987				
9. Office Building	8	Shear Wall/ Frame	Base 2nd Roof	0.39 0.41 0.48
10. Apartment Building	10	Shear Wall	Base 5th Roof	0.63 0.63 Lost

Building	Height	Framing System	Recorded Accelerations in g.	
11. Financial Building	6	Steel Perimeter Frame	Base 2nd 3rd Roof	0.22 0.21 0.24 0.30
12. Commercial Building	14	Shear Wall	Base 8th 12th Roof	0.12 0.19 0.14 0.21
13. Apartment Building	10	Precast Shear Wall	Base 4th 8th Roof	0.22 0.31 0.28 0.54
14. Dormitory	15	Prestressed Concrete	Base 7th 15th	0.094 0.088 0.110
15. Classroom Building	10	Steel Moment Frame	Base 6th 10th	0.140 0.082 0.070
16. Classroom Building	7	Shear Wall	Base 7th	Lost 0.260
17. Classroom Building	8	Shear Wall	Base 4th 8th	Lost 0.320 0.700
18. Dormitory	11	Shear Wall	Base 6th 11th	0.100 0.180 0.290
19. Office Building	13	Reinforced Concrete Frame	Base 2nd 8th Roof	0.26 0.18 0.13 0.14
20. Office Building	12	Steel Perimeter Frame	Base 6th Roof	0.30 0.47 0.28

Building	Height	Framing System	Recorded Accelerations in g.
21. Hotel	20	Reinforced Concrete Frame	Base 0.11 3rd 0.19 9th 0.12 16th 0.13 Roof 0.17
22. Hotel	7	Reinforced Concrete Frame	Base 0.17 2nd 0.18 3rd 0.20 Roof 0.20
LOMA PRIETA 1989			
23. Apartment Building	30	Reinforced Concrete Frame	Base 0.257 13th 0.270 21st 0.244 30th 0.366
24. Office Building	42	Steel Moment Frame	Base 0.108 Ground 0.136 25th 0.224 34th 0.182 42nd 0.228
25. Hospital	4	Steel Moment Frame	Base 0.15 2nd 0.26 Roof 0.61
26. Office Building	6	Reinforced Concrete Frame	Base 0.14 2nd 0.12 5th 0.22 Roof 0.32

INSTRUMENTED BUILDINGS
FRAMING TYPE

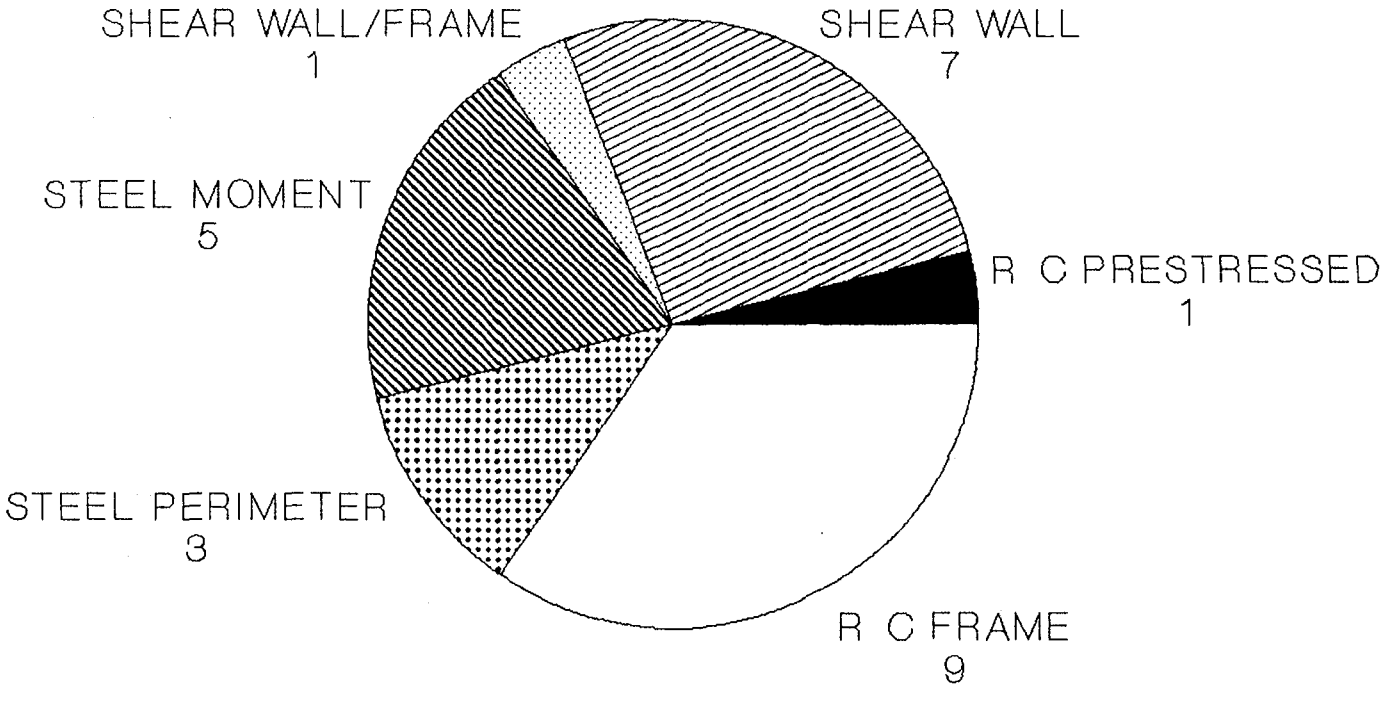

Figure 1.1 - Framing types of instrumented buildings.

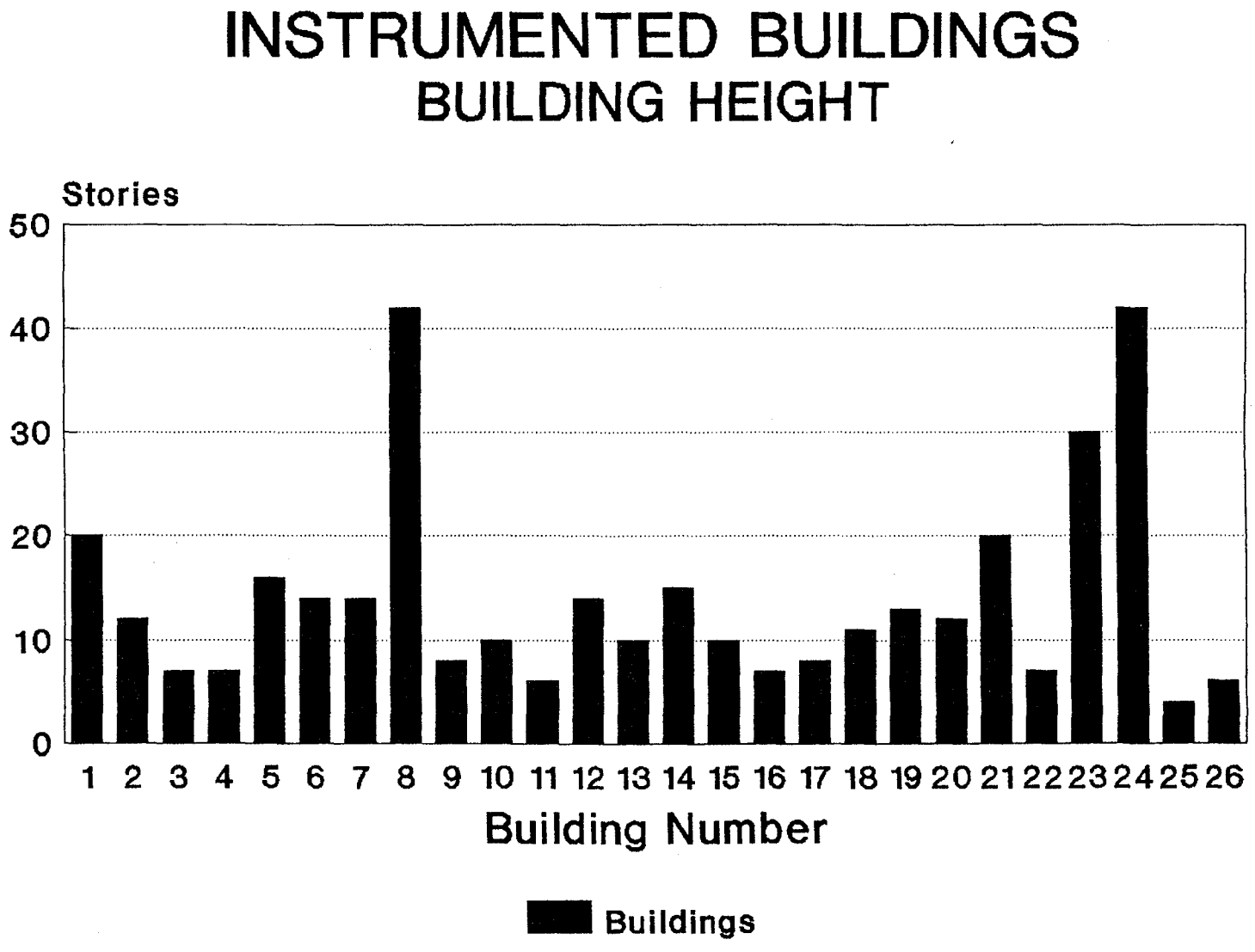

Figure 1.2 - Heights of instrumented buildings.

2. DESCRIPTION OF THE 30-STORY RC BUILDING, ITS DESIGN AND INSTRUMENTATION

2.1 GENERAL DESCRIPTION

The 30-story building selected for the case study of a high-rise reinforced concrete building built on soft soil is located at a latitude of 37.844° N and longitude 122.295° W. It contains 583 condominium units, with a five-level parking structure which is separate and is built on a separate foundation from the main building. An overall view of the building configuration is presented in Fig. 2.1, a typical plan is shown in Fig. 2.2, and the elevations of two sections (A-A and B-B) are presented in Fig. 2.3. As can be seen from Figs. 2.1 and 2.2, the building has one axis of symmetry and a three-winged, Y-shaped configuration. Structurally, the central core area contains two elevator shafts, and each wing contains a stairwell. The building was completed in 1983.

2.2 DESCRIPTION OF THE STRUCTURAL SYSTEM

2.2.1 Superstructure. Except for the shear walls, which are located in each wing and in the central core, and which run only from the foundation up to the second floor, the structural system can be classified as a special (ductile) moment resistant RC space frame. All the columns follow a continuous line from the foundation to the roof. Each wing has 18 columns and the central core 6 columns. In the west wing the space below the second floor is divided by the mezzanine floor. This mezzanine fits part of the parking structure that intersects the west wing up to the second floor level, as indicated in the sections shown in Fig. 2.3. Non-structural elements consist of precast lightweight concrete elements on all facades of the building with interior partitions located at beam lines.

2.2.2 Foundation. The site is underlain by several layers of silty fine sandfill, soft black silty clay (known locally as Bay Mud), and very stiff to hard silty clay (old Bay Mud). The depth of the Bay Mud is approximately 35 to 45 feet. Although it has been estimated that the site period could vary from 0.5 to 1.5 seconds, the records obtained during the Loma Prieta earthquake seem to indicate a period larger than 1.0 second. The superstructure is supported by 900 14 inch by 14 inch prestressed concrete piles, 60 to 70 feet long, along both the longitudinal and the transverse column lines. The base of the building rests on a five-foot thick reinforced concrete mat.

2.3 DESIGN CRITERIA AND STRUCTURAL MATERIALS

2.3.1 Design Criteria. Seismic criteria which included the seismicity of the site and two levels of earthquake, maximum probable and maximum credible, were specifically developed for the design of the building [4]. Earthquakes of magnitude 8.25 on the San Andreas fault and 7.5 on the Hayward fault were selected as bases for the development of the design spectra for the maximum credible earthquakes (MCEQ). A 10% damped design spectrum with a 10% probability of exceedance in 100 years was developed for the MCEQ. A 5% damped design spectrum with a 50% probability of exceedance in 50 years was developed for the maximum probable earthquakes (MPEQ). These design spectra, which are representative of free-field motions, are shown in Fig. 2.4 along with the response spectrum of the Loma Prieta ground motion recorded 328 feet (100 m) south of the building. It can be seen that the design spectra developed specifically for the site do not cover the characteristics of all possible motions at the site. Specifically, the predominant period of the site implied by the design spectra is consistent with a rock or firm soil site rather than a soft clay site like the one under consideration.

The design criteria required the building to resist the MPEQ elastically, to resist the MCEQ without major damage, and to preclude collapse of the structure. The following lateral load cases were considered in the analyses:

1. 1979 Uniform Building Code Lateral Earthquake Forces
2. 1979 Uniform Building Code Wind Loads
3. Response Spectrum Corresponding to the MPEQ
4. Response Spectrum Corresponding to the MCEQ

Linear Elastic Response Spectrum Analysis was used, along with the "Complete Quadratic Combination" (CQC), to combine the response of each mode. For the last two loading conditions, 80% of free-field spectral response was used in the design of the building, to account for soil-structure interaction. The code base shear coefficient for the first mode (analytically estimated to be 2.8 seconds) was 4% of the total weight of the building. The first mode responses for the MCEQ and MPEQ, in terms of shear coefficient, were 0.22 and 0.104, respectively. By considering the modal mass participation factors of the first mode in the dynamic analysis, the equivalent shear coefficients were of the order of 0.173 and 0.081 for the MCEQ and MPEQ, respectively. Wind shears at the base level were approximately 36% of the code seismic shears, and wind overturning moments were 30% of code seismic overturning moments, therefore wind loads did not govern the design of the structure members.

2.3.2 Structural Materials. The design compressive strength of the concrete was 6,500 psi (450 kg/cm^2) in the columns of the 1st to the 5th story of the building and in the interior

columns of the 20th and 21st floors. At other locations the concrete strength was 5,000 psi (346 kg/cm^2). The design yield strength for the reinforcing steel was 60 ksi (4,200 kg/cm^2). Specially manufactured high-strength wire was used for confinement reinforcement, column ties and beam stirrups. The beams were designed to resist the MCEQ without exceeding a curvature ductility of four, while the columns were designed to resist the same level of excitation without exceeding a curvature ductility of two.

2.4 INSTRUMENTATION

The Y Building forms a part of the strong-motion network instrumentation operated by the United States Geological Survey (USGS). The building is extensively instrumented, with sensors located on or within the structure at a sufficient number of locations to provide significant response data for a rigorous analysis of the structure's performance during strong earthquake motions [5]. Instrumentation of the building was completed in 1985.

The instrumentation consists of 21 CRA-1 analog acceleration sensors distributed over the three wings and central core on the 13th, 21st, and 31st floors, and at the ground level. Additionally, there is a 3-component CRA-1 free-field analog accelerometer 40 m (131 feet) north of the building, and a 3-component SMA-1 free-field analog accelerometer 100 m (328 feet) south of the building. Figure 2.5 shows the locations of the 21 sensors in the building.

It should be noted that only the ground floor was instrumented with vertical sensors. This is unfortunate, because it does not permit estimation of the effect of the vertical ground motion.

Figure 2.1 - Overall view of the thirty-story building

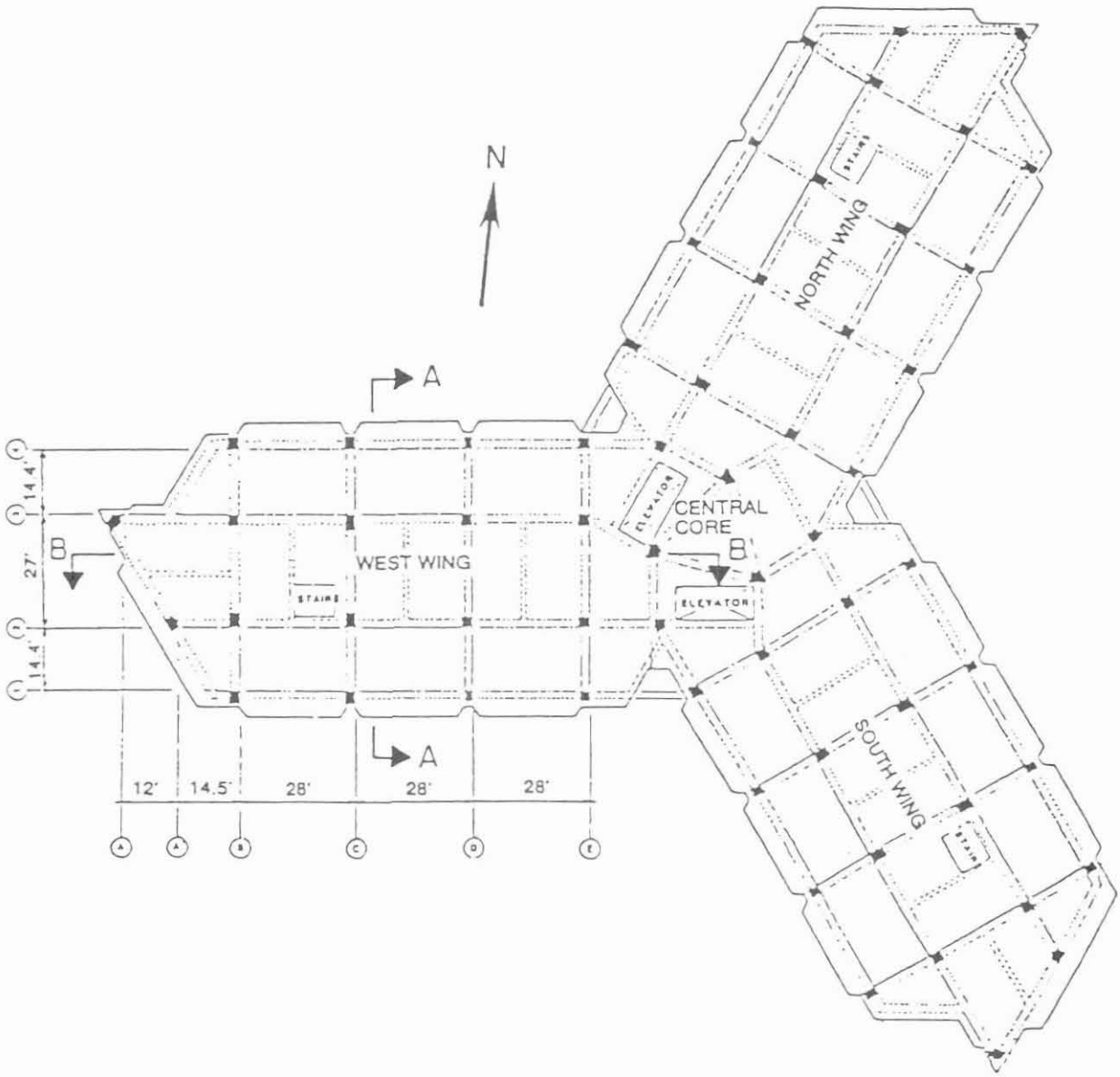

Figure 2.2 - Typical floor plan of the thirty-story building

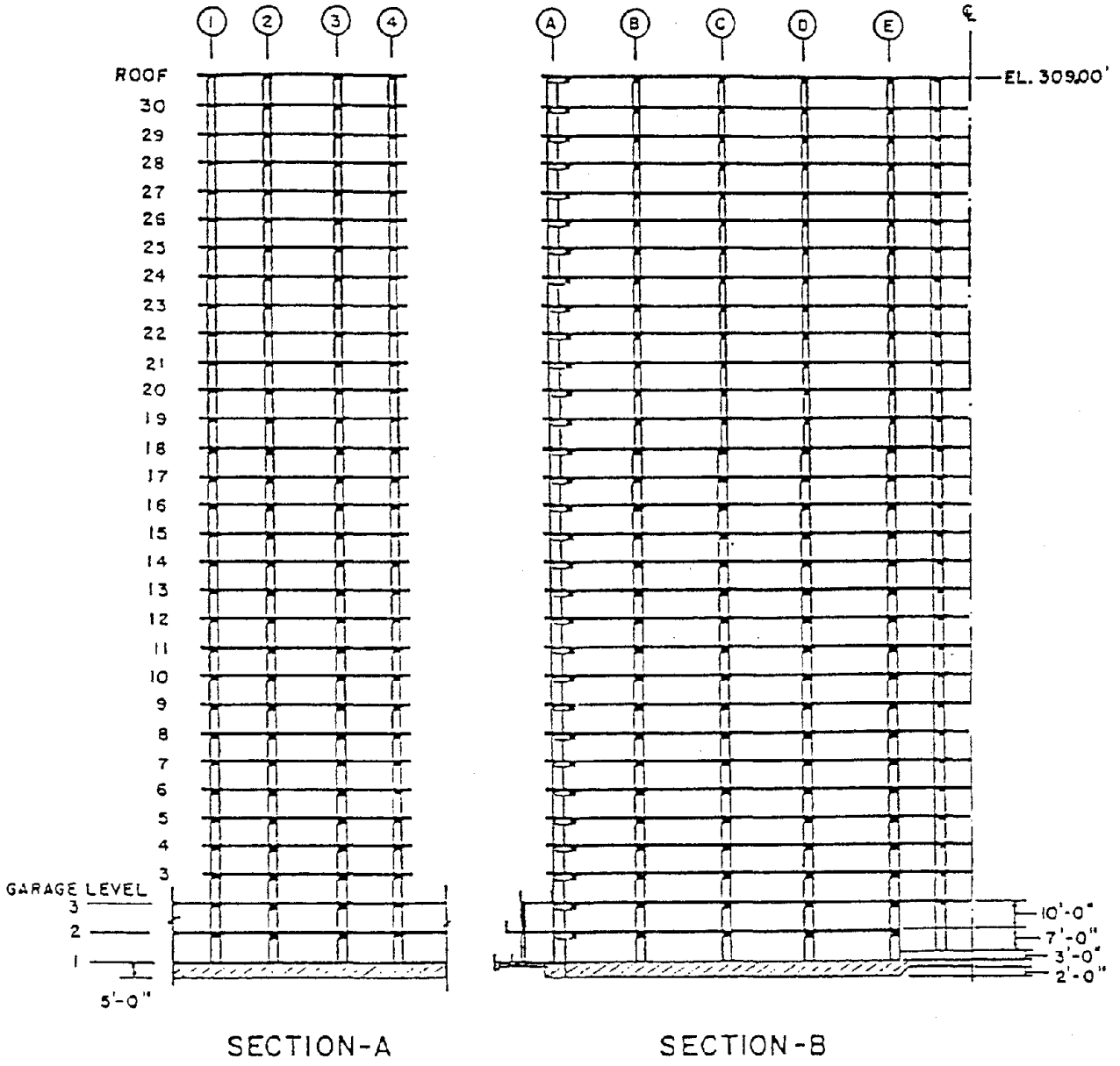

Figure 2.3 - Typical elevation (section) of the building -- west wing

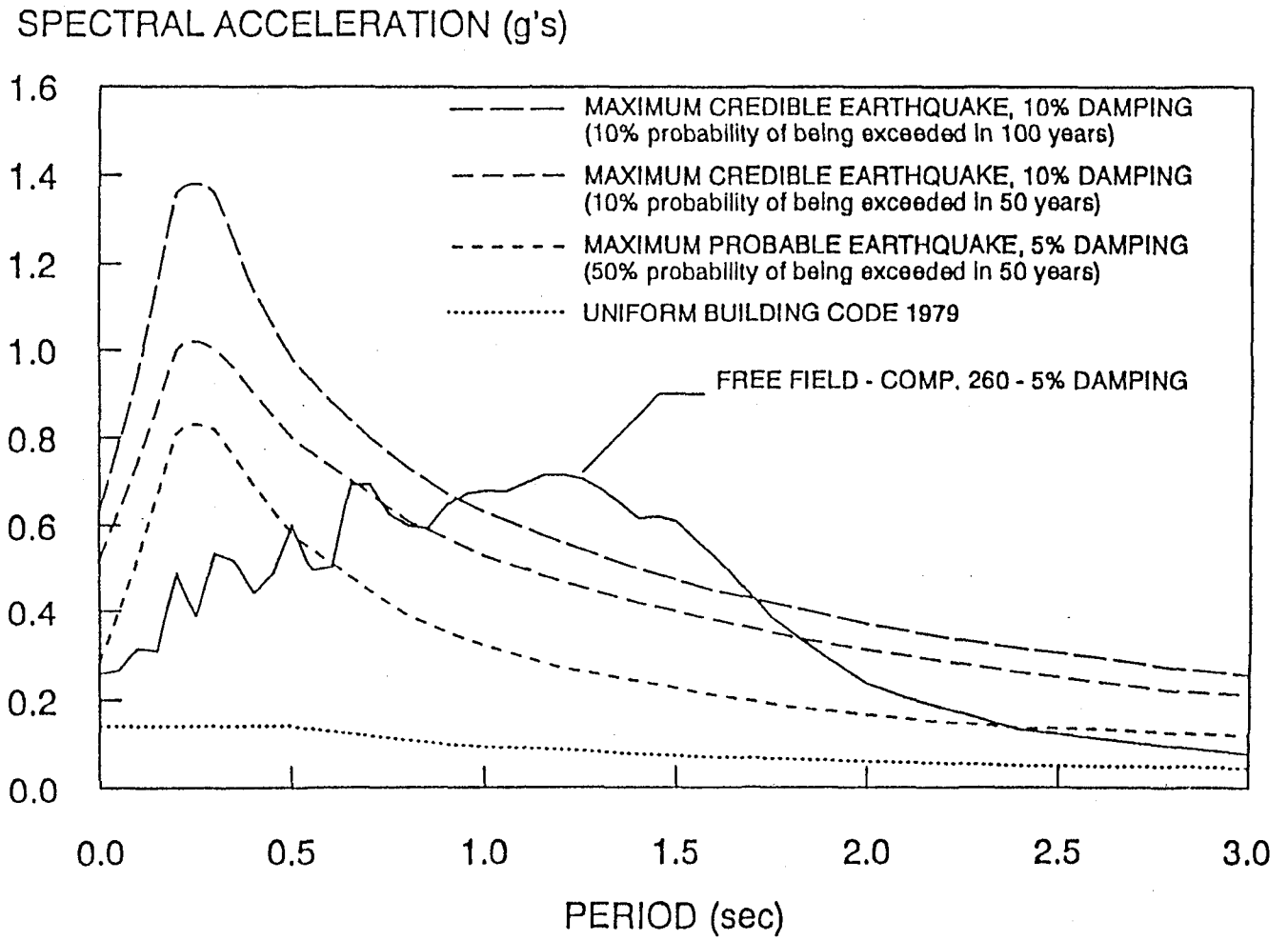

Figure 2.4 - Comparison of design spectra and the spectrum of the recorded free-field ground motion

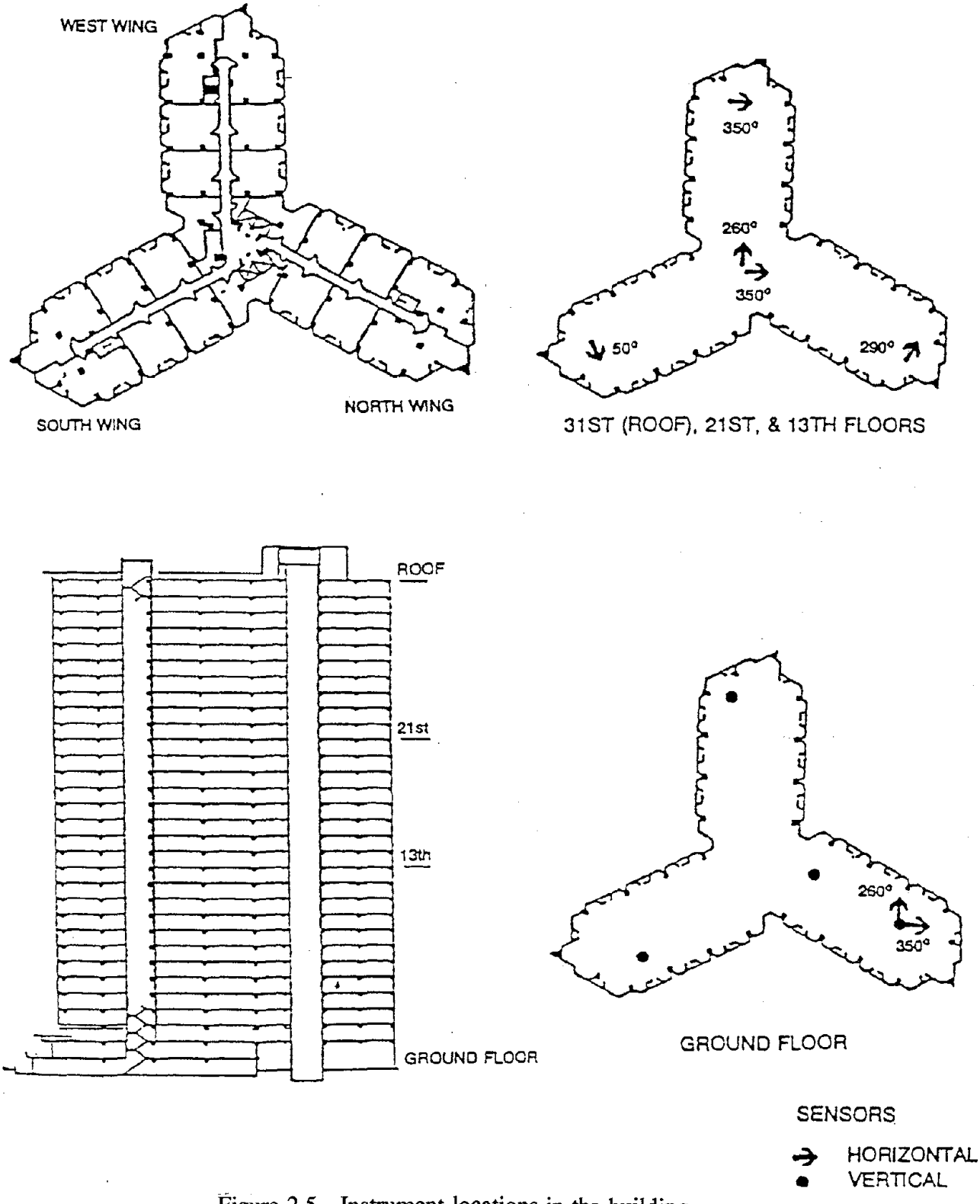

Figure 2.5 - Instrument locations in the building

3. RECORDED RESPONSE DURING THE LOMA PRIETA EARTHQUAKE

3.1 GENERAL REMARKS REGARDING THE LOMA PRIETA EARTHQUAKE

The 7.1 surface wave magnitude Loma Prieta earthquake, which occurred at 17:04 Pacific Daylight Time on 17 October, 1989, was centered approximately 16 km (10 miles) northeast of Santa Cruz at a hypocentral depth of about 18.5 km (11.5 miles). This earthquake, the largest magnitude earthquake in northern California since 1906, caused 62 deaths, approximately 3750 injuries, and more than 8 billion dollars in damage in the San Francisco Bay Area [6].

The Y Building is located approximately 97 km (60 miles) north of the epicenter. Major damage occurred within 5 km (3 miles) of the building, including the collapse of the Cypress Street Viaduct, the collapse of a segment of the San Francisco-Oakland Bay Bridge, damage to facilities at the Port of Oakland, and damage to several buildings in downtown Oakland.

The Y Building suffered only limited damage to non-structural components and no visible structural damage. The parking structure next to the building received flexural cracks in the floor system due to north-south motion of the structure, as well as severe shear cracking of two columns in the first story.

3.2 DESCRIPTION OF THE RECORDED RESPONSE

A total of 27 accelerograms were obtained from the Y Building in the Loma Prieta earthquake [5]. The records were collected and digitized by the USGS. Table 3.1 describes the digitized records obtained, as well as the location of the recording stations in the building.

Figures 3.1 to 3.9 show the recorded acceleration time-histories. It should be noted that the records on the free-field stations (Figs. 3.1 and 3.2) show that up-down motions were stronger than horizontal motions during the first 5 seconds. Similar observations can be made with respect to the recorded motion at ground level in the building (Figs. 3.3 and 3.4). This appears to agree with what some occupants reported after the earthquake. In general, the records obtained at ground level are characterized by a strong phase of approximately 8 seconds. For records obtained above the ground level (levels 13, 21 and 31) the strong phase extends for a duration of approximately 10 seconds.

The maximum peak ground acceleration, 0.26g, was recorded in the 260° component of the free-field instrument located approximately 100 m (328 feet) south of the building, whereas the peak acceleration recorded at the base of the building was 0.21g in the same direction. The ratios of peak structural to peak ground response are 1.72 and 1.53 in components 260° and 350°, respectively. Table 3.2 lists the peak acceleration recorded by each instrument. The largest acceleration (0.47g) was recorded at the 31st level of the north wing. For each record, velocity and displacement time-histories were computed by numerical integration of the recorded acceleration time-history. The integrated data were filtered with a high-pass Ormsby digital filter with a linear delay between a cut-off frequency of 0.20 Hz and a roll-off termination frequency of 0.18 Hz. At each step the time series were also corrected by a linear base-line correction [7, 8, 9]. The peak velocity and peak displacement for each record are also listed in Table 3.2. A maximum displacement of 19.5 cm (7.7 in.) was obtained at the central core and in the E-W direction. This resulted in an average drift index (roof displacement divided by the height of the building) of 0.002. Linear elastic response spectra of the horizontal motions recorded at ground level and at the free-field stations were

calculated by a direct integration method as proposed in Ref. 10. Figure 3.10 shows the linear elastic response spectra for 0, 2, 5, 10, and 20% damping of the horizontal ground motions recorded at the free-field station south of the building. In the figure the predominant period of the ground at the site is seen to be approximately 1.5 seconds (particularly well defined for the 260° component). Figure 3.11 shows the linear elastic response spectra for both horizontal components of ground motion (0, 2, 5, 10, 20% damping) recorded at the free-field station north of the building. Response spectra for the horizontal components of motion recorded at the ground floor of the building are shown in Fig. 3.12.

The principal direction of the ground motion recorded at the south free-field station was computed to be 294°. Figure 3.13 shows the time integral of accelerations squared for both recorded components and the principal direction. It can be seen that the energy in the principal direction is slightly larger than that of the 260° component and nearly twice the energy of the 350° component.

3.3 SYSTEM IDENTIFICATION OF DYNAMIC CHARACTERISTICS

The occurrence of a moderate or strong earthquake ground motion can be viewed as a full-scale, large-amplitude experiment on a structure: if the structural motion is recorded, it offers the opportunity to make a quantitative study of the structure at dynamic force and deflection levels directly relevant to earthquake-resistant design. A particularly important aspect of this quantitative study is the determination of the dynamic characteristics of the structure, which can be estimated through system identification techniques.

In this study, the following three frequency-domain system identification techniques were used.

1. Non-parametric, time-invariant
2. Non-parametric, time-variant (moving-window Fourier analysis)
3. Parametric, time-invariant

Despite some limitations, these approaches have been used successfully in the past to identify the dynamic characteristics of buildings that have been excited by earthquake ground motions [11-14].

In the first technique the structure is idealized by a non-parametric, time-invariant linear model in which a single input x(t) and output y(t) are characterized by an impulse response function h(t) in the following input-output relation.

$$y(t)=\int_0^{\infty} h(\tau)x(t-\tau)d\tau \tag{3.1}$$

The corresponding frequency domain model is given by the transfer function H(iω), the Fourier transform of h(t), and the input-output relation

$$Y(\omega)=H(i\omega)X(\omega) \tag{3.2}$$

where X(ω) and Y(ω) are the Fourier transform of the input and output time-series, respectively, which in their discrete form are defined as

$$X(\omega)_j=\frac{1}{n}\sum_{t=0}^{n-1} x(t)\ \exp(-i\omega_j t) \quad , \quad \omega_j=\frac{2\pi j}{n} \tag{3.3}$$

$$Y(\omega)_j=\frac{1}{n}\sum_{t=0}^{n-1} y(t)\ \exp(-i\omega_j t) \quad , \quad \omega_j=\frac{2\pi j}{n} \tag{3.4}$$

In this study, Equations 3.3 and 3.4 were computed using the Fast Fourier Transform algorithm [15].

The second system identification technique (non-parametric, time-variant) is essentially the same as the approach described above, except that in order to identify the variation of parameters in time, a window smaller than the total duration of the record, is "moved" in time. The size of the window is selected to be a function of the fundamental period of the building. In this study, a window with a duration of approximately four times the fundamental period of the building was used.

The third system identification technique is also done in the frequency domain, and was first proposed by McVerry [12]. The parameters of the mathematical model which describe the input-output relation of the building are selected to minimize the difference between the smoothed Fourier transform of the recorded acceleration time-histories and the Fourier transform of the computed response. The identification is done mode by mode by comparing the recorded and computed response only over a specified frequency band, which is chosen to be broad enough to include all the significant response due to a certain mode.

In order to increase the resolution of functions $X(\omega)$ and $Y(\omega)$, the input and output signals (in all three techniques), $x(t)$ and $y(t)$ (of length n) are extended by adding zeros at the end of the recorded signal. The new input time series is

$$x'(t)=\begin{matrix} x(t), & 0\le t<n \\ 0, & n\le t<n' \end{matrix} \tag{3.5}$$

where $n'> n$ is conveniently chosen to get adequate resolution in the Fourier transforms. The transform of the extended time series is

$$\begin{aligned} X'(\omega)_j &= \frac{1}{n'}\sum_{t=0}^{n'-1} x'(t)\ \exp(-i\omega_j t) \\ &= \frac{1}{n}\sum_{t=0}^{n-1} x(t)\ \exp(-i\omega_j t) \\ &= \frac{n}{n'}X(\omega)_j \end{aligned} \tag{3.6}$$

where $\omega'_j = 2\pi/n'$ is the *j*th Fourier frequency for the extended time series $x'(t)$ of length n'. We thus obtain (a multiple of) the required transform, but at the Fourier frequencies ω'_j whose spacing is $2\pi/n' < 2\pi/n$, resulting in an improved resolution.

However, improving the resolution by the method outlined above may emphasize the problem of *leakage* (appearance of nonzero terms in the transform because of a sinusoid of a different frequency) [16]. To reduce leakage, two types of time-domain digital filter were applied to the original time series before extending them. The two types of filter (or windows) employed are the split-cosine-bell data window and the Hanning data window, which is a particular case of the first window when the data is tapered 100%. Figures 3.14 and 3.15 compare these data windows to the rectangular box window (or boxcar). For the split-cosine-bell data window, tapering of 20% was sufficient to reduce most of the leakage. Both filters where implemented in the "S" programming environment [17], which was used to perform all of the signal processing analysis.

Figure 3.16 shows the Fourier amplitude spectra of input and output signals, functions $X(\omega)$ and $Y(\omega)$ for the 350° component recorded motions. The input signal (dotted line) corresponds to the motion recorded at the ground level, and the output signals (solid lines) correspond to the motions recorded in the central core at 31st, 21st, and 13th levels. Results are only shown for a 0 to 4 Hz window for easy identification of the first few modes of vibration. It can be seen that the ground has its strongest input in a band between 0.6 to 1.2 Hz and around 1.90 Hz. The response of the structure in the first region (0.6 to 1.2 Hz) is particularly strong at the 31st and 13th levels. The structural response at frequencies around 1.90 Hz is strong at the 31st and 21st levels. At the 21st floor there is also an important response at a frequency of 0.37 Hz.

Figure 3.17 shows the Fourier transforms of input and output motions recorded in the 350° component, but in this case the output signals correspond to motions recorded in the west wing at the 31st, 21st, and 13th levels. The same regions of strong structural response are seen and, in general, the comments regarding Fig. 3.16 also apply to Fig. 3.17.

Fourier amplitude spectra of input and output motions recorded in the 260° component are shown in Fig. 3.18. Here, the input signal (dotted line) corresponds to the acceleration time-history recorded at the ground level, and the output signals (solid lines) correspond to the motions recorded in the central core at the 31st, 21st, and 13th levels. The maximum input regions of the spectra are the same as those observed for the 350° component, that is, in a band between 0.7 to 1.0 Hz and around 1.90 Hz. For the 260° direction, the strongest building response is at frequencies around 0.93 Hz (particularly at the 31st and 13th levels). Important response also occurs for frequencies around 0.37 and 2.0 Hz.

In Fig. 3.18, the regions where there is a strong structural response for a smaller input suggest the presence of the natural periods of vibration of the building. Therefore, a better means of identification is obtained through the calculation of the transfer function of each combination of input and output signals. In order to reduce (to a certain extent) the variability and occurrence of peaks in the transfer functions that are results of measurement noise, the time series were smoothed through running medians [18].

Figure 3.19 shows the transfer functions corresponding to motions recorded in the central core in the 350° component. From this figure a first mode around a frequency of 0.39 Hz is evident. This first mode (350° component) is corroborated by the transfer functions of motions recorded at the west wing (also for the 350° component), which are shown in Fig. 3.20. In this figure the first mode is even more clearly defined (note the change in amplitude scale on each graph). The second mode (with larger amplitude at the 31st and 13th levels) occurs at a frequency of 1.12 Hz. The transfer functions corresponding to motions recorded in the central core in the 260° component are shown in Fig. 3.21. From this figure, 1st, 2nd, and 3rd modes were identified at 0.37, 0.94, and 1.81 Hz, respectively. Identified translational periods and mode shapes are summarized in Table 3.3, and the ratios of translational periods are shown in Table 3.4. The ratios reasonably follow what could be expected for moment-resistant frame (shear-type) buildings [19, 20].

The damping ratio in the first two modes was estimated using the half-power band-width method [20]. Values were found to vary with the filter and the degree of smoothing employed in computing the transfer functions, as was previously found by other researchers [21]. Since resolution, and particularly smoothing, introduced significant distortion in the

spectra, the length of the signal was extended to four times its original length to obtain a reasonable degree of resolution, and no smoothing or filters were used to estimate the damping ratios. For the first and second modes the damping was found to vary between 2.5% and 3% (Table 3.3).

3.4 COMPARISON OF DYNAMIC CHARACTERISTICS

Ambient and forced-vibration measurements of the building were made in 1983 [22]. Forced vibrations were produced by two rotating-mass vibration generators anchored to the roof level of the building. Each generator was capable of producing a maximum force of 5,000 lb. In Ref. 22, a description of the tests and the results for resonant frequencies, mode shapes and damping ratios for both types of excitation, are presented.

Table 3.5 compares the periods and frequencies obtained through ambient vibrations, small-amplitude forced vibrations, and those obtained in the present study. There is very good agreement between the periods obtained through ambient and forced vibrations. However, there exist very large differences between the small-amplitude measurements and the results from the records obtained in the Loma Prieta earthquake. For the 350° component, the ratio of fundamental period measured during the earthquake to that measured through ambient vibrations is 1.51. For the 260° component, this ratio is 1.57. Ambient and forced vibration tests of the building were done when construction of the structure had just finished. All the partitions were on the floors of the building, but only in a few stories were they installed in their final position. The tests were conducted before there were practically any live loads. An increase in mass due to the presence of live loads could partially explain

the change in periods from those observed from the earthquake records, but certainly does not explain all of the change.

Large differences between the periods of vibration obtained through ambient vibrations conducted immediately after completion of the construction and those observed during earthquakes have been reported in the literature [12, 23-29]. Table 3.6 summarizes changes in fundamental periods observed in other instrumented buildings. Fourteen of the buildings listed in this table also sustained no structural damage and insignificant non-structural damage. Of those 14 buildings that sustained no structural damage and insignificant non-structural damage, the periods of 10 buildings had previously been measured through ambient vibrations. The average T_{EQ}/T_{PRE} ratio for these 10 buildings (two translational first mode periods for each building) is 1.50. If this group of buildings is divided into reinforced concrete and steel buildings, the ratios are 1.56 and 1.44, respectively.

Using data from the San Fernando earthquake, Haviland et al. [28] performed a linear regression analysis on the observed changes in translational periods during earthquakes and proposed the following expression:

$$T_{sp} = 0.75T_{EQ} - 0.14 \tag{3.7}$$

where T_{sp} is the small amplitude period measurement prior to the earthquake, and T_{EQ} is the period measurement during the earthquake. Using this expression, the computed T_{EQ} for the Y Building is 2.47 seconds for both directions, which differs by 4.7% and 8.2% from those measured during the Loma Prieta earthquake in the 350° and 260° components, respectively. Thus, both the differences in period obtained during the earthquake and those obtained

through ambient vibrations follow the same pattern as that shown by other buildings where the same information was available.

Table 3.7 summarizes the results of similar observations made in Japan for an earthquake with magnitude 6.1 which occurred on July 1, 1968, about 45 km northwest of Tokyo [30]. For that set of buildings the ratio of fundamental period measured during the earthquake to the ambient vibration period is 1.20. A possible reason the ratio is smaller than that for the first set of buildings is that a smaller and more distant earthquake is causing very small vibration amplitudes of the buildings. Although no detailed description of the damage of the buildings is given, their maximum displacements indicate that the level of deformations was very small, and most likely no damage (either structural or non-structural) was observed.

Table 3.8 summarizes observed changes in fundamental periods in shaking table or pseudo-dynamic testing of model and prototype structures. Although the structures listed in Table 3.8 were tested under minor to severe earthquake ground motions, only the results from serviceability level earthquakes are reported here (except for the eccentrically-braced frame and moment-resistant full-scale steel frames tested in Tsukuba, which were not subjected to moderate testing prior to severe ground motions). The observed period changes varied from 1.04 to 1.91. Note that the highest ratio was obtained on the structure with non-structural components. In all of the cases where testing was done on only a bare structure, the highest ratio was 1.30. Comparing 1.91 with 1.30 reveals the importance of the role that non-structural components play in the change in T and therefore in the response of the whole building system.

A comparison of mode shapes measured for the Y Building through ambient vibrations, small-amplitude forced vibrations, and those identified in this study as a result of the Loma Prieta earthquake are shown in Figs. 3.22 and 3.23 for the 350° and 260° components, respectively. The mode shapes identified from the earthquake motions are in close agreement with those previously obtained using ambient and forced vibrations. The largest differences were observed for the third translational mode in the 350° component.

In order to identify possible changes in fundamental period during the earthquake, a moving-window Fourier analysis [37] was performed using the motion recorded at the 31st level in the west wing (350° component). Figures 3.24, 3.25, and 3.26 present the results of this analysis, presenting transfer functions for nine different windows. The transfer functions have been calculated for 10-second window lengths starting, from the beginning of the record and then offsetting the window by 5 seconds at each step. For each window, the length of the record was extended (by adding zeros) to obtain good resolution in the spectra. For the first two windows the response at the frequency of the fundamental mode, f_1 = 0.39 Hz, is not apparent. In the third window (10-20 seconds) the first mode response starts to become evident. It has to be noted that the story motion started at about 8 seconds. The first mode response increases further in the fourth and fifth windows, and from this point on decreases gradually toward the end of the record. From the moment the first mode response was evident (third window) to the end of the earthquake, no change in frequency was observed, despite changes of up to 400% in amplitude. For the 260° component, a 4% elongation of period was observed after the 14 second time mark.

3.5 EVALUATION OF TORSIONAL RESPONSE

From the amount of damage observed and reported in the different apartments, it appears that the non-structural damage was greater at the end of the wing than at or near the core, indicating the probability of torsion. The availability of records in the central core of the building and in the wings offers the opportunity for a careful study of the torsional response of the Y Building during the Loma Prieta Earthquake. In this section, results of analyses and comparisons, in the time and frequency domains, of motions recorded in the central core and wings of the building, are presented.

For the 350° component, motions were recorded in both the central core and the west wing. Figure 3.27 shows a comparison of recorded acceleration time-histories in the central core and the west wing at the 31st, 21st and 13th levels for the 350° component. The motion of the core and the west wing is almost the same at all three levels. Throughout the total length of the record there exists a very good match both in phase and amplitude. Small differences may be seen at the 13th level for 5 seconds after the 15 second mark. The difference that is shown at level 21 after 20 seconds is likely to be related to a digitization error of the acceleration time-history recorded at the core, where it seems likely that a whole cycle of the response was lost (skipped) in the digitization process.

In order to compare the response of the core with that of the north and south wings, the motion at the central core had to be computed for the same component that was recorded in these two wings. This was possible given the fact that records in two orthogonal directions were obtained at the central core. Figure 3.28 shows the comparison of recorded acceleration time-histories in the central core and the north wing at the 31st, 21st, and 13th levels for the

290° component, whereas Fig. 3.29 shows the comparison corresponding to the north wing (50° component). As shown in Figs. 3.27-3.29, the recorded motion at the central core is very similar to that in the wings, suggesting that the torsional response was not significant during the earthquake.

In order to identify specific frequencies at which there were differences between the core's motion and the motion at the wings, further analysis and comparison was carried out in the frequency domain. Figure 3.30 shows the comparison between the Fourier amplitude spectra of the accelerations recorded in the central core and those recorded in the west wing at the 31st, 21st and 13th levels for the 350° component. The spectra for the transfer functions presented in section 3.3 are only presented from 0 to 4 Hz, where the dominant frequencies of the building are located. As shown in this figure, the motion of the central core and the west wing is similar for practically all frequencies between 0 and 4 Hz. The first torsional mode frequency is 0.39 Hz. Figures 3.31 and 3.32 compare the Fourier amplitude spectra of motions recorded at the central core and motions recorded at the north and south wings, respectively. Again, it may be seen that the two motions are practically the same, indicating that there was very small (almost negligible) torsional movement in the building during the earthquake. Given the small amplitude of torsional motions in the building and mode interference, higher torsional mode frequencies could not be identified from the records.

3.6 EVALUATION OF SOIL-STRUCTURE INTERACTION AND ROCKING RESPONSE

The availability of free-field and ground floor records offers the opportunity to study the soil-structure interaction and rocking response of the building during the Loma Prieta

earthquake. In this section, results of analyses and comparisons, in time and frequency domains, of motions recorded at both of the free-field stations and the ground floor of the building, are presented.

Comparisons similar to those for the torsional response were made for the recorded acceleration time histories. Figure 3.33 compares the horizontal acceleration time-histories for the 350° component recorded at the ground floor (solid line) and at both free-field stations (dotted lines). The recorded motions are similar, although the motion recorded at the free-field station north of the building is closer to the ground floor motion than the motion recorded at the free-field station south of the building. Figure 3.34 shows the same type of comparison of recorded motions for the 260° component, which was slightly more intense. Again, the ground floor and free-field motions are similar. In general, it can be concluded that soil-structure effects were very small. As for the 350° component, small differences are more noticeable for the motion recorded in the free-field south of the building. The only significant difference in intensity occurred at the times when the free-field ground accelerations reached their maximum values (around 11 to 14 seconds): at these times the peak acceleration at the ground floor of the building was about 20% smaller than that of the free field.

Figures 3.35 and 3.36 compare horizontal free-field and ground floor motions in the frequency domain. As observed in the time domain, the motion recorded at the north free-field station is very similar to that recorded at the ground floor of the building. For the motion recorded south of the building, differences are more significant, especially for the 350° component (Fig. 3.35). These differences could be interpreted as consequences of soil-

structure interaction. On the other hand, differences between both of the free-field stations suggest that the observed differences in Figs. 3.35 and 3.36 are related more to loss of wave coherency due to spatial variation of the ground motion than to soil-structure interaction. However, this last suggestion can be obscured by the possibility that the record obtained at the so-called north free-field station (which was only 100 feet from the building) was actually affected by the response of the structure.

Some observations can be made by evaluating how elastic systems would behave under the motions recorded at the three locations. This evaluation is achieved by computing the linear elastic response spectra of a single-degree-of-freedom system (SDOFS) for the horizontal components of the recorded motion. Figures 3.37 and 3.38 show the comparisons of linear-elastic response spectra for horizontal components recorded at the three locations for 2% and 5% damping, respectively. It can be seen that for both horizontal components of motion, the response under the south free-field motion is greater than that for the other two locations for periods between 0.5 and 4 seconds, indicating a reduced response of up to 25% at the base of the building. The response of linear systems under the motions recorded at the north free-field station and under the motions recorded at the ground floor is practically the same for periods longer than 0.3 second.

Significant differences were observed between the periods of the structure obtained from the response to the earthquake and those determined from small vibration tests, and it was thought that one of the reasons could be that during the stronger earthquake motions significant rocking developed. The significance of rocking response in the building during the Loma Prieta earthquake was studied by comparing Fourier amplitude spectra of vertical

accelerations recorded at different locations of the ground floor and those recorded at the free-field stations. Figures 3.39 and 3.40 compare the Fourier spectra of the vertical accelerations recorded in each wing (at the ground floor) with those recorded at the north and south free-field stations, respectively. No changes in amplitude at frequencies close to the first translational mode in each direction (0.38 and 0.37 Hz) were observed, suggesting that there was no rocking, or at least that rocking did not influence the first mode. Further, in order to identify any evidence of rocking, the Fourier spectra of vertical accelerations recorded in the three wings at the ground floor of the building were compared with the Fourier spectrum of the vertical acceleration recorded at the central core of the building (ground floor). A larger amplitude of wing motion with respect to the core motion at frequencies corresponding to dominant modes of the building would indicate possible rocking response. Figure 3.41 presents such a comparison, and shows very little change in amplitude at frequencies corresponding to the first three modes of vibration in each direction.

3.7 CONCLUDING REMARKS

From analyses of the records of the free-field ground motions and of the response of the 30-story Y Building, obtained during the Loma Prieta earthquake, the following observations can be made regarding the dynamic characteristics of the building, its torsional response, the soil-structure interaction, and the rocking response.

3.7.1 Dynamic Characteristics. The analyses which were conducted using three different system identification techniques show the following:

(1) The first three translational modes have the following periods in seconds:

(a) in the E-W direction: 2.59; 0.89; and 0.46

(b) in the N-S direction: 2.69; 1.07; and 0.55

(2) Comparisons of the above identified dynamic characteristics with those obtained after the completion of construction of the superstructure using ambient and small-amplitude vibration tests show that periods of vibration with dominant modes obtained from earthquake records are significantly longer (54% and 59% for 1st modes) than those obtained from small amplitude vibration tests.

(3) A review of literature on recorded changes in vibration periods due to moderate shaking for existing buildings and for experimental models reveals that the changes observed in the Y Building follow reasonably well the changes reported for other RC buildings in the U.S., but are larger than those reported for Japanese buildings.

(4) No significant variations in the dynamic characteristics were identified in the two horizontal translational directions during the earthquake. Thus it is believed that the observed changes in the period of the Y Building occurred before the Loma Prieta earthquake.

3.7.2 Torsional Response. From detailed analyses and comparisons, in the time and frequency domains, of motions recorded in the central core and wings of the building, it has been concluded that during the 1989 Loma Prieta earthquake there was very small torsional movement in the building.

3.7.3 Soil-Structure Interaction and Rocking Response. The results obtained in detailed analyses and comparisons, in the time and frequency domains, of motions recorded during the 1989 Loma Prieta earthquake at both the free-field stations and on the ground floor of the building, indicate the following:

(1) Soil-structure interaction effects do not appear to be significant. Although small differences were noted between the intensity of the motions in the E-W direction when the free-field motions reached their highest values, the free-field intensity being somewhat larger, it is not clear whether these differences were due to soil-structure interaction or were consequences of the loss of wave coherency due to spatial variation of the ground motion.

(2) Rocking had only a negligible effect on the response of the building.

USGS FILENAME	NEW FILENAME	LEVEL	LOCATION	COMP.
USACA47.33	PLAZA1	Ground South	Free Field	350
USACA47.34	PLAZA2	Ground South	Free Field	UP
USACA47.35	PLAZA3	Ground South	Free Field	260
USACA47.36	PLAZA4	31st Level	West Wing	350
USACA47.37	PLAZA5	31st Level	South Wing	050
USACA47.38	PLAZA6	31st Level	North Wing	290
USACA47.39	PLAZA7	31st Level	Central Core	350
USACA47.40	PLAZA8	31st Level	Central Core	260
USACA47.41	PLAZA9	21st Floor	Central Core	350
USACA47.42	PLAZA10	21st Floor	West Wing	350
USACA47.43	PLAZA11	21st Floor	South Wing	050
USACA47.44	PLAZA12	21st Floor	North Wing	290
USACA47.45	PLAZA13	13th Floor	Central Core	350
USACA47.46	PLAZA14	13th Floor	Central Core	260
USACA47.47	PLAZA15	21st Floor	Central Core	260
USACA47.48	PLAZA16	13th Floor	West Wing	350
USACA47.49	PLAZA17	13th Floor	South Wing	050
USACA47.50	PLAZA18	13th Floor	North Wing	290
USACA47.51	PLAZA19	Ground Floor	West Wing	UP
USACA47.52	PLAZA20	Ground Floor	South Wing	UP
USACA47.53	PLAZA21	Ground Floor	Central Core	UP
USACA47.54	PLAZA22	Ground Floor	North Wing	260
USACA47.55	PLAZA23	Ground Floor	North Wing	UP
USACA47.56	PLAZA24	Ground Floor	North Wing	350
USACA47.57	PLAZA25	Ground North	Free Field	350
USACA47.58	PLAZA26	Ground North	Free Field	UP
USACA47.59	PLAZA27	Ground North	Free Field	260

Table 3.1 - Records obtained in the Y Building during the Loma Prieta Earthquake.

LEVEL	LOCATION	COMP.	FILENAME	PEAK ACC. [cm/sec^2]	PEAK VEL.[I] [cm/sec]	PEAK DISP.[II] [cm]
31st Level	West Wing	350	PLAZA4	257.4	30.69	5.83
31st Level	South Wing	050	PLAZA5	298.7	62.77	17.16
31st Level	North Wing	290	PLAZA6	466.7	70.08	17.32
31st Level	Central Core	350	PLAZA7	240.3	26.05	5.45
31st Level	Central Core	260	PLAZA8	359.1	77.42	19.45
21st Floor	West Wing	350	PLAZA10	185.6	13.02	3.77
21st Floor	South Wing	050	PLAZA11	165.4	26.05	8.46
21st Floor	North Wing	290	PLAZA12	235.9	30.08	6.60
21st Floor	Central Core	350	PLAZA9	179.4	15.00	5.98
21st Floor	Central Core	260	PLAZA15	239.2	32.1	8.76
13th Floor	West Wing	350	PLAZA16	206.3	19.21	2.77
13th Floor	South Wing	050	PLAZA17	218.4	34.42	7.80
13th Floor	North Wing	290	PLAZA18	303.0	40.84	8.11
13th Floor	Central Core	350	PLAZA13	265.6	25.37	4.24
13th Floor	Central Core	260	PLAZA14	253.7	40.13	9.10
Ground Floor	North Wing	350	PLAZA24	173.4	15.81	2.90
Ground Floor	North Wing	260	PLAZA22	208.21	37.40	6.66
Ground Floor	North Wing	UP	PLAZA23	46.8	4.17	0.94
Ground Floor	West Wing	UP	PLAZA19	55.9	4.36	0.90
Ground Floor	South Wing	UP	PLAZA20	55.4	4.34	0.87
Ground Floor	Central Core	UP	PLAZA21	37.5	4.24	0.79
Ground South	Free Field	350	PLAZA1	210.3	21.93	3.79
Ground South	Free Field	UP	PLAZA2	58.5	4.54	0.74
Ground South	Free Field	260	PLAZA3	252.26	40.84	8.15
Ground North	Free Field	350	PLAZA25	178.7	15.74	2.57
Ground North	Free Field	UP	PLAZA26	82.2	5.32	1.01
Ground North	Free Field	260	PLAZA27	225.23	37.94	6.67

I.- Velocities obtained from highpassed, baseline corrected integral with respect to time of recorded accelerations

II.- Displacements obtained from highpassed, baseline corrected integral with respect to time of computed velocities

Table 3.2 - **Peak responses in the building during the Loma Prieta Earthquake**

PARAMETER		350° COMPONENT (NS)			260° COMPONENT (EW)		
		1st MODE	2nd MODE	3rd MODE	1st MODE	2nd MODE	3rd MODE
Period [sec]		2.59	0.89	0.46	2.69	1.07	0.55
Frequency [Hz]		0.39	1.12	2.15	0.37	0.94	1.81
Damping Ratio [%]		2.4-2.9	2.5-3.0	-	2.5-2.9	2.5-3.0	-
Mode Shape	31st	1.00	1.00	1.00	1.00	1.00	1.00
	21st	0.69	-0.36	-1.02	0.63	-0.29	-0.79
	13th	0.38	-0.82	0.60	0.34	-0.84	0.34

Table 3.3 - Translational modes of vibration identified from earthquake records

MODE	350° COMPONENT (NS)		260° COMPONENT (EW)	
	FREQUENCY [Hz]	f_i / f_i	FREQUENCY [Hz]	f_i / f_i
1st	0.386	1.00	0.372	1.00
2nd	1.122	2.91	0.937	2.52
3rd	2.151	5.57	1.806	4.85

Table 3.4 - Ratios of translational mode frequencies

(a) TRANSLATIONAL MODAL FREQUENCIES [Hz]

COMPONENT	MODE	FORCED VIBRATION	AMBIENT VIBRATION	EARTHQUAKE RESPONSE
350° (NS)	1st	0.595	0.586	0.386
	2nd	1.675	1.685	1.222
	3rd	3.120	3.125	2.151
260° (EW)	1st	0.590	0.586	0.372
	2nd	1.660	1.685	0.937
	3rd	3.090	3.149	1.806

(b) TRANSLATIONAL PERIODS [sec]

COMPONENT	MODE	FORCED VIBRATION	AMBIENT VIBRATION	EARTHQUAKE RESPONSE
350° (NS)	1st	1.68	1.71	2.59
	2nd	0.60	0.59	0.89
	3rd	0.32	0.32	0.46
260° (EW)	1st	1.69	1.71	2.69
	2nd	0.60	0.59	1.07
	3rd	0.32	0.32	0.55

Table 3.5 - Comparison of dynamic characteristics

Building	No. of Stories	Construction[2]	Comp.	PERIOD [sec] T_{PRE}	T_{EQ}	T_{POST}	T_{EQ}/T_{PRE}	RESPONSE[1] TYPE	REF.
Tlatelolco K-1 Mexico City	14	RC MRF	Long. Transf.	1.04 1.68	- -	1.54 1.90	1.48[3] 1.13[3]	A	23
Tlatelolco K-5 Mexico City	14	RC MRF	Long. Transf.	1.07 1.54	- -	1.24 1.72	1.16[3] 1.12[3]	A	23
Jet Propulsion Lab. CalTech, CA	9	ST MRF	S28E S08W	0.91 0.88	1.26 1.42	1.01 1.16	1.38 1.61	B	12
Milikan Library CalTech, CA	9	RC MRF	NS EW	0.53 0.69	0.62 0.98	0.54 0.79	1.17 1.42	A	12
1900 Ave. of the Stars Los Angeles, CA	27	ST MRF	N44E S46E	3.30 3.30	4.37 4.24	3.60 3.60	1.32 1.28	A	12
Union Bank 445 Figueroa St.	39	ST MRF	S38W N52W	3.11 3.53	4.63 4.71	3.70 4.10	1.49 1.33	A	12
KB Valley Center Los Angeles, CA	18	ST MRF	S09W S81E	2.18 1.94	3.30 3.05	2.37 2.27	1.51 1.57	A	12
Kajima Building 250 E. First St.	15	ST MRF	N36E N54W	1.32 1.88	2.84 2.77	2.10 2.15	2.15 1.47	A	12
Sheraton-Universal 3838 Lankershim Blvd.	19	RC MRF	NS EW	1.22 1.26	1.98 2.24	1.40 1.50	1.62 1.78	B	12
Holiday Inn - Marengo 1640 Marengo St.	7	RC MRF	S52W N38W	0.49 0.53	1.17 1.06	0.63 0.64	2.39 2.00	B	12
Holiday Inn - Orion 8244 Orion St.	7	RC MRF	NS EW	0.48 0.52	1.42 1.20	0.68 0.72	2.96 2.31	C	12
Holiday Inn - Orchid 1760 North Orchid	22	RC MRF	NS EW	1.61 1.31	2.00 2.00	1.58 1.50	1.24 1.53	A	24
Bank of California 15250 Ventura Blvd.	12	RC MRF	N11E N79W	0.85 1.33	2.35 3.01	1.70 1.60	2.76 2.26	C	12
Hilton Hotel 15433 Ventura Blvd.	13	RC MRF	N12E N78W	0.62 0.71	1.60 1.30	0.77 0.91	2.58 1.83	A	24
Muir Medical Center 7080 Hollywood	11	RC MRF	NS EW	0.90 1.03	1.40 1.60	1.02 1.14	1.56 1.55	A	24
Wilshire Christian 616 South Normandie	16	RC MRF	NS EW	- -	1.10 1.80	0.85 1.17	1.29[4] 1.54[4]	A	24
Mohn Olympic 1625 Olympic	10	RC MRF	N28E N62W	- -	1.30 1.40	1.05 1.21	1.24[4] 1.16[4]	A	24
1901 Ave. of the Stars Los Angeles, CA	20	ST MRF	N46W S44W	2.63 2.45	3.50 3.60	2.80 2.72	1.33 1.47	B	24
Certified Life Tower 14724 Ventura Blvd.	14	RC MRF	N78W S12W	0.88 0.81	1.20 1.10	0.96 0.90	1.36 1.36	A	24
Imperial Services County El Centro, CA	6	RC MRF RC SW	EW NS	0.65 0.45	1.00 0.50	0.83 0.52	1.54 1.11	D	25, 26
Shinjuku Building Tokyo, Japan	29	ST MRF	NS EW	2.41 2.34	2.73 2.73	- -	1.13 1.17	A	27

[1]RESPONSE TYPES:

A: Buildings which sustained no structural damage and insignificant nonstructural damage.
B: Buildings which sustained no structural damage but sustained some nonstructural damage.
C: Buildings which sustained minor structural and nonstructural damage.
D: Buildings which sustained significant structural and nonstructural damage.

[2]RC = Reinforced Concrete, ST = Steel, MRF = Moment-Resistant Frame, SW = Shear Walls.

[3]T_{POST}/T_{PRE}

[4]T_{EQ}/T_{POST}

Table 3.6 - Changes in fundamental period reported in the literature

BUILDING	No. OF STORIES	CONSTRUCTION §	COMP.	PERIOD [sec] T_{PRE}	PERIOD [sec] T_{EQ}	T_{EQ}/T_{PRE}	MAX. DISP. [cm] §§
Metropolitan Municipal Office Bldg.- 1	8	SRC	NS	0.63	0.75	1.19	2.0
			EW	0.46	0.54	1.17	1.3
Metropolitan Municipal Office Bldg.- 2	9	SRC	NS	0.61	0.80	1.31	1.0
			EW	0.63	0.85	1.35	1.9
Daini Sennari	9	SRC	NS	0.66	0.77	1.17	1.7
			EW	0.32	0.36	1.13	0.3
Tokyo Tatemono	8	SRC	NS	0.40	0.44	1.10	0.6
			EW	0.39	0.43	1.10	0.9
Uyeno Matsuzakaya Department Store	7	RC	NS	0.54	0.73	1.35	1.3
			EW	0.54	0.75	1.39	1.5
Marubutsu Department Store	8	SRC	NS	0.42	0.53	1.26	1.2
			EW	0.58	0.71	1.22	2.8
Shimizu Construction Main Office	9	SRC	NS	0.46	0.51	1.11	0.7
			EW	0.44	0.52	1.18	1.5
Ohbayashi-gumi	9	SRC	NS	0.59	0.70	1.19	1.0
			EW	0.65	0.79	1.22	1.3
Engineering Bldg. No.5 Tokyo University	7	RC	NS	0.36	0.39	1.08	0.6
			EW	0.37	0.40	1.08	0.6
San-ai Dream Center	9	SRC	NS	0.65	0.80	1.23	1.0
			EW	0.76	0.86	1.13	1.4
Higashi-Shinjuku Den-Den	8	SRC	NS	0.42	0.47	1.12	0.7
			EW	0.36	0.40	1.11	0.3
Shin-Tokyo	9	SRC	NS	0.46	0.52	1.13	0.6
			EW	0.49	0.57	1.16	0.8
Mitsui No.3 Detached Bldg.	10	SRC	NS	0.60	0.73	1.22	1.1
			EW	0.54	0.64	1.19	1.2
Hotel New-Otani	17	SRC	NS	1.06	1.30	1.23	4.6
			EW	1.05	1.31	1.25	3.4
Keio Bldg.	8	SRC	NS	0.45	0.54	1.20	0.7
			EW	0.62	0.72	1.16	1.5
Fuji Bank Head Office	16	SRC	NS	0.96	1.27	1.32	5.3
			EW	0.98	1.26	1.29	4.4
Hotel Empire	21	SRC	NS	1.27	1.39	1.09	4.6
			EW	1.24	1.40	1.13	7.7

§ RC=Reinforced Concrete, SRC=Steel Reinforced Concrete
§§ Approximate values

Table 3.7 - Changes in fundamental period reported in Reference 30

BUILDING	No. OF STORIES	CONSTRUCTION §§	PERIOD [sec]		T_{POST}/T_{PRE}	RESPONSE § TYPE	REF.
			T_{PRE}	T_{POST}			
Full-scale prototype Tsukuba, Japan	7	RC DUAL SYSTEM	0.43	0.55 (1)	1.28	C	31
Full-scale prototype † Tsukuba, Japan	7	RC DUAL SYSTEM §	0.47	0.90 (2)	1.91	B	31
1/5-scale model UC Berkeley	7	RC DUAL SYSTEM	0.21	0.27 (3)	1.30	B	32
Full-scale prototype Tsukuba, Japan	6	ST CBF	0.61	0.71 (4)	1.16	B	33
0.3-scale model UC Berkeley	6	ST CBF	0.34	0.36 (5)	1.06	B	34
Full-scale prototype Tsukuba, Japan	6	ST EBF	0.68	0.81 (6)	1.19	C	33
0.3-scale model UC Berkeley	6	ST EBF	0.32	0.33 (7)	1.04	B	35
Full-scale prototype Tsukuba, Japan	6	ST MRF	0.87	1.13 (8)	1.16	B	33
1/4-scale model UC Berkeley	6	RC MRF	0.27	0.32 (9)	1.19	B	36

§ RESPONSE TYPES:
A.- Buildings which sustained no structural damage and insignificant nonstructural damage
B.- Buildings with insignificant structural damage and some nonstructural damage (if any)
C.- Buildings which sustained minor structural damage and nonstructural damage
D.- Buildings which sustained significant structural and nonstructural damage

§§ RC=Reinforced Concrete, ST=Steel, MRF=Moment-Resistant Frames, SW=Shear Walls, CSF=Concentrically-Braced Frames, EBF=Eccentrically-Braced Frames

† Repaired and non-structural components added

(1) After 0.11g Miyagi-Ken-Oki record (PSD-2)
(2) After 0.11g Miyagi-Ken-Oki record (PSD-6)
(3) After 0.10g Miyagi-Ken-Oki record
(4) After 0.25g Miyagi-Ken-Oki record (moderate testing)
(5) After 0.10g Miyagi-Ken-Oki record
(6) After 0.50g Taft record
(7) After 0.27g Miyagi-Ken-Oki record
(8) After 0.36g El Centro record
(9) After 0.16g El Centro record

Table 3.8 - Changes in fundamental period from experimental research

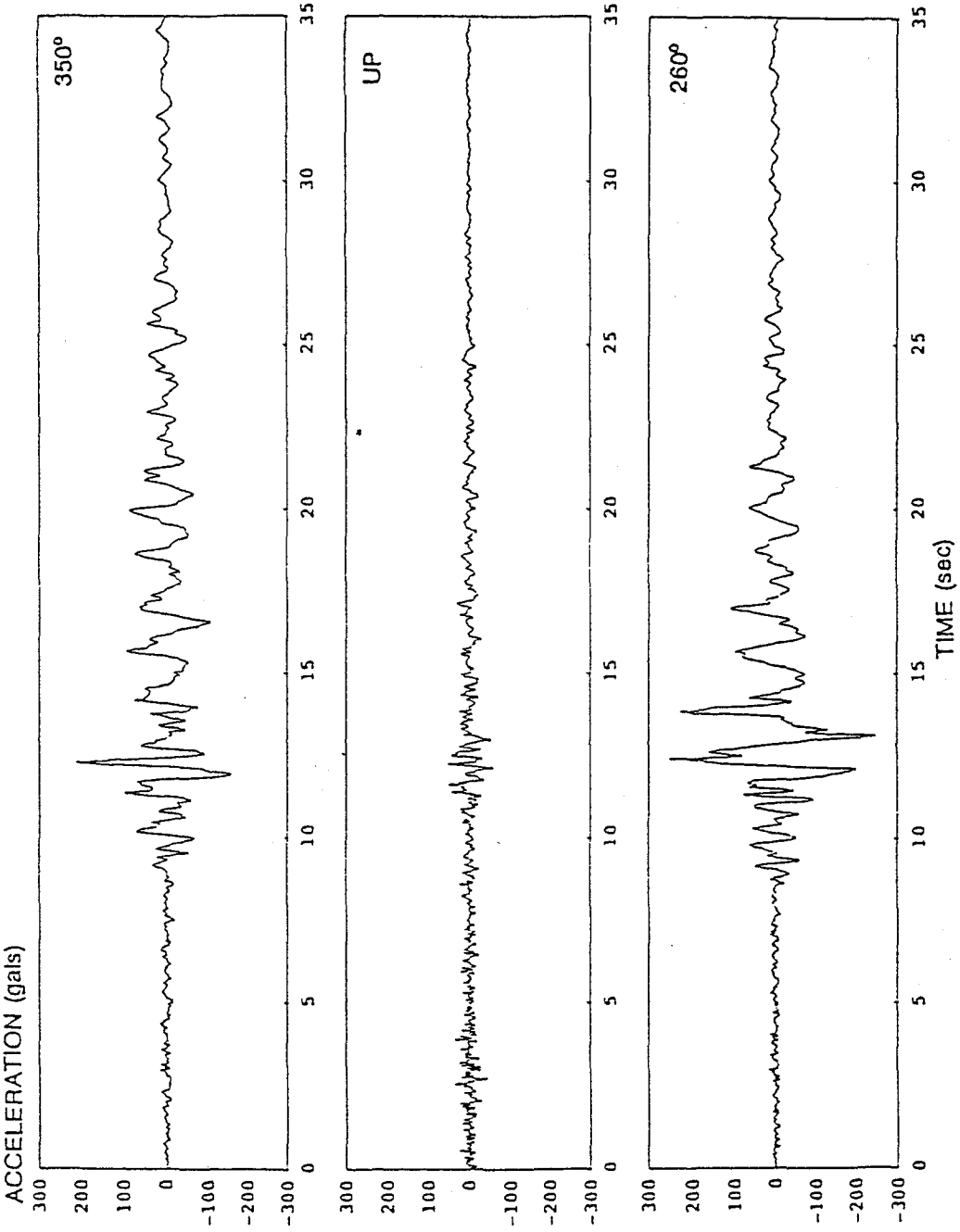

Figure 3.1 - Acceleration time-histories recorded on the south free-field station

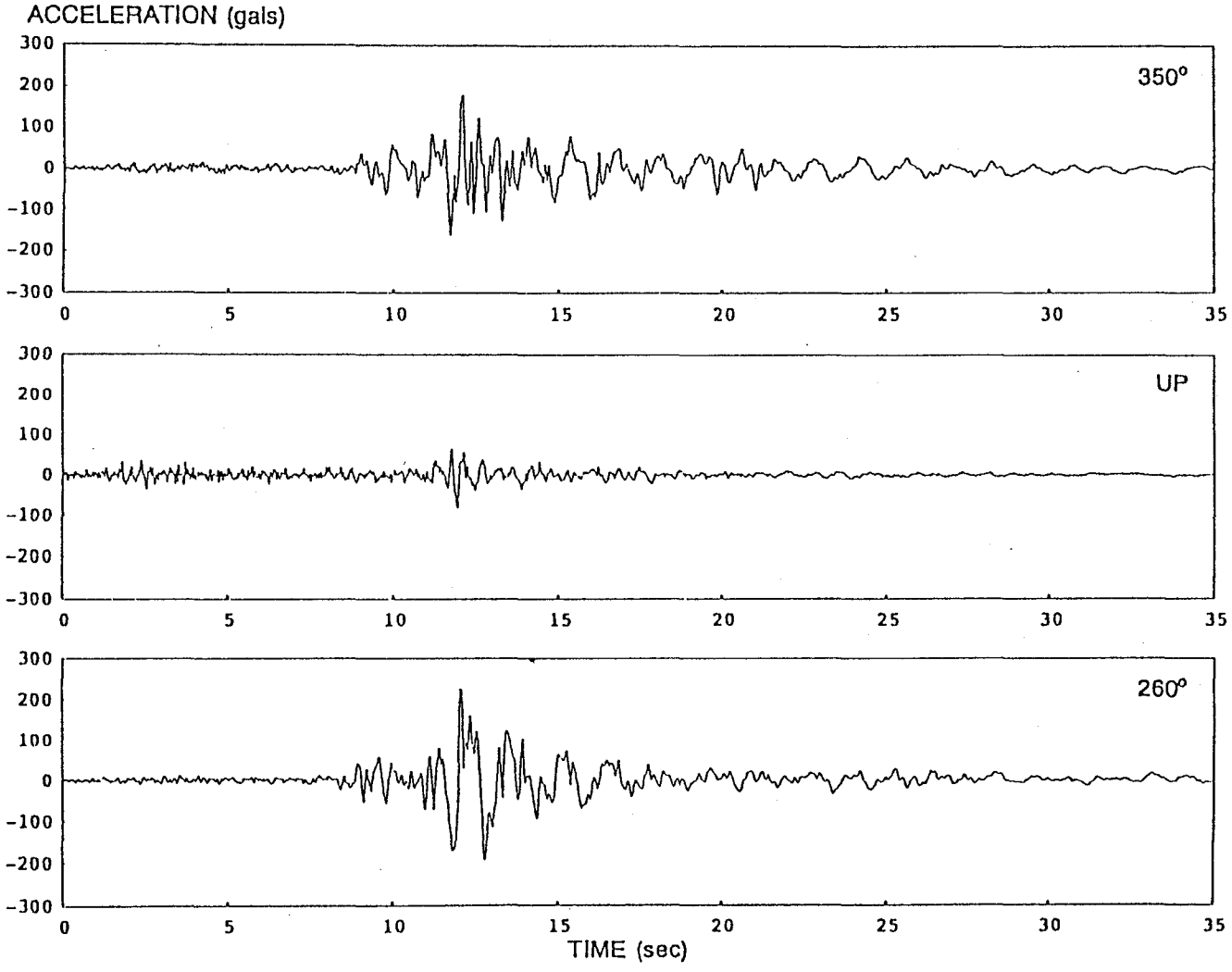

Figure 3.2 - Acceleration time-histories recorded on the north free-field station

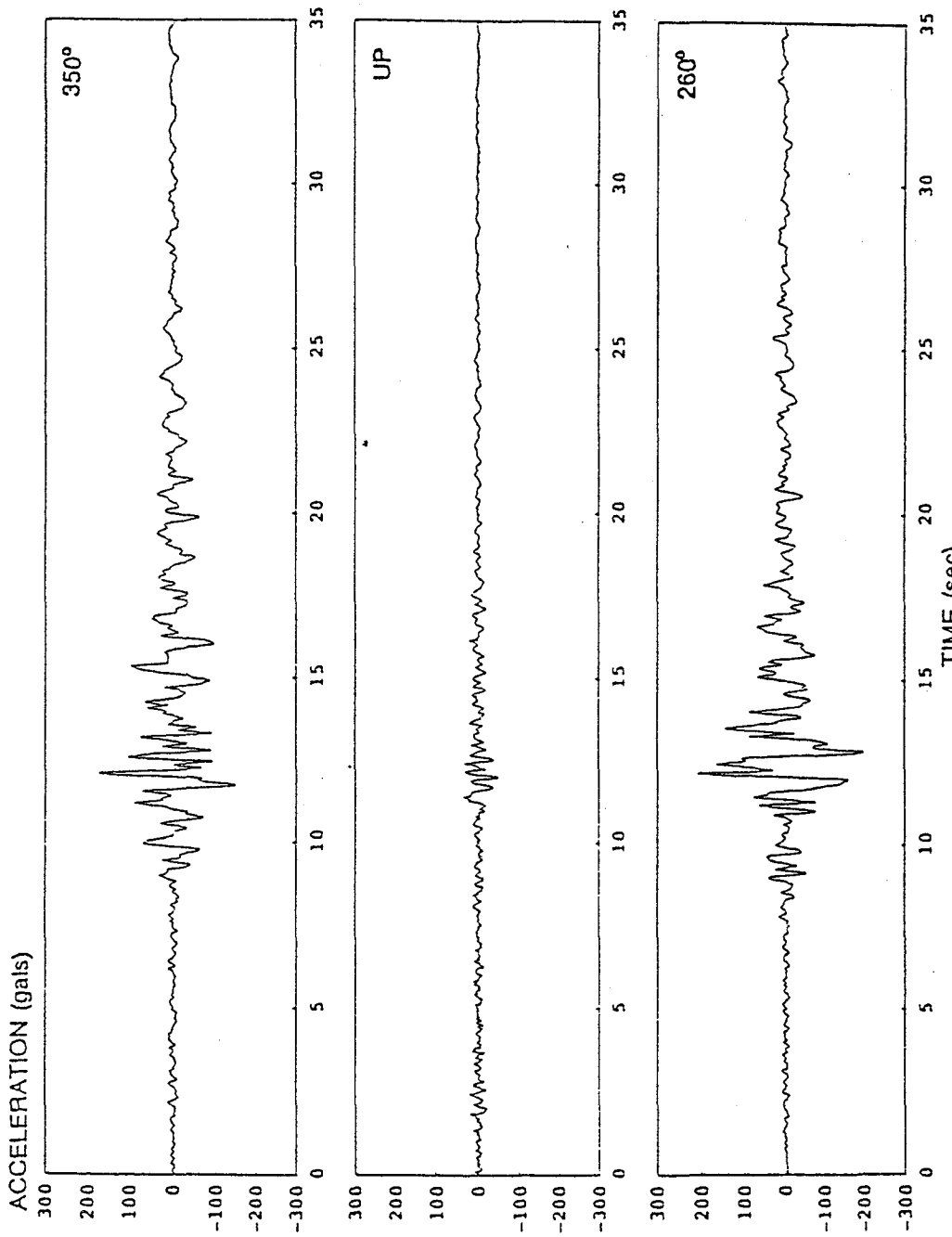

Figure 3.3 - Acceleration time-histories recorded on the ground floor of the north wing

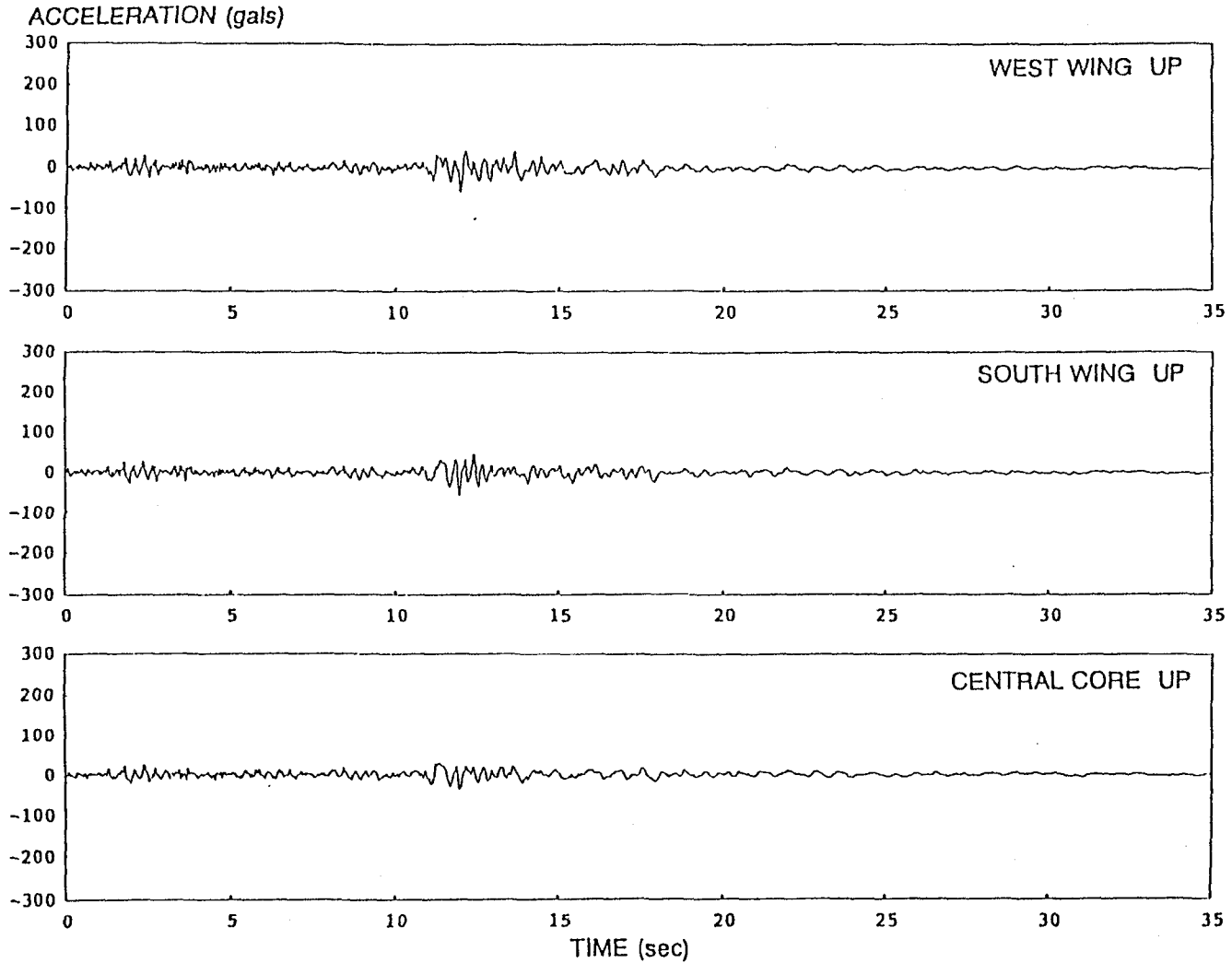

Figure 3.4 - Vertical acceleration time-histories recorded on the ground floor .

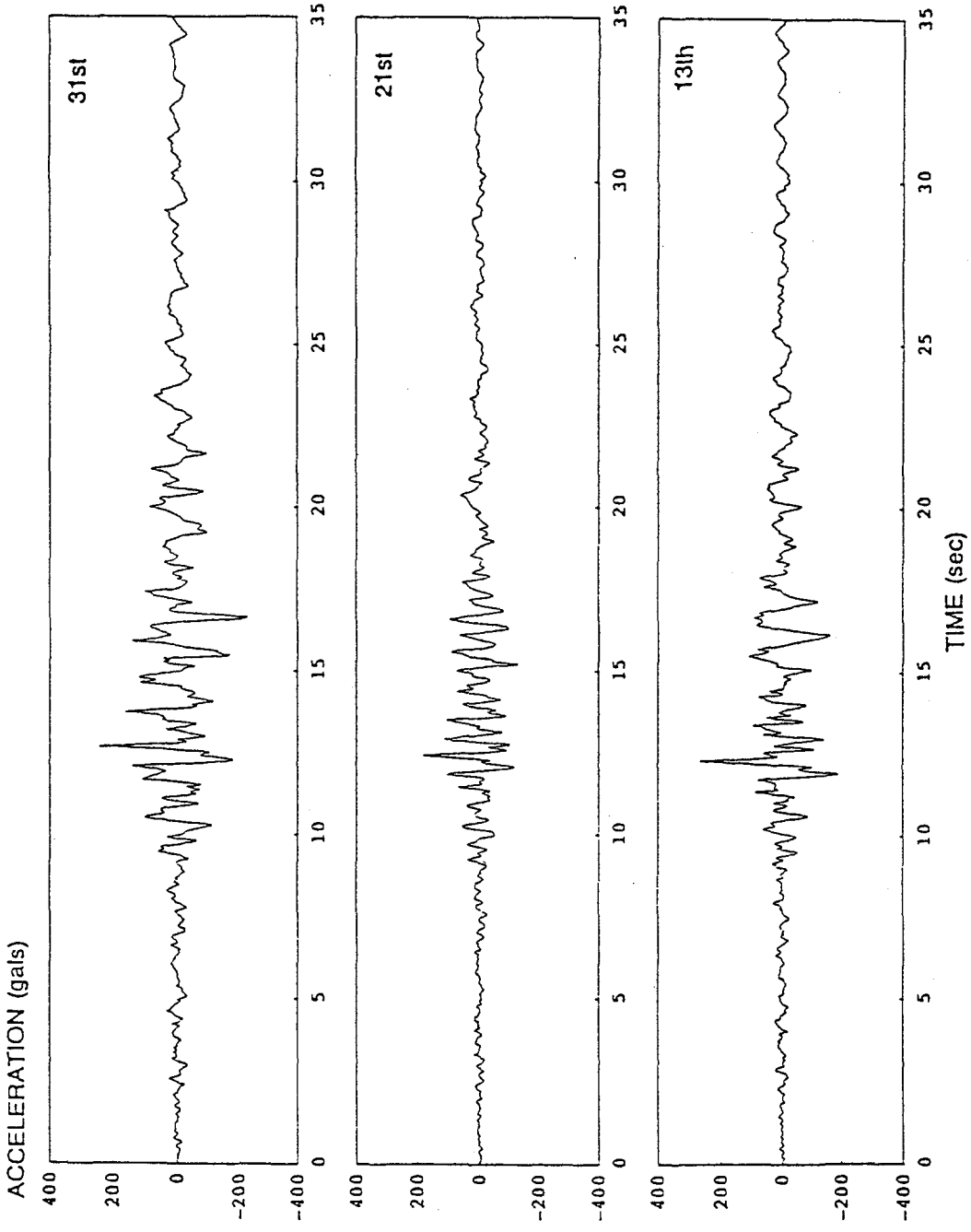

Figure 3.5 - Acceleration time-histories recorded at 31st, 21st and 13th floors in the central core (component 350°)

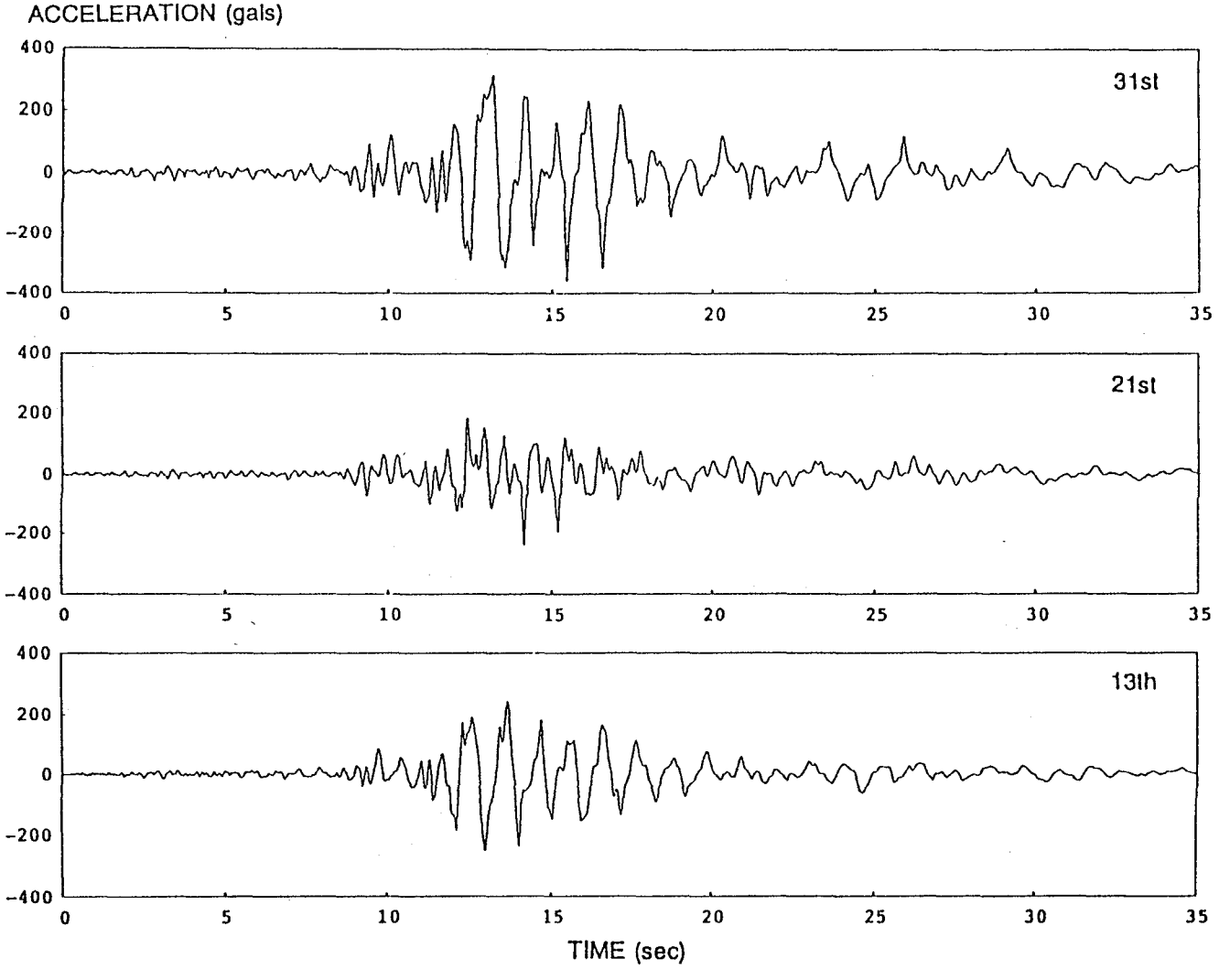

Figure 3.6 - Acceleration time-histories recorded at 31st, 21st and 13th floors in the central core (component 260°)

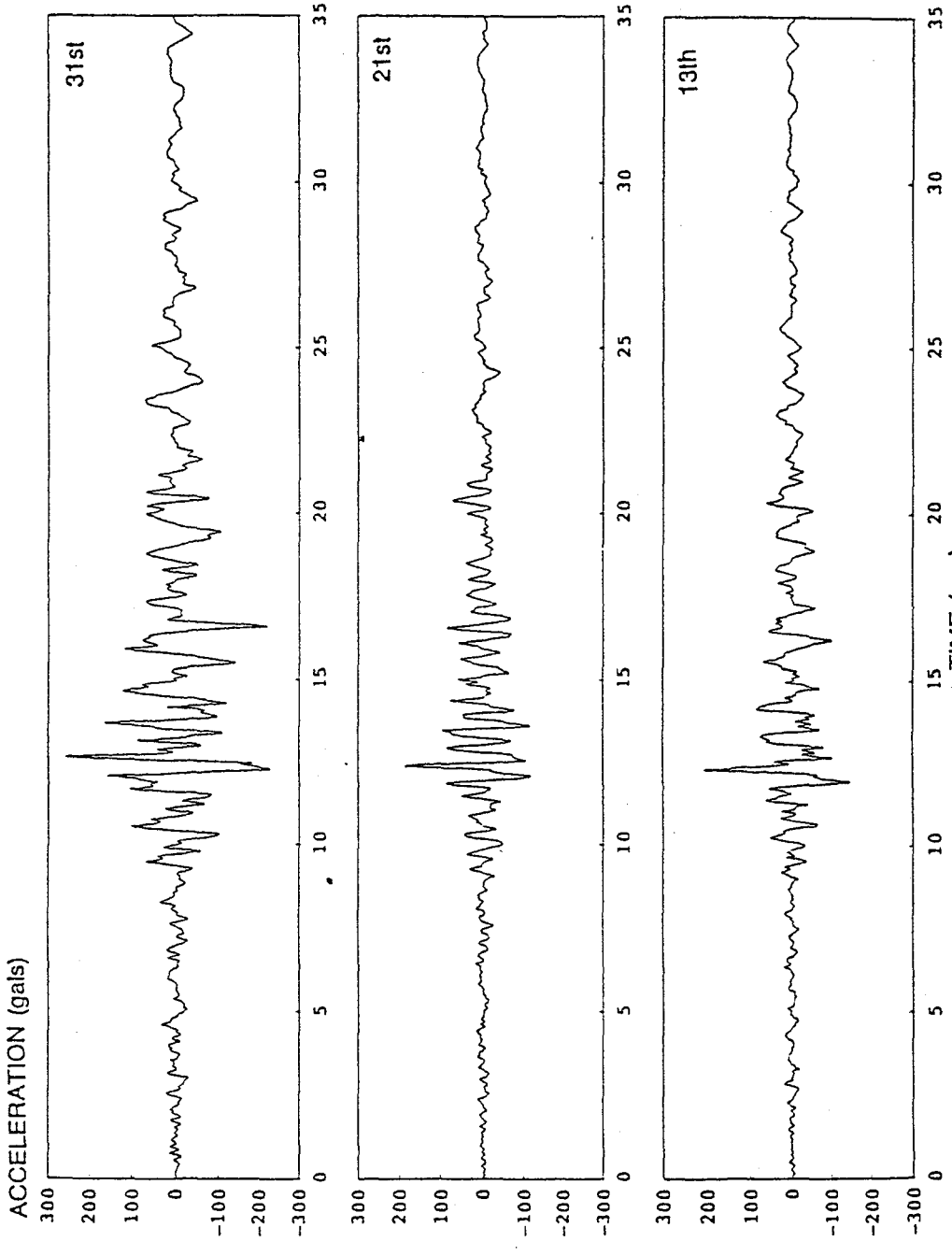

Figure 3.7 - Acceleration time-histories recorded at 31st, 21st and 13th floors in the west wing (component 350°)

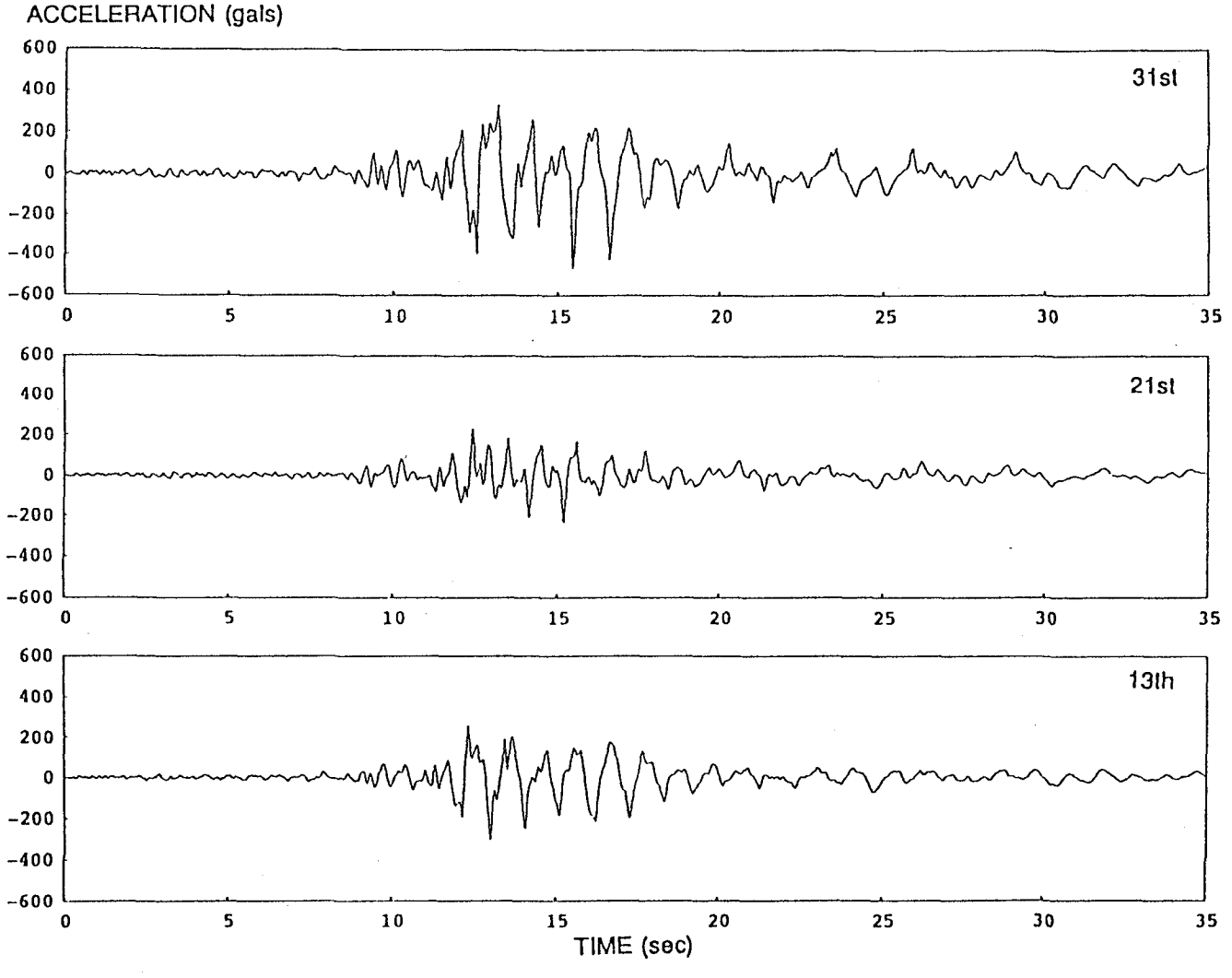

Figure 3.8 - Acceleration time-histories recorded at 31st, 21st and 13th floors in the north wing (component 290°)

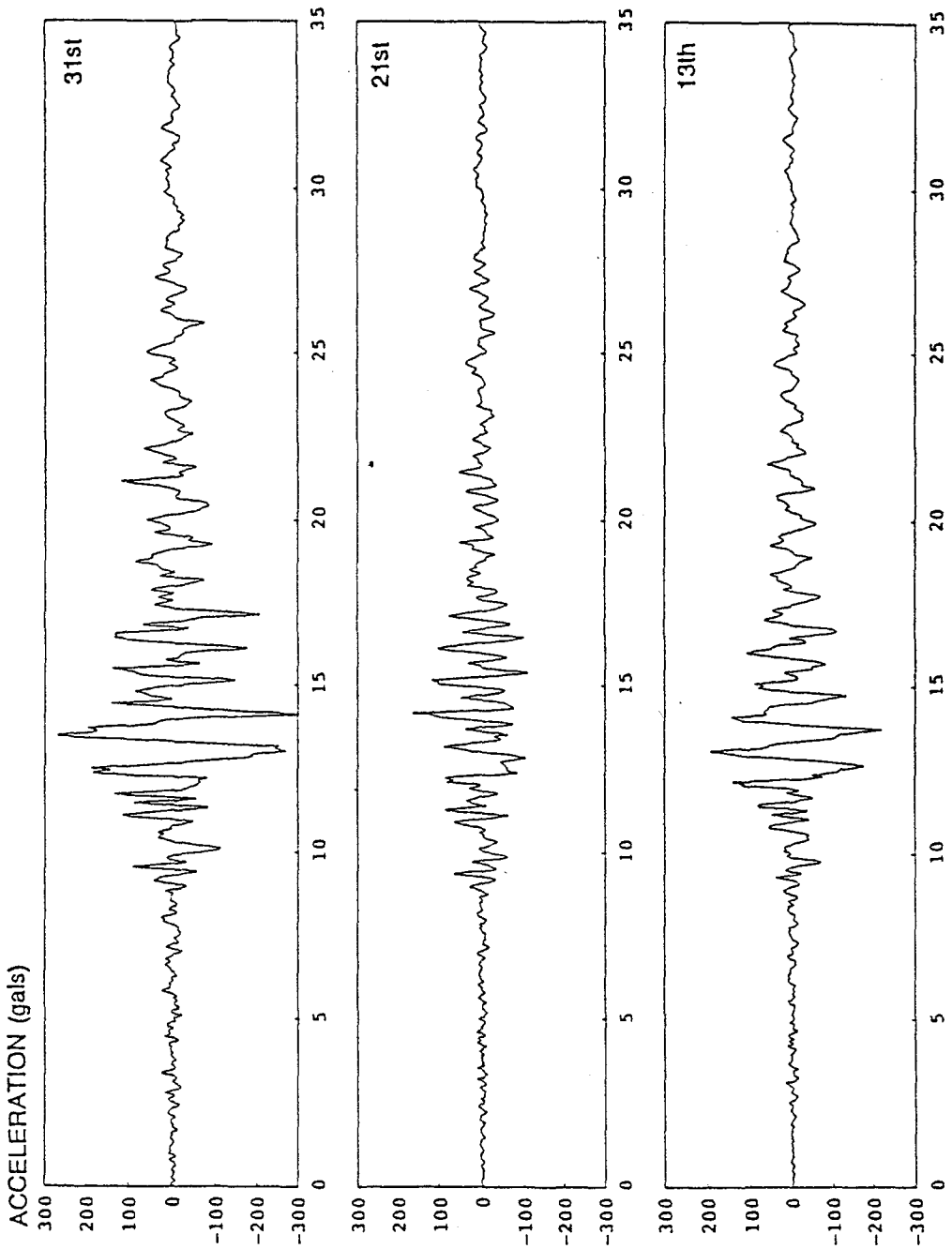

Figure 3.9 - Acceleration time-histories recorded at 31st, 21st and 13th floors in the south wing (component 50°)

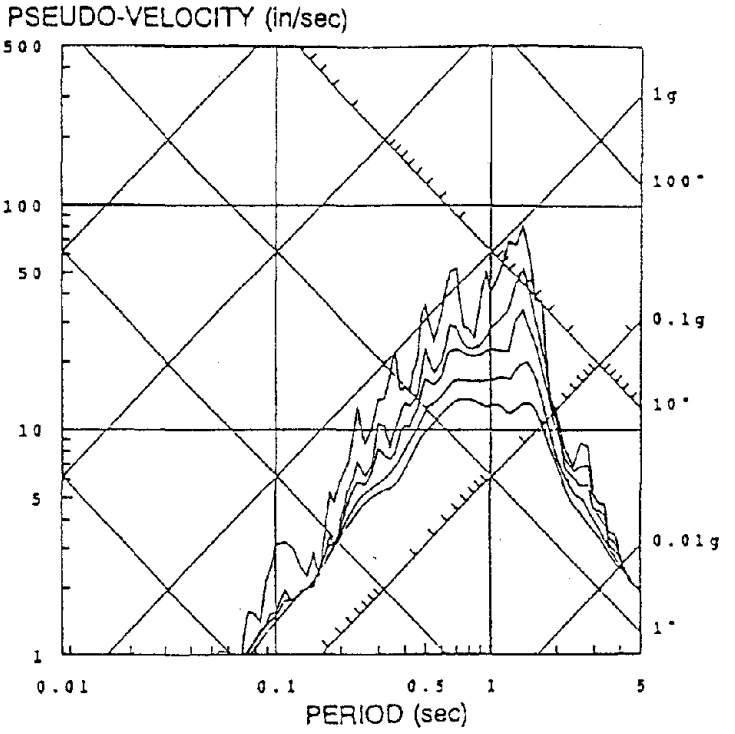

(A) 350° COMPONENT

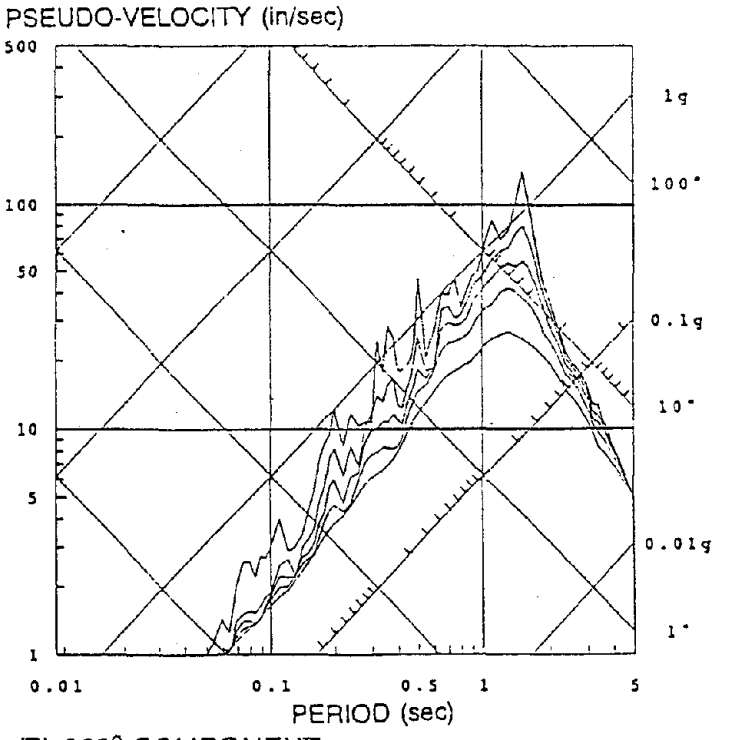

(B) 260° COMPONENT

Figure 3.10 - Linear-elastic response spectra of the horizontal ground motions recorded at the south free-field station (0, 2, 5, 10, and 20% damping).

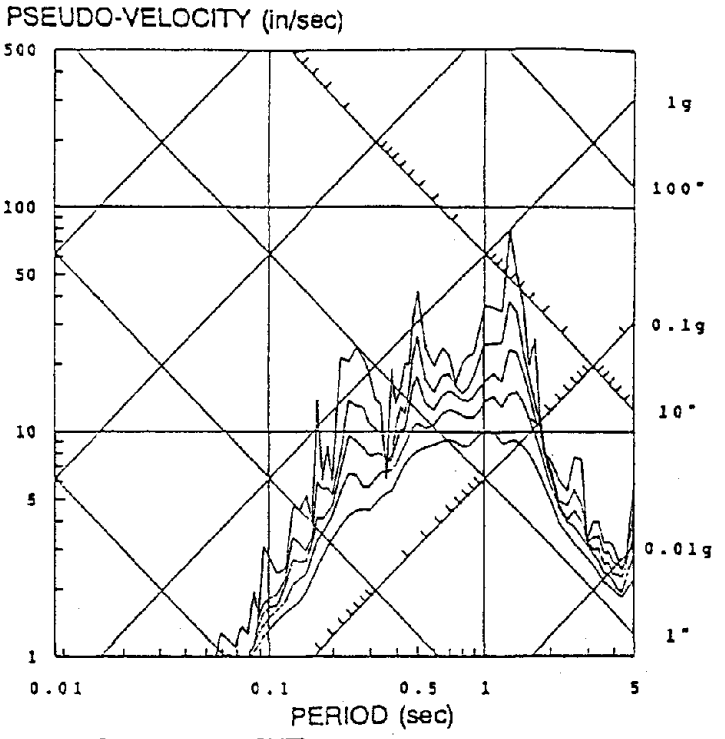

(A) 350° COMPONENT

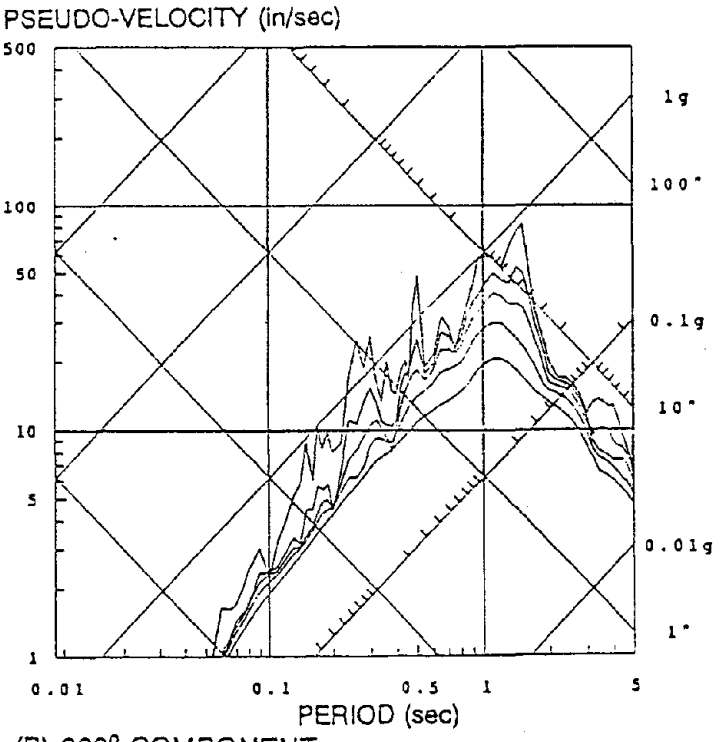

(B) 260° COMPONENT

Figure 3.11 - Linear-elastic response spectra of the horizontal ground motions recorded at the north free-field station (0, 2, 5, 10, and 20% damping).

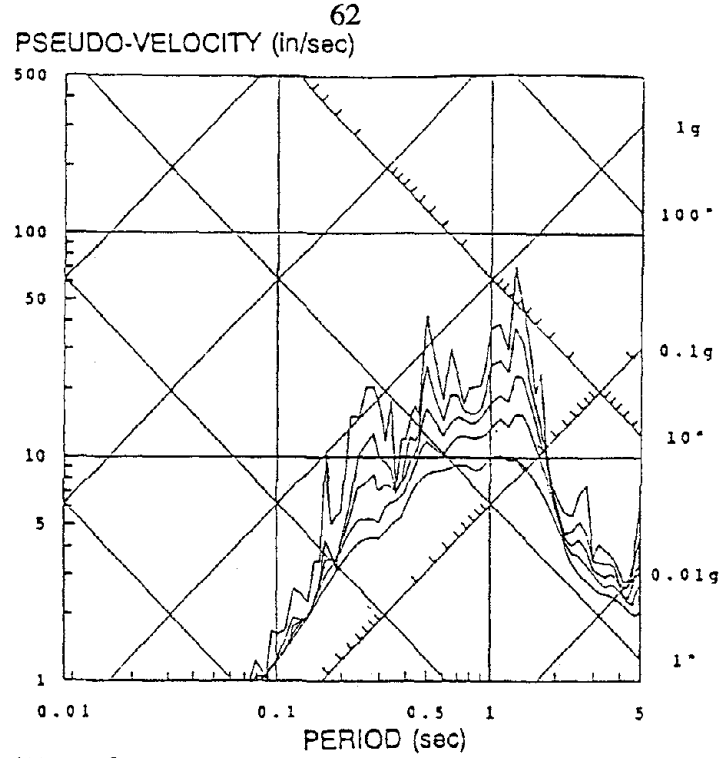

(A) 350° COMPONENT

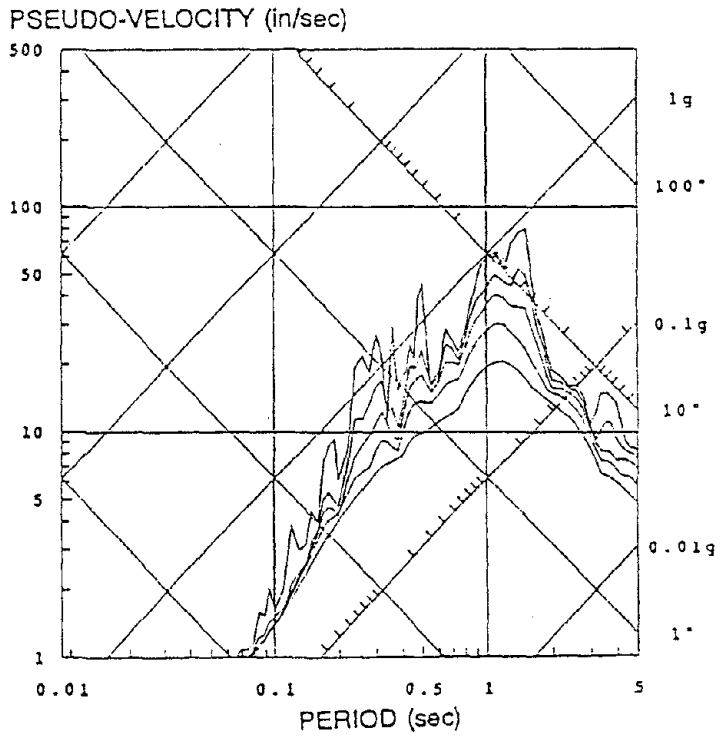

(B) 260° COMPONENT

Figure 3.12 - Linear-elastic response spectra of the horizontal ground motions recorded on the ground floor of the building (0, 2, 5, 10, and 20% damping).

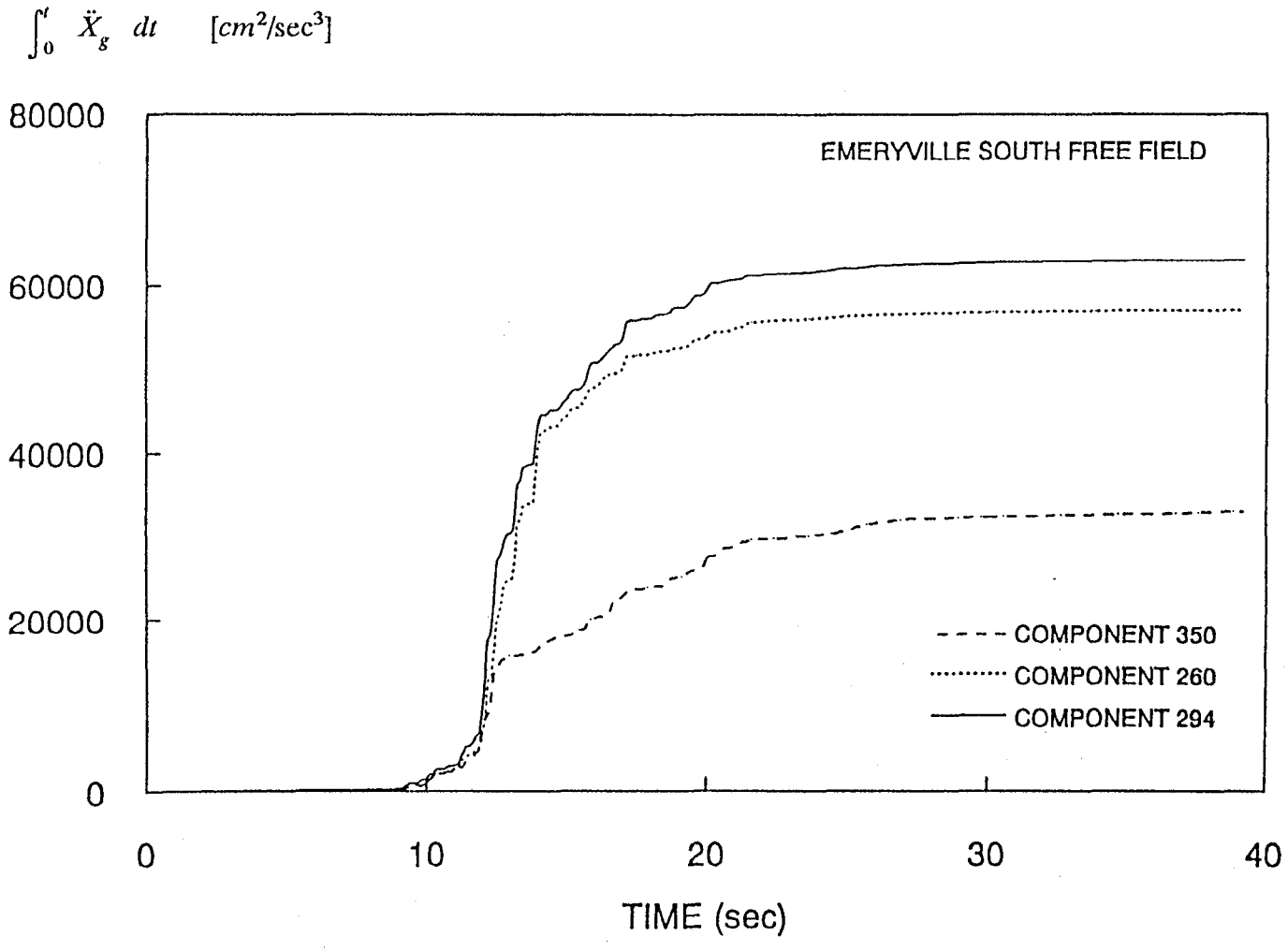

Figure 3.13 - Time Integral of accelerations squared for the 350°, 260°, and 294° components of the ground motion recorded at the south free-field station.

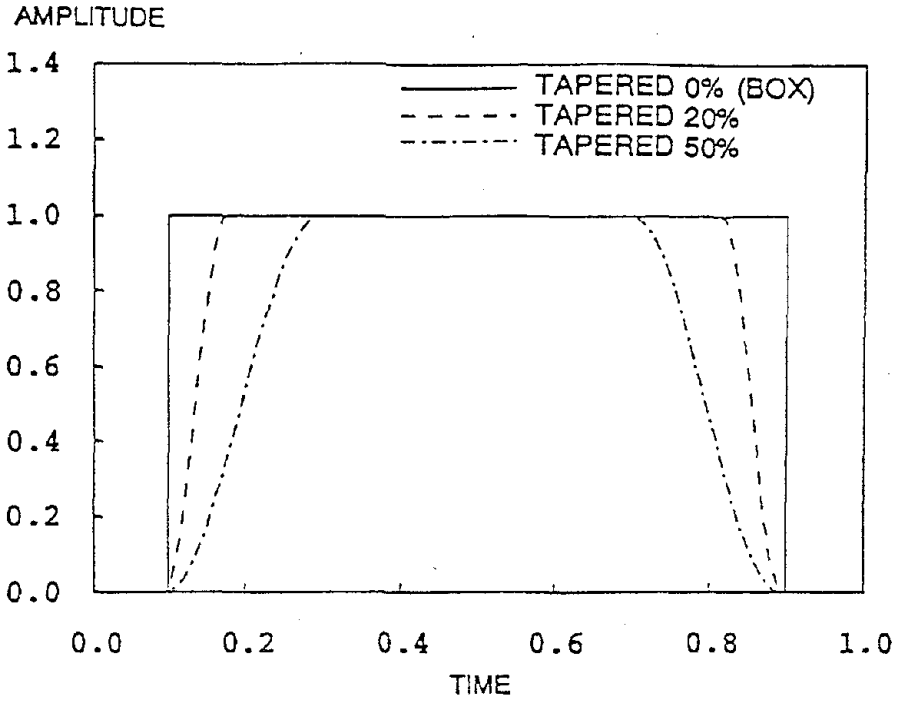

Figure 3.14 - Comparison between the box data window and the split-cosine-bell data window for different levels of tapering.

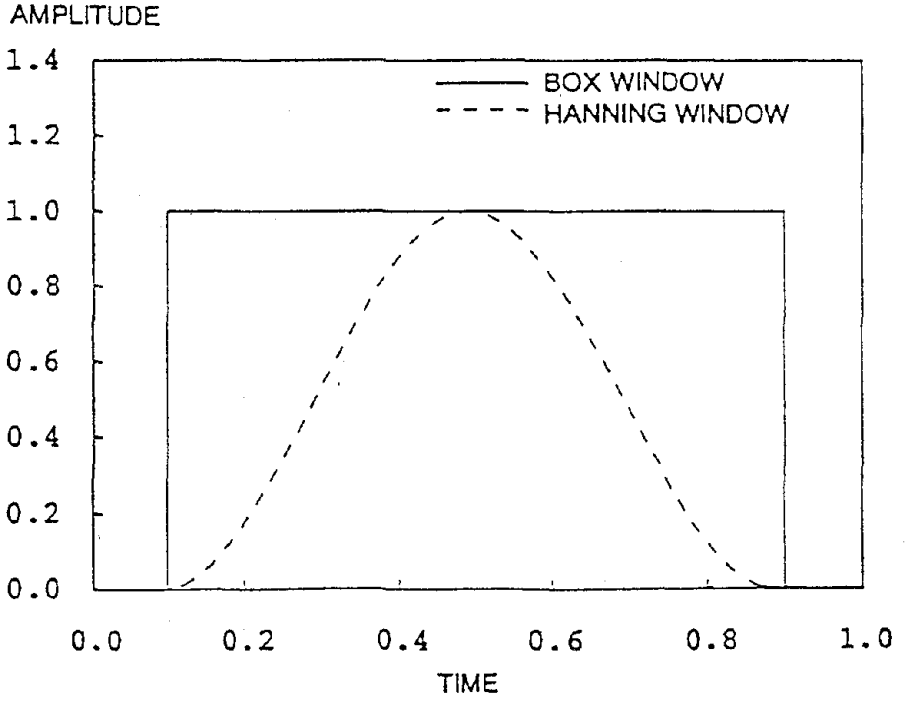

Figure 3.15 - Comparison between the box data window and the Hanning data window.

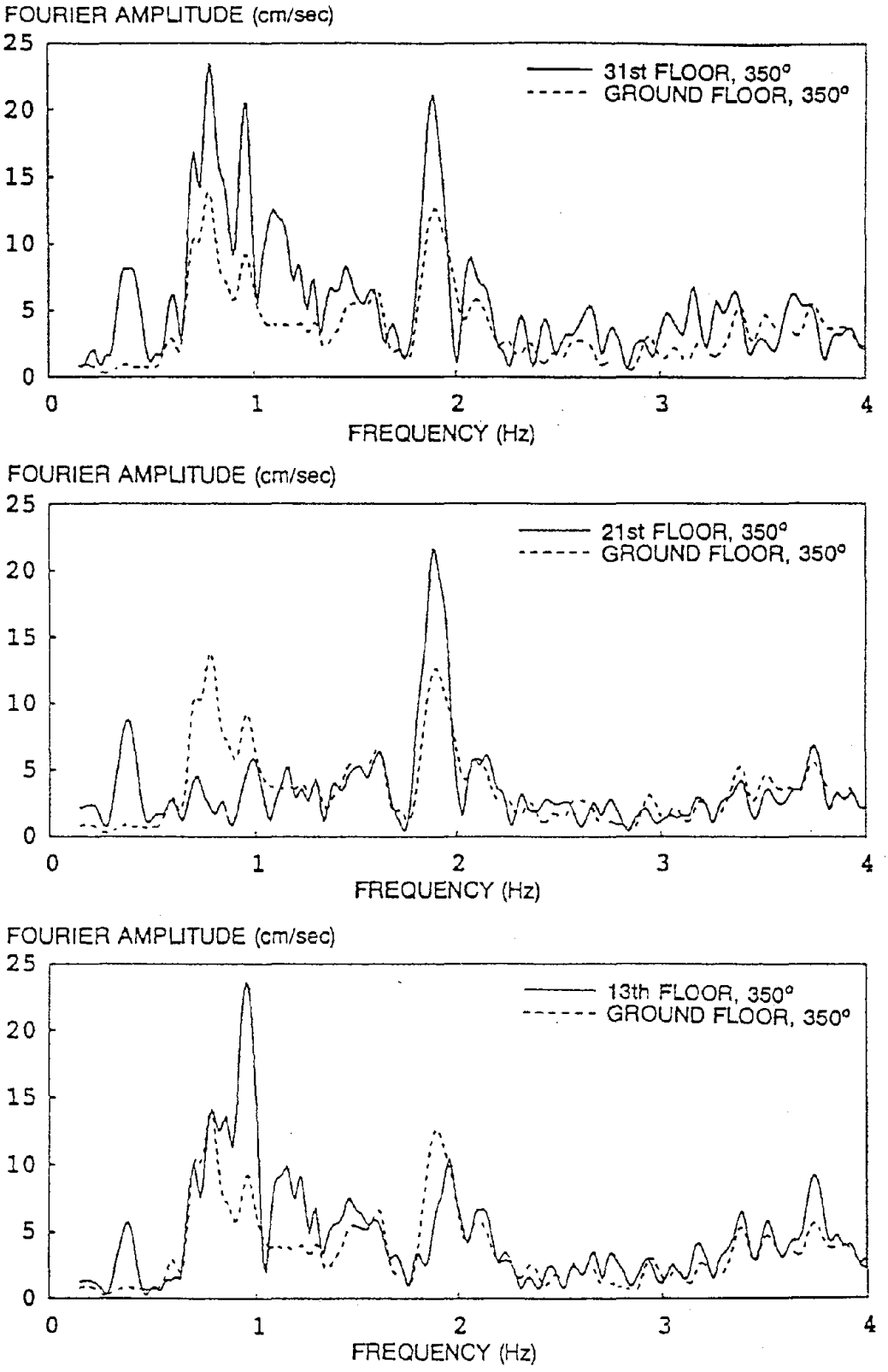

Figure 3.16 - Fourier amplitude spectra of input and output recorded accelerations in the central core for the 350° component.

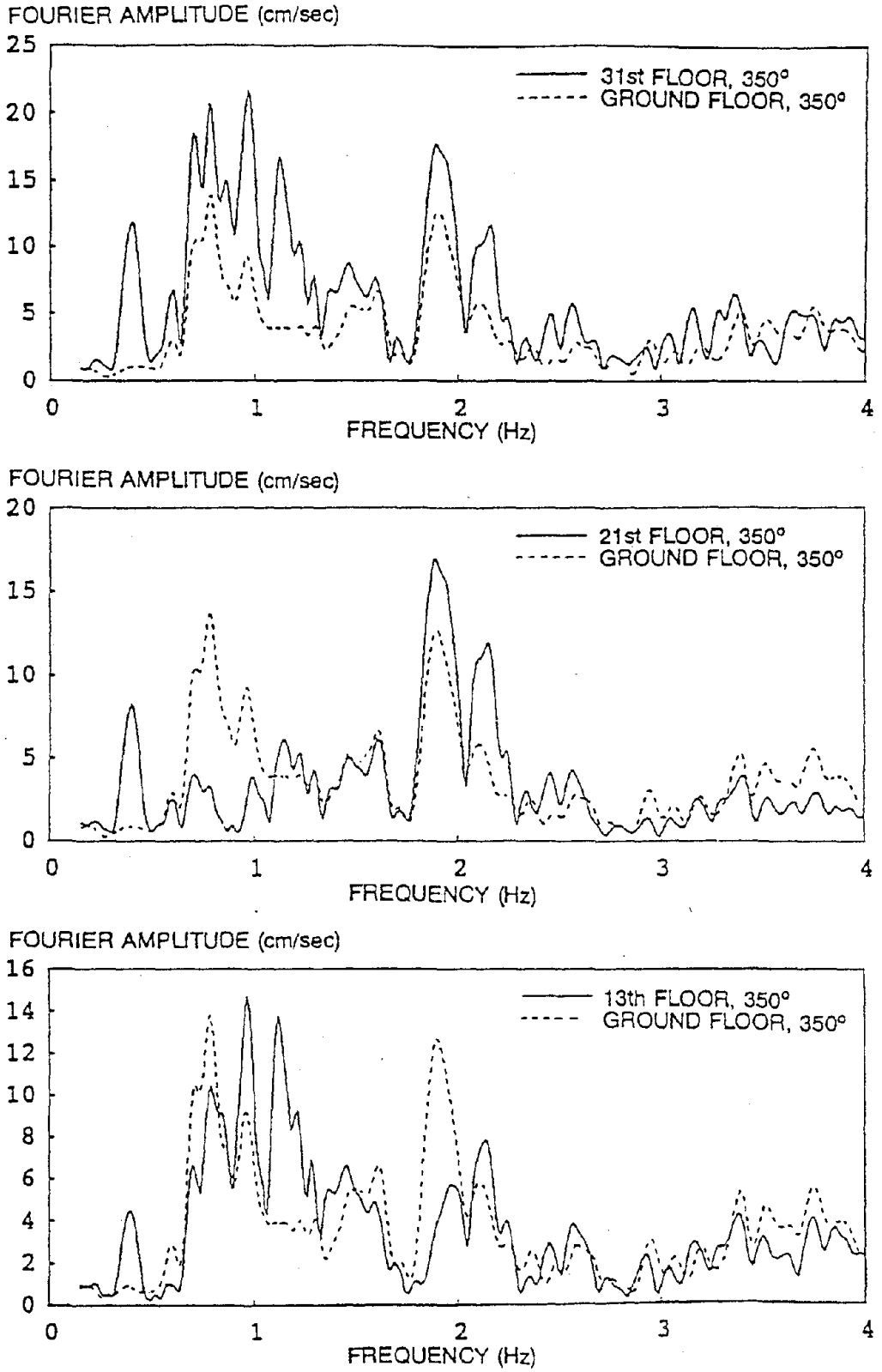

Figure 3.17 - Fourier amplitude spectra of input and output recorded accelerations in the west wing for the 350° component.

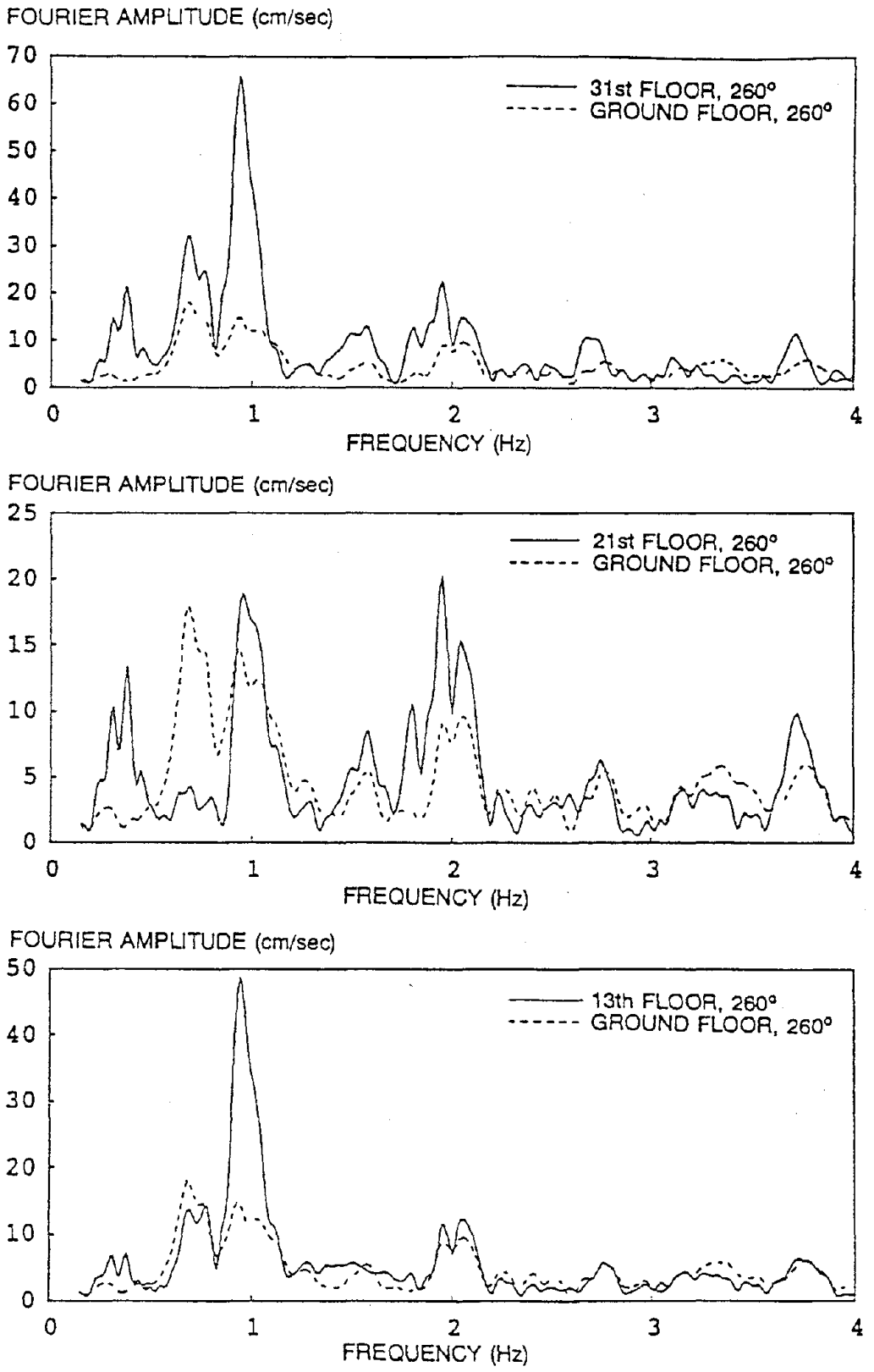

Figure 3.18 - Fourier amplitude spectra of input and output recorded accelerations in the central core for the 260° component.

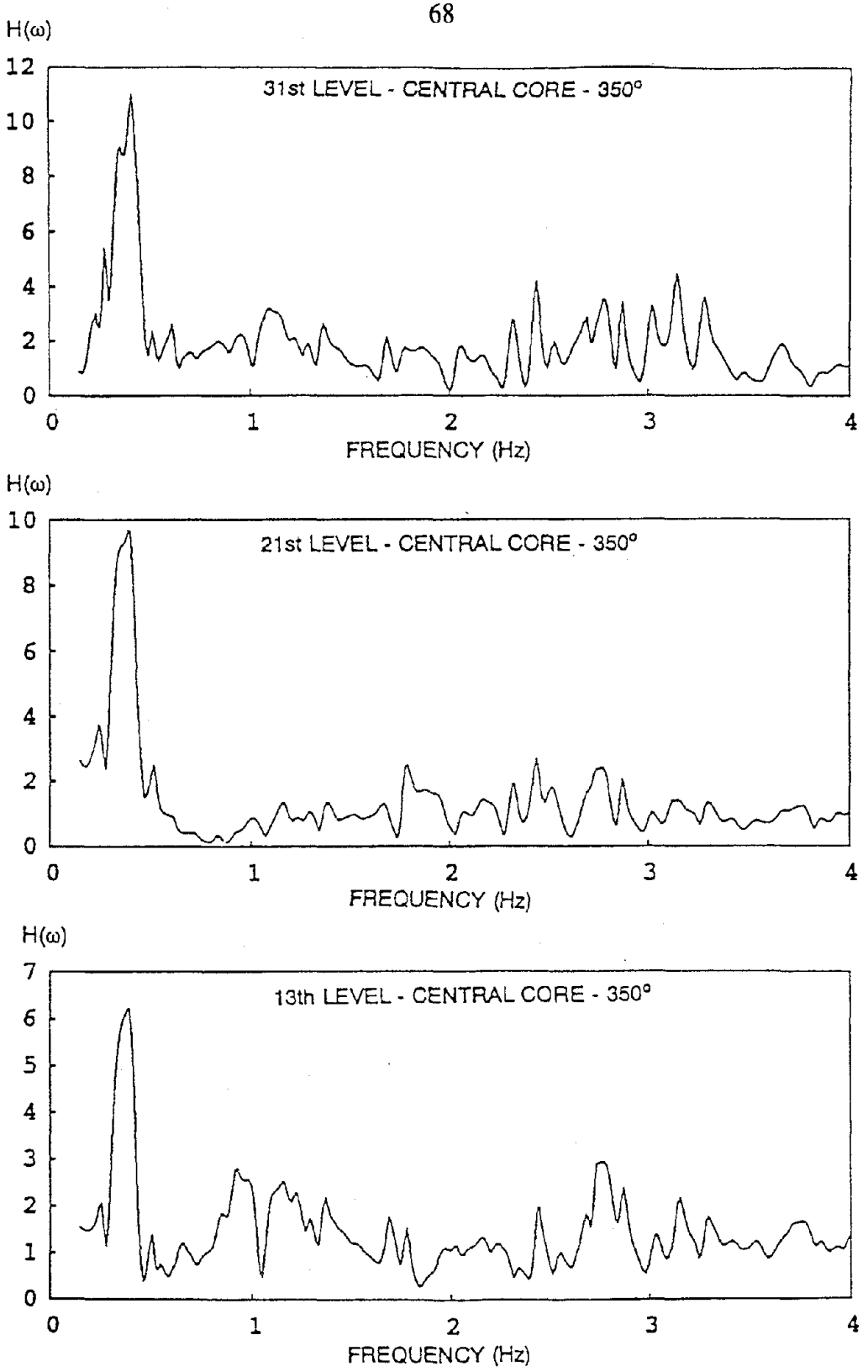

Figure 3.19 - Computed acceleration transfer functions in the central core for the 350° component.

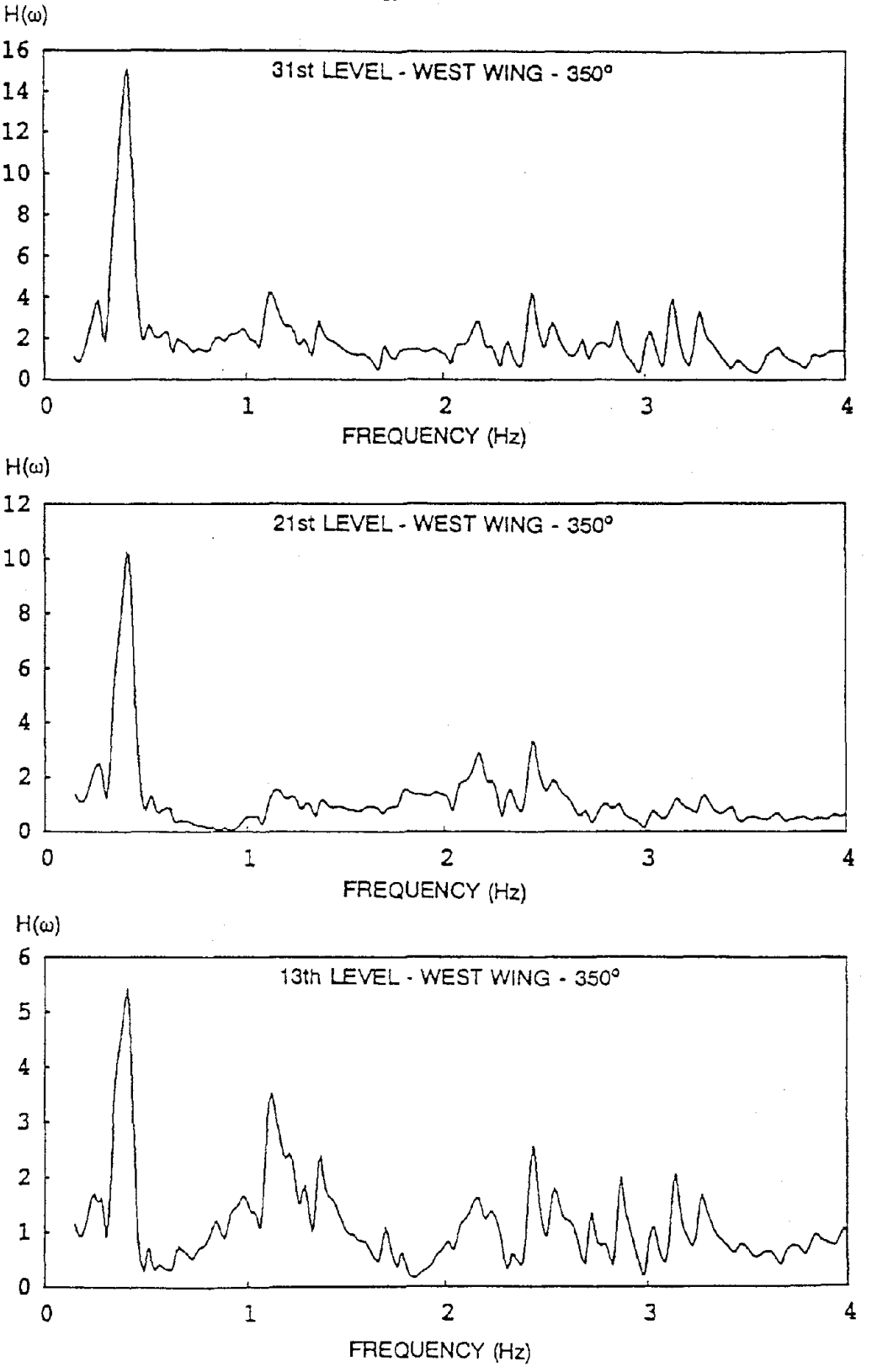

Figure 3.20 - Computed acceleration transfer functions in the west wing for the 350° component.

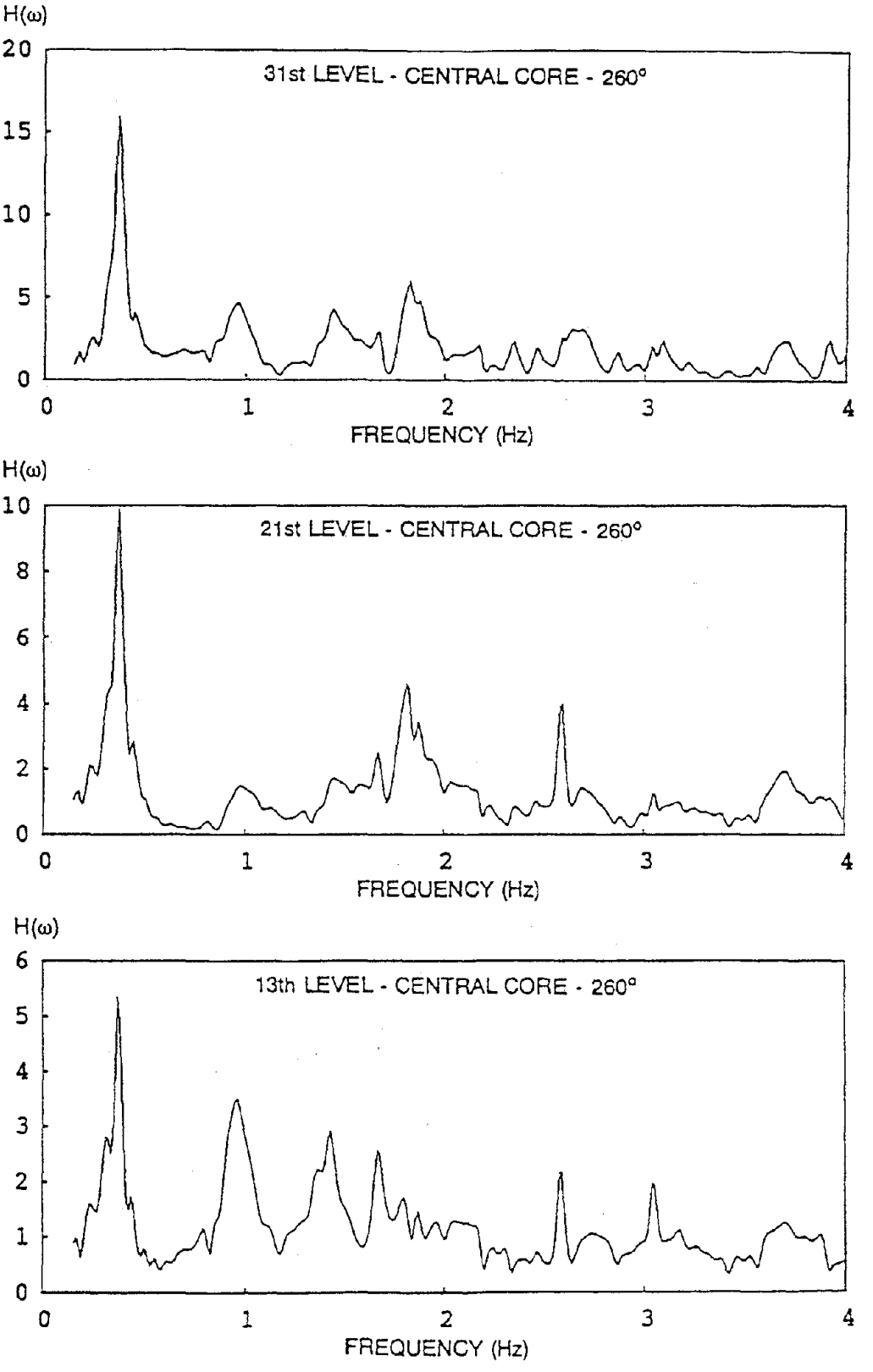

Figure 3.21 - Computed acceleration transfer functions in the central core for the 260° component.

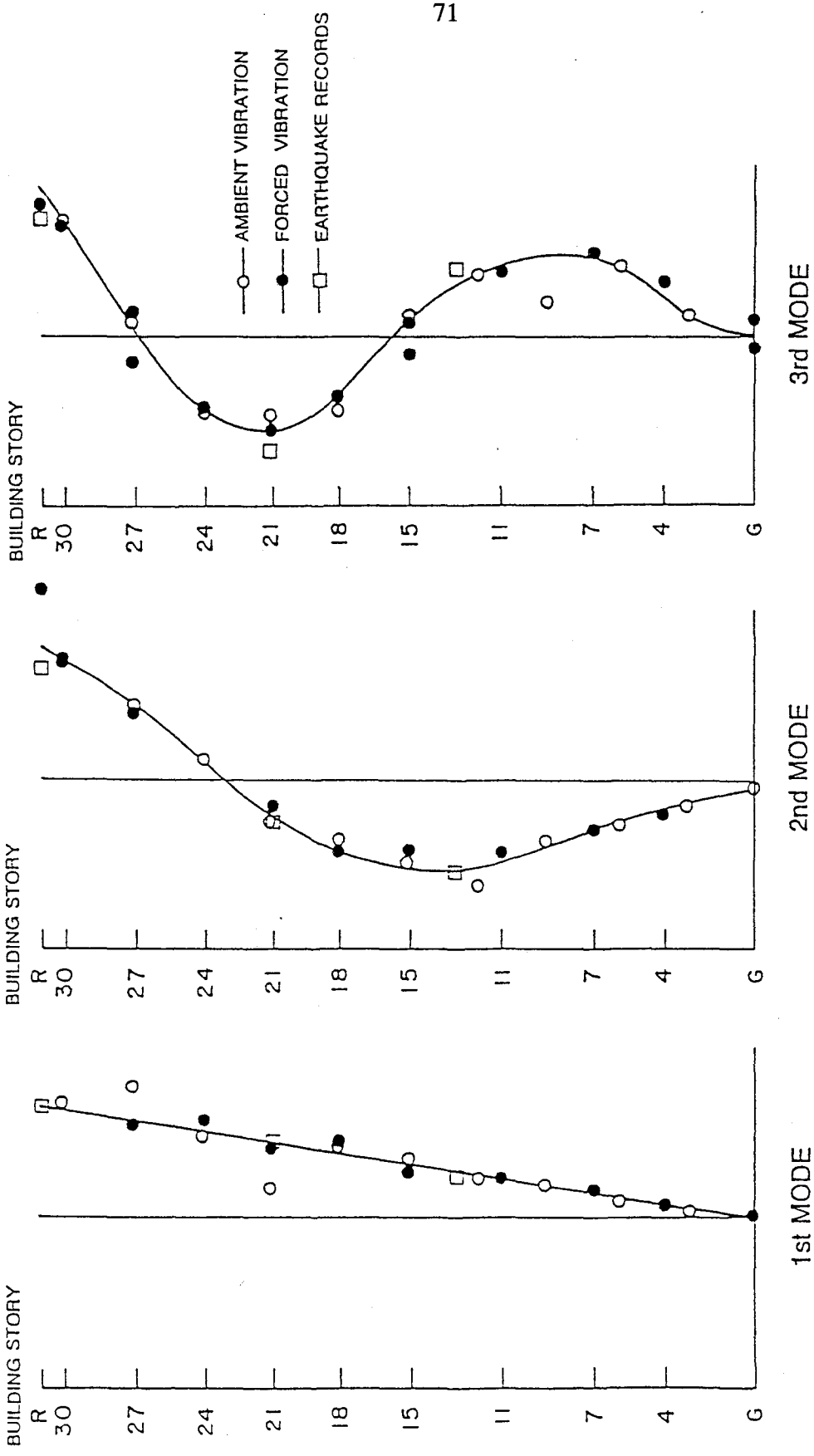

Figure 3.22 - Comparison of translational mode shapes of the building (350° component) obtained through three different procedures

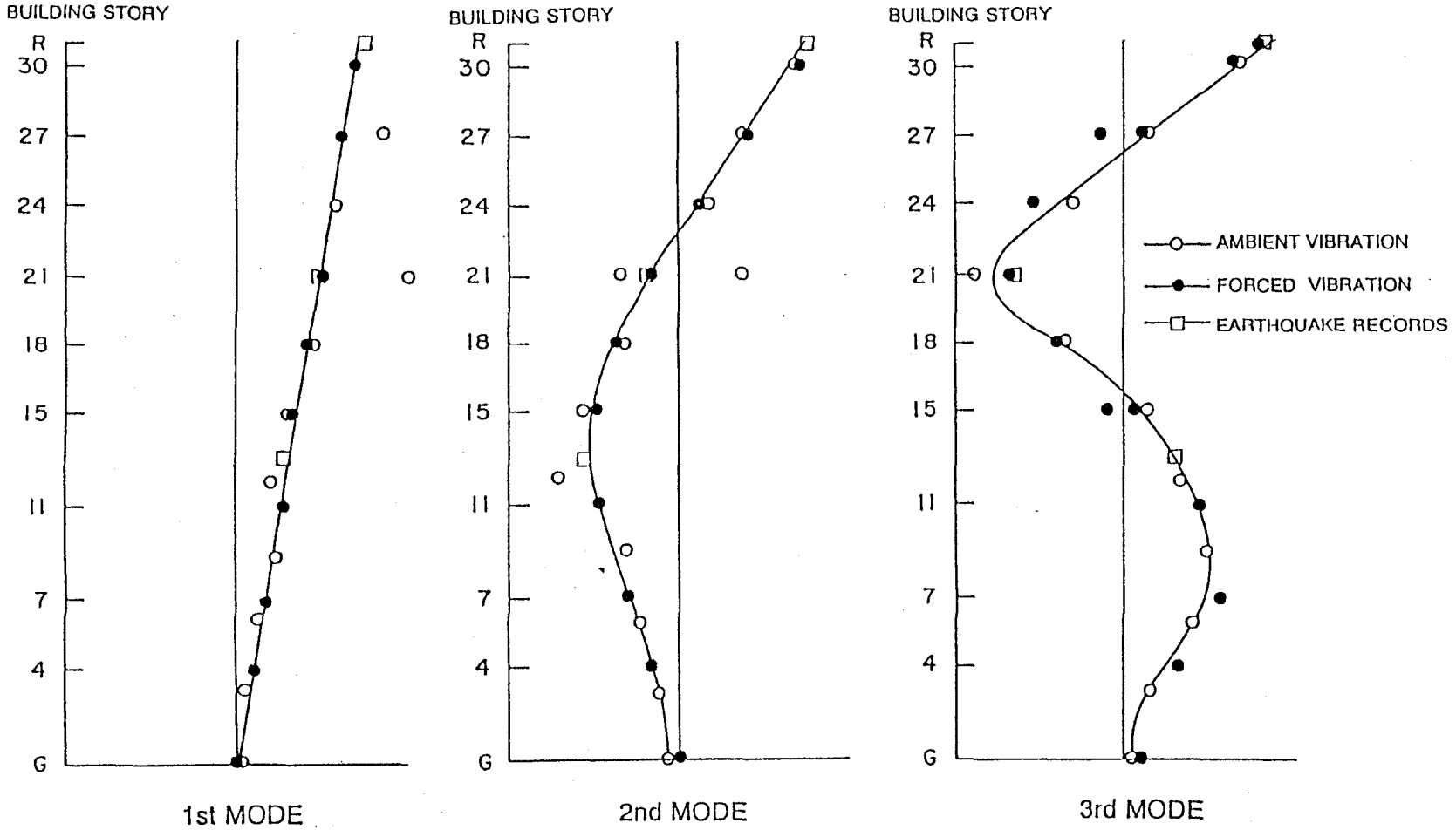

Figure 3.23 - Comparison of translational mode shapes of the building (260° component) obtained through three different procedures.

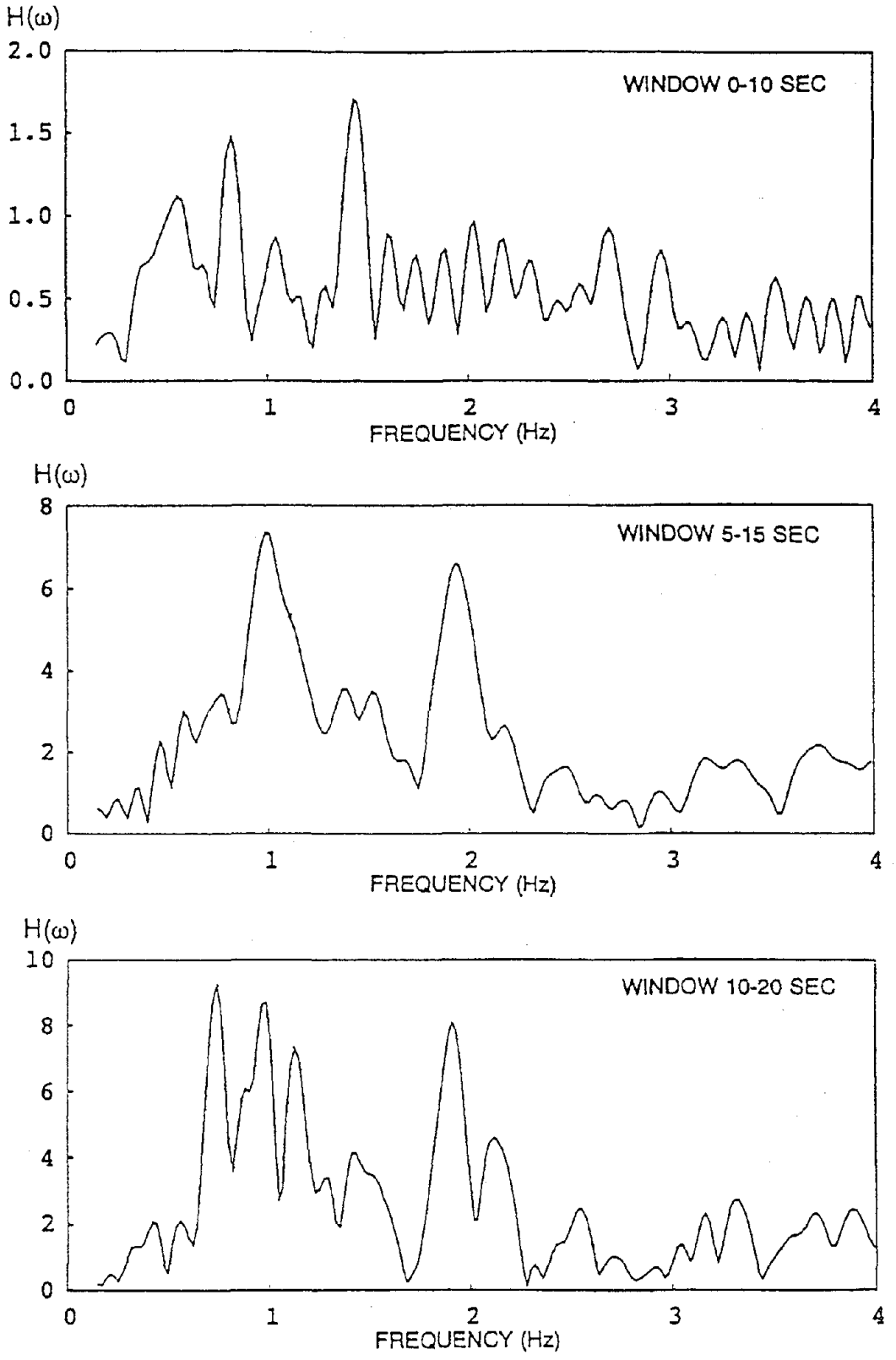

Figure 3.24 - Moving window Fourier analysis using the west wing roof acceleration (windows 0-10, 5-15, and 10-20 seconds).

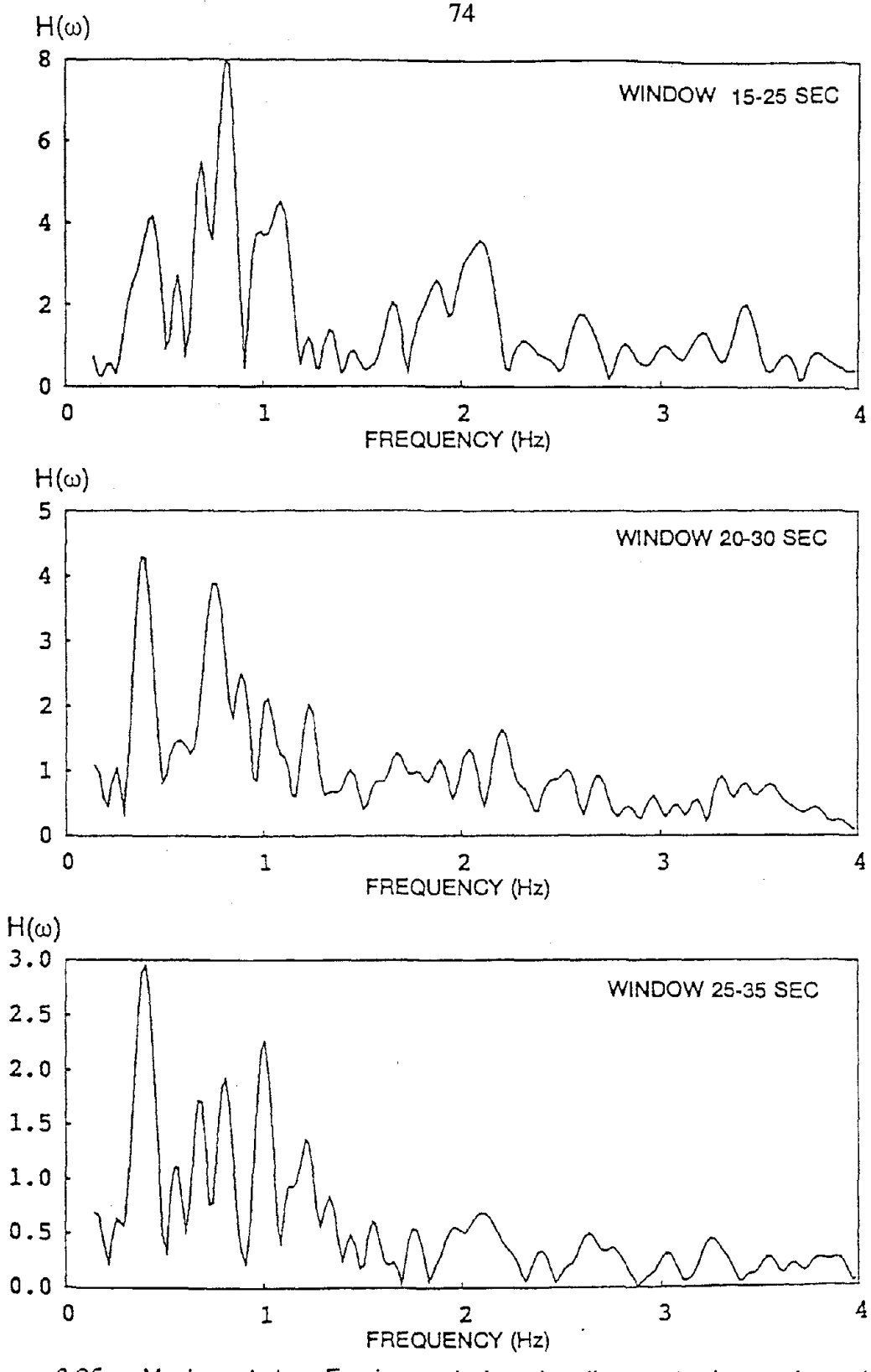

Figure 3.25 - Moving window Fourier analysis using the west wing roof acceleration (windows 15-25, 20-30, and 25-35 seconds).

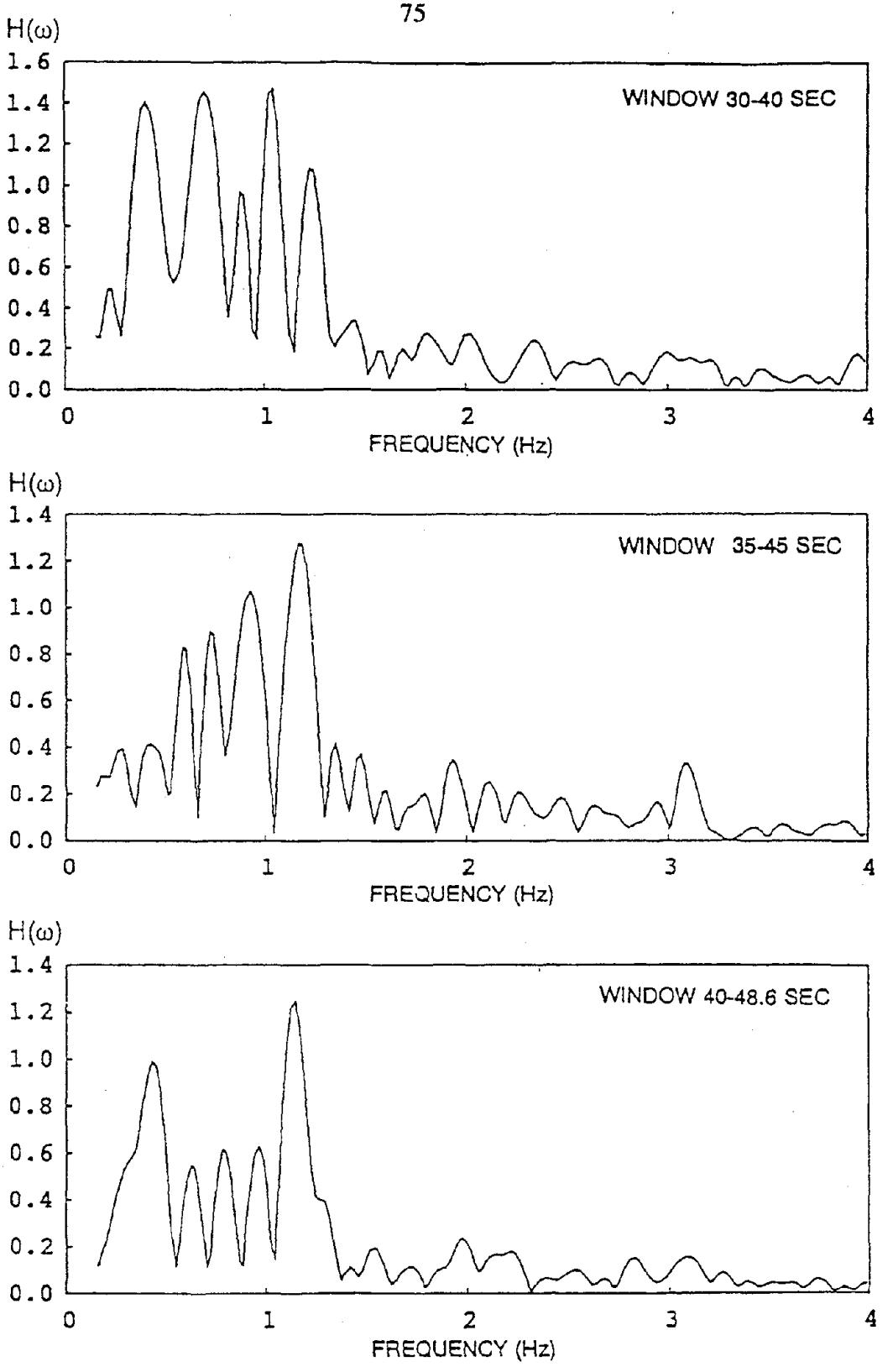

Figure 3.26 - Moving window Fourier analysis using the west wing roof acceleration (windows 30-40, 35-45, and 40-48.6 seconds).

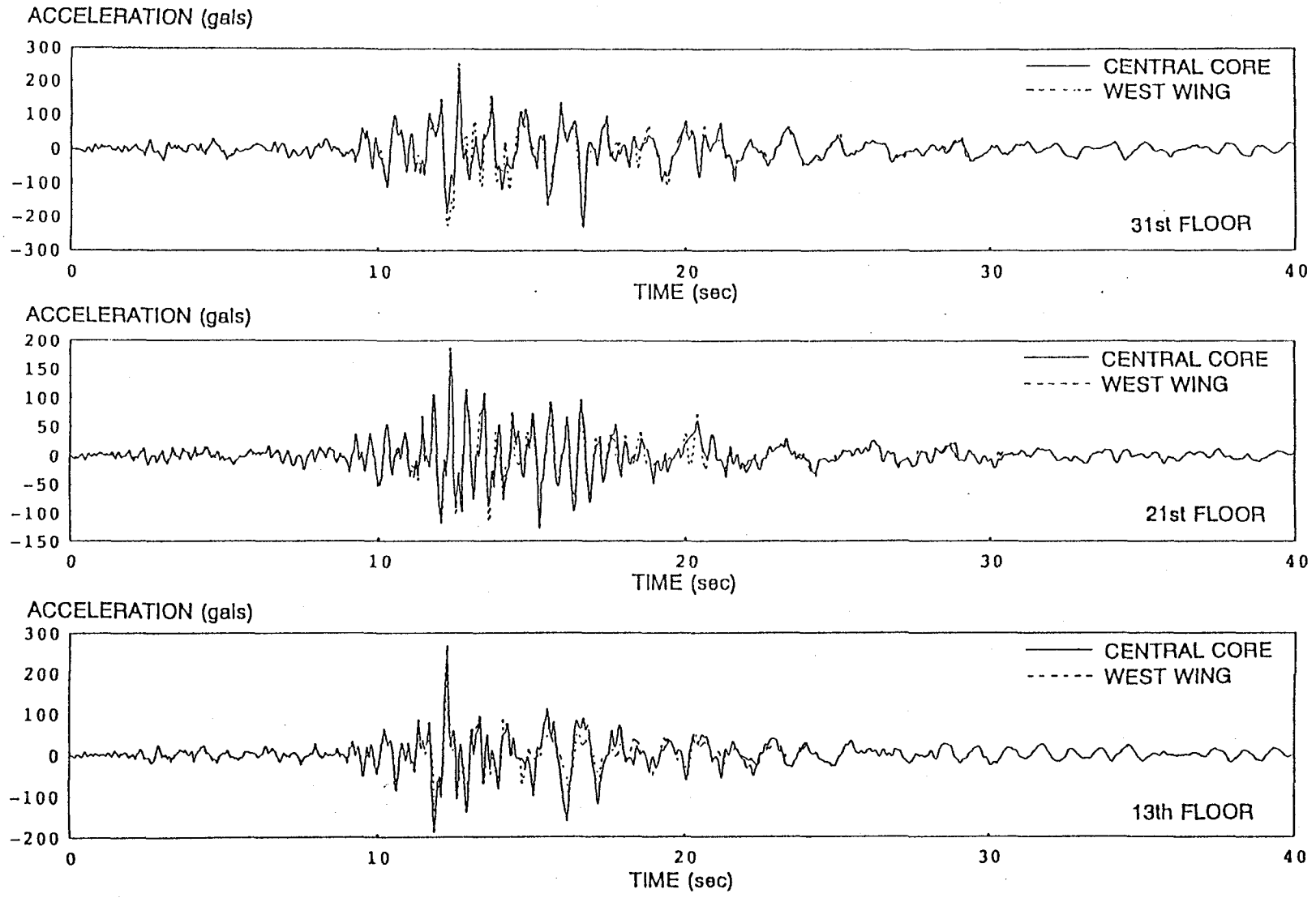

Figure 3.27 - Comparison of acceleration time-histories recorded in the central core and west wing of the building at the 31st, 21st, and 13th floors (350° component).

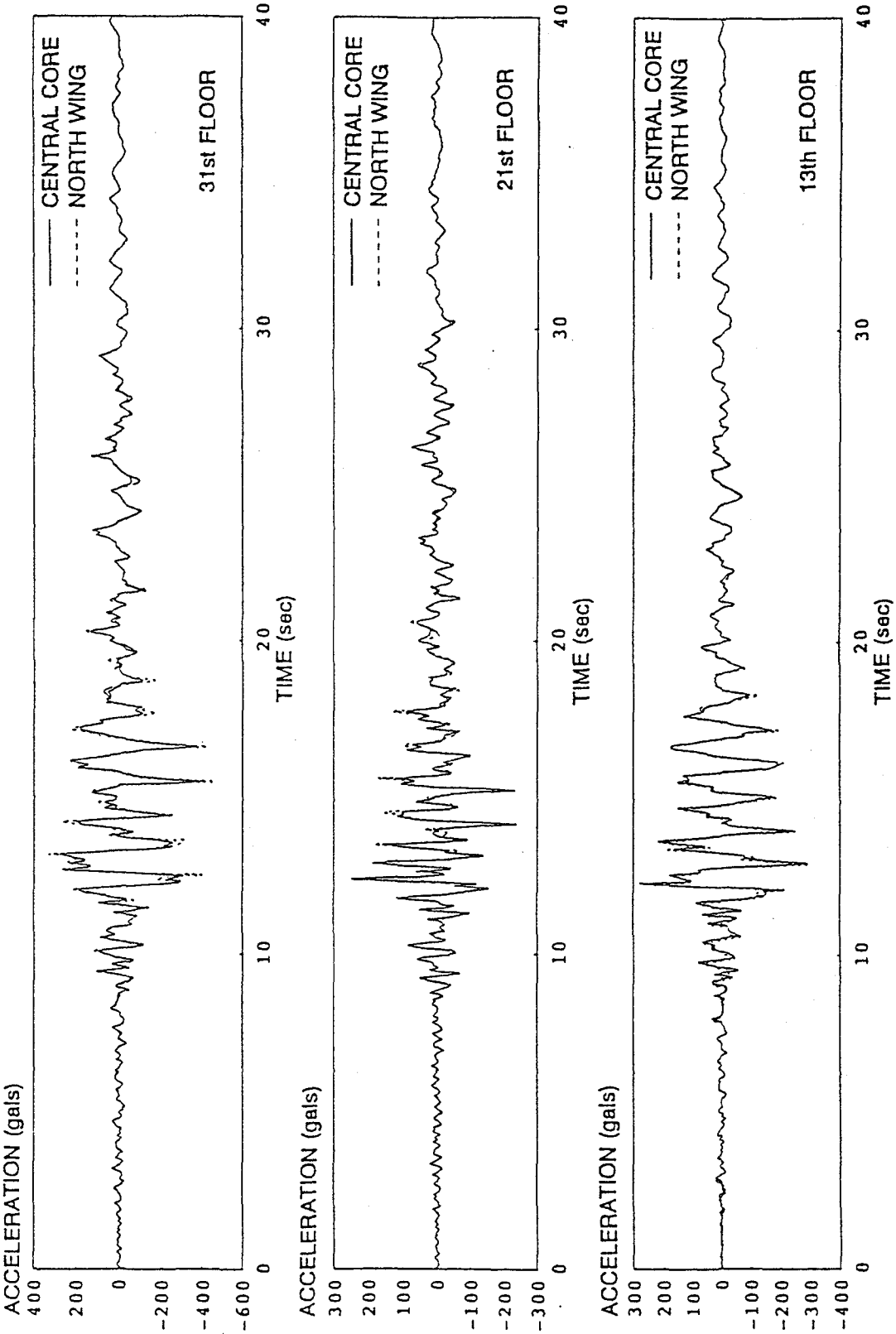

Figure 3.28 - Comparison of acceleration time-histories recorded in the central core and north wing of the building at the 31st, 21st, and 13th floors (290° component).

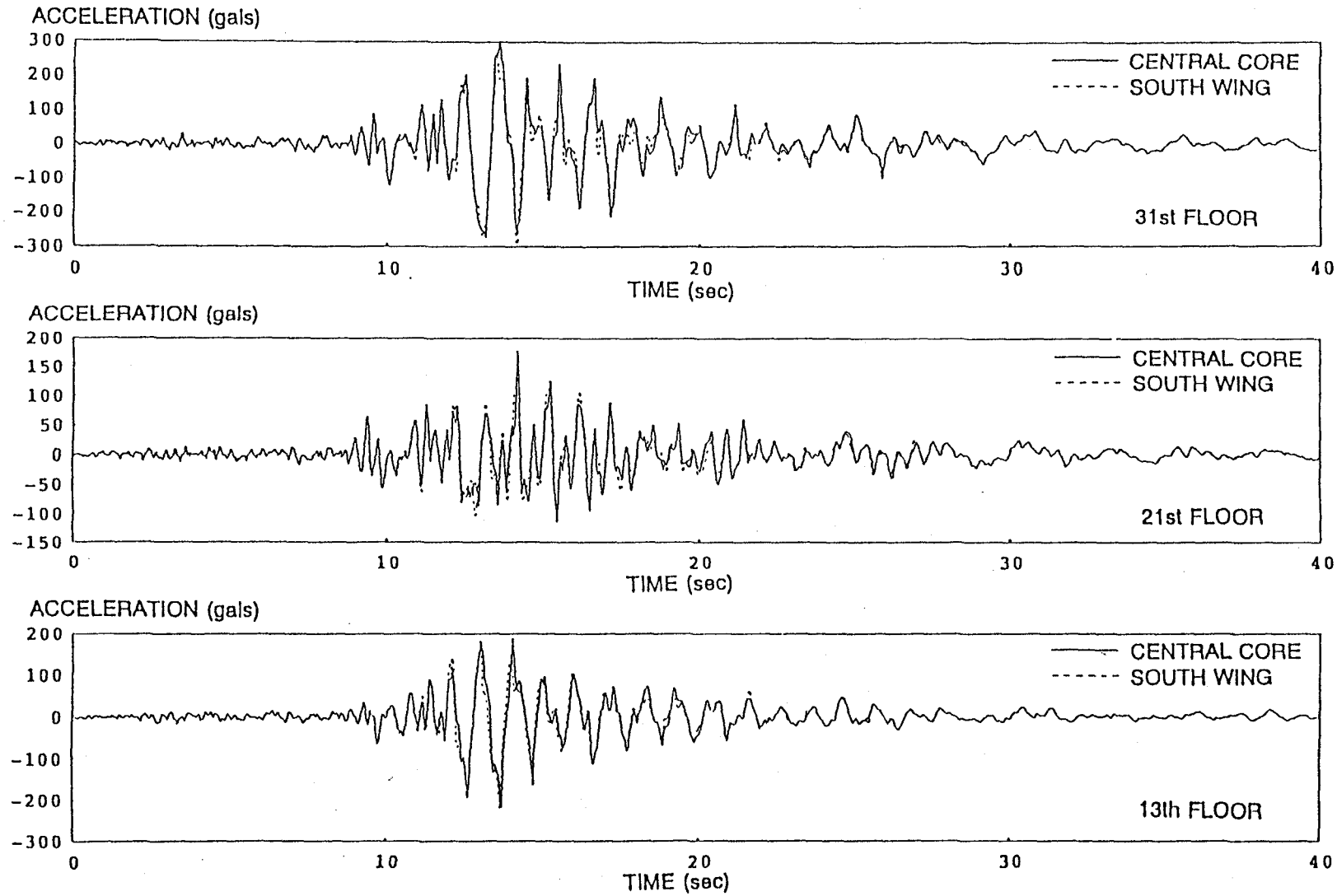

Figure 3.29 - Comparison of acceleration time-histories recorded in the central core and south wing of the building at the 31st, 21st, and 13th floors (50° component).

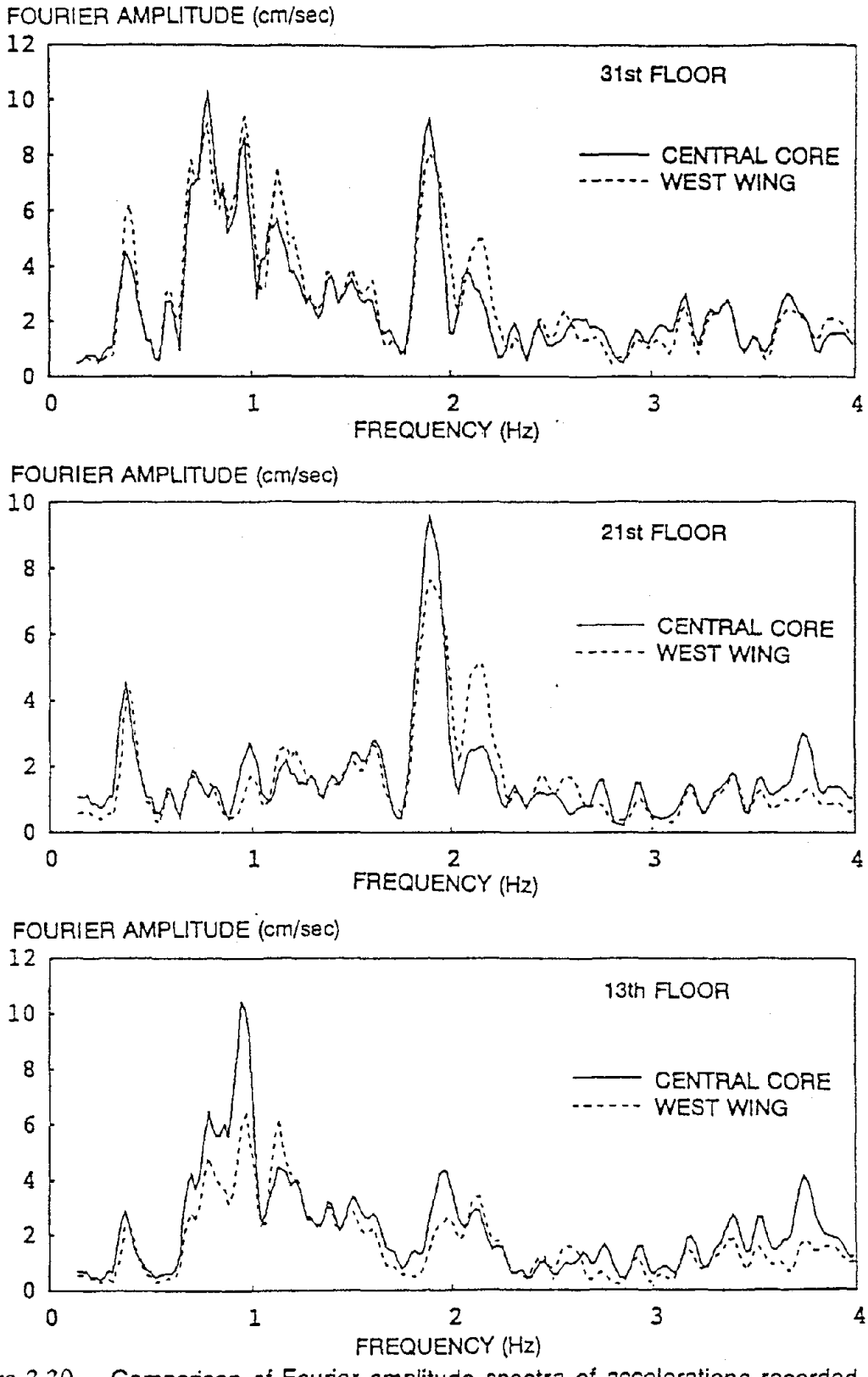

Figure 3.30 - Comparison of Fourier amplitude spectra of accelerations recorded in the central core with those recorded in the west wing at the 31st, 21st, and 13th floors (350° component).

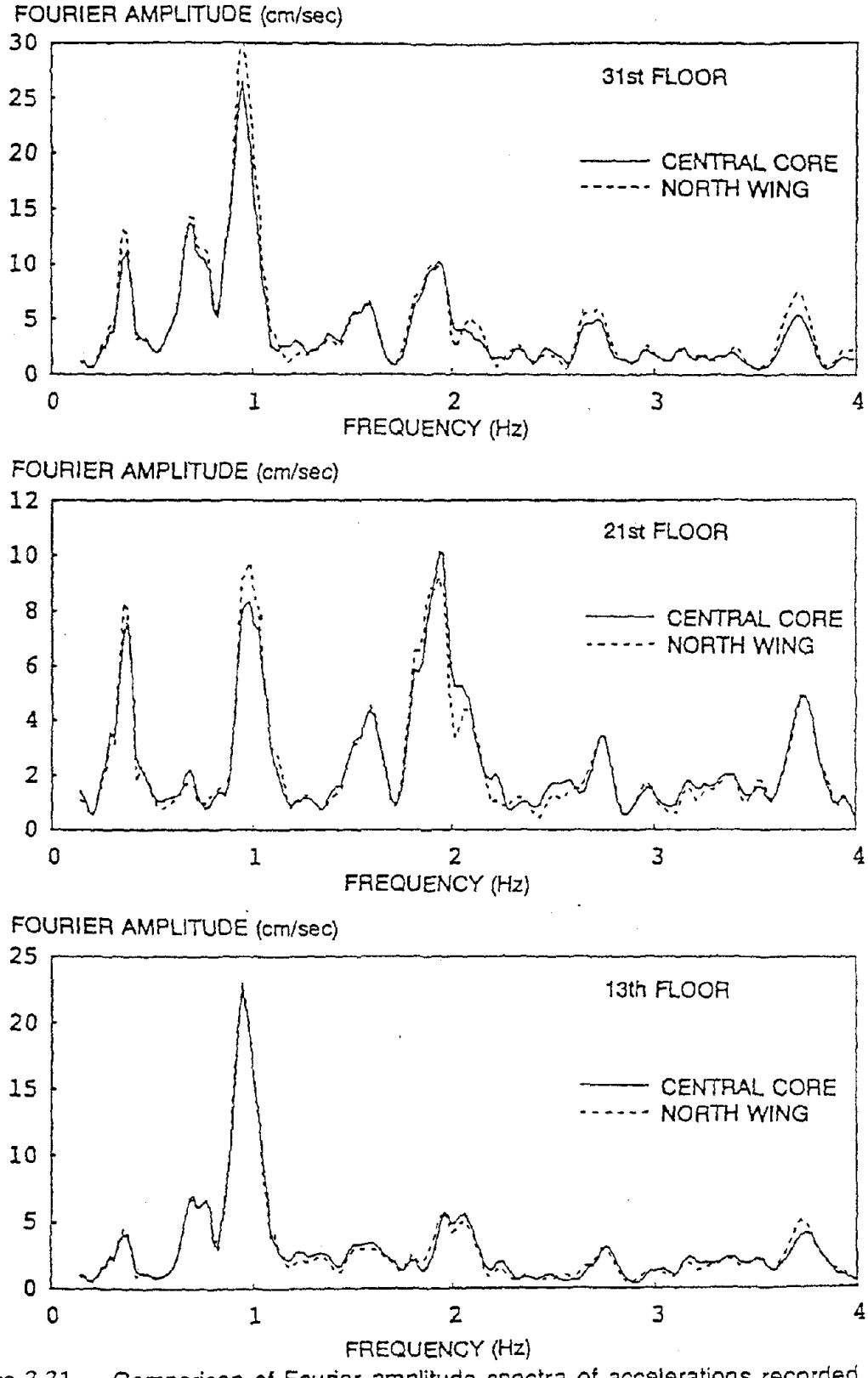

Figure 3.31 - Comparison of Fourier amplitude spectra of accelerations recorded in the central core with those recorded in the north wing at the 31st, 21st, and 13th floors (290° component).

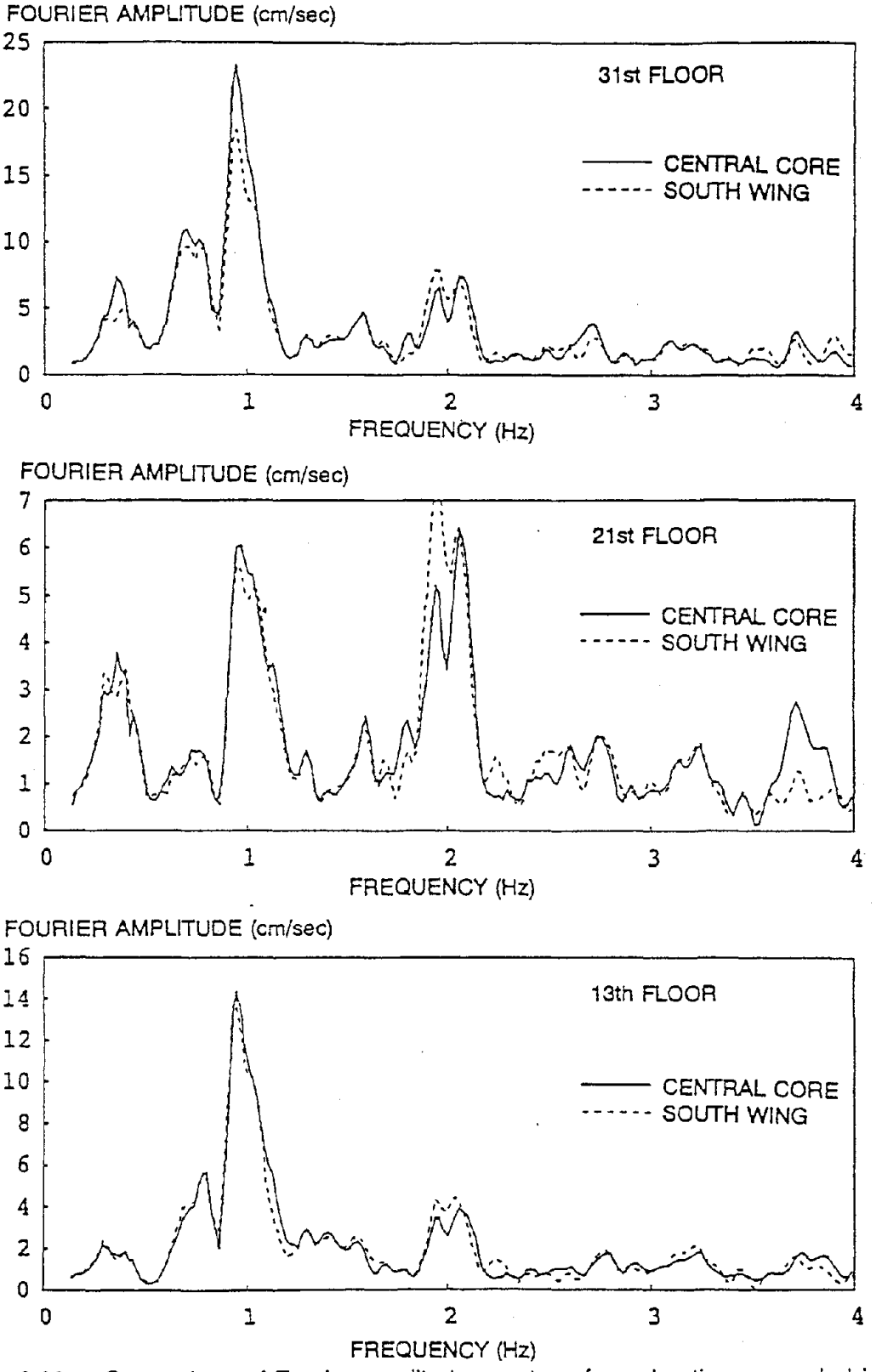

Figure 3.32 - Comparison of Fourier amplitude spectra of accelerations recorded in the central core with those recorded in the south wing at the 31st, 21st, and 13th floors (50° component).

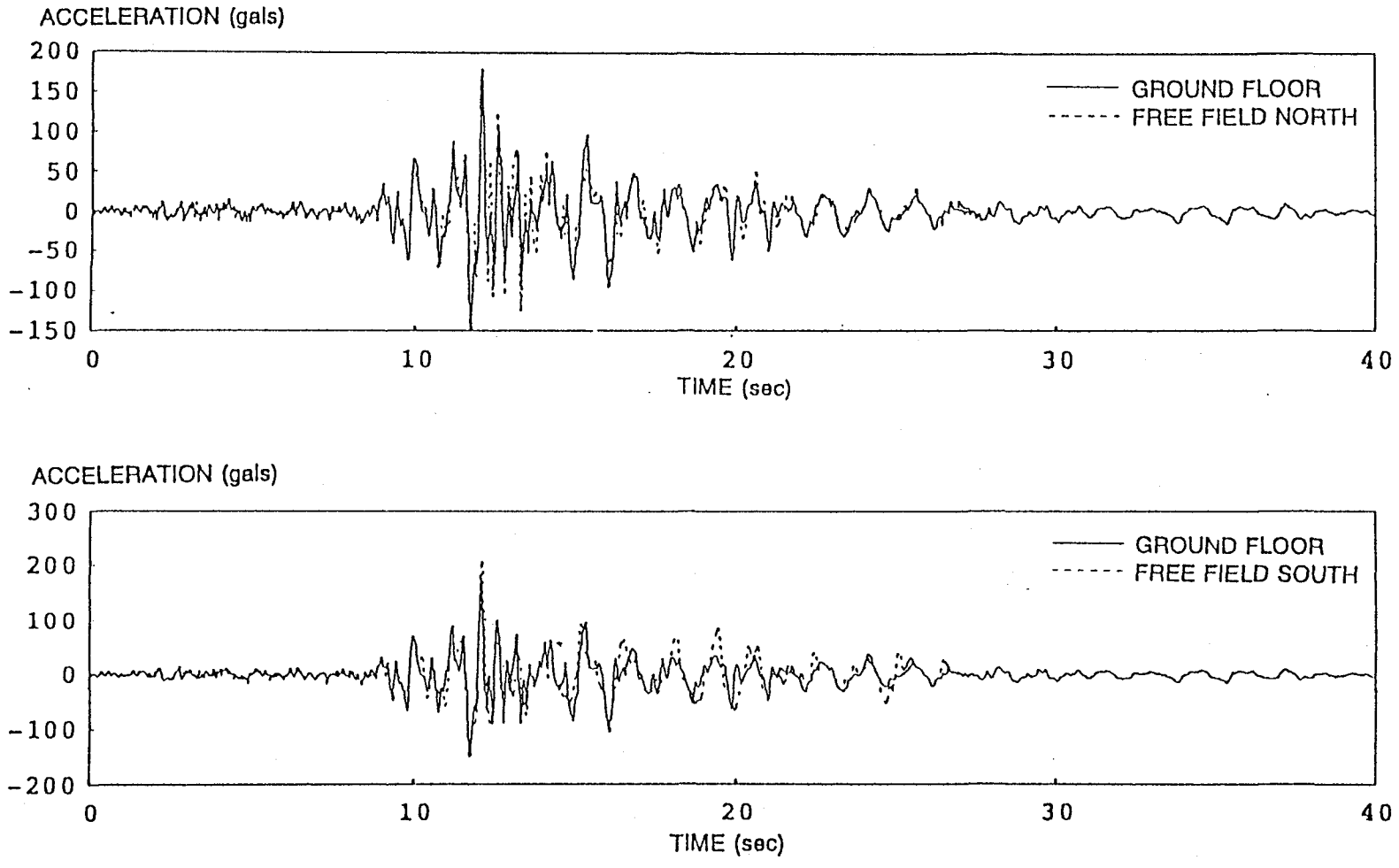

Figure 3.33 - Comparison of horizontal acceleration time-histories recorded in the 350° component at the ground level of the building with those recorded at the free-field stations.

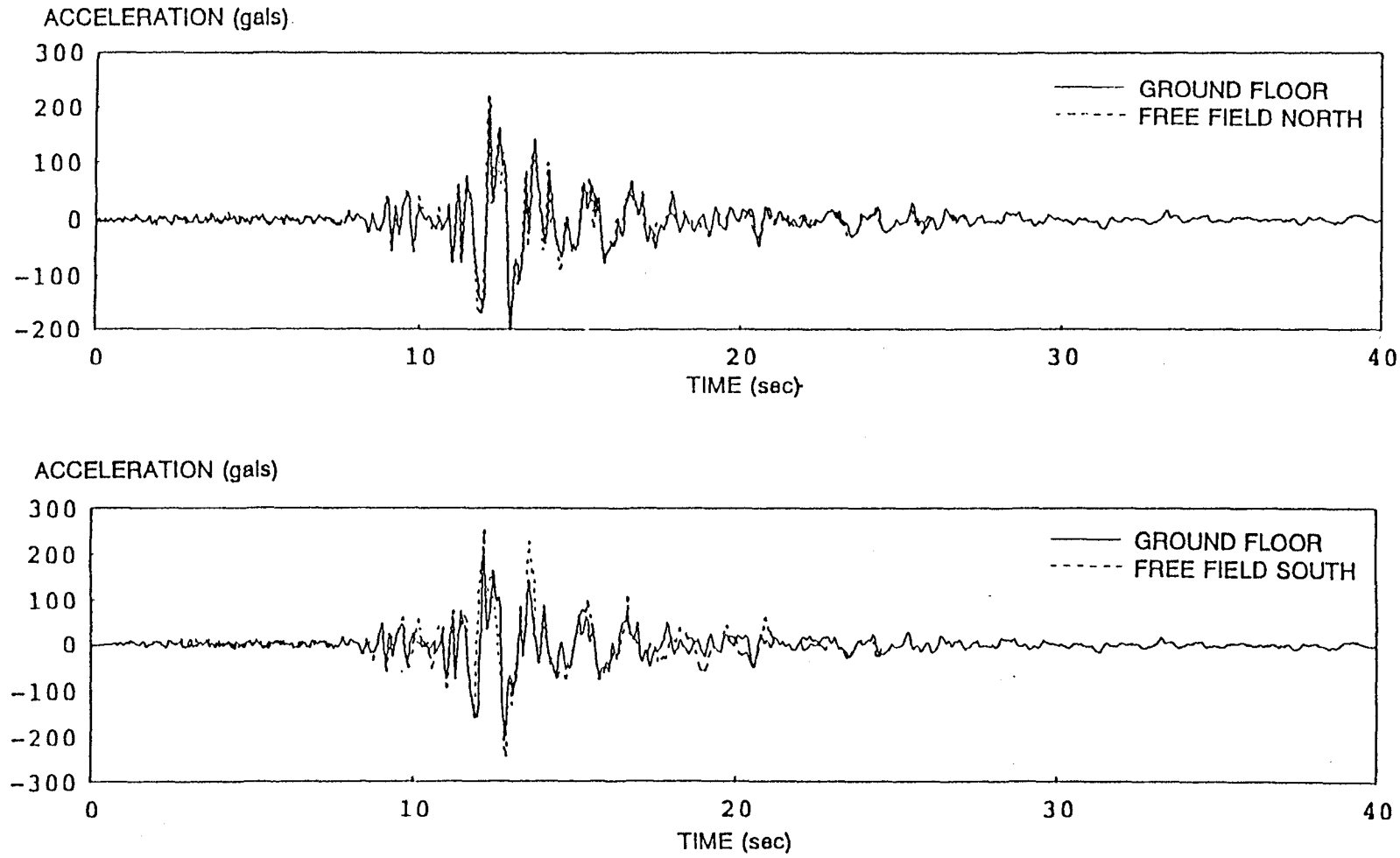

Figure 3.34 - Comparison of horizontal acceleration time-histories recorded in the 260° component at the ground level of the building with those recorded at the free-field stations.

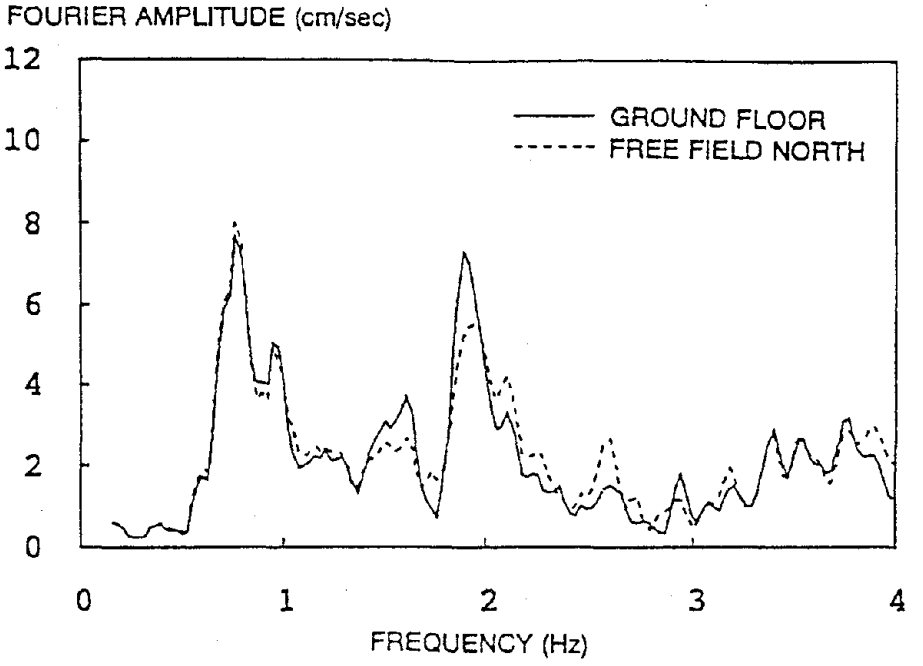

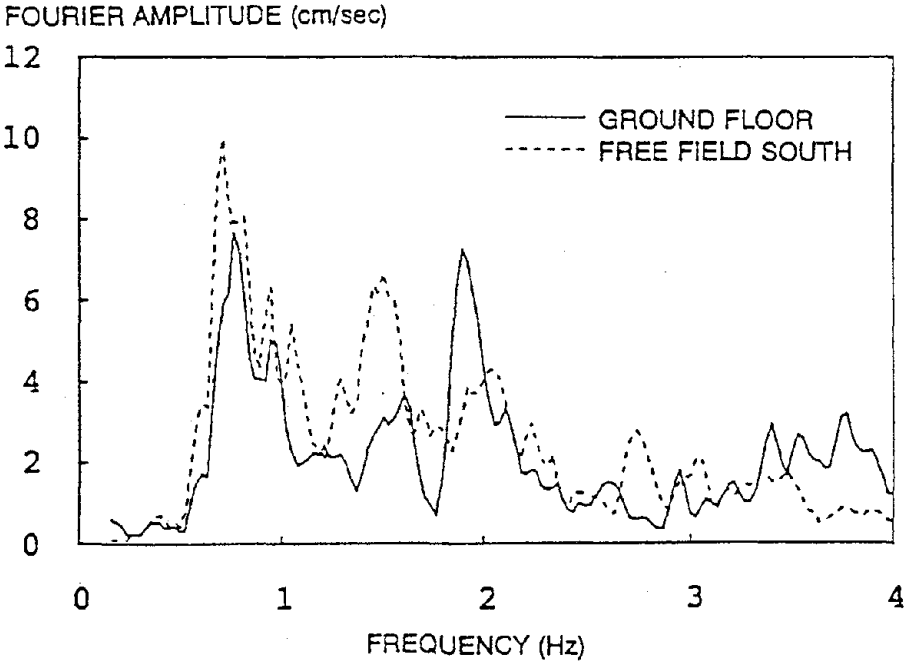

Figure 3.35 - Comparison of Fourier amplitude spectra of horizontal accelerations recorded in the 350° component at the ground level of the building with those recorded at the free-field stations.

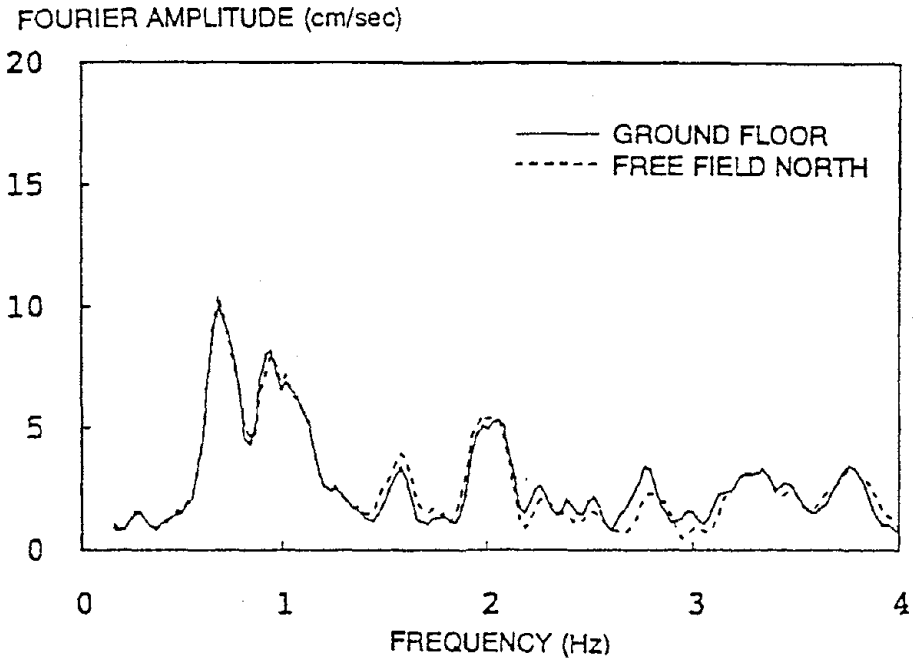

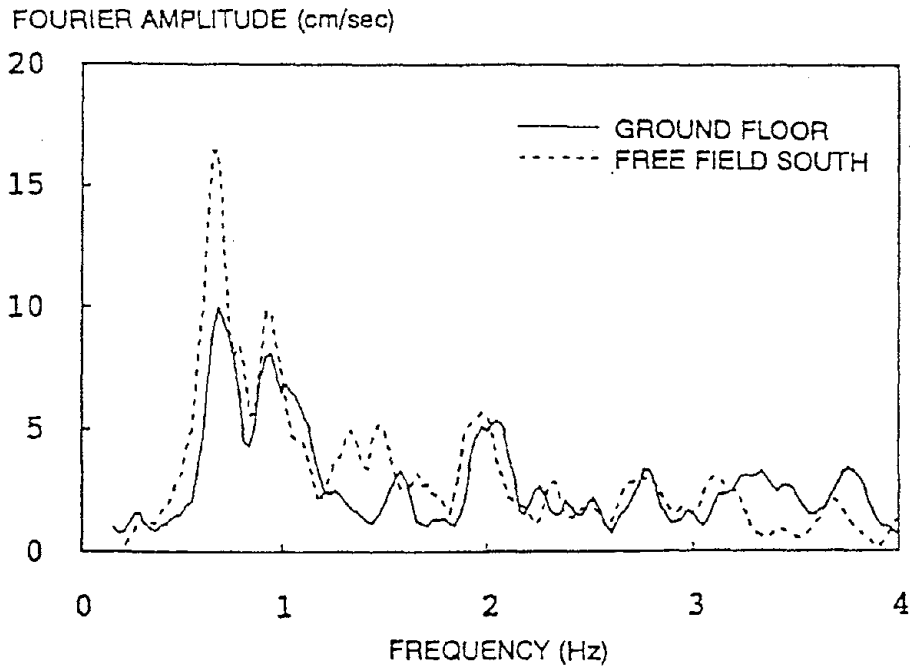

Figure 3.36 - Comparison of Fourier amplitude spectra of horizontal accelerations recorded in the 260° component at the ground level of the building with those recorded at the free-field stations.

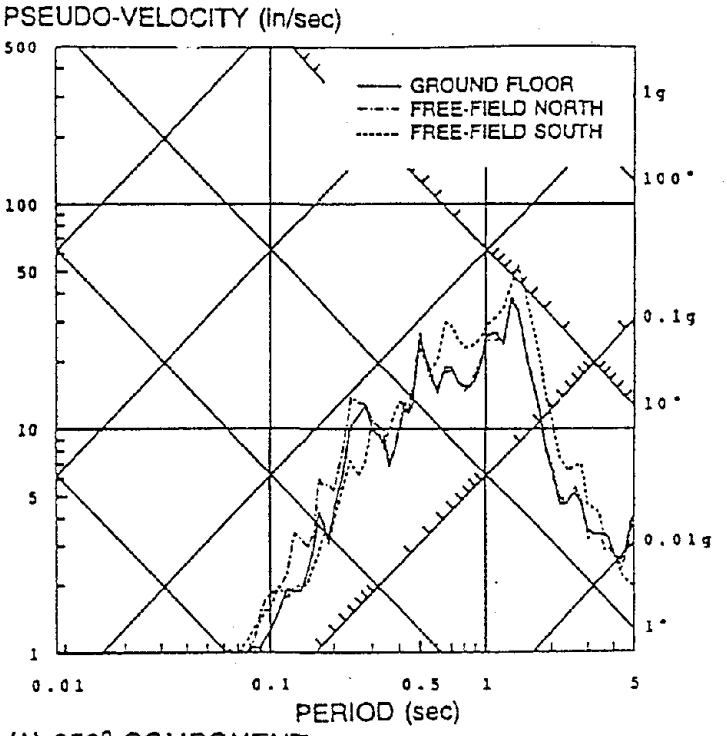

(A) 350° COMPONENT

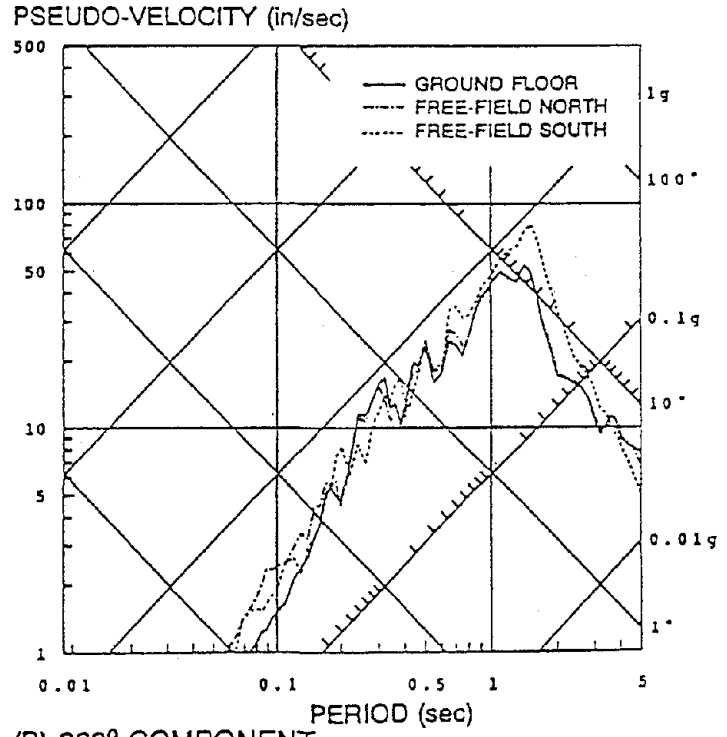

(B) 260° COMPONENT

Figure 3.37 - Comparisons of 2% damped linear-elastic response spectra of horizontal ground motions recorded at the ground floor of the building and those of motions recorded at both free-field stations.

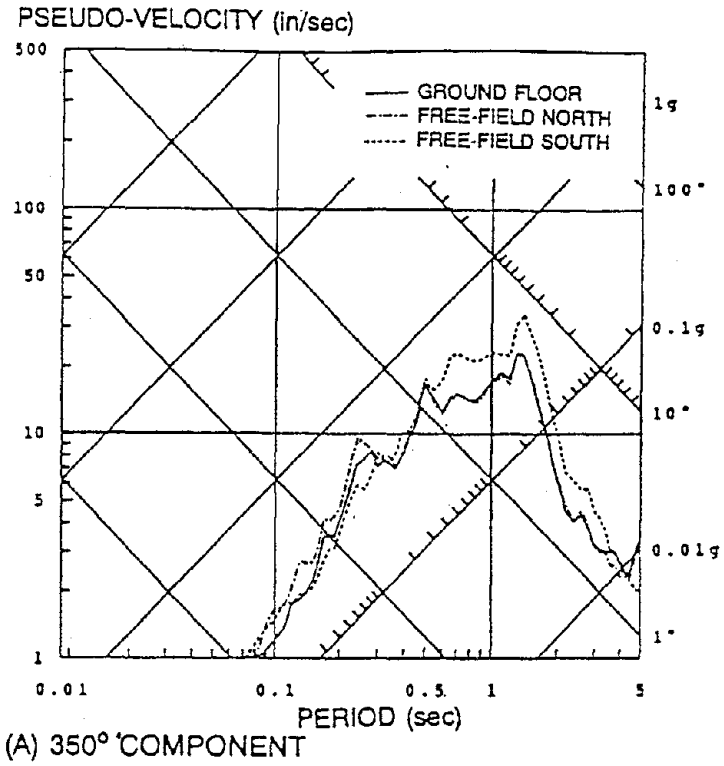

(A) 350° COMPONENT

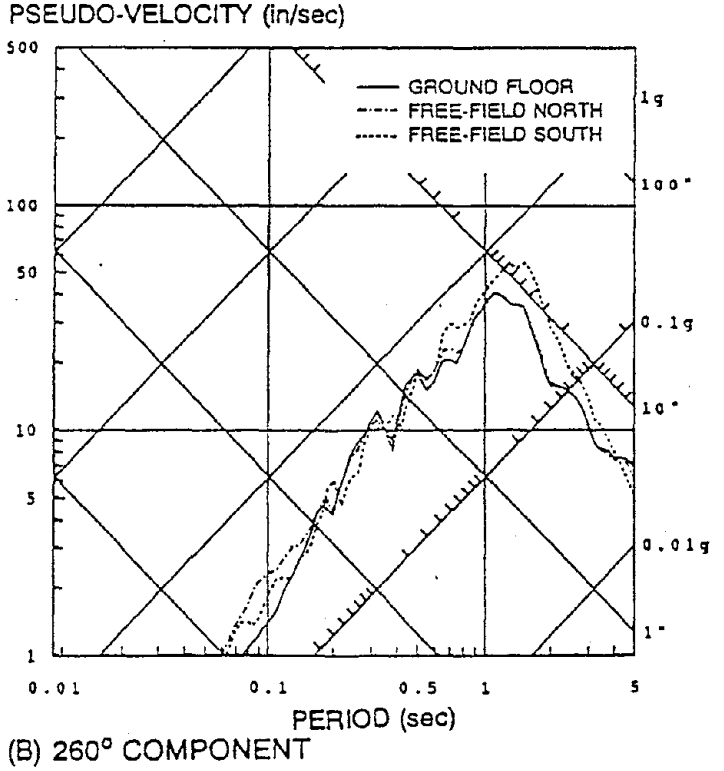

(B) 260° COMPONENT

Figure 3.38 - Comparisons of 5% damped linear-elastic response spectra of horizontal ground motions recorded at the ground floor of the building and those of motions recorded at both free-field stations

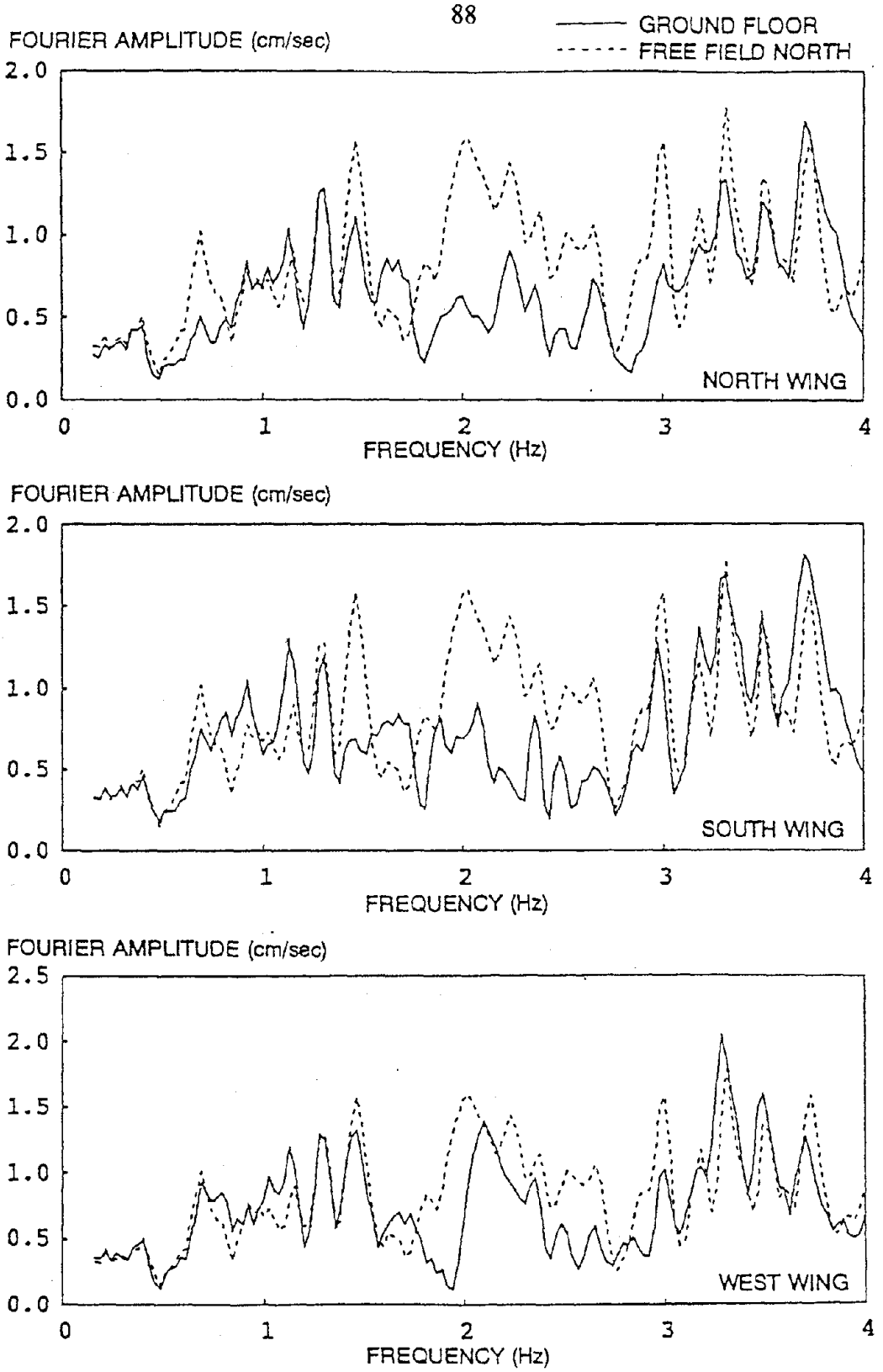

Figure 3.39 - Comparison of Fourier amplitude spectra of vertical accelerations recorded at the ground floor of the building and of those recorded at the north free-field station.

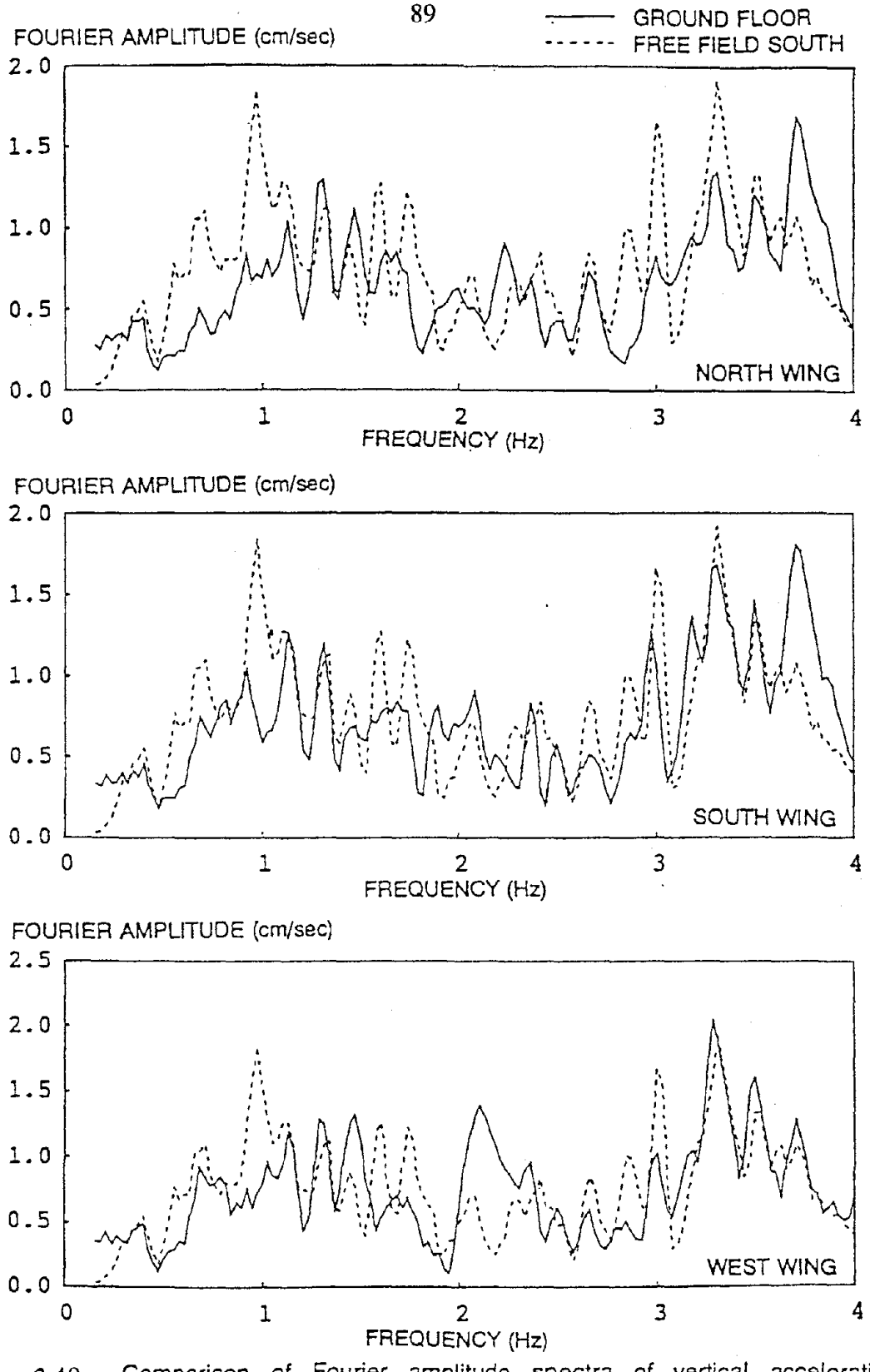

Figure 3.40 - Comparison of Fourier amplitude spectra of vertical accelerations recorded at the ground floor of the building and of those recorded at the south free-field station.

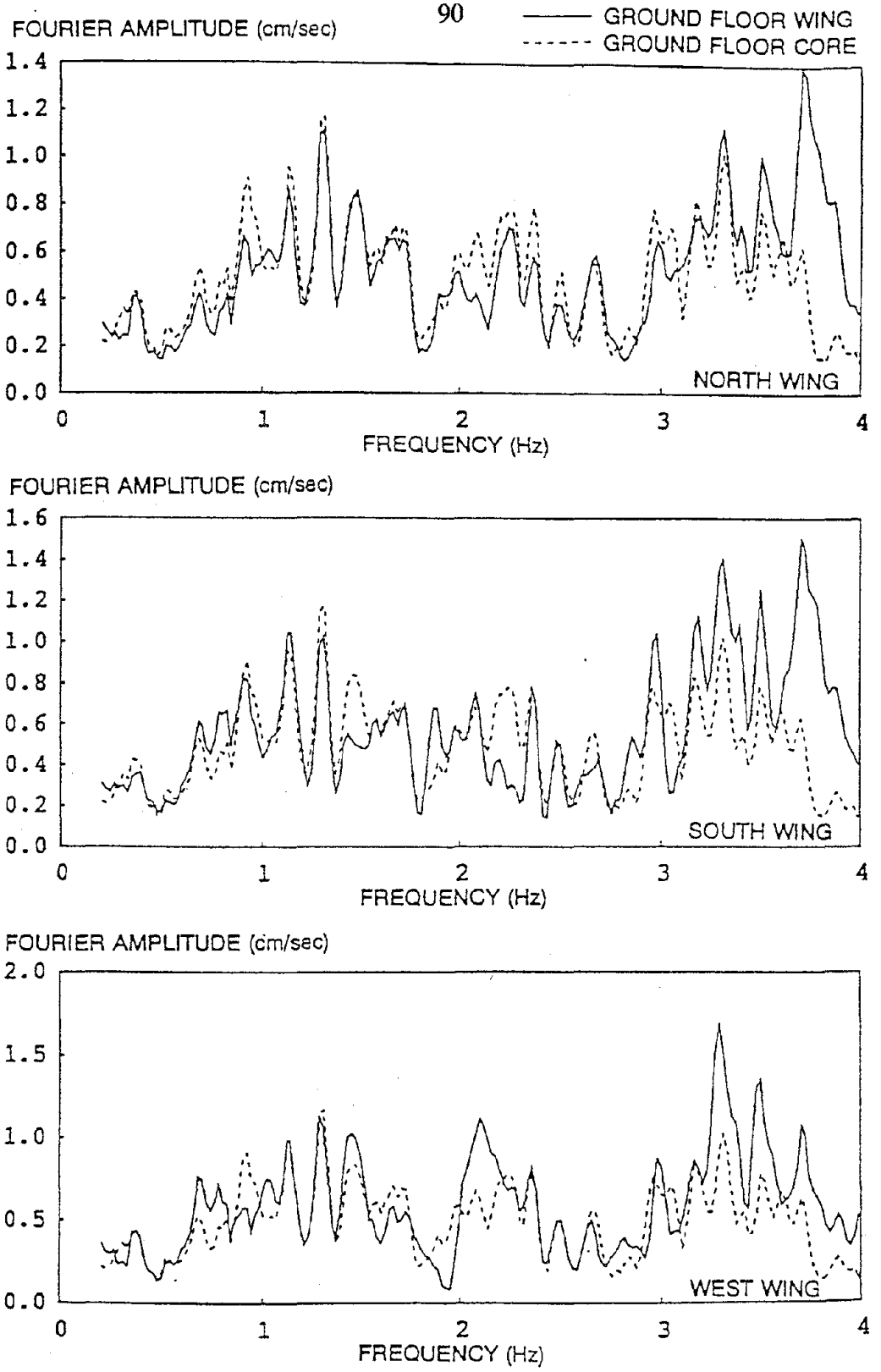

Figure 3.41 - Comparison of Fourier amplitude spectra of vertical accelerations recorded at the ground floor, in the wings and in the central core.

4. LINEAR ELASTIC SEISMIC RESPONSE ANALYSES

4.1 INTRODUCTORY REMARKS

During the last two decades there have been significant advances in the development of computer programs for seismic response analysis of structures. Because of the uncertainties involved in the formulation of realistic three-dimensional (3-D) mathematical models of the whole building system (soil-foundation, superstructure and non-structural components), questions have been raised regarding the reliability of these programs for predicting the actual response of real structures when subjected to critical seismic ground motions which can occur during the service life of a structure. In order to answer these questions there has been a need to calibrate predictions based on the use of these analytical models with the results of experiments. The best experiment is when earthquake ground motions occur and there are properly instrumented structures which can record reliably the actual building response to ground motions recorded at the base.

Because the thirty-story Y Building is extensively instrumented and produced a large number of excellent response records during the October 17, 1989 Loma Prieta earthquake, these data offer an excellent opportunity to evaluate the reliability of the existing analytical capability to predict the seismic response of a real structure. One of the main questions that need to be answered is whether very sophisticated finite element models are required or whether acceptable predictions can be obtained using simplified models.

The recorded response of the Y Building also offers an excellent opportunity to evaluate the soundness of present seismic design code methodologies. Are the magnitude and distribution

of seismic design forces adequate for medium and high-rise buildings which have longer periods of vibration? Does the dynamic response analysis procedure outlined in the codes result in an accurate prediction of the seismic response of these structures, particularly if they are buildings which have an irregular plan?

To answer the above questions, a series of analytical studies have been conducted to analyze the response of the Y Building to the Loma Prieta Earthquake. Two different types of models were used for these analyses: simplified, cantilever (stick) models in which each floor level has a translational degree of freedom, and detailed, 3-D finite element models which consider all structural members. Working independently, the Kajima research team developed a 3-D linear elastic model of the building and conducted a series of analyses of the response of the model when subjected to five earthquake ground motion records that are considered typical for seismic design in Japan.

4.2 SIMPLIFIED MODEL ANALYSES

4.2.1 Description of the Simplified Model. This model consists of two-dimensional (2-D) shear elements with only one translational degree of freedom per floor. Therefore, a total of 31 degrees of freedom were necessary to model the response of the Y Building in one of its principal directions. Formulation of the simplified model requires knowledge of two characteristics of the structure out of the following three: (a) reactive mass; (b) lateral stiffness; and (c) vibration mode shape and frequency. In order to have an accurate model, the required mechanical characteristics must be obtained from one or more of the following: (1) ambient or forced vibration measurements; (2) system identification of recorded response, and (3) analytical calculation from a detailed mathematical model. The model used in this

study was derived using (a) and (c) above. The vibration mode shapes and frequencies were identified from the recorded earthquake response (Chapter 3) and the reactive mass at each floor level was estimated from a copy of the structural drawings. In this case the following masses were used: roof, 8.5 kip-sec^2/in.; typical floor, 11.08 kip-sec^2/in.; 2nd floor, 16.2 kip-sec^2/in. Using this data, the equation of motion for the nth mode can be written as

$$\ddot{Y}_n + 2\lambda_n \omega_n \dot{Y}_n + \omega_n^2 Y_n = \{\phi\}_n^T [M] \{1\} \ddot{v}_g / M_n^* \quad (4.1)$$

where

$M_n^* = \{\phi\}_n^T [M] \{\phi\}_n$ = generalized mass of the nth mode

$K_n^* = \omega_n^2 M_n^*$ = generalized stiffness of the nth mode

$C_n^* = 2\lambda_n \omega_n M_n^*$= generalized damping of the nth mode

Y_n = amplitude of response for the nth mode

ϕ_n = shape of the nth mode of vibration

$\ddot{v}_g$ = ground acceleration

Equation 4.1 is solved by step by step integration for each mode and the total response is obtained by modal superposition as

$$\{v\} = [\phi] \{Y\} \quad (4.2)$$

The purpose of the simplified model was to have a relatively small model (31 degrees of freedom versus 6816 degrees of freedom for the detailed 3-D finite element model) which could perform time-history analyses quickly in order to conduct parametric studies and code evaluations. Two types of studies were conducted: spectral analyses and time-history analyses.

4.2.2 Response Spectrum Analyses. In order to evaluate the soundness of the seismic code methodology to estimate the displacement demands on the building in moderate earthquake ground motions, response spectrum dynamic analyses were conducted using the following three spectra:

(a) 1979 Uniform Building Code

(b) 1988 Uniform Building Code

(c) Response spectrum of the 260° component of the ground motion recorded at the south free-field station (5% damping).

A comparison of these three spectra is shown in Fig. 4.1. The spectrum corresponding to the 1979 UBC was constructed using a framing factor (K) of 0.67 and a soil factor (S) of 1.5, while the 1988 UBC spectrum is based on a response modification factor (R_w) of 12 and S=2.0. It can be seen that both design spectra are very similar and that the small difference is mainly due to the difference in the soil factors. The 5% damped response spectrum of the Loma Prieta earthquake record is significantly larger than either of the code spectra.

4.2.3 Time-History Analyses

4.2.3.1 Component at 350°. A comparison of the recorded response at the roof level with that calculated in the time domain using all three modes and 3% damping is shown in Fig. 4.2. The comparisons include the absolute acceleration, relative velocity, and relative displacement of the west wing. Relative motions correspond to the difference of the motion at the roof and the recorded motions at the ground floor of the building. This ground floor record was also used as input for the simplified analyses. As shown in this figure, apart from the first 10 seconds, correlation between the recorded and calculated response is good except

possibly at 14 seconds. Large differences between the recorded and computed response at the beginning of the signals were also observed by McVerry using the same identification technique [12].

It was found that the relative importance of each mode in the total response depends on the response function (absolute acceleration, relative velocity or relative displacement). For relative displacement the first mode response dominated the total response; for relative velocity the first two modes dominated the response; whereas for absolute acceleration at least three modes were needed to capture adequately the recorded response. Improvement of the calculated acceleration time-history at the roof level of the west wing with the inclusion of the higher modes is shown in Fig. 4.3.

In order to study the correlation between the recorded and the calculated response over the height of the building, comparisons were made for all levels where records were obtained. Relative velocity time-histories at the 31st, 22nd and 13th floors are shown in Fig. 4.4. As before, it can be seen that with exception of the first 10 seconds, correlation is very good. Slightly larger differences are observed at the 13th level between the 12 and 15 second time marks.

4.2.3.2 Component at 260°. Recorded and calculated values for time-histories of absolute acceleration, relative velocity and relative displacement are compared in Fig. 4.5. Comparisons are made at the roof level of the central core. The ground floor record in the 260° direction was used as input for the simplified analyses. It can be seen that correlation in amplitude is reasonably good, although after 27 seconds the calculated response shifts

slightly out of phase with respect to the recorded response. It is clear from this figure that if better correlation is sought, a time-variant model is necessary.

The improvement in the correlation between the recorded and calculated roof absolute acceleration with the inclusion of higher modes is shown in Fig. 4.6. Comparison of recorded and calculated relative velocity time-histories over the height of the building is shown in Fig. 4.7. It can be seen that the participation of the second mode after the first 20 seconds is overestimated in the time-invariant model.

4.2.4 Concluding Remarks. Based on the studies just described, the following conclusions are drawn:

1. The relative importance of each mode in the total response depends on the response parameter. For relative displacement, the first mode is dominant; for relative velocity, the first two modes are dominant; and for absolute acceleration, at least the first three modes are required to capture the response.

2. The simplified model can produce an accurate estimate of the overall response in each of the principal directions of the structural system provided there is little cross-coupling of the modes and that information about the mechanical characteristics of the structure is available either from experimental measurements or detailed finite element models.

4.3 THREE-DIMENSIONAL LINEAR ELASTIC ANALYSES

Detailed three-dimensional finite element models of the structure were developed in order to evaluate the response of this irregular structure to the two horizontal components of ground motion recorded at the base. These models will provide an opportunity to evaluate the ability of current computer programs to reproduce the actual, recorded response, given the input base motion. In addition, they will be used to evaluate the effect of the earthquake on the individual members of the structure and to evaluate the developed inertia forces relative to the specified building code requirements. Critical comparisons will be made between the calculated response and the corresponding recorded values. These comparisons will include acceleration time-history, displacement time-history, and floor response spectra.

4.3.1 Mathematical Models. Several alternative computer programs which could have been used to evaluate the elastic, dynamic response of the building, are available on a commercial basis. The SAP90 [38] program was selected for use in the initial phase of this study for the following reasons:

1. An extended memory version, SAP90 Plus, which has large capacity and permitted modeling the structure in detail for computation on a personal computer (IBM PS/2 with 8MB of memory and 120MB disk), is available.

2. The program allows the user to plot the time-history response of any node point. This feature was crucial for comparison of the calculated results with the recorded response.

3. The program permits consideration of a discontinuous, rigid floor diaphragm through the use of a master node-slave node option. This feature was essential for modeling the discontinuous floor diaphragm at the mezzanine level. It also greatly reduces the amount of modeling required to represent the in-plane effect of the floor diaphragm and also reduces the time required to perform a dynamic analysis.

The completed SAP90 model of the structure consisting of 2,362 nodes, 5,700 elements and 6,816 degrees of freedom, is shown in an isometric view in Fig. 4.8. A plan view of the model is shown in Fig. 4.9 which details the three wings and the center core. An elevation view in the north-south direction is shown in Fig. 4.10. Here the mezzanine floor in the west wing can be clearly seen. An elevation view in the east-west direction is shown in Fig. 4.11. As noted previously, the ultimate compressive strength for the reinforced concrete used in the building is 5000 psi, with the exception that the columns of the first four floors and the interior columns of the 20th and 21st floors have a compressive strength of 6500 psi. These higher strength members are shown in Fig. 4.12. The mezzanine level of the west wing and the second story level of the structure are shown in Fig. 4.13. Columns that are located in the center of bays represent the shear walls in the bottom two story levels which are modeled as short, cantilever columns having the mechanical properties of the wall.

4.3.2 Weight (Mass) Determination. In order to obtain the mode shapes and periods of vibration and to perform the dynamic response analysis, the self weight (mass) of the structure must be estimated as accurately as possible. The initial estimate of the weight of the structure in kips is detailed as follows:

Roof Weight

Columns	333
Girders	1338
Exterior Walls	132
Floor Slab	1474
Roofing (6 psf)	140
Total Roof Weight	3417 kips

Typical Floor Weight

Floors 19 through 30

Columns	667
Girders	1338
Exterior Walls	264
Floor Slab	1452
Finish Floor (2 psf)	47
Partition (15 psf)	350
Total Floor Weight	4118 kips

Typical Floor Weight

Floors 3 through 18

Columns	667
Girders	1860
Exterior Walls	264
Floor Slab	1452
Finish Floor (2 psf)	47

	Partition (15 psf)	350
	Total Floor Weight	4640 kips

Second Floor Weight

	Columns	667
	Girders	1860
	Floor Slab	1981
	Exterior Walls	264
	Finish Floor (2 psf)	51
	Partition (15 psf)	381
	Total Floor Weight	5203 kips

Mezzanine Floor Weight

	Columns	252
	Girders	521
	Walls	88
	Slab	773
	Finish Floor	19
	Partition	140
	Total Floor Weight	1793 kips

Total Building Weight = 134,069 kips

4.3.3 Modeling Considerations for Reinforced Concrete. Reinforced concrete is a nonhomogenous material which is normally placed monolithically. This results in the

following modeling considerations, which are necesaary considerations for working with reinforced concrete.

4.3.3.1 Finite Width Joints Because of the size of the beam and column members, the clear span of the beams and columns can be reduced significantly. This stiffens the structure. The program accounts for this condition by the inclusion of rigid offsets on the ends of the frame elements. There is no bending or shear deformation within the rigid offset which extends from the centerline of the joint to the face of the support. It is possible that the use of rigid offsets may stiffen the structure too much, since deformations do occur in the joint region. To account for this behavior, the program includes a rigid joint reduction factor which reduces the length of the offset, thereby reducing the joint stiffness and approximating the deformation that occurs in the joint region. Analyses based on the centerline to centerline dimensions are identified as having zero width joints.

4.3.3.2 Effective Beam Section Initially, monolithic slab and beam construction results in a tee section for the beams, with the flange having the slab thickness and effective width specified by ACI [39] to be equal to the smaller of the following: (a) eight times the slab thickness on each side of the beam plus the web width, (b) one fourth the beam span, or (c) the beam spacing. Under service loads, cracking occurs in the concrete, causing sections under negative moment to act as rectangular sections and sections under positive moment to continue to act as a tee section. Furthermore, the cracking that occurs at certain sections along the beam span reduces the properties of these sections from those of the gross section to those of the cracked-transformed section used in working stress analysis, and this results in a beam of variable cross section whose effective section is somewhere between the gross

and cracked-transformed values, depending on the force level. Use of the cracked-transformed section for the entire beam span represents a lower bound on the beam stiffness.

4.3.3.3 SAP90 Models The above modeling considerations were incorporated in different SAP90 models of the Y Building which are identified in the following manner:

Model 1 - Finite width joints, tee beams, gross section properties.

Model 2 - Finite width joints, rectangular beams, gross section properties.

Model 3 - Finite width beam and zero width column joints, rectangular beams, gross section properties.

Model 4 - Zero width joints, rectangular beams, gross section properties.

Model 5 - Finite width joints with 50% reduction factor, rectangular beams, gross section properties.

Model 6 - Finite width joints, average cracked, transformed section properties considering tee section at center and rectangular section at supports.

Model 7 - Finite width joints with 50% reduction factor, average cracked transformed section properties considering tee section at center and rectangular section at supports.

4.3.4 Modal Analyses. The results of the modal analyses of the various building models listed above are summarized in Table 4.1. Here it can be seen that Model-1, which uses finite width joints and tee sections for the beams and girders, gives the best approximation of the results measured in the ambient and small amplitude forced vibration tests: however, this model is still more flexible than the actual structure. At the time of the ambient tests,

the structure was unoccupied and the vertical loading was largely due to the self weight of the structural members. Since the lateral deformations were quite small, the tee sections of the girders were considered to be effective in both tension and compression. Also, the mass of the structure was reduced to represent the condition of the structure at the time of the tests.

The building has experienced several small earthquakes since its completion and has most recently been subjected to the ground motion from the Loma Prieta earthquake. This has caused some cracking in the concrete members, which is to be expected under service loads. Consequently, the periods of vibration of the structure have lengthened as indicated by the recorded values given in Table 4.1. When cracking occurs, the effective section of the girders under negative moment becomes a rectangular section, and under extensive cracking the effective section is reduced from the gross section to the cracked-transformed section. For these reasons, models considering rectangular sections and various joint rigidities were considered.

Model-6 incorporates an estimate of the moment of inertia of the cracked, transformed section. This was done by calculating the moment of inertia of the cracked transformed section at the two ends of the member and at midspan. The average value used in the computations was obtained by averaging the two end values (negative moment) and then averaging this value with the midspan value (positive moment). As can be seen from Table 4.1, this model tends to overestimate the recorded period, indicating that the amount of cracking was not as extensive over the entire building as assumed in the model.

Model-7 considers the cracked transformed section in combination with a 50% reduction factor in the stiffness of the rigid, finite width joint size. This model estimates the stiffness of the structure just prior to or just at the initiation of yielding of the reinforcing steel and gives an estimate of the upper bound of the period. The models which produce the best estimates of the recorded periods are Model-3, Model-4, and Model-5. Models 3 and 4 give a better estimate of the first mode (N-S) and Model 5 gives a better estimate of the second mode (E-W). Model-3 represents the effect of cracking by the convenient use of the rectangular section and the zero width joint. However, it is recognized that the use of a zero width joint and a rectangular cross section is an oversimplification.

These results illustrate the complexity involved in developing an analytical model for the analysis and design of a reinforced concrete structure. For this building, the period has increased from a value of 1.77 seconds in the "as built" condition to 2.69 seconds during the moderate response to the Loma Prieta earthquake, an increase of 52%. Calculations shown for Model-7 indicate that the period of this structure could lengthen to approximately 3.15 seconds with little or no yielding of the reinforcing steel. In this case the period has increased by a factor of 1.8 with a corresponding decrease in the stiffness by a factor of 3. The above discussion clearly illustrates the uncertainty that designers must consider in predicting the seismic behavior of a reinforced concrete structure. The actual stiffness of members, their connections and supports can vary significantly and have a significant effect on the overall response. This also indicates the importance of recorded response data for evaluating the dynamic characteristics of actual buildings.

The deformed plan shapes for the first three modes are shown in Figs. 4.14, 4.15 and 4.16. The translational mode in the north-south (Y) direction is shown in Fig. 4.14. Here it can be seen that this is a translational mode that has some torsional component due to the asymmetry of the geometry which is accentuated by the mezzanine slab in the west wing. The translational mode in the east-west (X) direction is shown in Fig. 4.15. Here the structure is almost symmetrical about the east-west (X) axis and the displaced shape is almost pure translation. The third mode, shown in Fig. 4.16, is a torsional mode which is readily apparent from the displaced shape.

4.3.5 Dynamic Response Analysis. Using the accelerations recorded on the ground floor in the north wing as input, the time-history response of the model was evaluated. In these analyses, **accelerations recorded in the north-south (Y) and east-west (X) directions were applied simultaneously to the model**, and the dynamic response calculated using the modal time-history approach. On the basis of the results of the studies conducted using the simplified model and the UBC requirement that at least 90% of the total reactive mass participate in the response, fifteen modes of vibration (five transverse modes in each principal direction and five torsional modes) were used in the dynamic analyses. **In order to evaluate better the comparison between the frequency content of the recorded and the calculated floor accelerations,** floor response spectra were generated for both motions. This was done by passing the recorded floor accelerations through a SDOF oscillator and generating a response spectrum with 5% of critical damping. Similarly, the floor accelerations which were calculated using the 3-D finite element model were passed through the SDOF oscillator, generating another floor response spectrum. These spectra were then plotted on the same tripartite graph for comparison. Initially the damping in the structure was assumed to be 3%

in all modes. Because of its reasonable accuracy in estimating the periods and its overall simplicity, Model-3 was used for the comparison of calculated versus recorded response. Results using either Model-4 or Model-5 would probably give better comparisons in some cases and worse in others.

The roof spectra in the east-west direction are shown in Fig. 4.17. Here it can be seen that while there is a good match between the recorded and calculated spectral values for the range of period of interest, the calculated results tend to fall above the recorded values. This response comparison can be improved by a slight increase in the amount of damping. It is also of interest to note that the peak response occurs at a period of approximately 1.0 seconds which is the fifth mode of vibration or second mode in the X direction. The peak due to the first mode occurs at about 2.6 seconds but is much smaller. The corresponding acceleration time-history at the roof level is shown in Fig. 4.18. Here it can be seen that the match is quite good with regard to frequency and that only the magnitude of some of the acceleration peaks tend to be higher than the recorded values.

If the modal damping in the 3-D model is increased to 5% in all modes, the spectra shown in Fig. 4.19 are obtained for the calculated acceleration at the roof level. Here it can be seen that the match is much better with respect to the amplitude of the maximum responses. However, this figure also indicates that the percentage of critical damping may be even higher in the higher modes. A similar result can be seen in Fig. 4.20, which shows the corresponding time-histories at the roof level. This indicates that the damping determined from the dynamic response analysis is higher than that obtained from a Fourier analysis of the recorded motion (Table 3.3). In performing the Fourier analysis, assumptions must be

made about the characteristics of the filters and the amount of smoothing used to process the records. These assumptions will affect the amount of damping obtained from the analysis and, therefore, the higher value obtained from the response analysis is thought to be more representative of the actual damping in the structure. The time-history displacement response at the roof level is presented in Fig. 4.21. Here it can be seen that the recorded value is about 9 inches whereas the calculated value is about 10 inches.

In order to evaluate the relative importance of earthquake motions in the N-S and E-W directions, the seismic energy input to the structure in these two directions was evaluated. This was done by considering the product of the recorded base displacement and the developed base shear. In incremental form this is expressed as

$$\text{Input Energy} = \sum V \times \Delta v_g \qquad (4.3)$$

The time-history of the base shear in the E-W (X) direction is shown in Fig. 4.22 and the corresponding values for the N-S (Y) direction are shown in Fig. 4.23. Here it can be seen that the maximum base shear in the E-W (X) direction is approximately 8000 kips compared with only 4500 in the N-S (Y) direction. The dominance of the E-W (X) direction is also shown in the time-history of the input energies shown in Fig. 4.24, which indicates that the input energy in the E-W (X) direction is almost 2.5 times that in the N-S (Y) direction. This indicates that the main response of this structure will be in the E-W (X) direction although the fault rupture occurred in a predominately N-S (Y) direction.

The floor slab of this building was modeled as a rigid floor diaphragm using the master-slave option in SAP90. This eliminated the need to model the slab using plate elements and

thereby reduced the complexity of the model and the number of degrees of freedom. The mass of a story level is lumped at the master node which was located at the center of the core structure. For this reason, the time-history comparisons are made between this master node and the instrument located nearest the core region of the structure.

The data recorded on channel 13 (N-S) in the core region of the 13th floor are compared with the calculated results in Figs. 4.25 (a), (b) and (c). The acceleration response is shown in Fig. 4.25 (a), the displacement response in Fig. 4.25 (b) and the calculated floor spectra in Fig. 4.25 (c). Here it can be seen that there is good correlation between the calculated and recorded values with a maximum acceleration of 0.27g and a maximum displacement of 2.5 inches at this level. Similar data for channel 14 (E-W) are shown in Figs. 4.26 (a), (b) and (c). In this direction the maximum recorded acceleration was 0.30g and the maximum recorded displacement was 4.3 inches although the calculated value reached 5.0 inches.

The data recorded on channel 9 (N-S) at the 21st level are compared with the calculated values in Figs. 4.27 (a), (b) and (c). The accelerations, shown in Fig. 4.27 (a), have a maximum value of 0.2g, and the recorded displacement, shown in Fig. 4.27 (b), has a maximum value of 4.0 inches, which in this case is significantly larger than the recorded value. The floor spectra, shown in Fig. 4.27 (c), do not agree as well as in the previous case at the 13th level. Similar data for channel 15 (E-W) are shown in Figs. 4.28 (a), (b) and (c). As shown in Fig. 4.28 (a), the maximum recorded acceleration is 0.25g while the maximum calculated value is 0.22g. The maximum recorded displacement, Fig. 4.28 (b), is 4.5 inches which is almost the same as the calculated value of 4.4 inches. The floor spectra given in Fig. 4.28 (c) are also in better agreement than in the N-S direction.

The data recorded on channel 7 (N-S) at the roof level are compared with the calculated values in Figs. 4.29 (a), (b) and (c). The accelerations, shown in Fig. 4.29 (a) have a maximum recorded value of 0.24g compared with a maximum calculated value of 0.31g. Corresponding values for the displacement, presented in Fig. 4.29 (b), are 2.9 inches recorded and 3.2 inches calculated. Agreement between the floor spectra, shown in Fig. 4.29 (c), is not good between the period range of 0.4 second and 1.5 seconds. Data for channel 8 (E-W) is shown in Fig. 4.30 (a), (b) and (c). At this level, the maximum recorded acceleration is 0.32g compared with a calculated value of 0.44g as seen in Fig. 4.30 (a). The maximum recorded displacement as shown in Fig. 4.30 (b) is 8.6 inches compared with the calculated value of 10.1 inches. Good agreement is obtained between the floor spectra calculated for these two motions as seen in Fig. 4.30 (c).

4.3.6 Static Lateral Force Analysis (1979 UBC). The design is based on the 1979 edition of the Uniform Building Code [40], with the lateral force requirements supplemented by the use of site specific design response spectra. The dynamic response spectrum analysis will be discussed in detail in a later section. Lateral forces specified in building codes are defined in terms of base shear and have the general form:

$$V = C_s W_e \tag{4.4}$$

where C_s is the design seismic resistance coefficient and W_e is the weight of the reactive mass (total seismic dead load in this case). In the 1979 edition of the code, the base shear is given by the expression

$$V = (ZKCIS)W \tag{4.5}$$

The fundamental period of vibration can be estimated as T = 0.1N, which in this case results in a period of T = (0.1)(31) = 3.1 seconds.

$$C = \frac{1}{(15\sqrt{T})} = 0.038 \tag{4.6}$$

Because of the relatively soft soil conditions at the site (Bay Mud), the soil coefficient was taken as S = 1.5. The remaining coefficients are the framing factor, K = 0.67, the occupancy importance factor, I = 1.0 and the seismic zone factor, Z = 1.0. Using these values, the base shear in terms of the weight is estimated to be

$$V = (1.0)(0.67)(0.038)(1.0)(1.5)*W = 0.038W \tag{4.7}$$

The total dead weight of the structure is estimated to be 134,069 kips which results in a base shear of V = 5119 kips. Since the period is greater than 0.7 second, a portion of the base shear must be applied at the roof to account for the effect of the higher modes of vibration. This concentrated load is given as

$$F_t = 0.07TV = 1111 \text{ kips} \tag{4.8}$$

The remaining base shear which will be distributed over the height of the structure is

$$V - F_t = 4008 \text{ kips} \tag{4.9}$$

The lateral displacement analyses of the model under lateral seismic and wind loads specified by the 1979 Uniform Building Code are presented in Figs. 4.31 and 4.32, respectively. The lateral displacement in the E-W (X) direction due to code seismic load is shown in Fig. 4.31 where it can be seen that the maximum deflection at the roof level is 9.71 inches. In this case the code loads have been increased by the factor 1/K = 1.49 for use in the displacement

analysis. The displacement under wind loads, shown in Fig. 4.32, has a maximum value of 2.2 inches at the roof level. This clearly indicates that the seismic load is the controlling lateral force for this structure.

4.3.7 Design Response Spectra Analyses. The design criteria for this structure are described by Tai, Yang and Lin [4] and have already been discussed in section 2.3.1. The design spectra are taken as representative of the free-field motion that might occur at the site under the MPEQ or MCEQ. In order to account for a reduction of the free-field motion at the base of the structure due to interaction effects, the members were designed to remain elastic for 80% of the maximum probable design spectrum (MPDS) and the structure was designed to avoid major damage and collapse for 80% of the maximum credible design spectrum (MCDS). These two free-field spectra are compared with the 1979 UBC requirements in Fig. 4.33.

In order to perform a comprehensive design response analysis of the building, a mathematical model of the structure was developed for use with the ETABS [41] program. This program is more design oriented and has the following features which were essential for this part of the investigation:

1. Envelopes of maximum story displacement, maximum interstory drift, maximum inertia force and maximum story shear are output as part of the dynamic analysis.

2. A post processor program, CONKER, is available to perform the following analyses:

(a) The capacity of the columns is checked against a three-dimensional interaction curve which considers the effect of axial load and moments about the two principal axes.

(b) Critical positive and negative moments in the beams resulting from various loading conditions are summarized. However, the program does not check the capacity of the beams.

An isometric view of the ETABS model is shown in Fig. 4.34. It can be seen that this model looks almost exactly the same as the SAP90 model except that the shear walls in the bottom two floors are clearly visible. This is due to the use of an isoparametric finite element to model the walls in ETABS as compared to a column element in SAP90. A plan view is shown in Fig. 4.35 indicating the location of the base shear walls. An elevation looking in the E-W (X) direction is shown in Fig. 4.36 and a similar view in the N-S (Y) direction is shown in Fig. 4.37. Here again, the walls in the bottom floors are readily apparent. An isometric view of the lower two floors is shown in Fig. 4.38. Here the location of the walls can be clearly seen along with the location of the mezzanine floor. Gravity loads on a typical floor are input as uniformly distributed beam loads as shown in Fig. 4.39.

In order to validate the ETABS model, critical comparisons were made with the response data obtained from the SAP90 model. The periods for the first nine modes of vibration are compared in Table 4.2. These nine modes represent 87.5% of the participating mass in each direction. A plan view showing the displaced shape of the first mode is shown in Fig. 4.40. This indicates that the first mode is almost a pure translational mode in the N-S (Y) direction.

The displaced shape of the second mode, shown in Fig. 4.41, indicates that this mode is a translational mode in the E-W (X) direction. The displaced shape of the third mode, shown in Fig. 4.42, indicates that this is primarily a torsional mode.

Envelopes of maximum lateral displacement are shown in Fig. 4.43. One pair of values compares the ETABS solution with the SAP90 solution under the static lateral forces required by UBC 1979. The other pair of curves compares the results obtained using a dynamic time-history analysis for the recorded base motion. As can be seen in this figure, the differences between the results obtained from these two computer programs are very small. In addition, a comparison of the code versus the recorded base results indicates that the displacement response for this building due to this earthquake is very near the code requirement. The dynamic response curves also indicate that the higher modes are beginning to influence the maximum displacement envelopes above the 16th story level.

When performing a response spectrum analysis, the method of combining the modal responses must be selected. Two common means of doing this are the square root of the sum of the squares (SRSS) method and the complete quadratic combination (CQC) method. The SRSS method has been shown to give a good approximation of the actual response for two-dimensional structural systems. However, for three-dimensional systems and particularly those systems that have closely-spaced modes in two orthogonal directions, the CQC method has been shown to give improved estimates of actual response [42]. The effects of using these two methods for this structure are presented in terms of the story shears in Fig. 4.44. Here, it can be seen that use of the CQC method results in an increase in the story shear of approximately 17% for the maximum probable spectrum and approximately 22% for the

maximum credible spectrum. In the following computations, the CQC method will be used to combine modal responses.

The effect of using a 2-D model to evaluate the story shears in each of the principal directions is shown in Figs 4.45 and 4.46. The story shears in the E-W (X) direction for the MPDS and MCDS are shown in Fig. 4.45. The values obtained from the 3-D model are identified as 3-D and those obtained by constraining the displacements to the E-W (X) direction are identified as X. It can be seen that adding the constraint causes a slight increase in the story shears, but this increase is very small. Therefore it is concluded that with the proper 2-D model, the story shears can be accurately estimated in the E-W (X) direction. A similar result is shown in Fig. 4.46 for the N-S (Y) direction. Comparing these two figures also indicates that the story shears in each direction are almost identical. Recall that the periods of vibration in these two directions are also quite similar.

A plan view of the displaced shape in the E-W (X) direction under code lateral forces is shown in Fig. 4.47. A similar plot for forces acting in the N-S (Y) direction is shown in Fig. 4.48. In both cases the deformation is almost pure translation with the maximum deflections being approximately equal in each direction.

Recorded acceleration time-histories during four recent strong motion earthquakes are shown in Fig. 4.49. Linear elastic response spectra for these earthquakes are compared with the design criteria which includes CODE, MPDS, and MCDS in Fig. 4.50. The UBC 1979 is the building code used for the design of the structure, whereas UBC 1988 represents the normalized design spectrum for a soft soil site contained in the current code, with Z = 0.4,

I = 1.0, S = 1.5, and R_w = 1.0. The maximum probable and maximum credible spectra are the site specific design spectra used for the building design. Considering a building period of 2.7 seconds, it can be seen that the seismic coefficient specified in the 1979 UBC is about half of the spectral acceleration recorded at the site (Emeryville). This would imply that had the building been designed for the minimum lateral forces specified in the code, there would have been considerably more damage.

It is interesting to note that the spectral acceleration for the MPDS is greater than that recorded at the site for a period of 2.7 seconds. This indicates that during the Loma Prieta earthquake most of the members should have responded in an elastic manner since this was the original design criteria. Considering the second mode in the E-W direction which has a period of 0.96 second, it can be seen that the spectrum from the recorded motion exceeds the design criterion by about 100% (the spectrum for the motion at the site indicates that the base motion has a strong component at a period of 0.75 second). As has been shown in the response comparisons presented previously, this recorded motion tends to excite the second mode response of the building in the E-W direction.

The Hollister ground motion was recorded close to the epicenter of the Loma Prieta earthquake [48 km (29.8 miles) southeast], with the strongest motion in the N-S direction. It can be seen that this record has a very high spectral acceleration at a period of 0.8 second (second mode in the E-W direction); however, the spectral acceleration drops off considerably at a period of 2.7 seconds (first mode in E-W direction) although it is above the MPDS. The Hachinohe record was recorded in the coastal city of Hachinohe, Japan. Although this record has a peak acceleration of only 0.19g, it can be seen that its spectrum exceeds the MPDS

between 0.6 and 1.5 seconds and between 2.0 and 3.1 seconds. These are the period ranges that contain the first two modes of vibration in each direction.

The James Road record which was obtained during the October 15, 1989 Imperial Valley earthquake, was recorded close to the fault [approximately 10 km (6.2 miles)] north of the epicenter, and has a maximum velocity of 37.6 in./sec (95.5 cm/sec). As can be seen from the response spectrum, this motion has a high spectral acceleration at 2.7 seconds (first mode) and also at 1.0 seconds (second mode in E-W direction). Considering the first mode, the spectral acceleration of 0.47g is 235% greater than the 0.14g of the MPDS and 52% greater than the 0.31g of the MCDS. This would indicate the probability of considerable inelastic deformation in the frame since the design criteria for the MCDS were a ductility demand of four in the beams and a ductility demand of 2 in the columns [4].

The envelopes of maximum lateral displacement based on elastic response are shown in Fig. 4.51. As mentioned earlier, the displacement response to the recorded motions closely approximates that specified in the code and is less than that required by the MPDS. This strongly suggests that the response of the building for this earthquake was predominately elastic. The displacement response for the Hollister motion falls between the MPDS and MCDS requirements. For this motion some inelastic deformation would be expected but it should be less than the design requirement of the MCDS. The increased displacement above the 21st floor shows the effect of the strong spectral acceleration in the second mode (east-west direction) for this ground motion.

Finally, the time-history analysis for the James Road motion results in an elastic deformation of 50 inches at the roof level which is clearly quite high. It should also be noted that the 1979 UBC required that framing elements that are not part of the lateral force resisting system shall be shown to be adequate for 3/K times the distortions resulting from the code required lateral forces. This requirement was equivalent to the displacement requirement for a maximum credible earthquake. Multiplying the 1979 UBC displacements, shown in Fig. 4.51, by 3.0 results in a maximum roof displacement of 28 inches which compares well with the response of 31 inches due to the MCDS and is greater than the 24.5 inches obtained from the Hollister ground motion.

The envelopes of maximum interstory drift indices are shown in Fig. 4.52. These results indicate that the interstory drift indices due to the recorded ground motion exceed the code requirement, particularly in the upper stories. In fact, the interstory drift indices in the upper stories (17-31) exceed even those required by the MPDS. This might imply that some minor damage to the non-structural components in the upper stories occurred during the Loma Prieta earthquake. It can also be seen that there is a bulge in the interstory drift envelope just above the 18th floor. A similar but more pronounced bulge appears in the same region for the MCDS, and for the Hollister and James Road recorded motions.

There are two factors which contribute to this behavior: (a) there is a change in column section at the 19th floor, and (b) this building has a high second mode response which is accentuated by the high spectral accelerations for this mode in both the Hollister and James Road records. The other bulge in the interstory drift curves occurs at the top of the second floor and this indicates the stiffening effect of the shear walls that extend from the base to

this level. The maximum interstory drift index of over 2.2% under the James Road record is extremely high. Story drifts of this order are getting close to the maximum rotation that can be expected to be available from well-detailed beam to column connections.

The envelope of maximum story shears is shown in Fig. 4.53. Here it can be seen that the 1979 UBC requirement is clearly a minimum. The story shears due to the MPDS tend to approximate those due to the motion recorded at the site. However, the strong contribution of the second mode causes the values due to the recorded motion to be higher in the upper floors and lower in the bottom floors. In the upper floors the story shear exceeds the MPDS values by a substantial amount and approaches those of the MCDS. This indicates that in the upper floors, critical members may be close to yield or in fact may have experienced some yielding of the reinforcing steel. A similar type of response can also be seen for the MCDS and the Hollister motion. It seems likely that the Hollister motion would have caused substantial yielding in the upper floors of the building. The James Road motion generates story shears that exceed the others by a substantial margin, being almost nine times greater than the code values at the base.

When the interstory drifts begin to exceed 2%, it is possible that interaction of the axial load with the lateral displacement (P-Δ) may need to be considered in the analysis. The influence of the P-Δ effect on the lateral displacement envelopes is shown in Fig. 4.54. From this figure it is clear that even under the James Road record the P-Δ effect is small.

The relative damage potential of these earthquake ground motions with respect to this building can be evaluated by considering the input energy. As mentioned previously, the

input energy is calculated by summing the product of the base shear and the incremental base displacements. The time history of input energy is shown in Fig. 4.55 for an elastic system. Here, the effect of the James Road record on this building is readily apparent, being four times that of Hollister and twenty-two times that of Emeryville. This clearly indicates that the ground motion due to the Loma Prieta earthquake was not a severe test for this building. The time history of the base shears is shown in Fig. 4.56 and the corresponding time history for the base displacement is shown in Fig. 4.57. It can be seen that the ground displacements recorded at Emeryville during the Loma Prieta earthquake are small (approximately 4 inches or less), whereas the maximum displacement recorded at James Road during the Imperial Valley earthquake is over 30 inches.

4.4 LINEAR ELASTIC ANALYSES CONDUCTED BY THE KAJIMA TEAM

4.4.1 General Remarks. It has been shown [1] that although the U.S. and Japanese seismic codes for buildings base their design recommendations for the extreme level of earthquake safety (or survival) on the same peak ground acceleration (0.4g), the design forces specified by the Japanese code for this level of motion are considerably higher than those specified by the U.S. codes. Therefore, it was considered important to study the behavior of the Y Building with regard to the **Japanese Seismic Design Methodology**. Such a study was conducted by a team of researchers from Kajima.

4.4.2 Research Objectives of the Kajima Study. The objectives of the study conducted by the Kajima research team were the following: (1) to analyze the U.S. designed Y Building according to typical "Japanese Seismic Design Methodology"; (2) to compare the calculated response with that of a typical Japanese RC building with particular emphasis on differences

in the use of the ductility and drift concepts; and (3) to identify and/or clarify the main differences between the U.S. and Japanese seismic design methodologies and resulting designs.

4.4.3 Scope of the Kajima Studies. To accomplish the above objectives, the Kajima researchers conducted linear elastic and nonlinear (inelastic) analyses of the Y-Building using a 3-D frame model. The model was developed from the same drawings and information that were used by the U.S. researchers. The studies followed the flow chart illustrated in Fig 4.58. In accordance with this chart, the first step involved the development of a 3-D Linear Elastic Vibration Model. Once this model was established, different response analyses were conducted following the procedure described below:

Step 1. The 3-D elastic model was used to perform the following analyses: static analysis for what is considered to be the design seismic service load; modal analysis for natural periods and mode shapes; and response analysis for service ground motions scaled to a maximum ground velocity of 25 cm/sec.

Step 2. Based on the results of the static analysis, a simplified, equivalent bending-shearing, cantilever model was developed. The natural periods and vibration mode shapes of this model were compared with those of the 3-D elastic model and shown to agree well.

Step 3. Considering the flexural cracking and the yielding of the reinforcing bars, the elastic-plastic characteristics were estimated for the beams and columns. On the basis of these

estimations, the nonlinear restoring force characteristics were set up for the shearing deformation of each frame which was expressed as the bending-shearing element.

Step 4. Using the simplified nonlinear 3-D model, the earthquake response analyses for selected ground motions scaled to a maximum velocity of 50 cm/sec. were conducted. On the basis of the results obtained from these analyses, the seismic safety of the building was evaluated.

In this chapter, only the results obtained from the linear elastic analyses are summarized, discussed and compared with the results obtained by the U.S (CUREe) researchers. The results obtained in the nonlinear analyses are discussed in detail in the next chapter.

4.4.4 3-D Linear Elastic Model. The 3-D linear elastic model is based on the following assumptions and discretizations:

(1) The mass of the structure is lumped at the story levels resulting in a 31-lumped mass model which is fixed at the ground level.

(2) In developing the member stiffness matrix, bending, shearing, and axial deformation were considered for the columns, bending and shearing deformation for the beams and shearing deformation for the joint panel between the beams and columns. Shear walls were represented by equivalent brace members.

(3) Each floor level has three degrees of freedom; two translations and a rotation about a vertical axis. Story elements are linked together by a rigid floor diaphragm. Details of the 3-D frame analysis method are given in Appendix 4.1.

4.4.5 Mechanical Characteristics and Ground Motions.

4.4.5.1 Estimation of Reactive Mass. The estimated weight of the reactive mass at each floor level is summarized in Table 4.3. When these weights are compared with those estimated by the U.S. researchers, some minor differences can be seen (132,500 kips vs. 134,069 kips). These differences are mainly due to the manner of estimating the reactive weight of the partitions and the fact that the Japanese code (BSL) requires that part of the live load be included in the reactive mass (see footnote for Table 4.3).

4.4.5.2 Seismic Design Forces at Service Level. According to the BSL, the static equivalent lateral base shear for this type of building is based on a total base shear coefficient of 0.10. The distribution of the total base shear along the height of the building is given in Table 4.3. When these design forces are compared with those specified by the 1979 UBC at the time the building was designed or those required by the more recent 1988 UBC, it can be seen that the total base shear required by the BSL is about 2.5 times larger.

4.4.5.3 Ground Motions and Damping. The five earthquake records shown in Table 4.4 were selected as the typical input ground motions for seismic design in Japan. The acceleration time-histories of these records are shown in Fig. 4.59, and the acceleration response spectra are shown in Fig. 4.60. A viscous damping coefficient of 3% of critical was adopted for the vibration of the model in the first mode.

4.4.6 Results of Linear Elastic Analyses. The values of the natural periods and the dominant directions of each mode of vibration of the 3-D linear elastic model are shown in Table 4.5. The mode shape and natural period corresponding to each of the first nine modes, normalized by its participation factor are shown in Figs. 4.61 through 4.69. These figures show that the torsional modes are very small.

Results of the seismic response analyses of the 3-D model when subjected to the earthquake ground motions of Table 4.4 are summarized by the plots of Figs. 4.70 to 4.73. From these figures it is clear that except for a few upper stories, the maximum story shears in the E-W (X) direction as well as in the N-S (Y) direction are developed by the El Centro ground motion (scaled PGA = 0.21g) and the Hachinohe ground motion (scaled PGA = 0.115g). The interstory drift indices, shown in Fig 4.73, start to increase significantly at the third story level (at the end of the base shear walls) and again at the nineteenth story, reaching their peak values at the 21st and 22nd stories. At the 19th story there is a change in column and beam dimensions. These changes together with the significant participation of the 4th and 5th modes are the main reasons for this increase. The interstory drift index at the 22nd story reaches a value larger than 1/200, which is considered to be unacceptable according to Japanese practice. Thus the Kajima researchers concluded that the rigidity of the upper stories does not seem adequate when compared with that of typical Japanese RC tall buildings.

4.5 COMPARISON OF U.S. AND JAPANESE DESIGN CRITERIA

4.5.1 General Remarks. The building code used in the design of the Y Building was the 1979 UBC. However, the designers wisely decided to use site specific design response

spectra and dynamic spectral analysis procedures to determine the lateral force requirements. The minimum lateral force requirements of the 1979 UBC have been discussed in an earlier section (see Figs. 4.51 to 4.53). Therefore, in this section, emphasis will be placed on the requirements of the 1988 UBC*, the site design spectra and the Japanese Code (BSL). The Japanese requirements consider two levels of earthquake motion, one having a peak velocity of 25 cm/sec and the other having a peak velocity of 50 cm/sec. These two levels are similar to the maximum probable earthquake and the maximum credible earthquake used in the design of the Y Building, with the exception that **the structure is expected to have a displacement ductility of less than unity for both levels of earthquake under the Japanese code.** This requirement allows cracking of the concrete but only limited yielding of the steel reinforcement. This will be discussed in detail in the next chapter which considers inelastic behavior.

In the figures that follow, Figs. 4.74 to 4.76, the maximum probable and maximum credible spectra are the free-field site spectra used in the design of the Y Building. The UBC 1988 spectrum, which is the normalized response spectrum specified in the code for the dynamic lateral force procedure for soft to medium clays and sand soil conditions, is taken as representative of the MCDS. This spectrum, arbitrarily scaled by 0.5, is taken as representative of the maximum probable condition. **Note that both spectra are not reduced by the structural system coefficient, R_w.** The two earthquake time-histories normalized to

*It should be noted that the 1988 edition of the UBC is the first edition that, because of the height of the Y Building (309'>240') and its irregularity, requires that this building be designed using lateral dynamic procedure.

a maximum velocity of either 25 cm/sec or 50 cm/sec are representative of current Japanese design practice.

4.5.2 Maximum Lateral Displacement. The envelopes of maximum lateral displacement are shown in Fig. 4.74. Here it can be seen that the displacements due to the MPDS envelop those of the normalized El Centro motion. However, the same is not true for the normalized (25 cm/sec) Hachinohe motion. The MPDS produces a good estimate of lateral displacement in the lower half of the building but the Hachinohe motions exceed those of the MPDS in the upper half. This is due to the fact that the MPDS, as far as its frequency (period) content, is a rather narrow band spectrum (see Figs. 4.33 and 4.50). The stronger input of the Hachinohe record at the 4th and 5th modes (0.95 second) of the building has increased the response in the upper floor levels. The UBC 1988 spectrum for soft soil (S=1.5) has a broader band and if scaled by 0.5, the resulting displacements envelop the time-history responses normalized to 25 cm/sec at all story levels.

The Hachinohe record normalized to 50 cm/sec closely approximates the displacement requirements of the MCDS. As before, the one exception is in the upper floor levels where the higher mode response of the Hachinohe record is not captured by the narrow band MCDS. The displacements due to the 1988 UBC spectrum envelop both time-history responses normalized to 50 cm/sec and also the MCDS. It should be noted that for both levels of earthquake, the normalized El Centro motion results in the least displacement response.

4.5.3 Interstory Drift Index (Story Drift Angle). The envelopes of maximum interstory drift are shown in Fig. 4.75. The results presented here show that in the upper floors (19-31) the interstory drifts due to the MPDS are less than those of the time-history records normalized to 25 cm/sec. As mentioned previously, this is due to the higher mode response which is not estimated accurately in the MPDS. It is also of interest to note that the normalized El Centro motion results in the critical IDI in the upper nine story levels. It can also be seen that the scaled 1988 UBC spectrum does a good job of enveloping the normalized time histories and the MPDS. As mentioned previously (section 4.4.6), Japanese practice limits the IDI for the 25 cm/sec earthquake to 1/200. This figure also indicates that this building does not meet this requirement in story levels 18-26.

Similar results are obtained when considering the time-history motions scaled to 50 cm/sec and the MCDS. It can be seen that the MCDS results in a good estimate of maximum interstory drift in the lower 15 floors but fails to capture the maximum response in the upper floors. As before, the normalized El Centro motion becomes the critical motion for interstory drift in the upper floors. It is also interesting to note that the 1988 UBC spectrum envelopes the normalized time histories at all story levels with the possible exception of floors 28-29, where the comparison is quite close.

4.5.4 Maximum Story Shear. The envelopes of maximum story shear are shown in Fig. 4.76. Here it can be seen that the story shear due to the MPDS is exceeded in the lower six floors (normalized El Centro) and in the upper half of the building (normalized El Centro and normalized Hachinohe). The scaled 1988 UBC spectrum envelops the normalized time history records in the lower 21 stories and gives a reasonable estimate of the shears in the

upper stories. The MCDS results in a good estimate of the story shear in the lower half of the building but is exceeded substantially by the shears due to the normalized El Centro motion in the upper nine stories.

4.5.5 Concluding Remarks. The evaluation of the comparisons given above can be summarized as follows:

1. A relatively narrow band design spectrum which has a peak acceleration at 0.25 second (Fig.4.33) was specified for this soft-soil site. This design spectrum does not accurately represent the seismic input of the possible ground motions that can occur at the building site, such as those recorded during the Loma Prieta earthquake, particularly regarding the exciting of the 4th or 5th mode (0.95 second) which has a significant influence on the response of the upper floors of the building. Improved estimates of the building response are obtained by using the normalized earthquake motions representative of Japanese design practice.

2. The 1988 UBC spectrum with R_w equal to unity results in response envelopes which are similar to those obtained from earthquake ground motions normalized to 50 cm/sec in Japanese practice. Scaling this spectrum by 0.5 results in building response envelopes which are similar to those obtained from the ground motions normalized to 25 cm/sec.

3. Since reinforced concrete cracks at relatively low force levels, a reinforced concrete structure is in fact a weakly nonlinear structural system under service loads. The

analyses have shown that this can result in considerable variation in the dynamic properties of the structure. The effect of the cracks and the contribution of the slabs to the stiffness of the beam and the effective stiffness of beam-to-column joints is also hard to evaluate and can have a significant effect on the mechanical properties. These modeling considerations emphasize the importance of comparing results of analytic studies with recorded building response, as well as the need to consider a band of values for the fundamental periods rather than just a single deterministic value.

4. The CQC method of modal combination must be used for three-dimensional systems having closely spaced modes in two orthogonal directions. This study has shown that the use of the CQC method results in an increase in the story shears of approximately 17% over those from the SRSS for the MPDS.

5. The recorded base motion results in an acceleration spectrum that has relatively high values (exceeding the MCDS) in the period range of 0.9 to 1.5 seconds, which includes the 4th and 5th (2nd mode E-W and 2nd mode N-S) modes of the building. This tends to excite a strong second translational mode response which increases the story shears in the upper floors by as much as 50% over those obtained from the MPDS.

6. Calculations of the input energy for an elastic system indicate that the motions recorded from the Loma Prieta earthquake were not a severe test for the Y Building. Motions recorded nearer the epicenter at Hollister produce an input energy 5.6 times

greater than the recorded base motions, and motions recorded at James Road during the 1979 Imperial Valley earthquake produce an input energy 22 times greater.

7. Studies conducted by the Kajima research team indicate that the upper floors of the building are too flexible and do not meet the requirements of Japanese practice for tall buildings.

8. The results obtained point out clearly the danger of designing a building for site spectra having a very narrow band (i.e., peaking at a certain period, supposedly equal to the predominant period of the soil, T_g). Design site spectra should consider the uncertainties involved in estimating the T of the structure and the T_g of the soil.

Table 4. 1. Modal Analysis Summary

Model	Mode 1 N-S	Mode 2 E-W	Mode 3 Torsion	Mode 4 N-S	Mode 5 E-W	Mode 6 Torsion
AMBIENT TEST	1.77	1.69	1.68	0.60	0.60	0.59
Model-1	2.00	1.99	1.89	0.70	0.70	0.62
Model-2	2.34	2.34	2.16	0.82	0.82	0.72
Model-3	2.65	2.65	2.41	0.94	0.94	0.82
Model-4	2.74	2.73	2.49	0.97	0.97	0.85
Model-5	2.54	2.54	2.32	0.90	0.90	0.78
Model-6	2.91	2.84	2.56	1.02	0.96	0..86
Model-7	3.15	3.08	2.76	1.12	1.05	0.94
RECORDED	2.69	2.59	---	1.07	0.89	---

TABLE 4. 2. Periods of Vibration (Seconds)

(Mode)	1	2	3	4	5	6	7	8	9
ETABS	2.70	2.69	2.44	.964	.960	.842	.520	.518	.477
SAP90	2.74	2.73	2.49	.974	.971	.852	.525	.524	.453

1st Natural Period(sec)= 2.19
Base Shear Coefficient = 0.10

Story	Height (cm)	Weight (ton)	Rotat. Inert. (ton·cm²)	Shear Coef.	Design Load (ton)
31	289.6	1646	7350001660	0.448	737.7
30	289.6	1722	7689998340	0.341	1149.5
29	289.6	1722	7689998340	0.294	1496.5
28	289.6	1722	7689998340	0.265	1807.8
27	289.6	1759	7850000380	0.245	2100.2
26	289.6	1759	7850000380	0.230	2372.7
25	289.6	1759	7850000380	0.217	2628.6
24	289.6	1759	7850000380	0.207	2870.3
23	289.6	1759	7850000380	0.199	3099.3
22	289.6	1759	7850000380	0.191	3316.6
21	289.6	1759	7850000380	0.184	3523.2
20	289.6	1759	7850000380	0.178	3719.7
19	289.6	1759	7850000380	0.173	3906.6
18	289.6	2053	9170001920	0.167	4113.1
17	289.6	2053	9170001920	0.161	4307.7
16	289.6	2053	9170001920	0.156	4490.7
15	289.6	2053	9170001920	0.151	4662.5
14	289.6	2053	9170001920	0.147	4823.5
13	289.6	2053	9170001920	0.142	4973.9
12	289.6	2053	9170001920	0.138	5113.8
11	289.6	2053	9170001920	0.134	5243.6
10	289.6	2053	9170001920	0.130	5363.3
9	289.6	2115	9440002050	0.127	5476.3
8	289.6	2115	9440002050	0.123	5578.9
7	289.6	2115	9440002050	0.119	5671.3
6	289.6	2115	9440002050	0.116	5753.5
5	289.6	2115	9440002050	0.113	5825.6
4	289.6	2115	9440002050	0.109	5887.8
3	289.6	2115	9440002050	0.106	5940.2
2	304.8	2115	9440002050	0.103	5982.7
1	304.8	2115	9440002050	0.100	6015.5
Total	9008.0	60155	268560035830		

Table 4.3 - Weight of reactive mass and code design forces.*

*Weight includes dead load, partition load (100 kg/m²) and live load (600 kg/m² for residential area.

Name		Acceleration		Time
		Velocity =25cm/s	Velocity =50cm/s	
EL CENTRO	1940(NS)	0.261g	0.522g	30 sec
TAFT	1952(EW)	0.253g	0.507g	30 sec
TOKYO101	1956(NS)	0.310g	0.619g	11 sec
SENDAI TH038	1978(EW)	0.169g	0.339g	35 sec
HACHINOHE	1968(EW)	0.115g	0.231g	80 sec

Table 4.4 - Earthquake ground motions selected to check seismic design in Japan

Mode	Natural Period(sec)	Dominant Direction
1	2.19	Y
2	2.19	X
3	1.84	Torsion
4	0.80	Y
5	0.80	X
6	0.64	Torsion
7	0.43	Y
8	0.43	X
9	0.34	Torsion

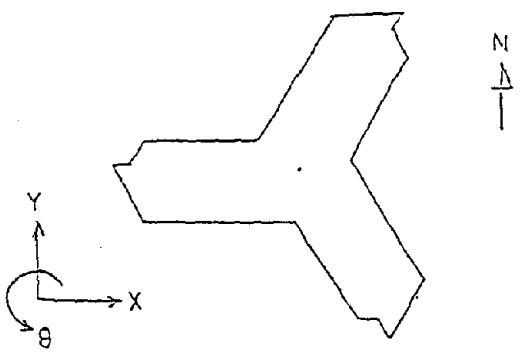

Table 4.5 - Natural period

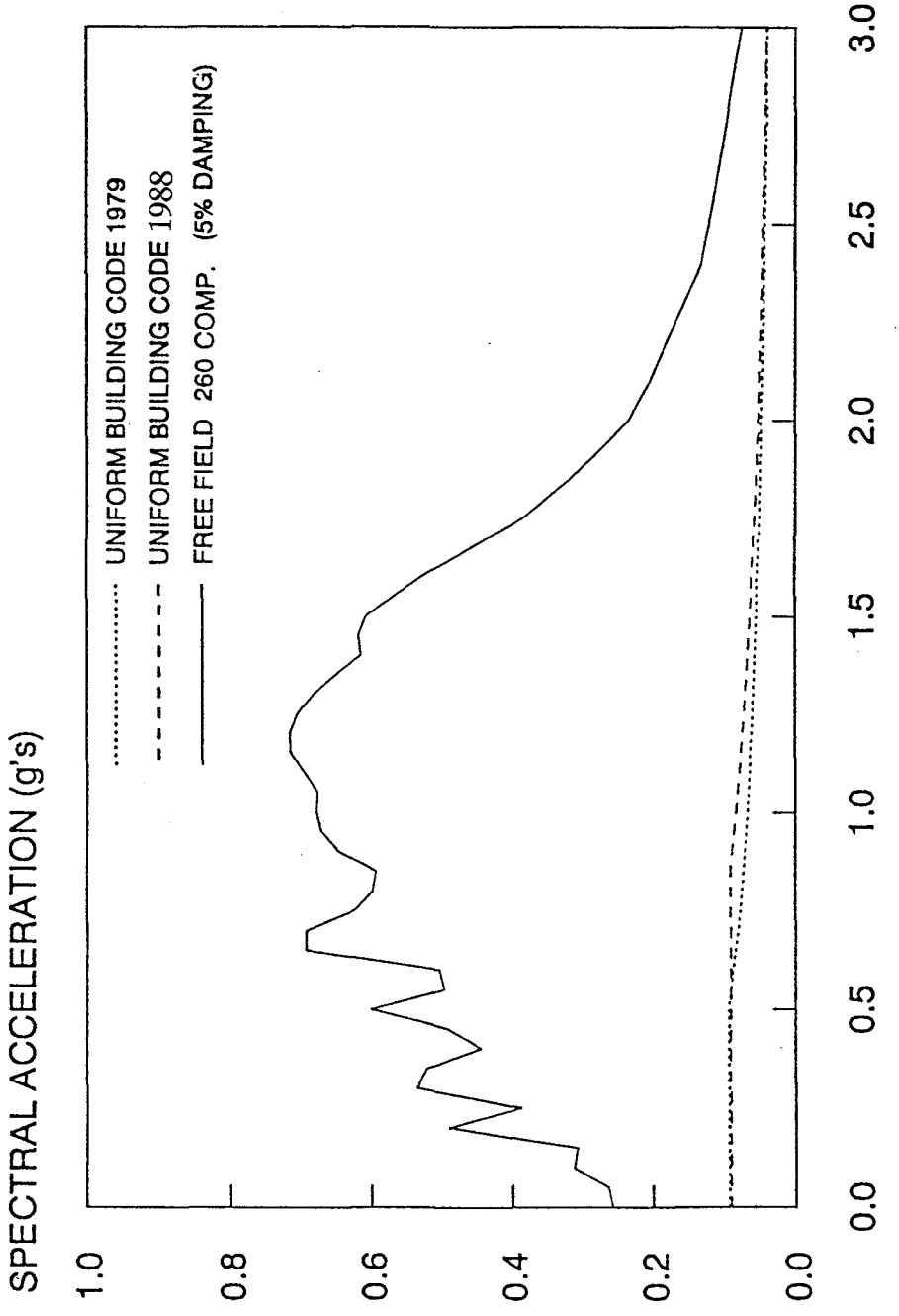

Figure 4.1 - Code vs. recorded response spectra

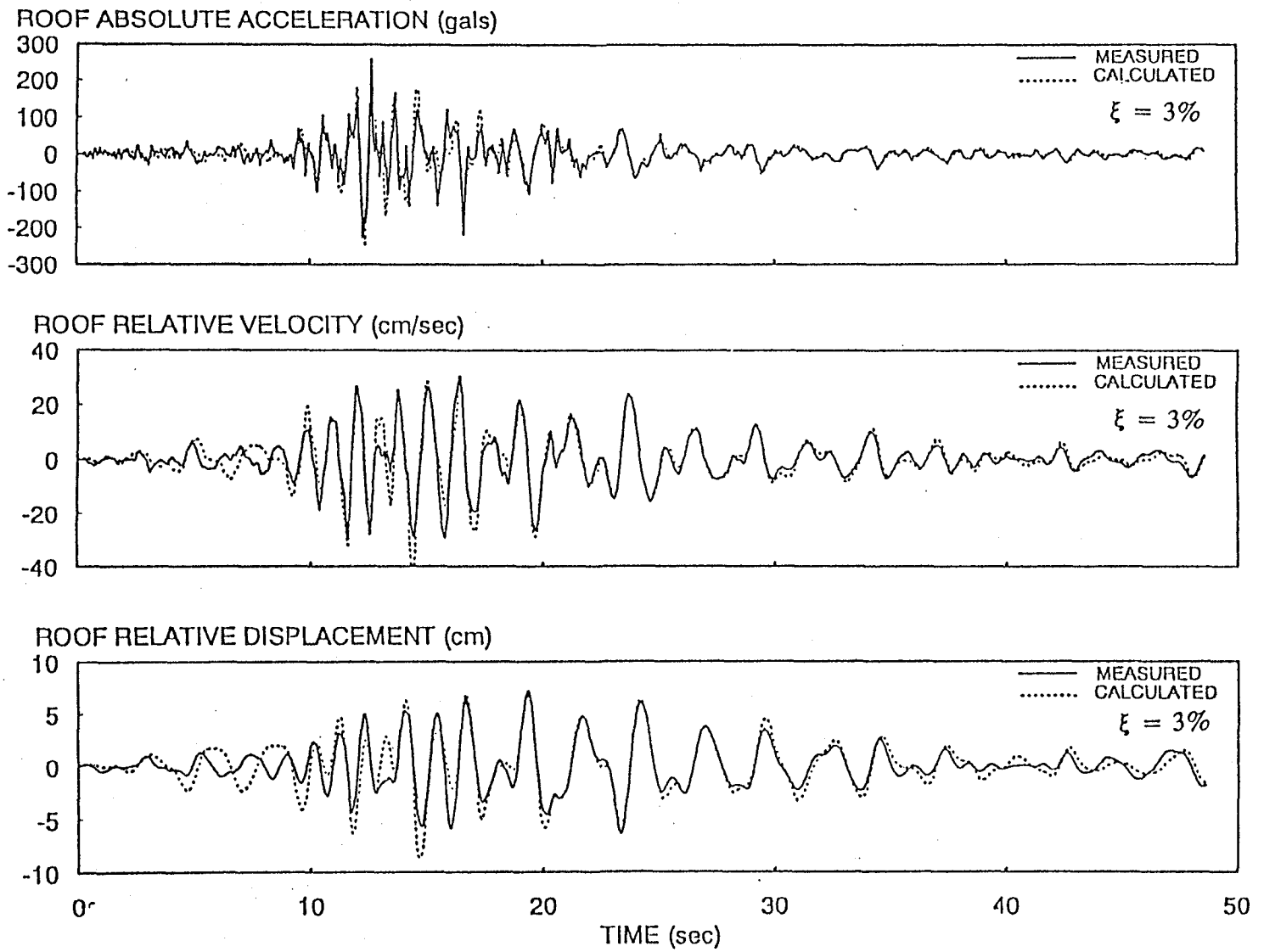

Figure 4.2 - Comparison of measured and calculated (ξ = 3%) response at the roof level of the west wing (350° component)

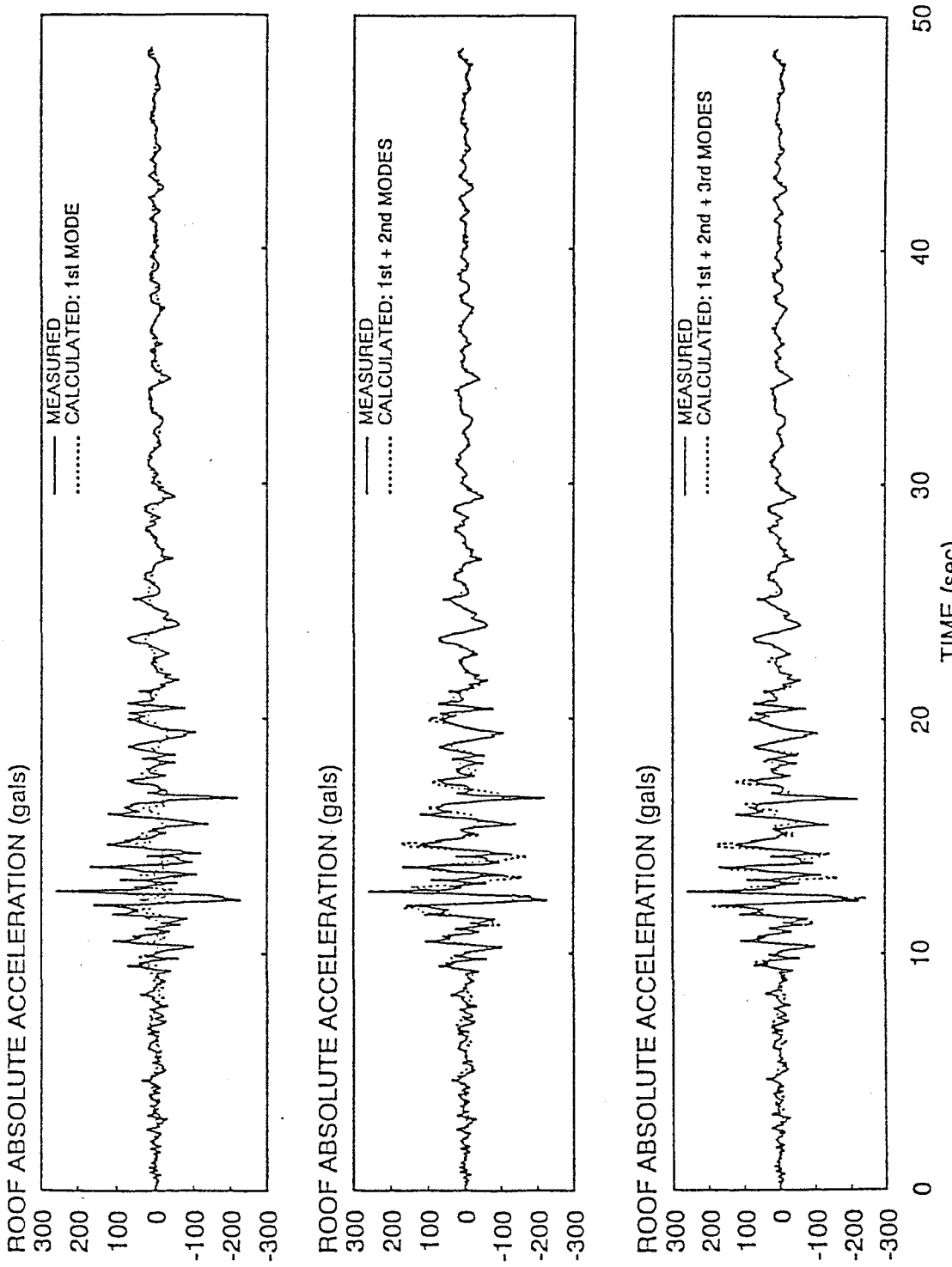

Figure 4.3 - Influence of higher modes on acceleration response (350° component)

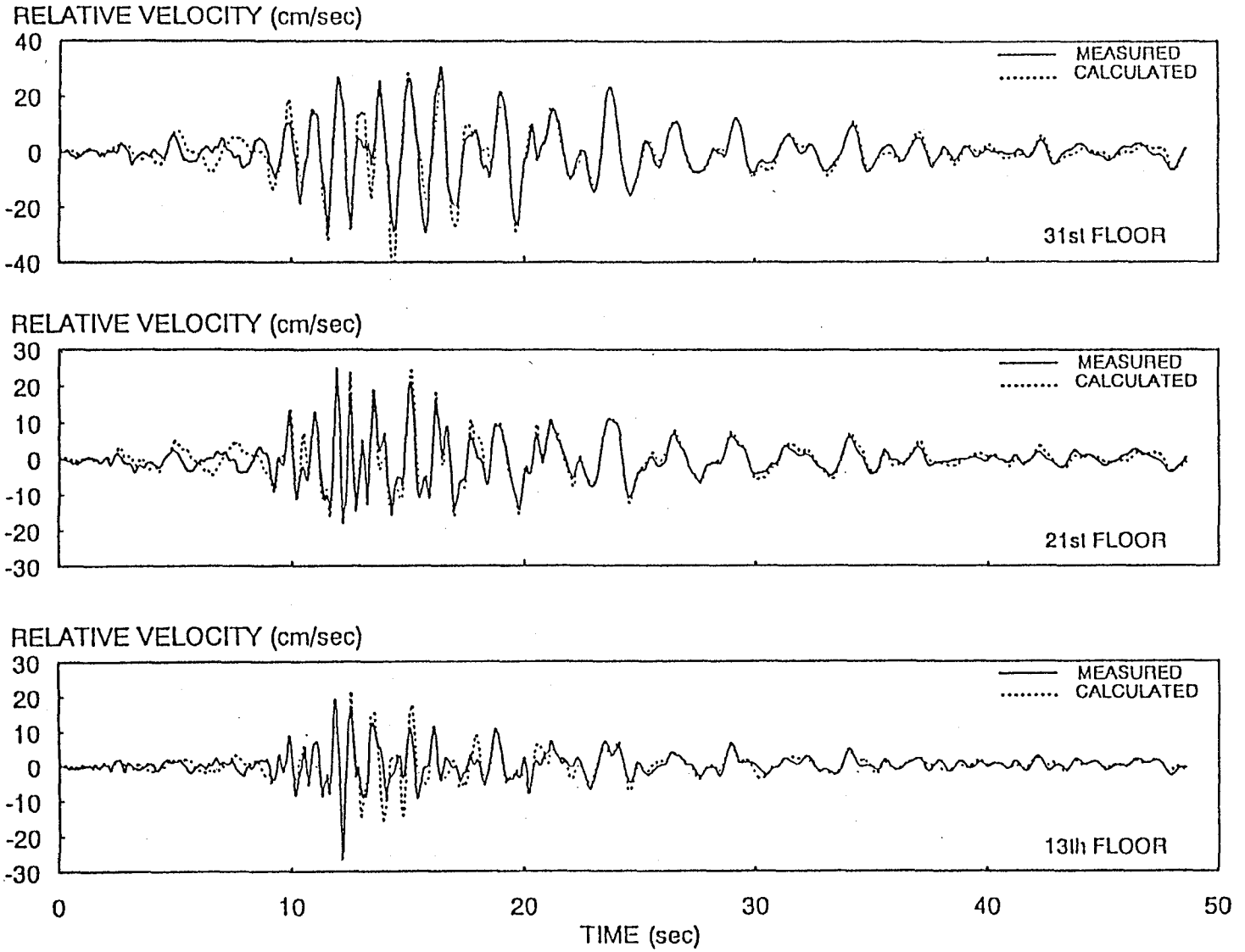

Figure 4.4 - Measured vs. calculated velocity (350° component)

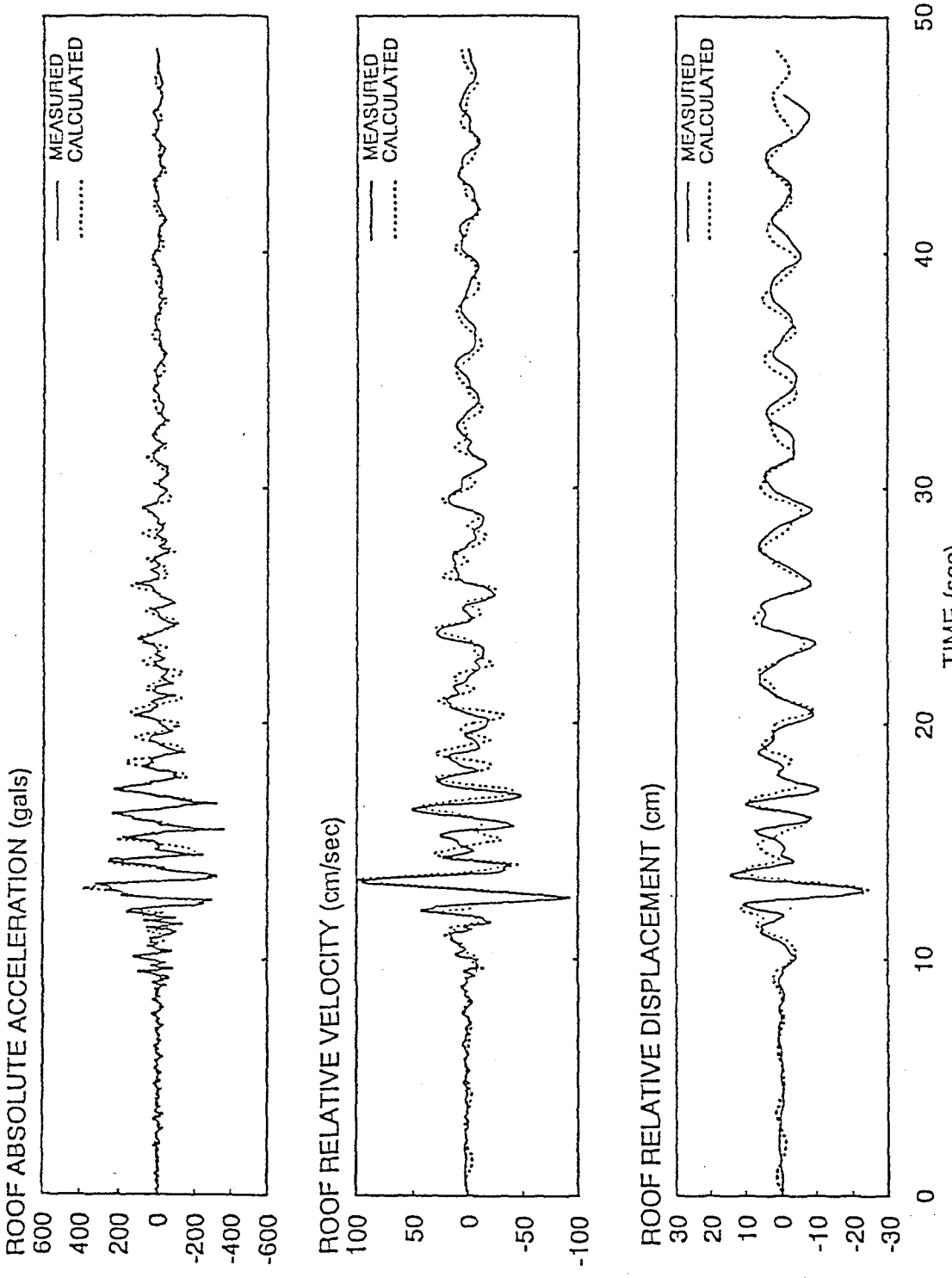

Figure 4.5 - Comparison of measured and calculated response at the roof level of central core of the building (260° component)

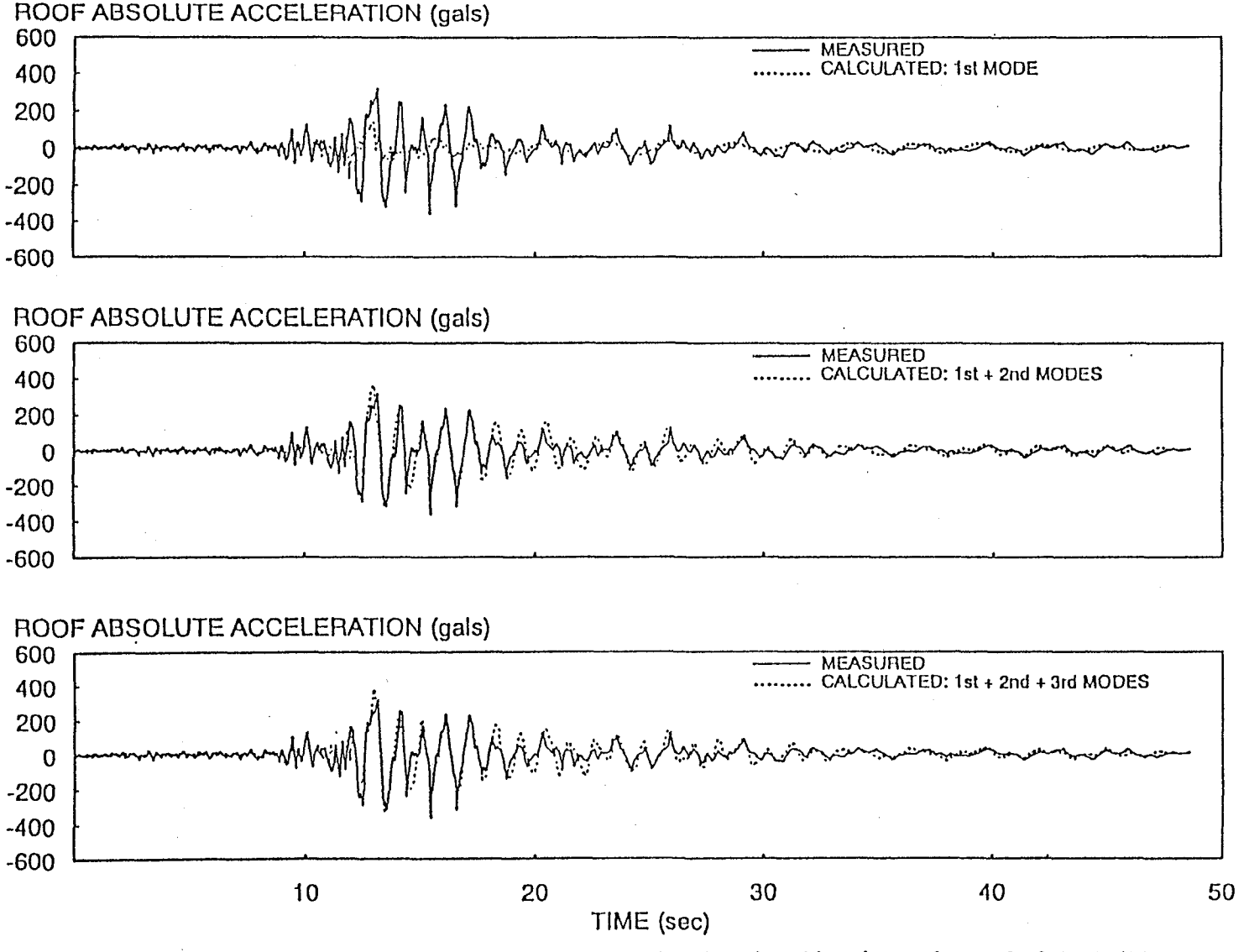

Figure 4.6 - Influence of higher modes in calculated acceleration time-histories at the roof of the building (260° component)

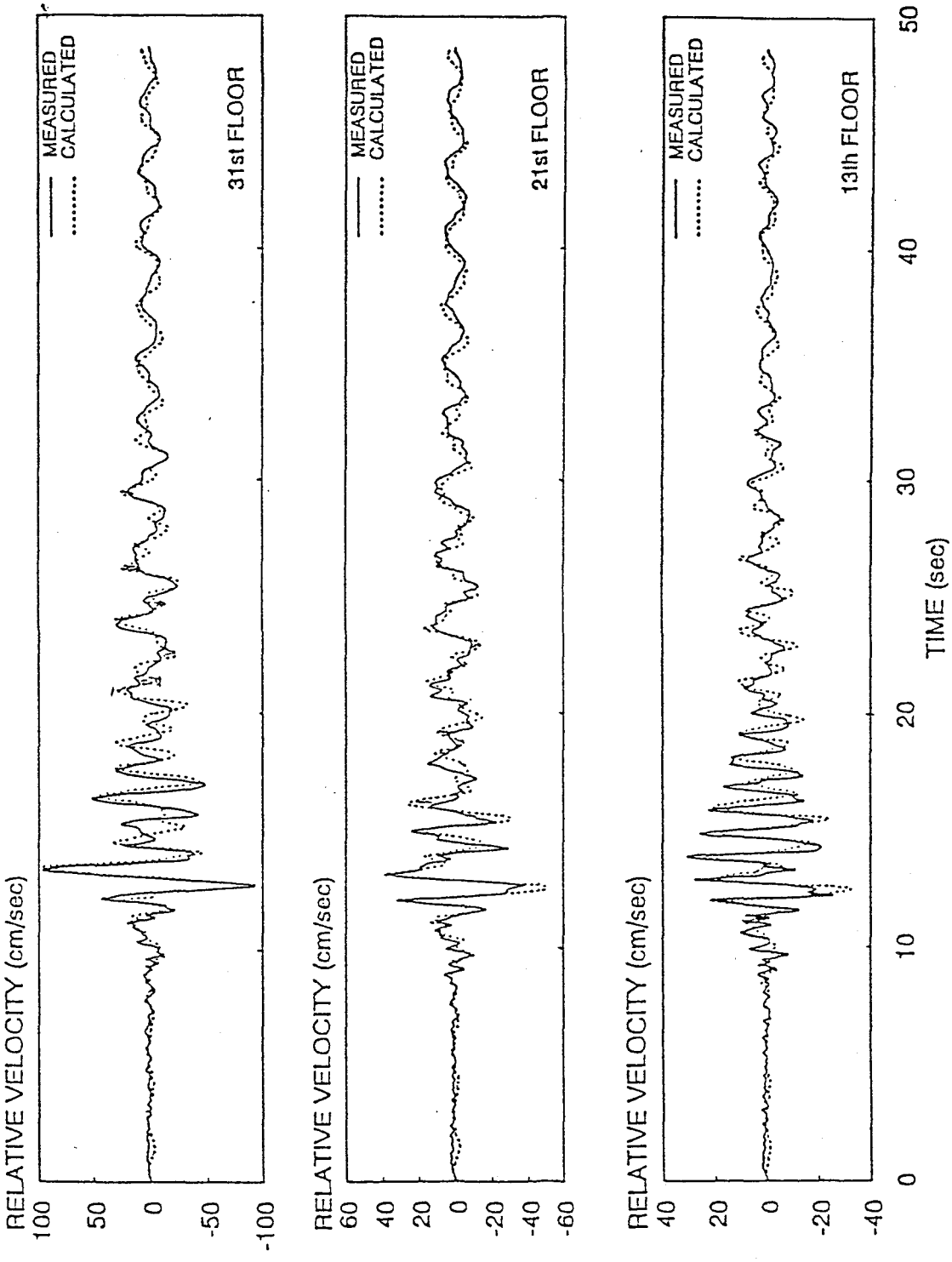

Figure 4.7 - Comparison of measured and calculated velocity time-histories along the height of the building (260° component)

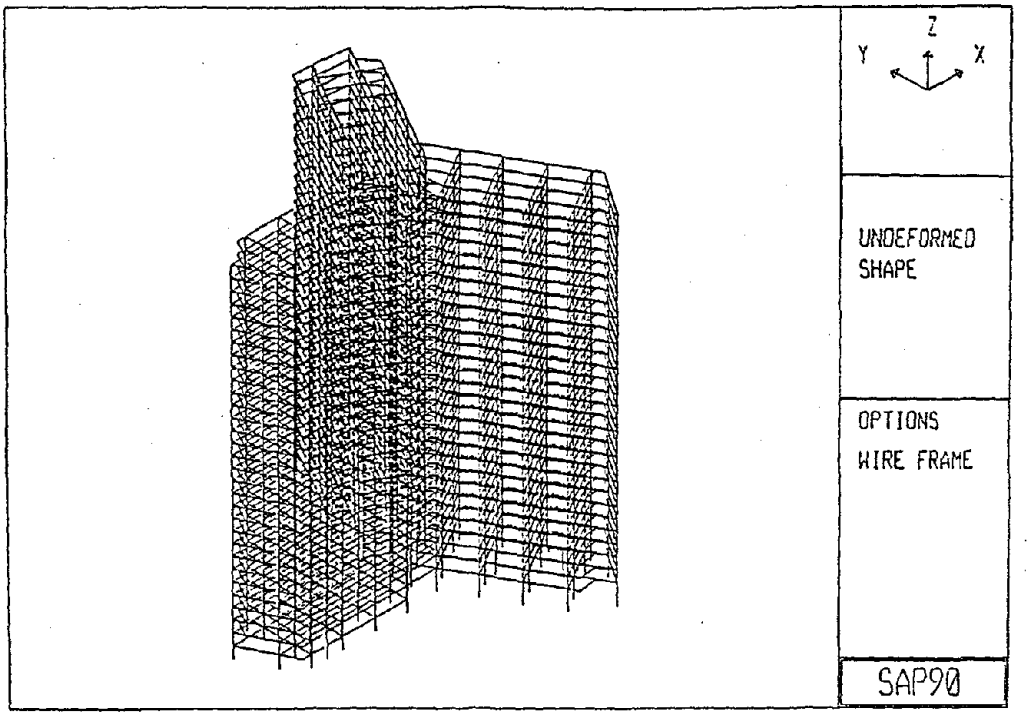

Figure 4.8 - Isometric view of the building, SAP90

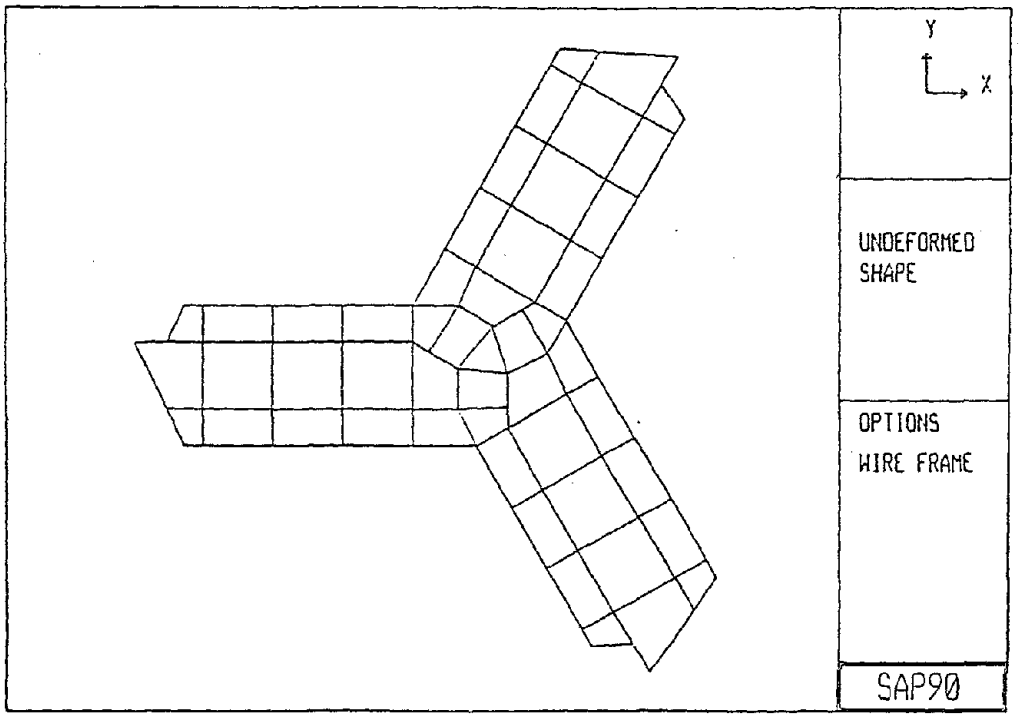

Figure 4.9 - Plan view of Y Building, SAP90

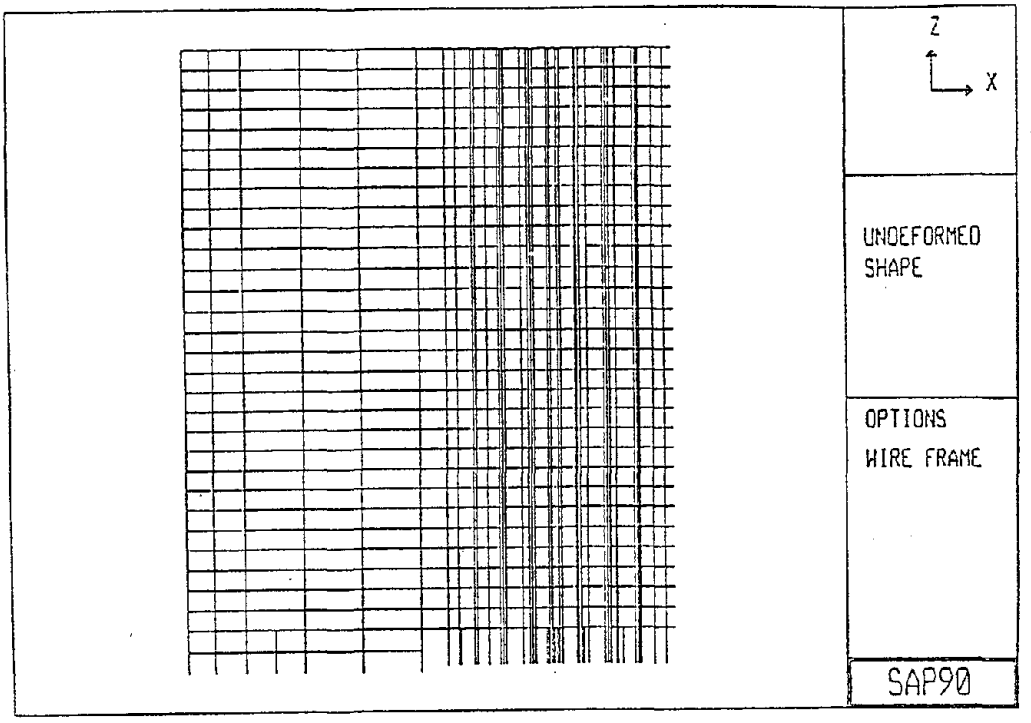

Figure 4.10 - South elevation of Y Building, SAP90

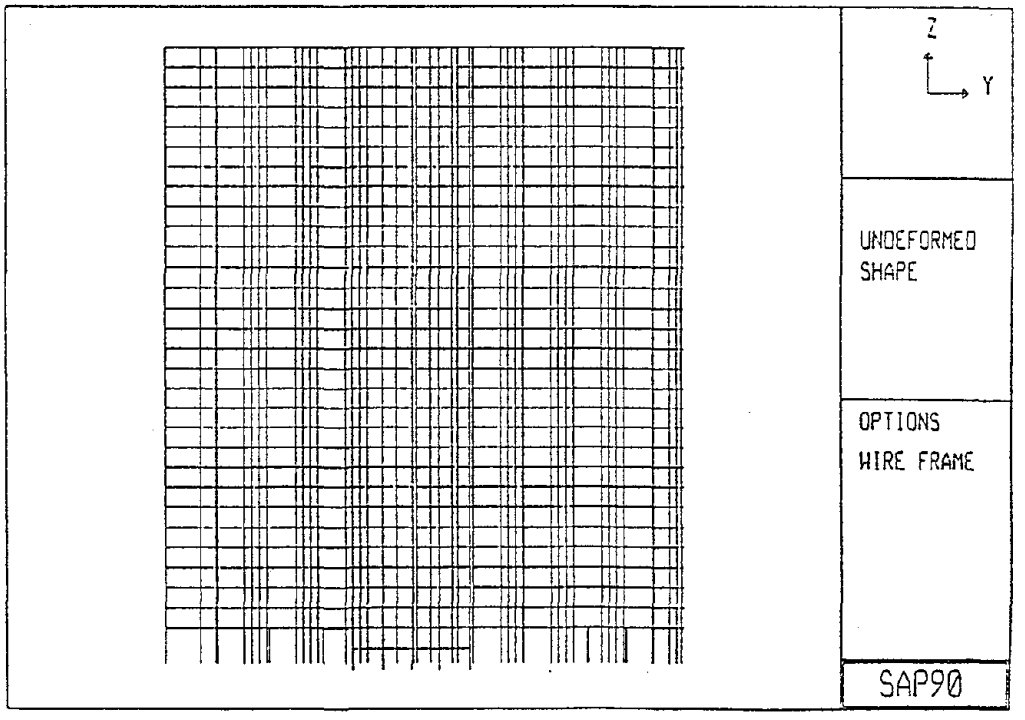

Figure 4.11 - West elevation of the Y Building, SAP90

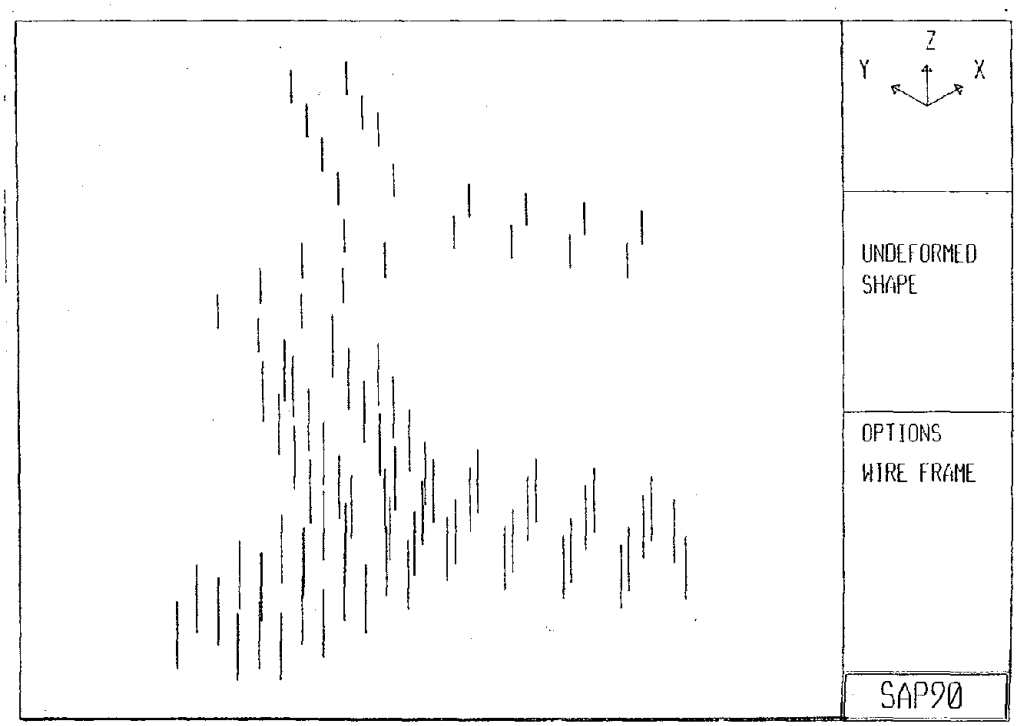

Figure 4.12 - Isometric view of high strength columns, SAP90

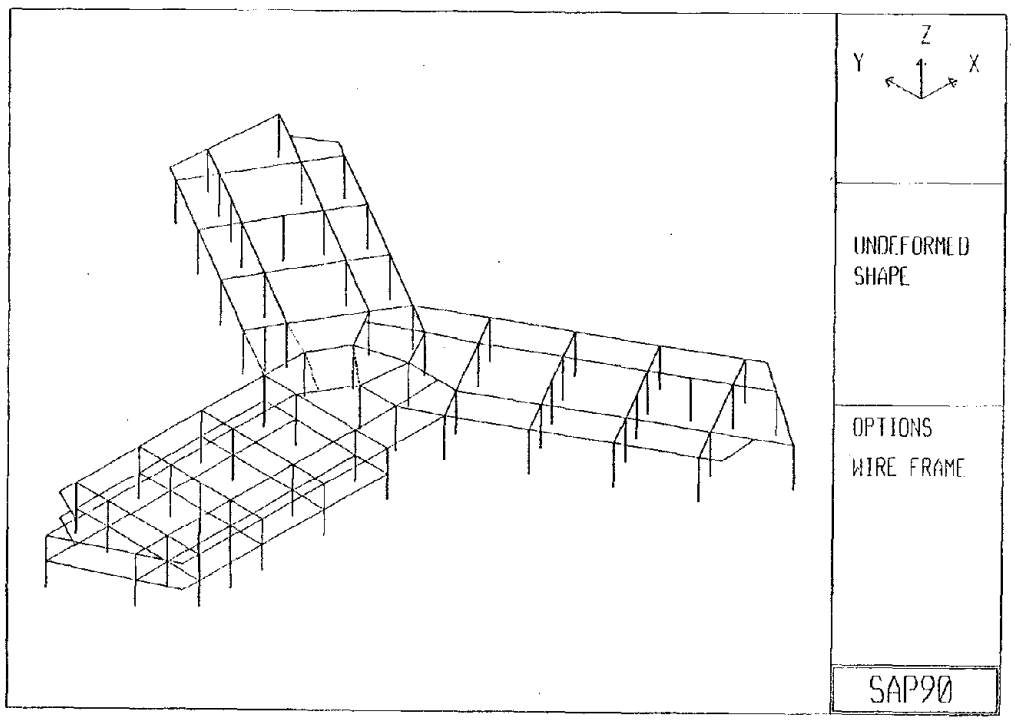

Figure 4.13 - Isometric view of mezzanine and 2nd floor, SAP 90

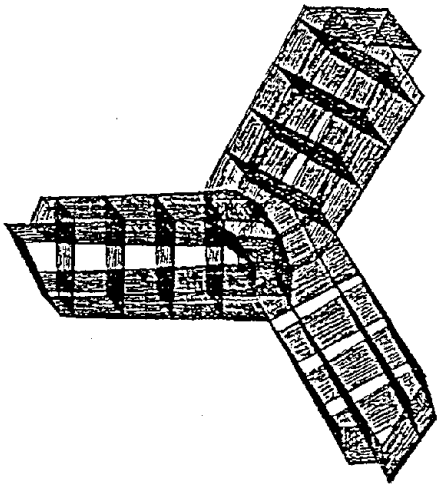

Figure 4.14 - Plan view of 1st vibration mode shape, SAP90

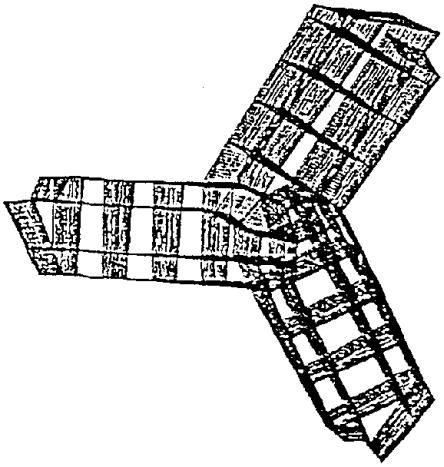

Figure 4.15 - Plan view of 2nd vibration mode shape, SAP90

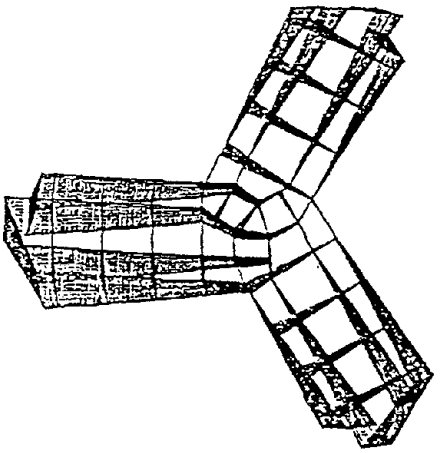

Figure 4.16 - Plan view of 3rd vibration mode shape, SAP90

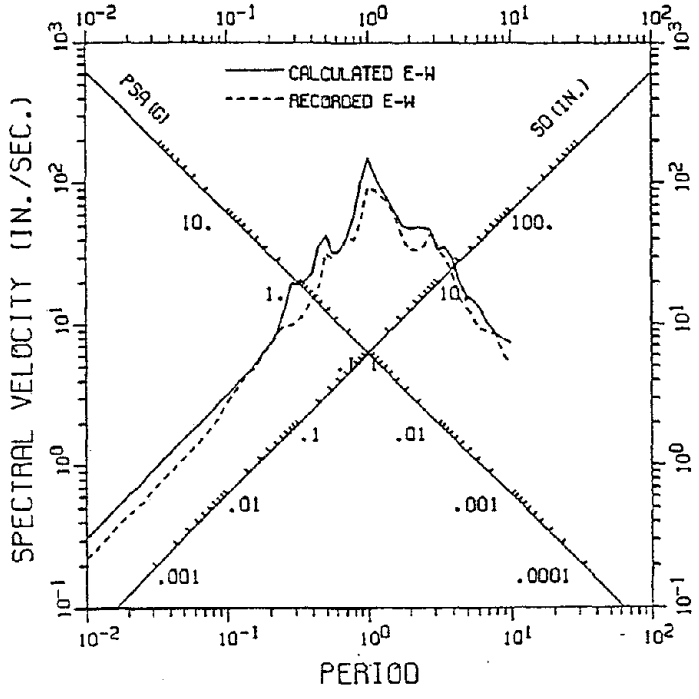

Figure 4.17 - Calculated vs. recorded roof spectra, 3% damping

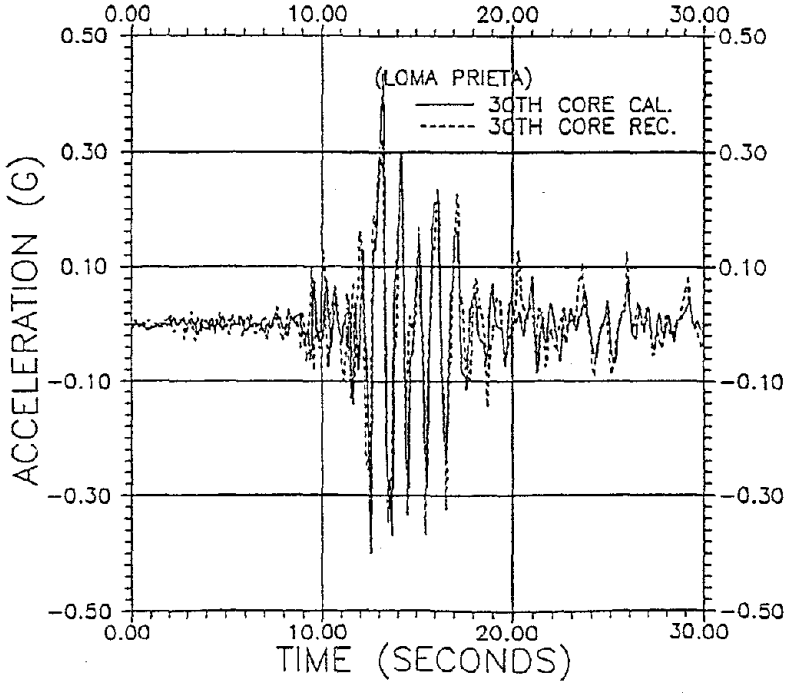

Figure 4.18 - Calculated vs. recorded roof accelerations, roof, 3% damping

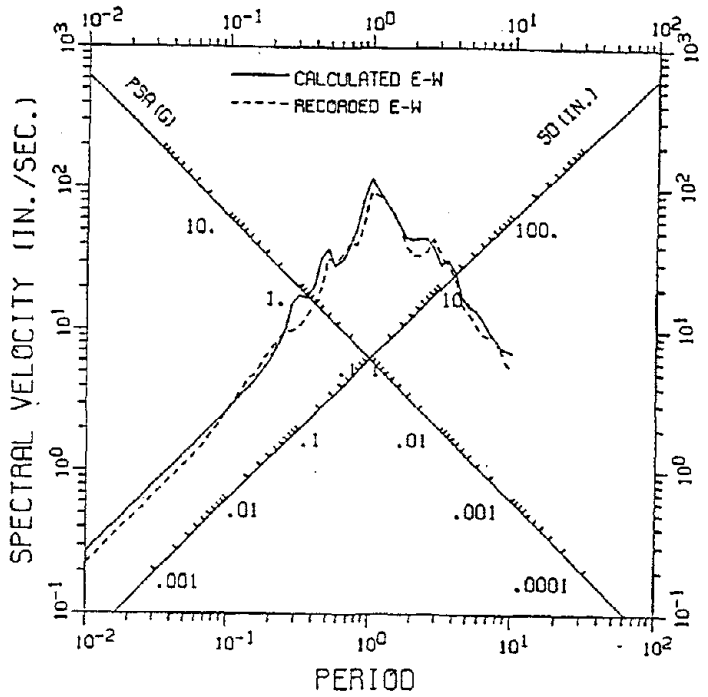

Figure 4.19 - Calculated vs. recorded roof spectra, 5% damping

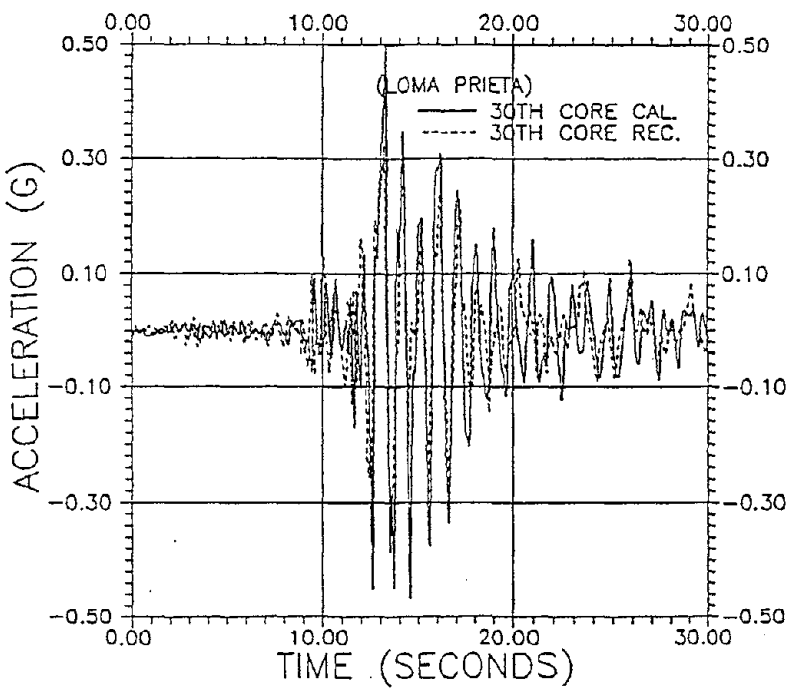

Figure 4.20 - Calculated vs. recorded accelerations, roof, 5% damping

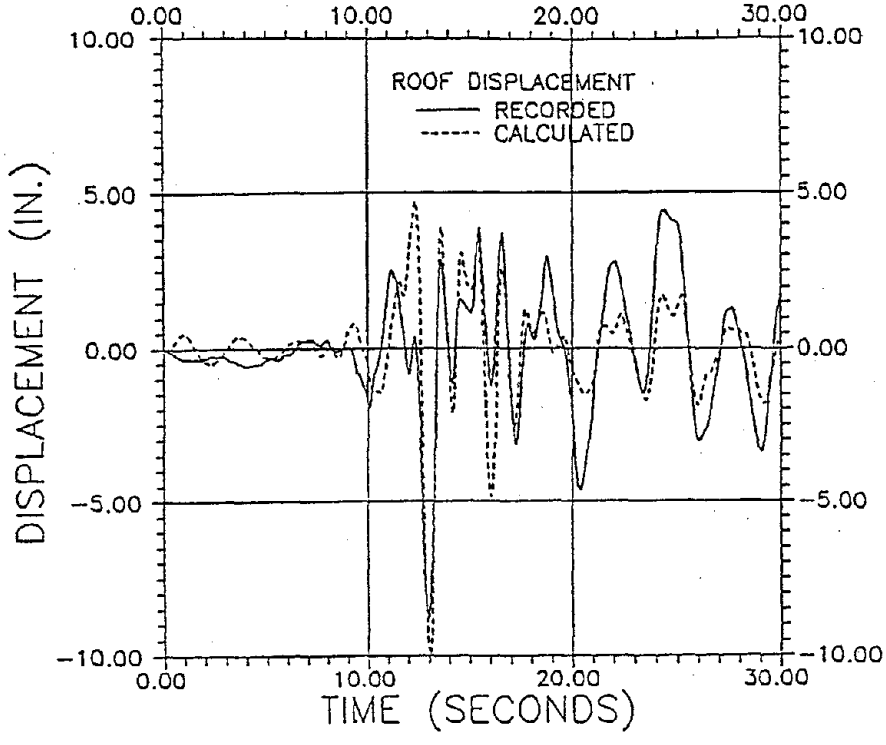

Figure 4.21 - Calculated vs. recorded displacement, roof, 5% damping

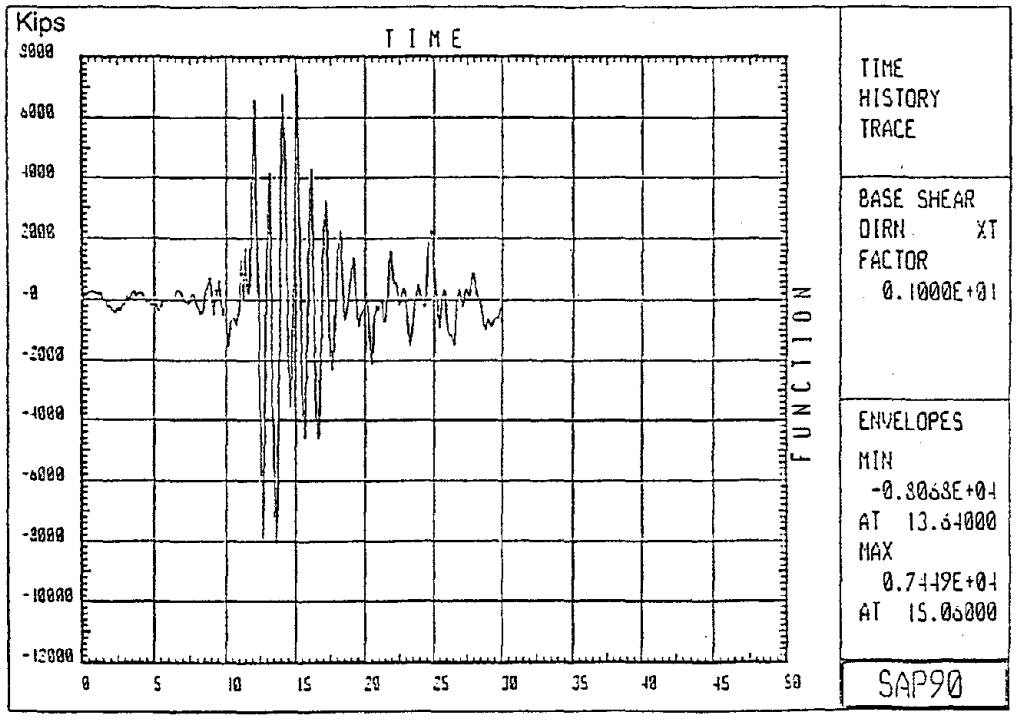

Figure 4.22 - Base shear response, E-W, recorded base motion, 260°

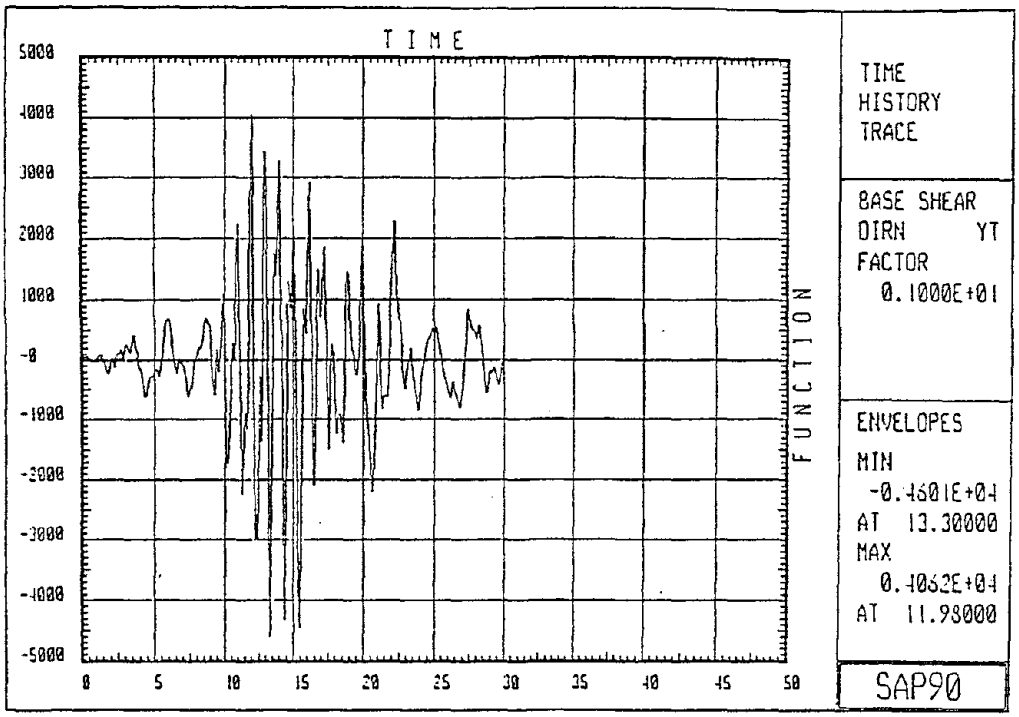

Figure 4.23 - Base shear response, N-S, recorded base motion, 350°

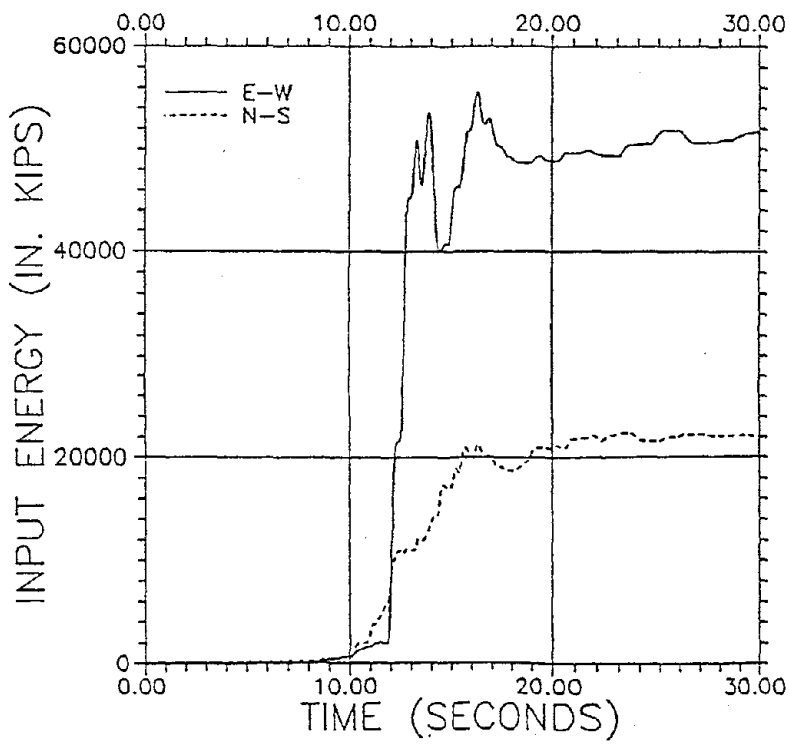

Figure 4.24 - Comparison of input energy, E-W vs. N-W, elastic

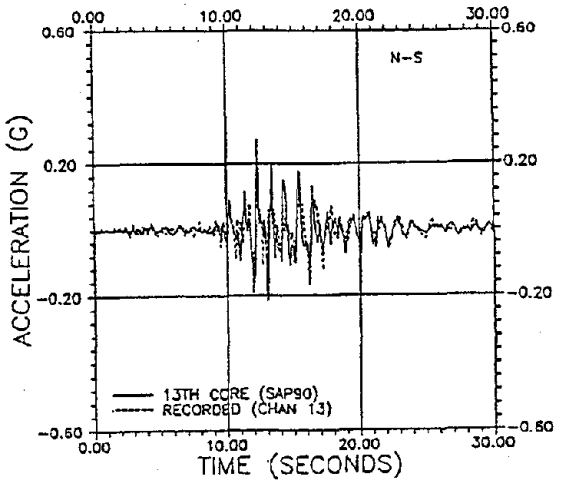

(a) acceleration

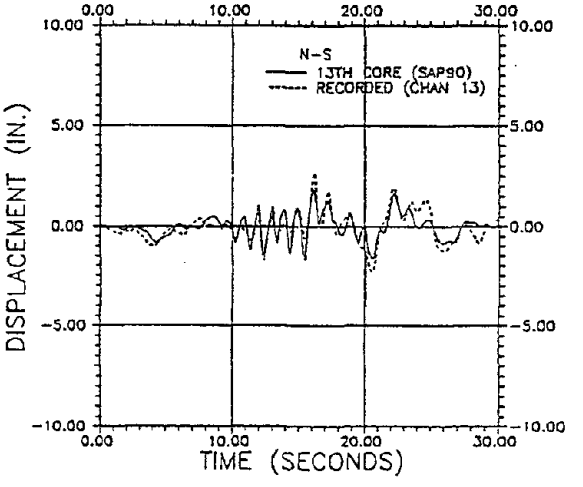

(b) displacement

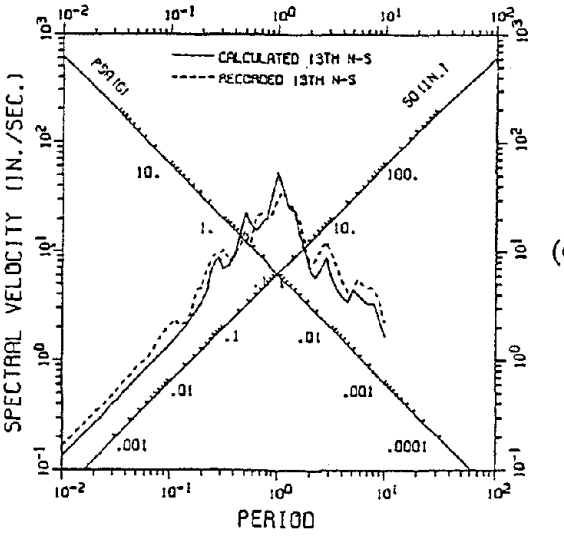

(c) floor spectra

Figure 4.25 - Calculated vs. recorded response, 13th level, N-S

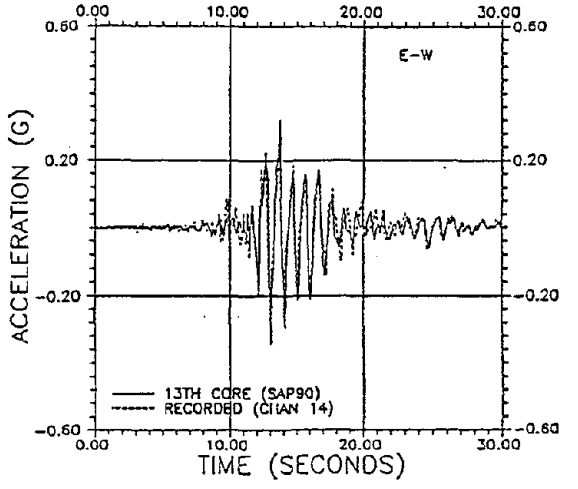

(a) acceleration

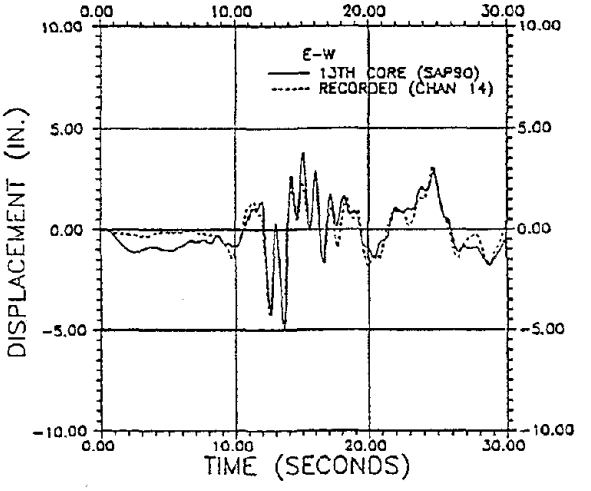

(b) displacement

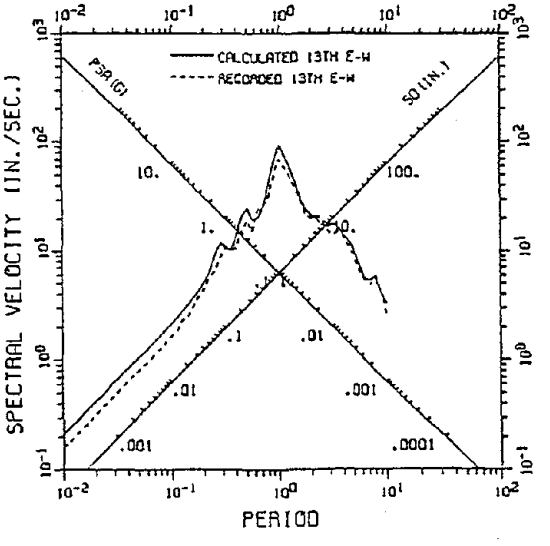

(c) floor spectra

Figure 4.26 - Calculated vs. recorded response, 13th level, E-W

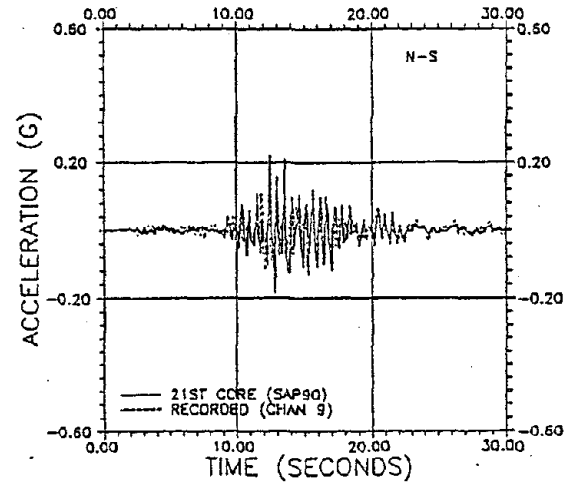

(a) acceleration

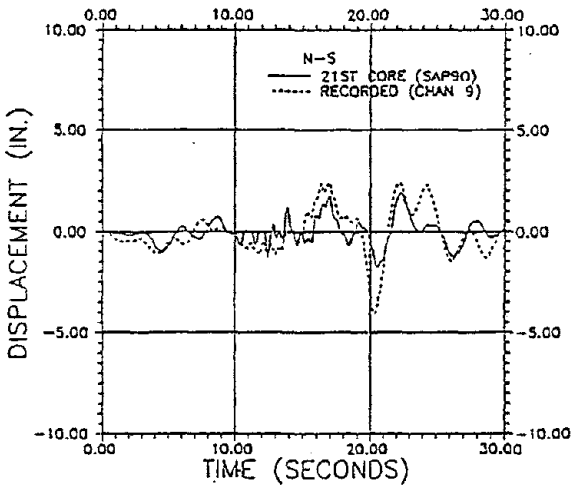

(b) displacement

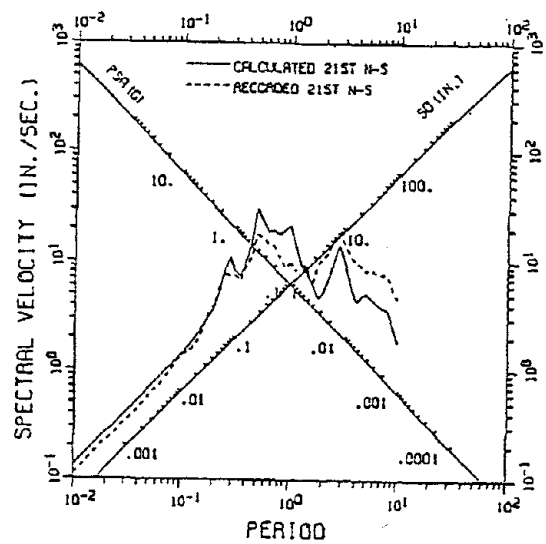

(c) floor spectra

Figure 4.27 - Calculated vs. recorded response, 21st level, N-S

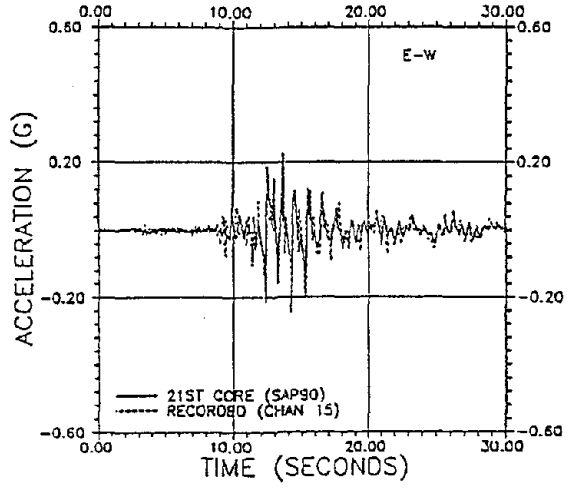

(a) acceleration

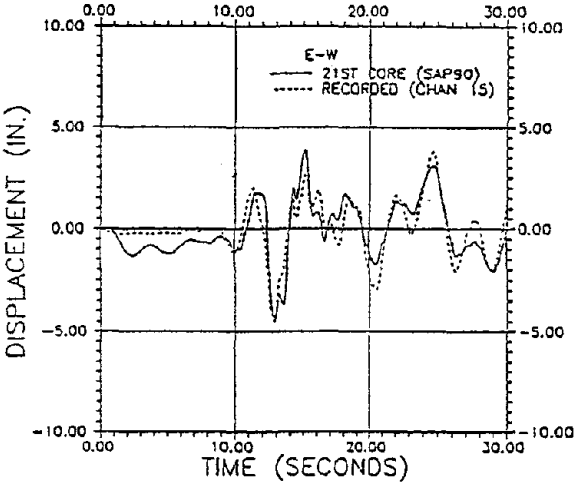

(b) displacement

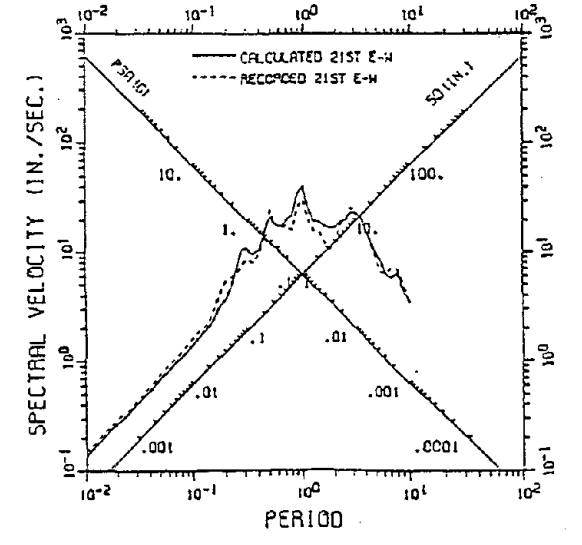

(c) floor spectra

Figure 4.28 - Calculated vs. recorded response, 21st level, E-W

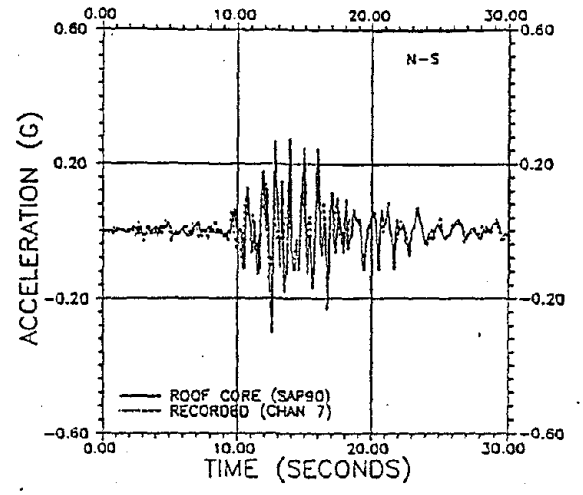

(a) acceleration

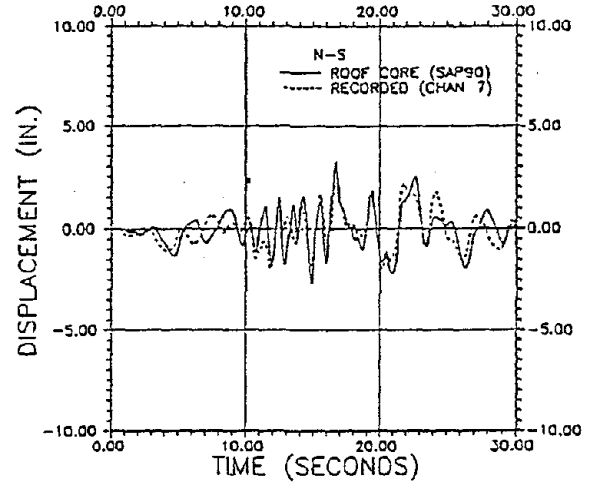

(b) displacement

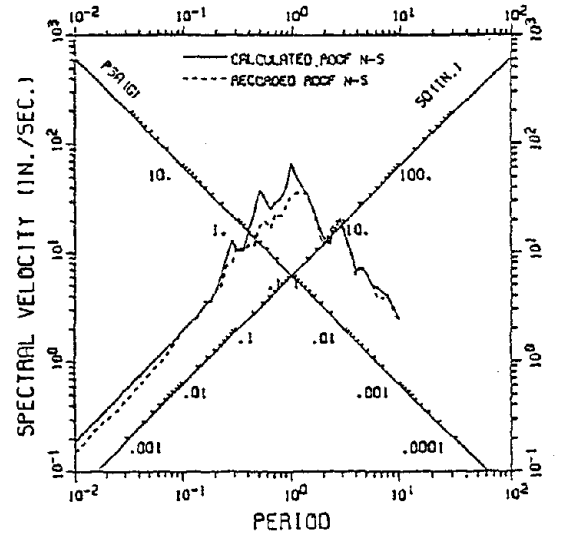

(c) floor spectra

Figure 4.29 - Calculated vs. recorded response, roof level, N-S

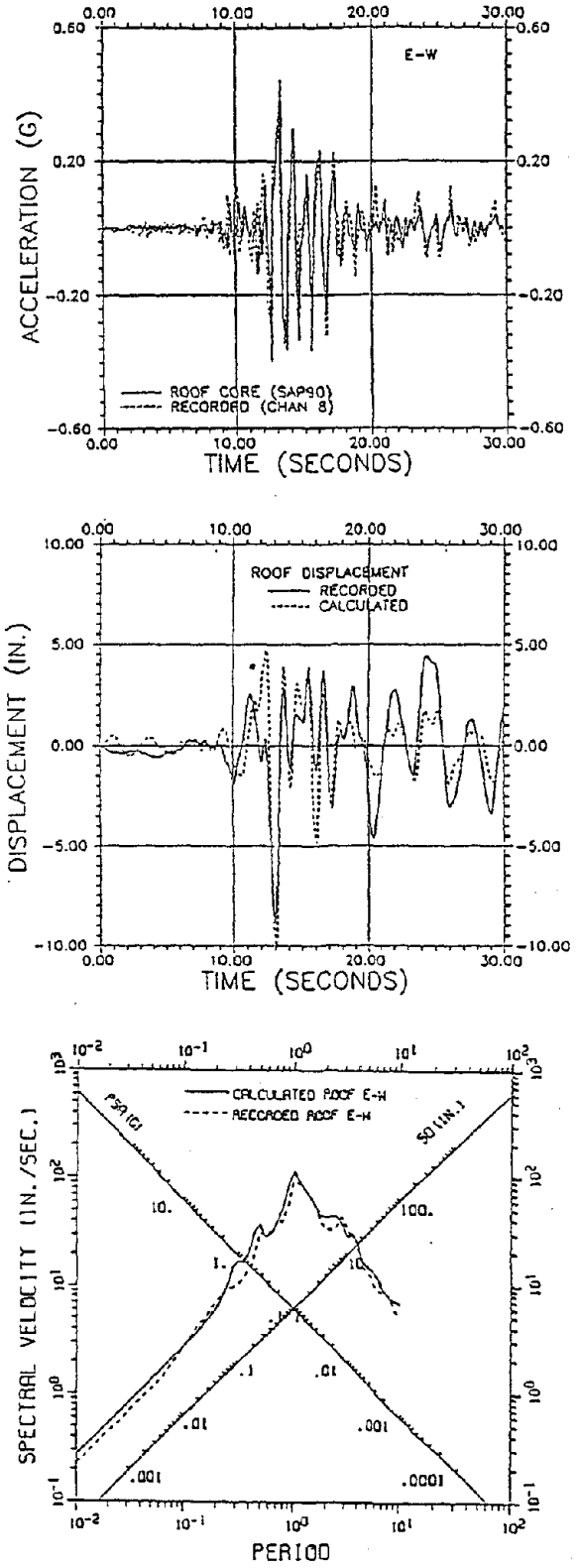

(a) acceleration

(b) displacement

(c) floor spectra

Figure 4.30 - Calculated vs. recorded response, roof level, E-W

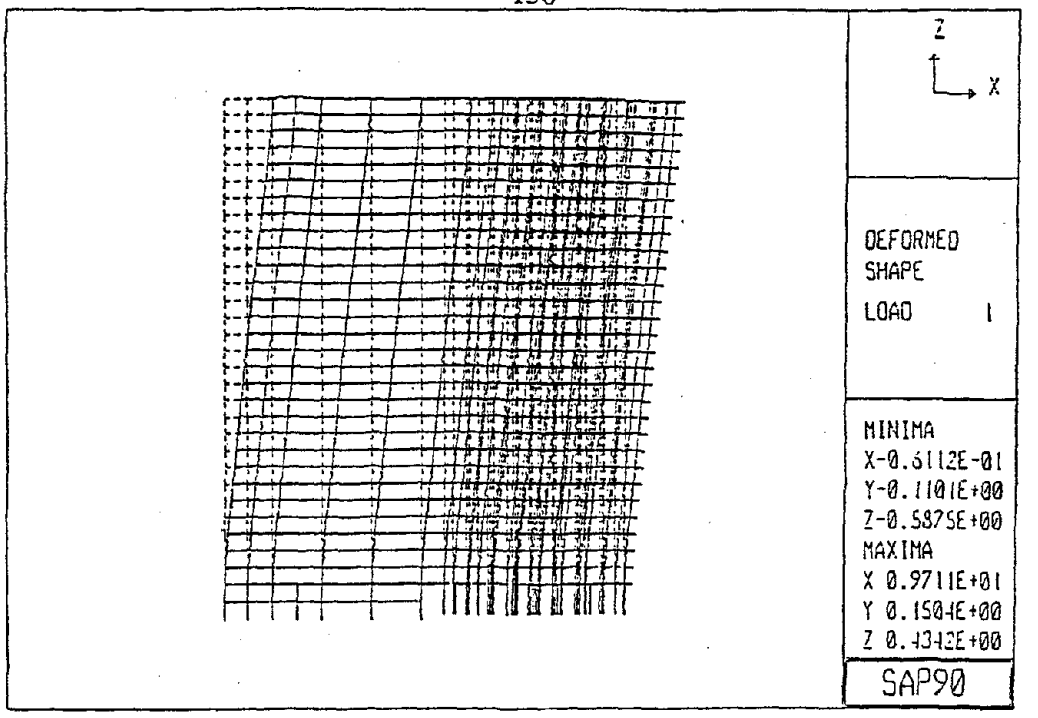

Figure 4.31 - Static deformed shape, 1979 UBC seismic

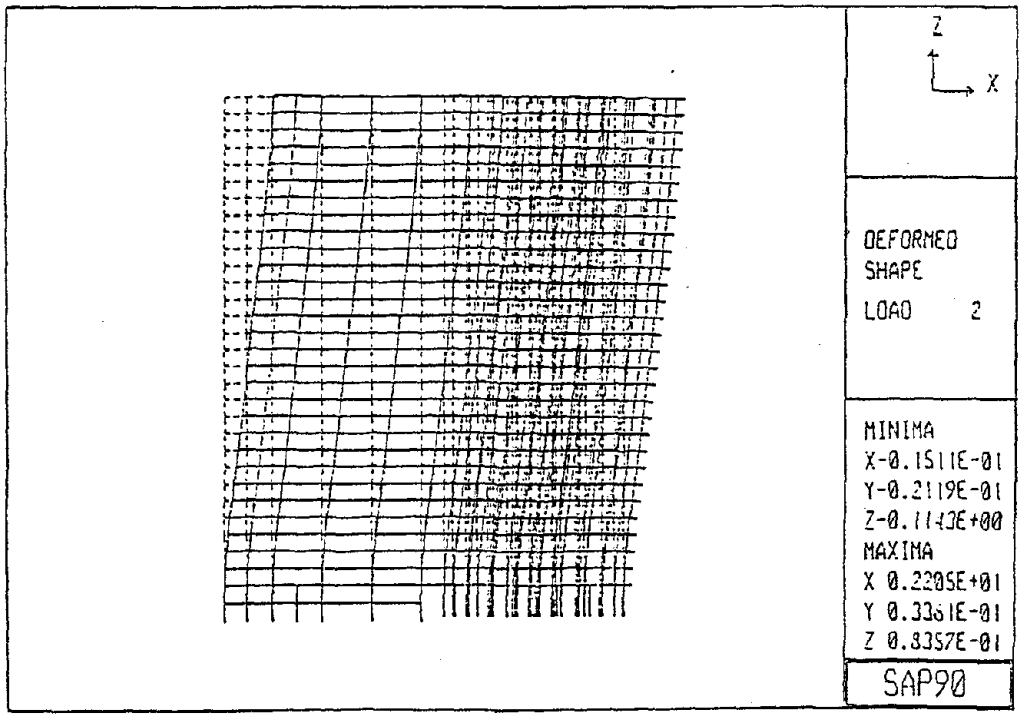

Figure 4.32 - Static deformed shape, 1979 UBC wind

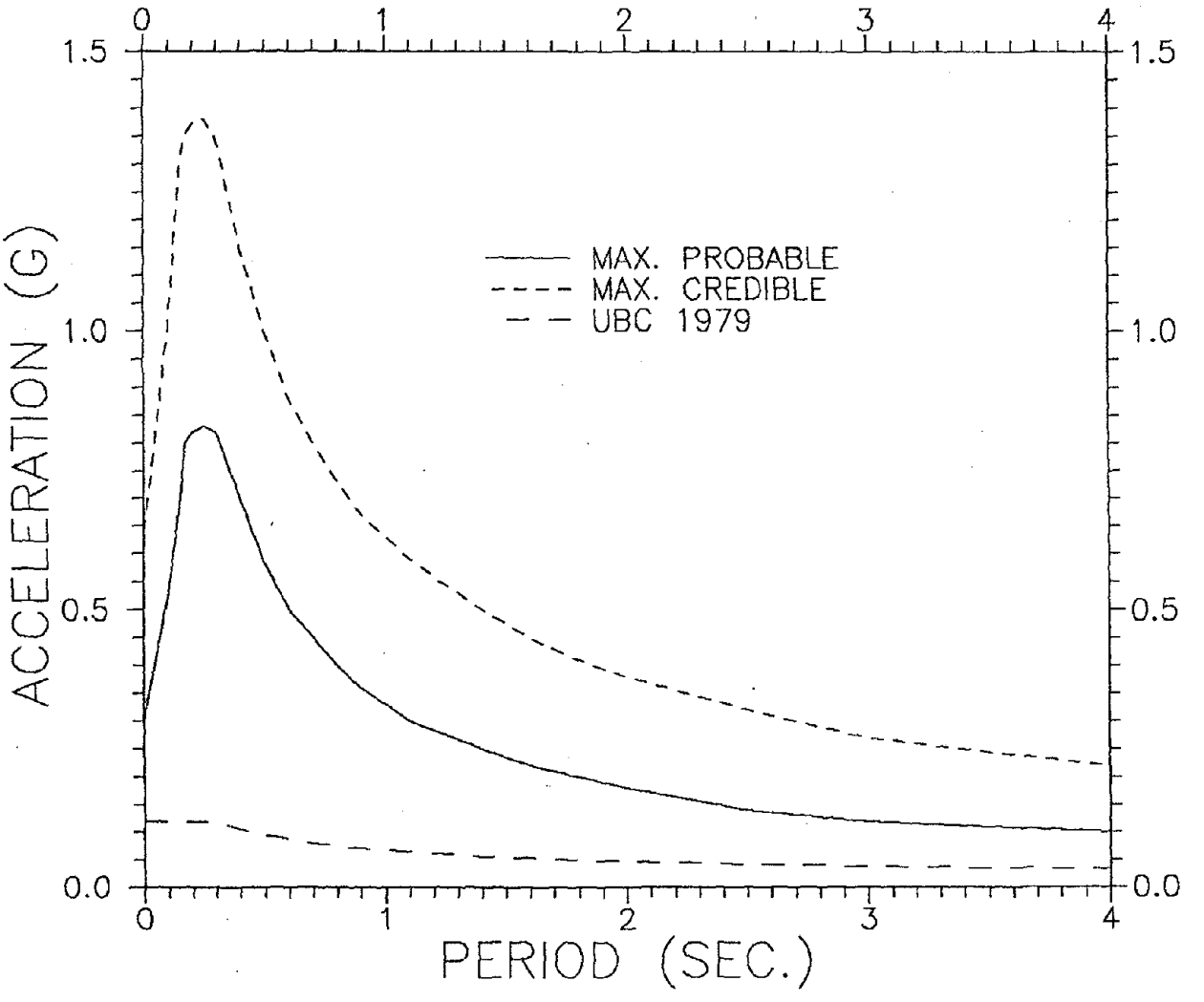

Fig. 4. 33 - Site spectra vs. 1979 UBC spectrum.

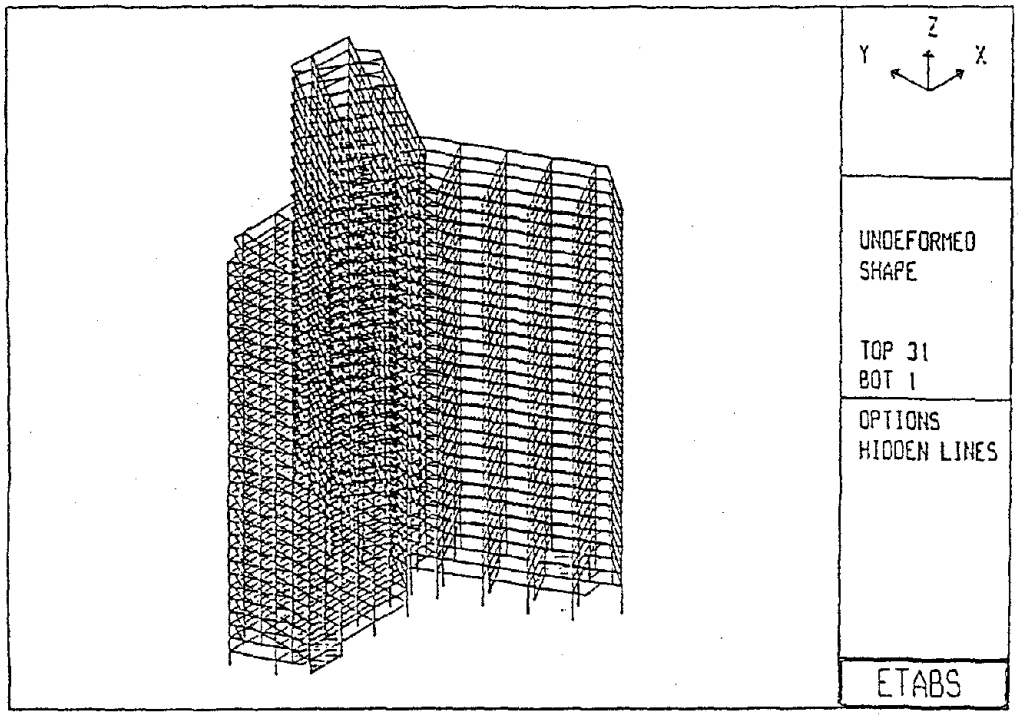

Figure 4.34 - Isometric view of Y Building, ETABS

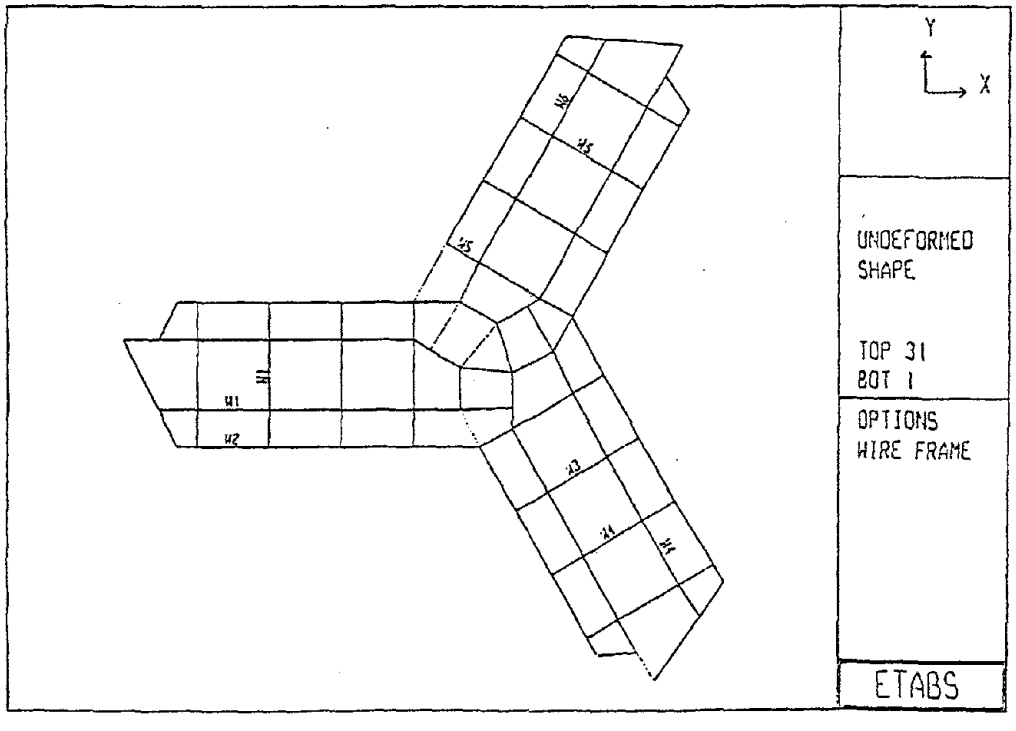

Figure 4.35 - Plan view of Y Building, ETABS

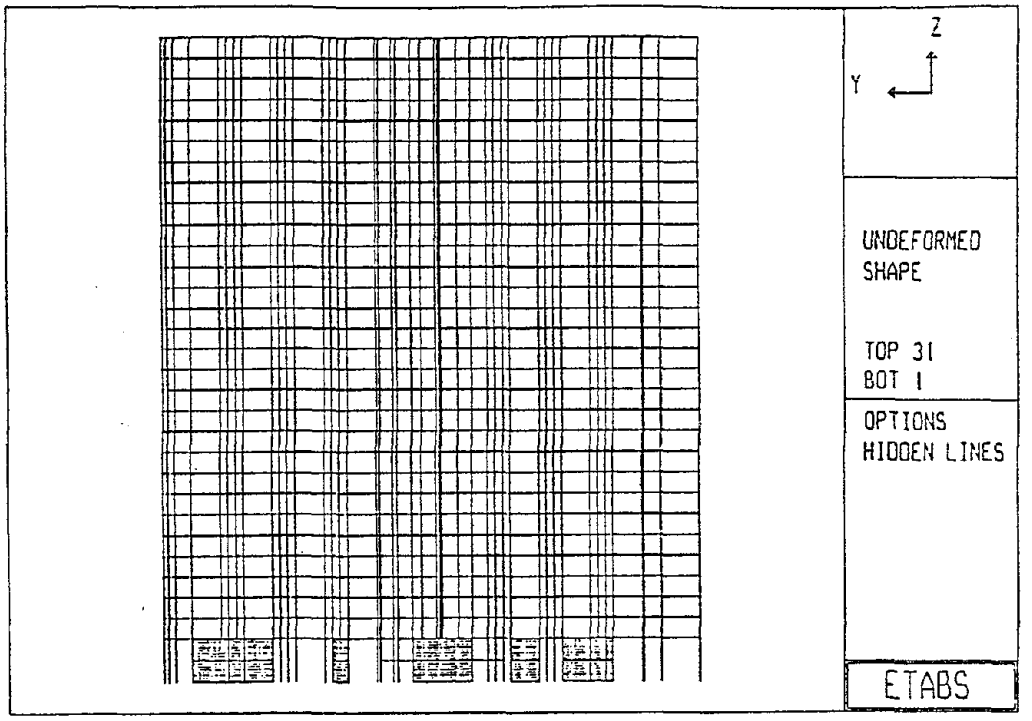

Figure 4.36 - West elevation of Y Building, ETABS

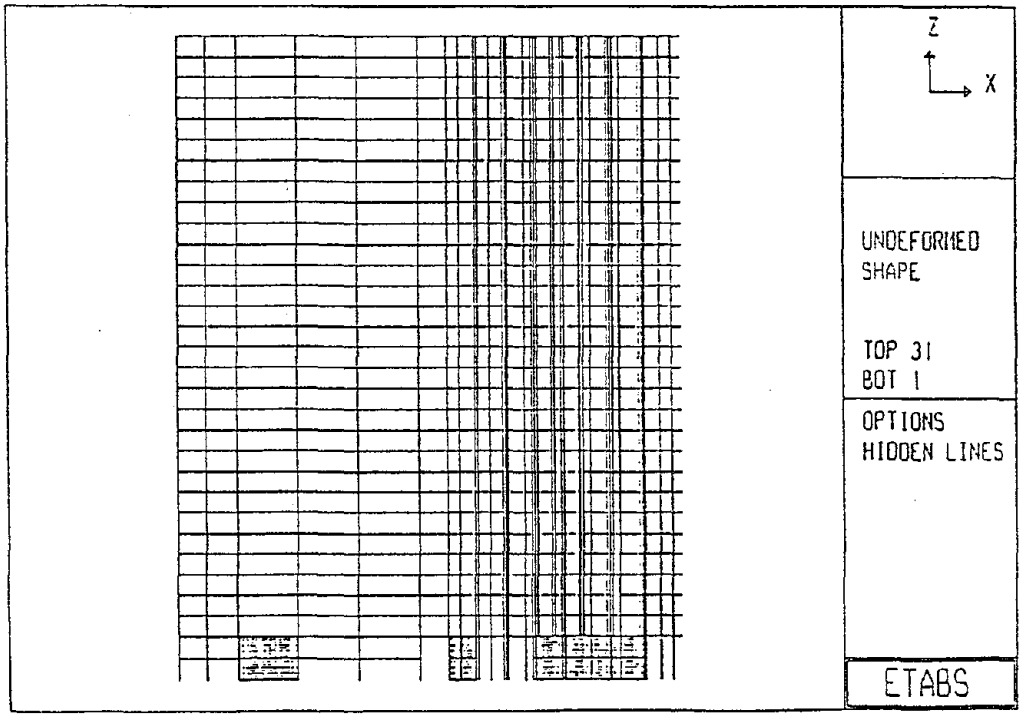

Figure 4.37 - North elevation of Y Building, ETABS

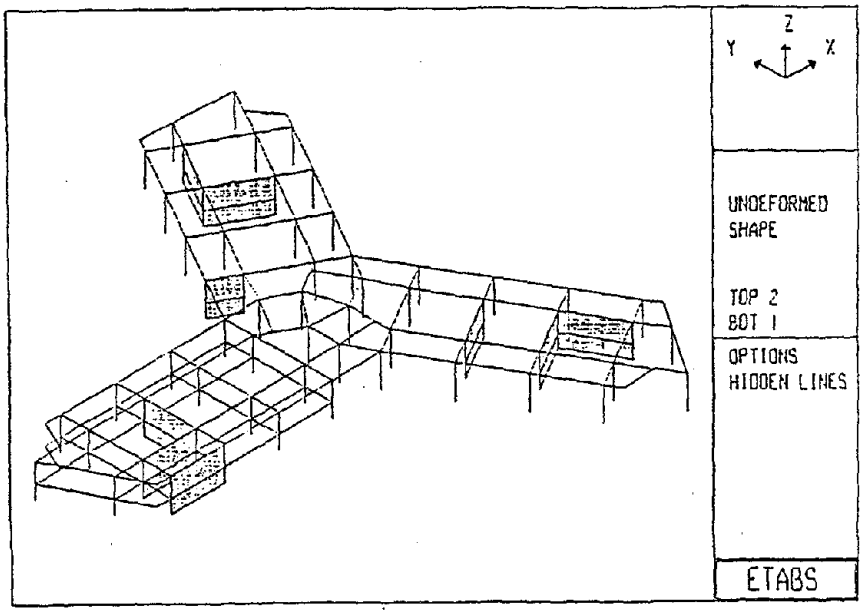

Figure 4.38 - Isometric view of mezzanine and 2nd floor, ETABS

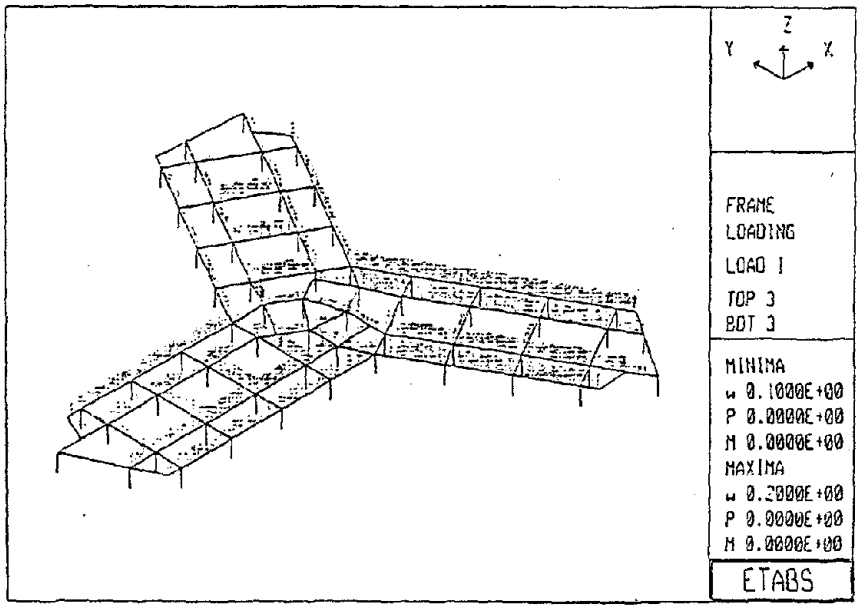

Figure 4.39 - Gravity loading, typical floor, ETABS

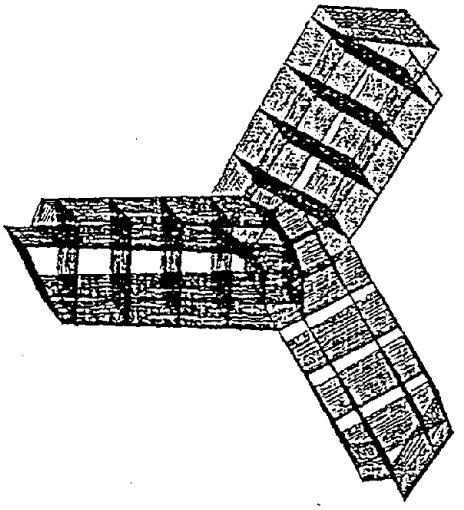

Figure 4.40 - Plan view of 1st vibration mode shape, ETABS

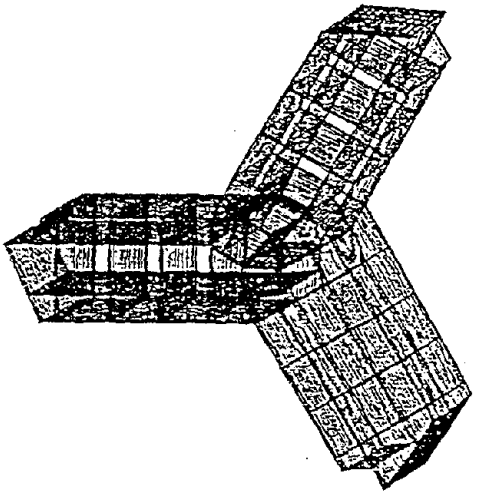

Figure 4.41 - Plan view of 2nd vibration mode shape, ETABS

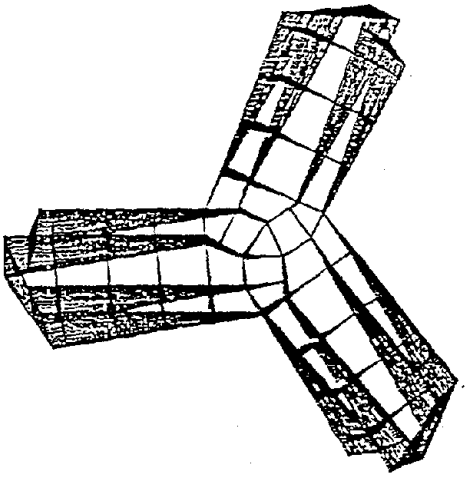

Figure 4.42 - Plan view of 3rd vibration mode shape, ETABS

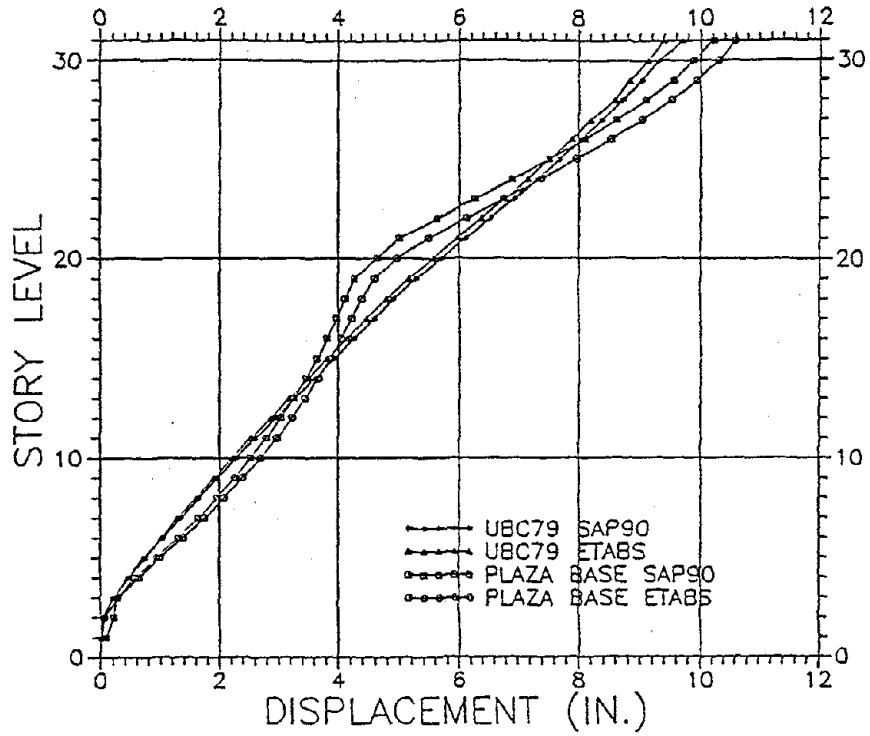

Figure 4.43 - Maximum floor displacement, SAP90 vs. ETABS

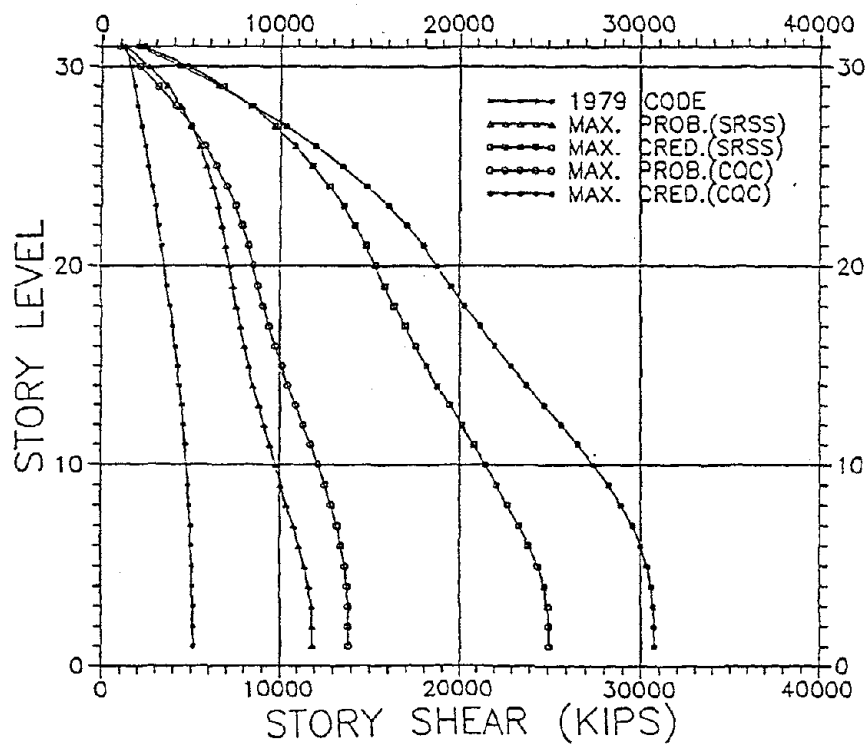

Figure 4.44 - Maximum story shear, SRSS vs. CQC

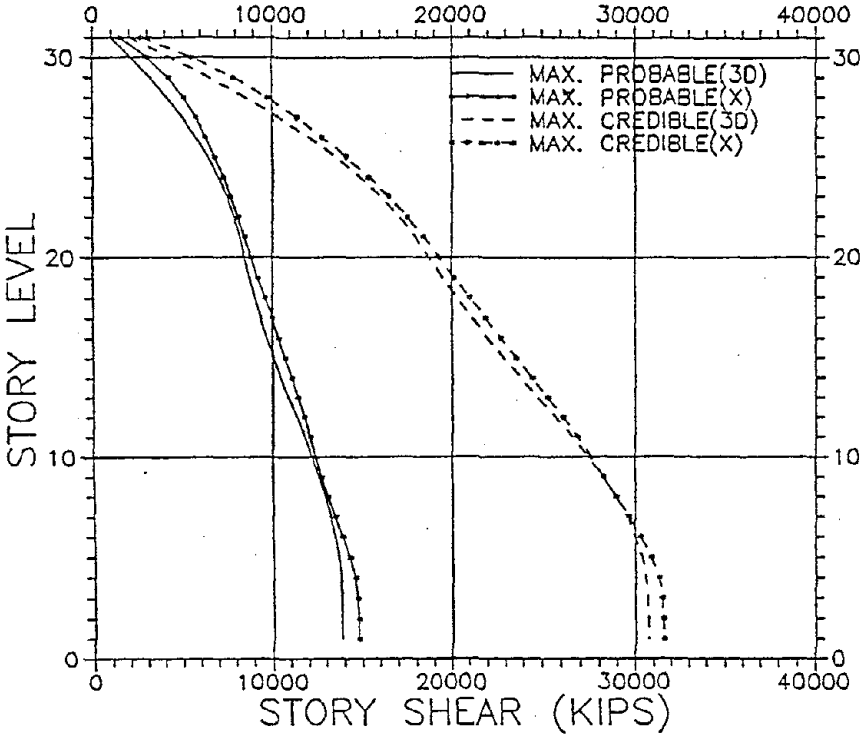

Figure 4.45 - Maximum story shear, 3D vs. 2D, E-W

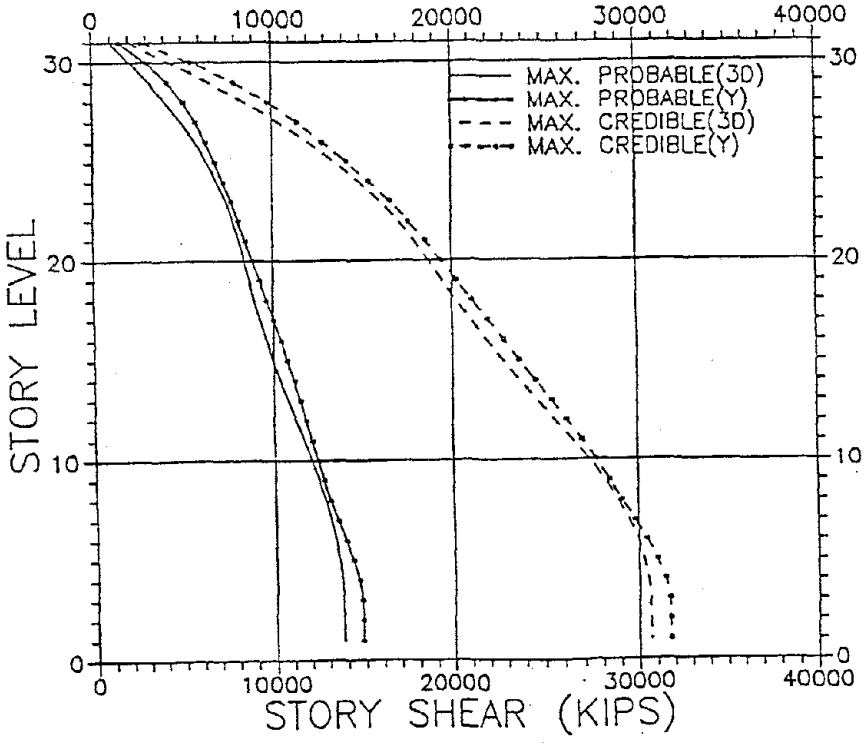

Figure 4.46 - Maximum story shear, 3D vs. 2D, N-S

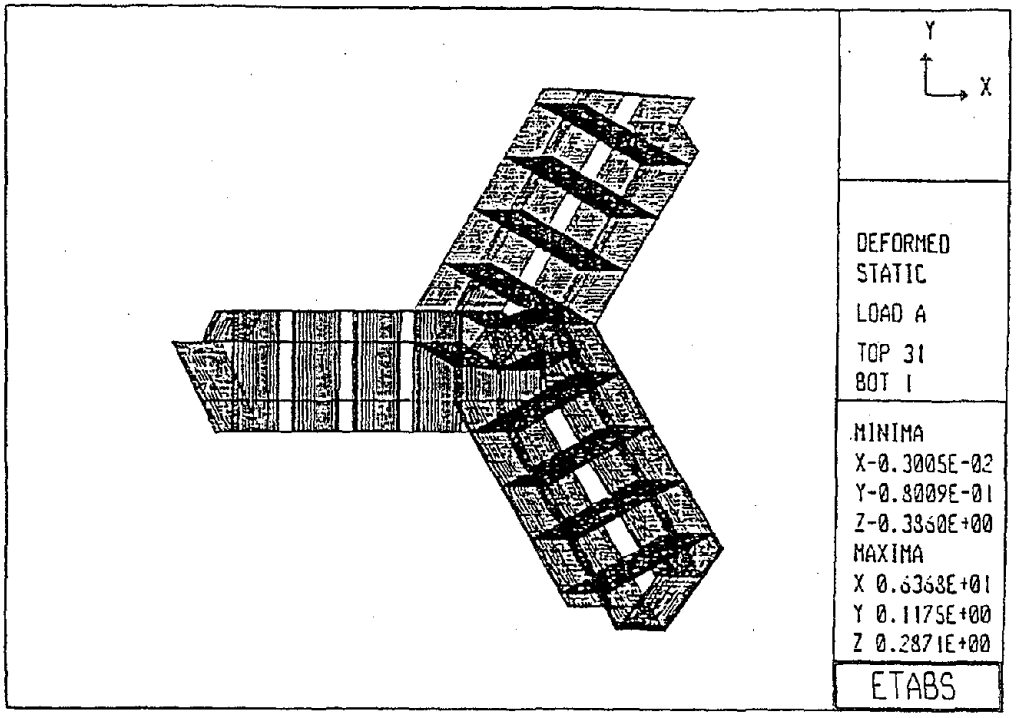

Figure 4.47 - Plan view of static deformed shape in the E-W direction for UBC 1979 seismic forces

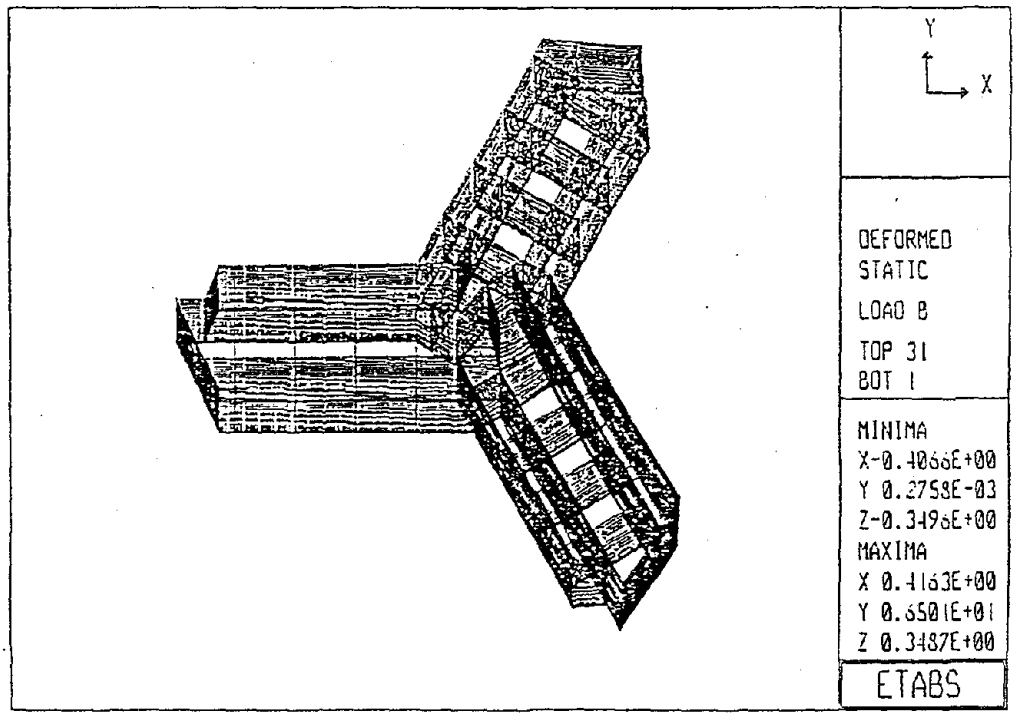

Figure 4.48 - Plan view of static deformed shape in the N-S direction for UBC 1979 seismic forces

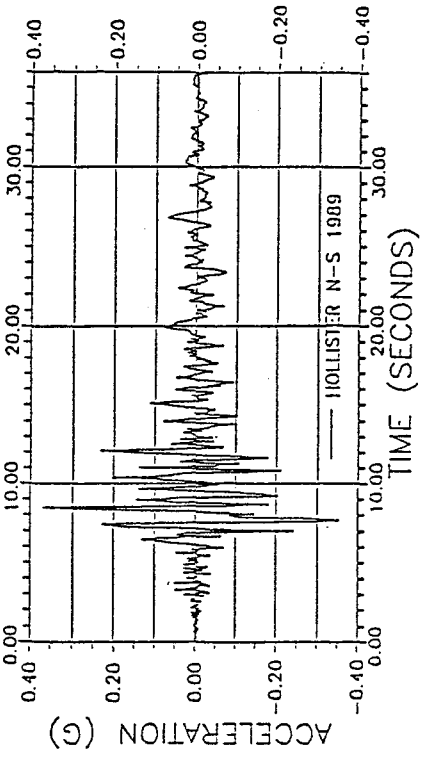

(a) Emeryville, 1989

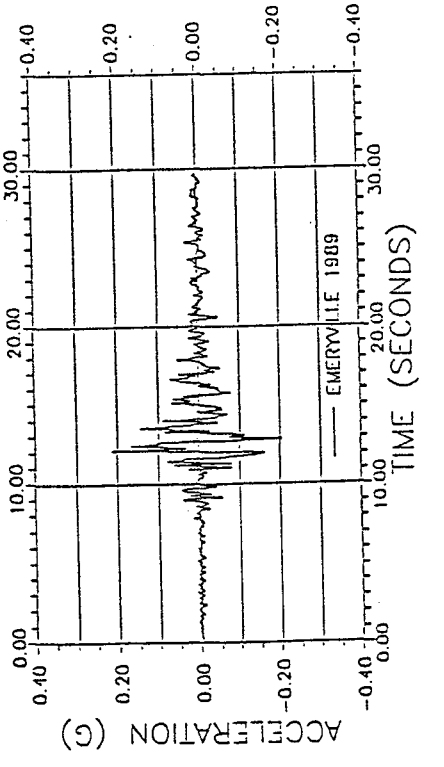

(b) Hollister, 1989

(c) James Road, 1979

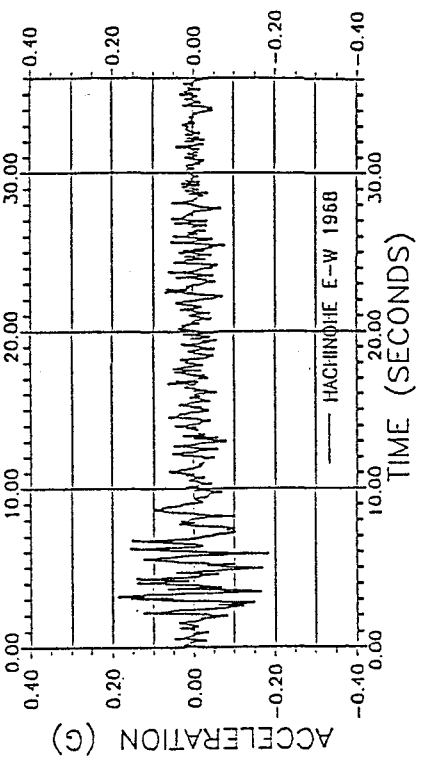

(d) Hachinohe, 1968

Figure 4.49 - Recorded earthquake ground accelerations

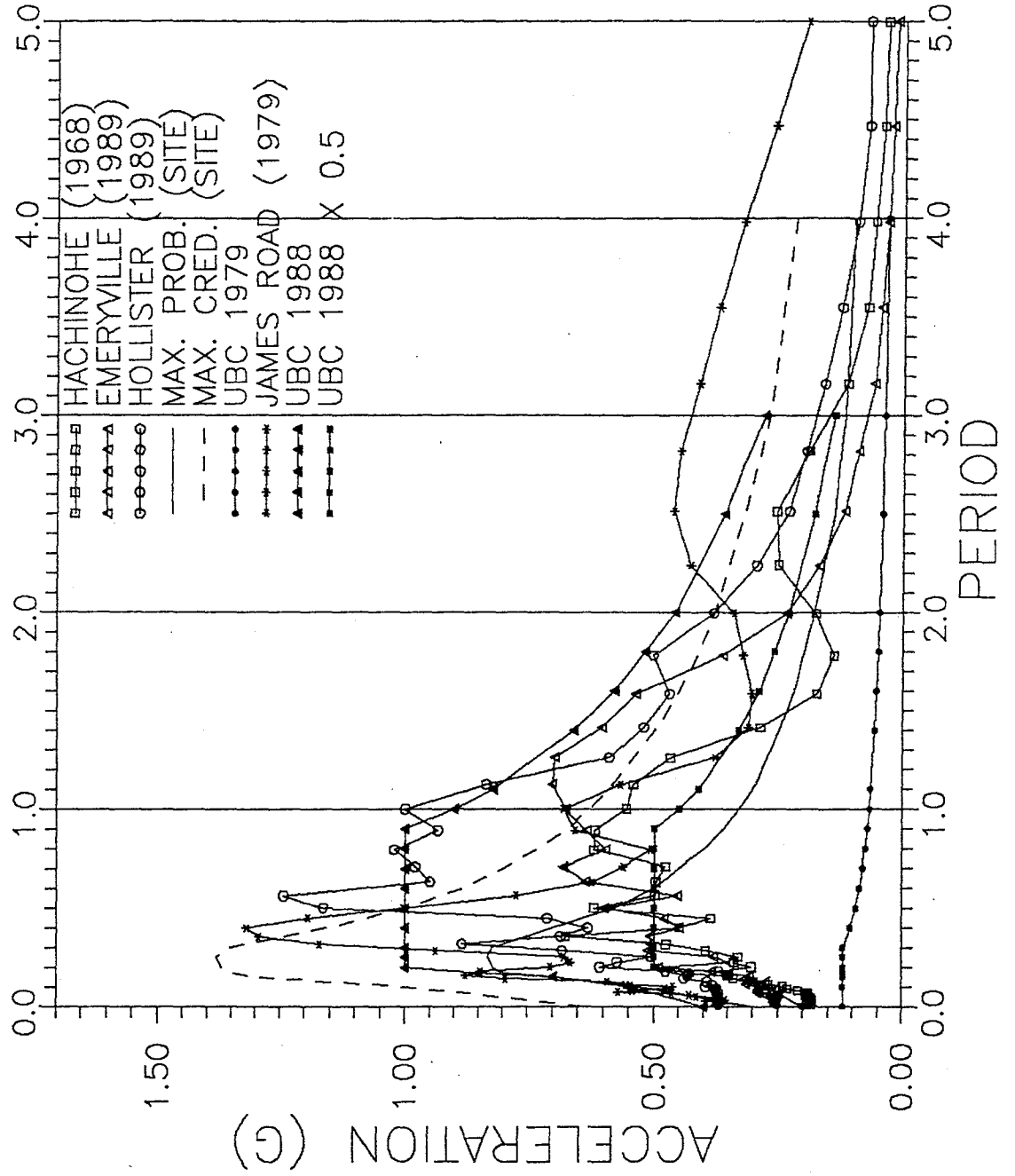

Fig. 4. 50 - Response spectra vs. design spectra.

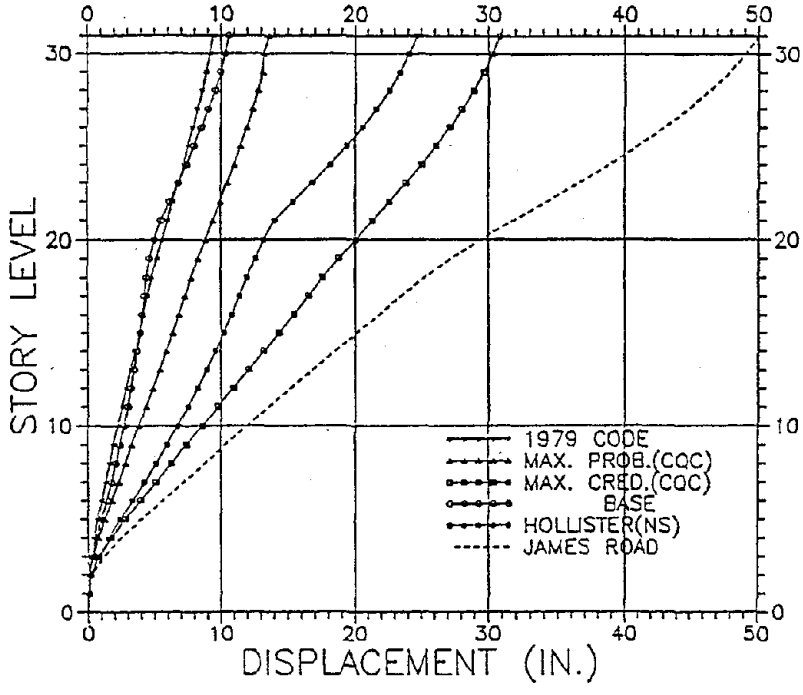

Figure 4.51 - Envelopes of maximum floor displacement

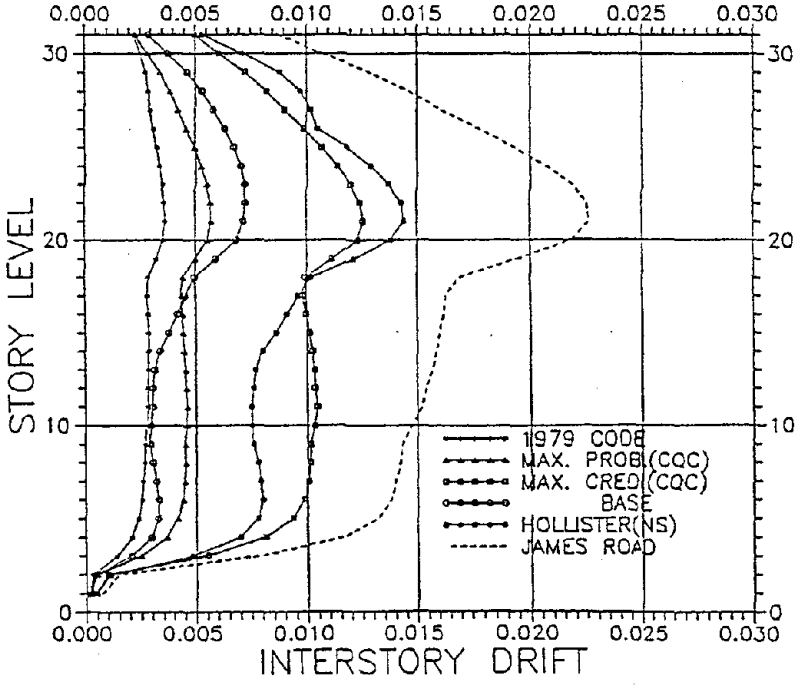

Figure 4.52 - Envelopes of maximum interstory drift

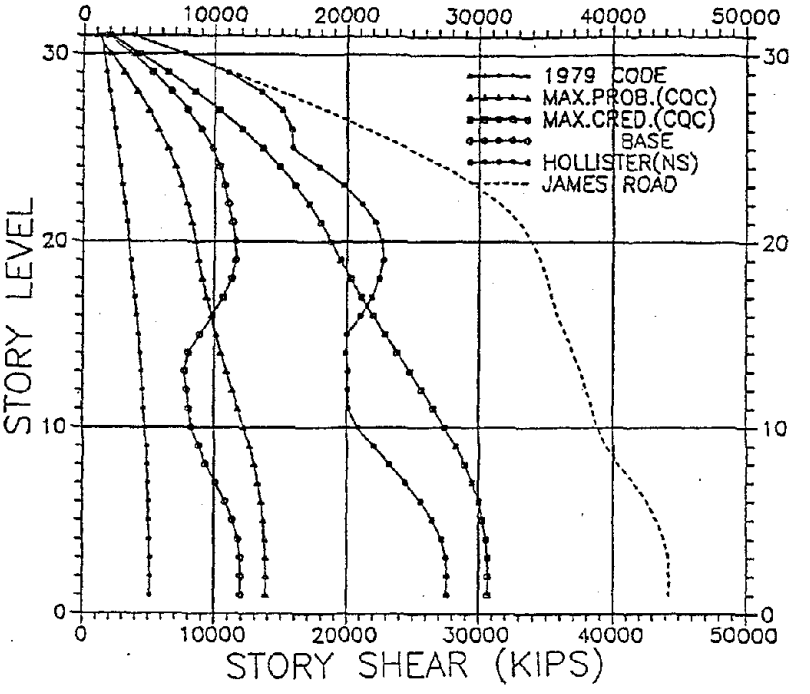

Figure 4.53 - Envelopes of maximum story shear

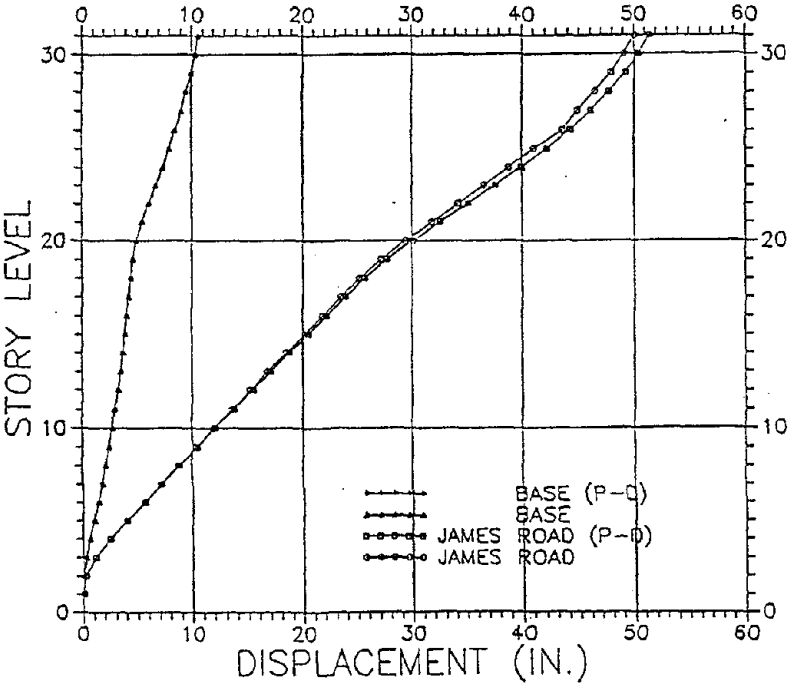

Figure 4.54 - Effect of P-delta on maximum floor displacement

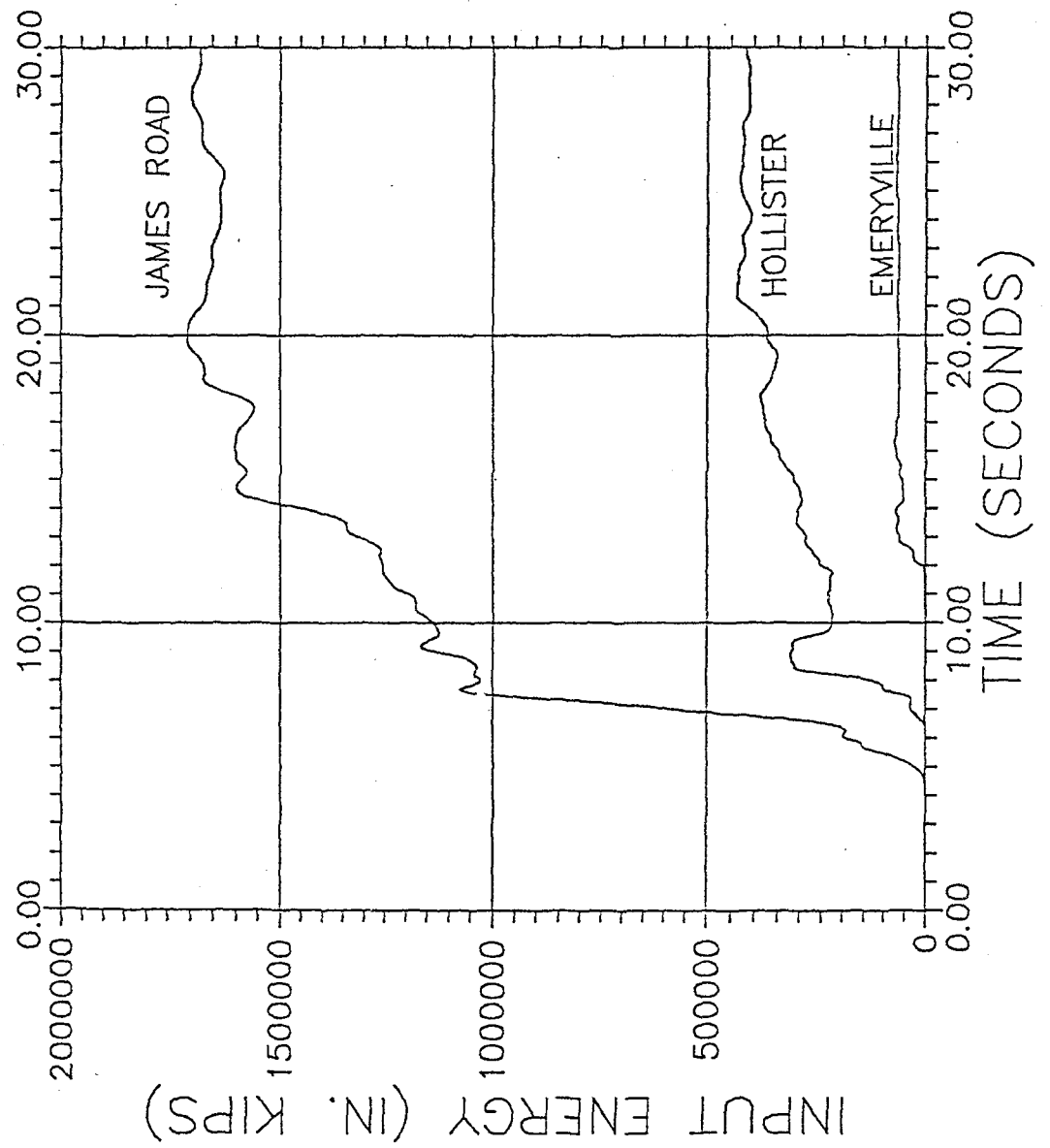

Figure 4.55 - Elastic input energy, earthquake ground motions

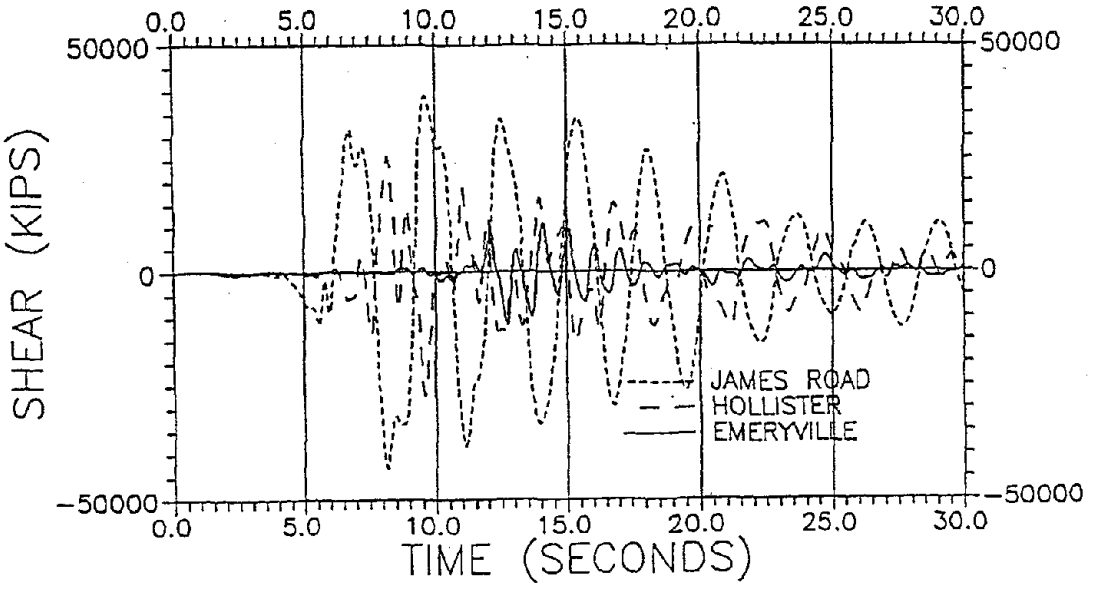

Figure 4.56 - Base shear response, earthquake ground motions

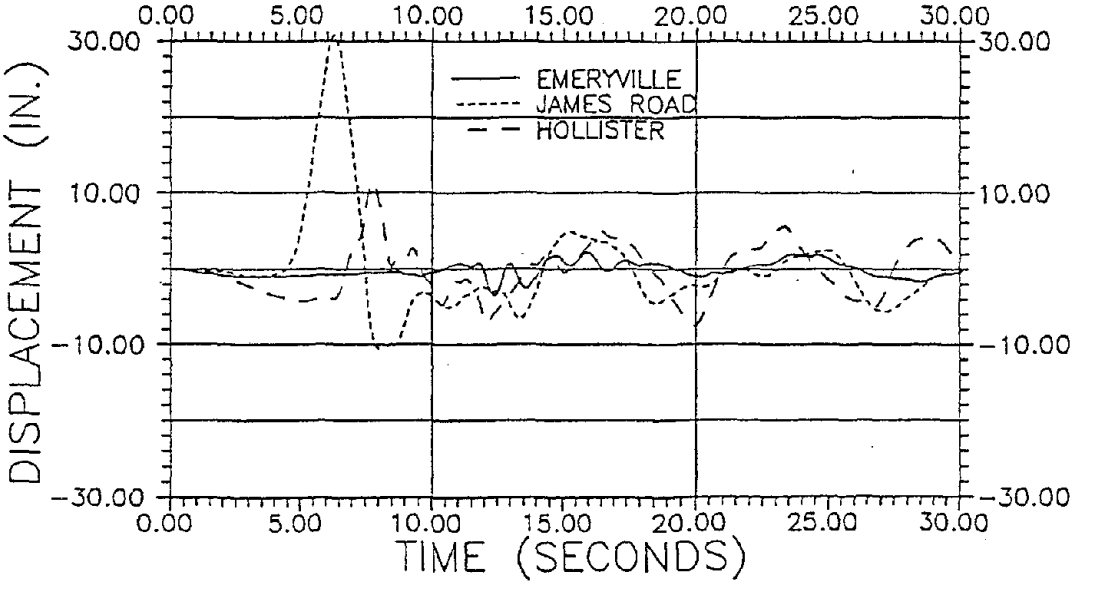

Figure 4.57 - Base displacement, earthquake ground motions

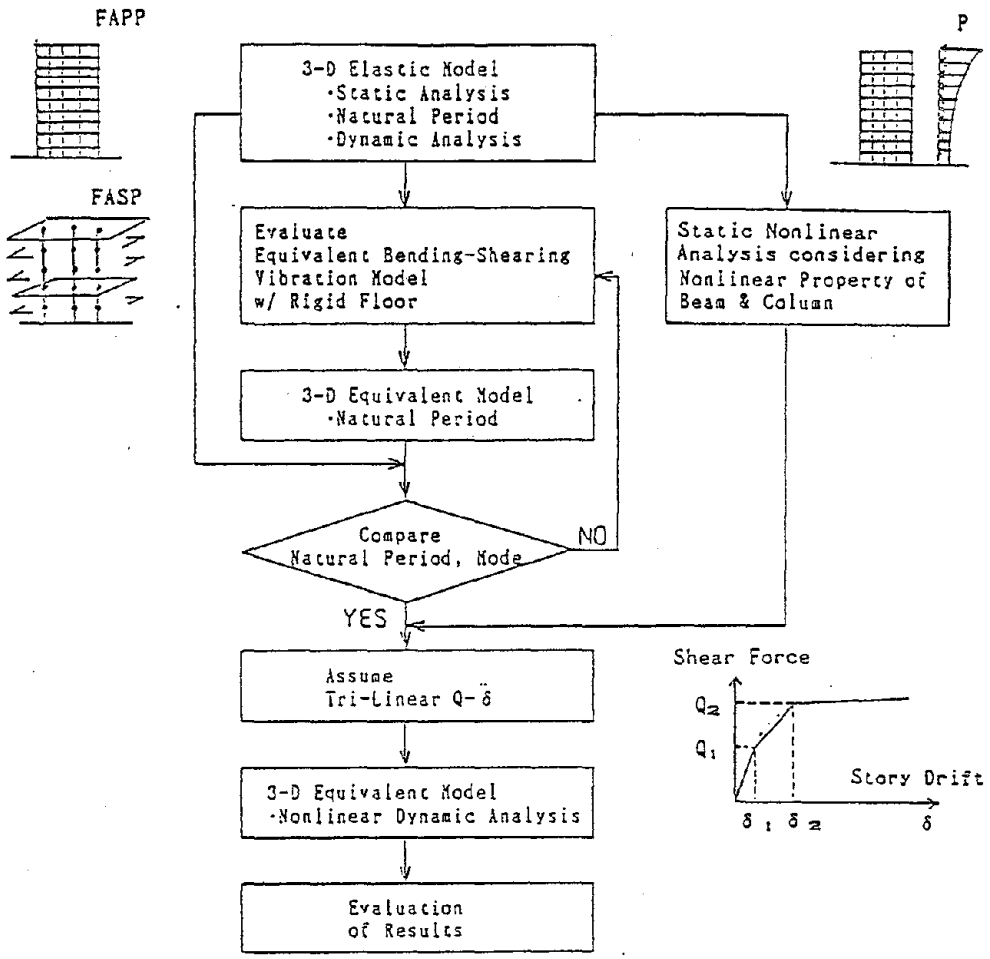

Figure 4.58 - Flow chart of earthquake response analysis

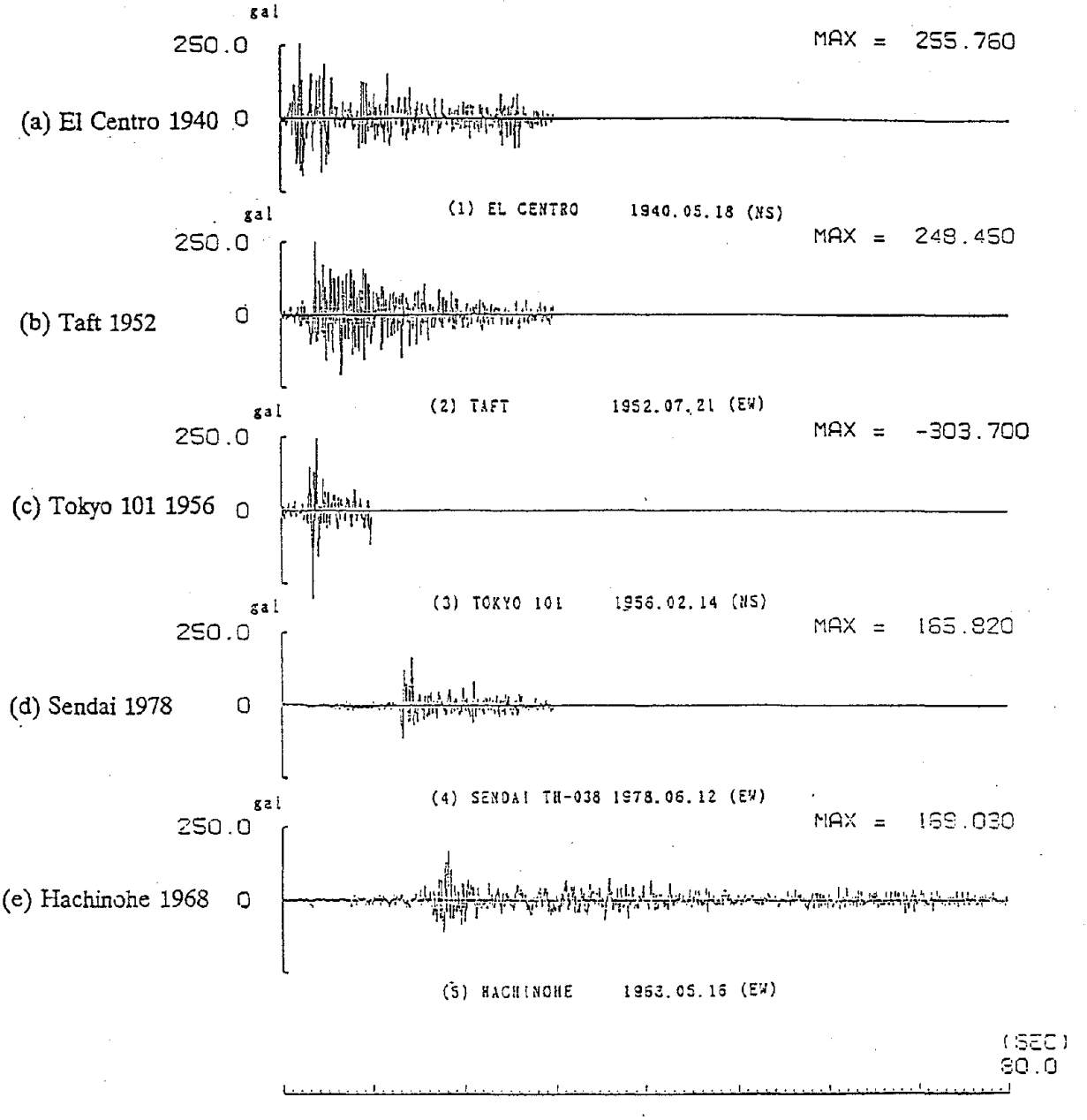

Figure 4.59 - Input earthquake record (standard earthquake at seismic design)

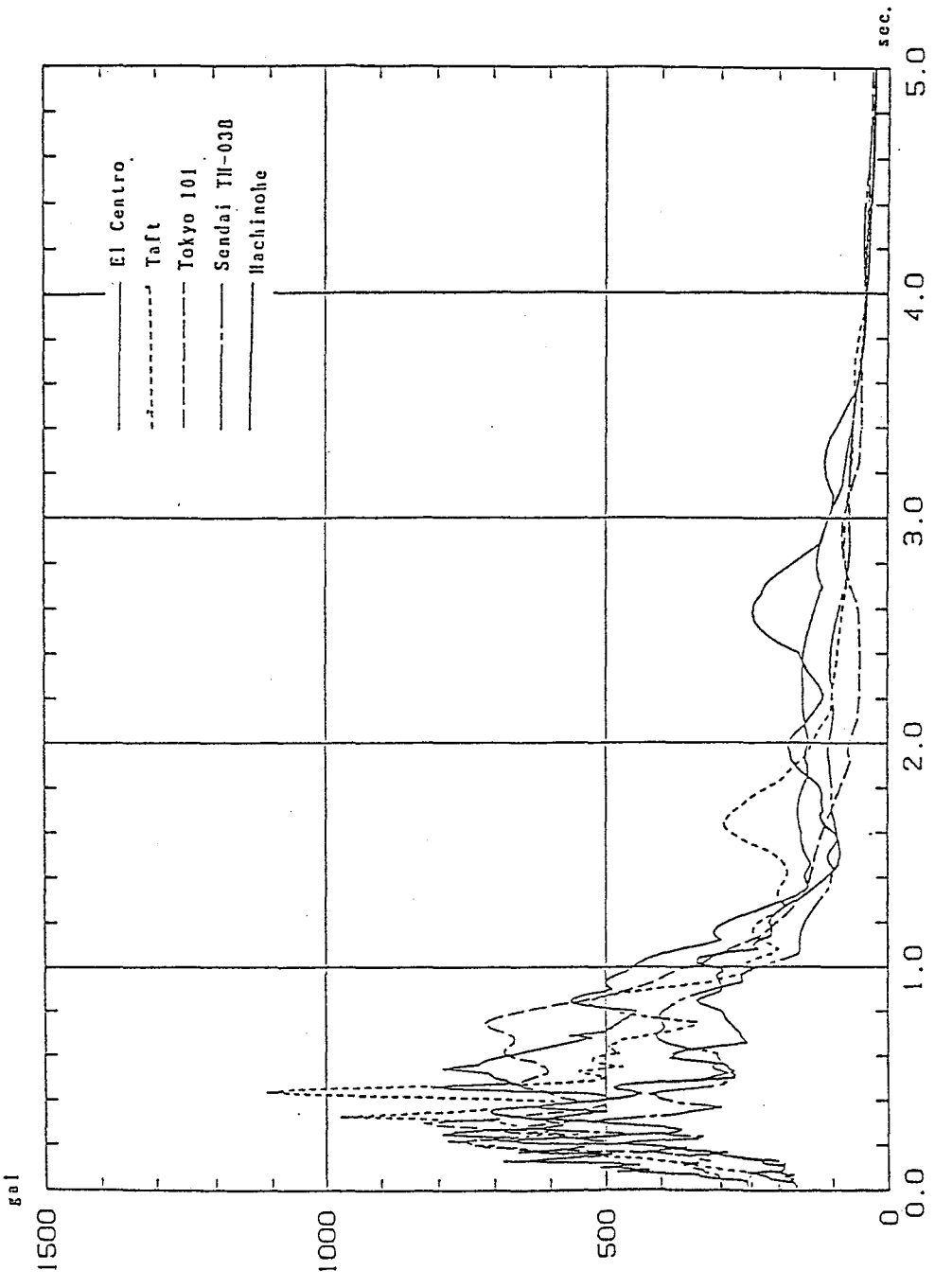

Figure 4.60 - Acceleration response spectra of input earthquakes (maximum velocity normalized to 25 cm/sec, 3% damping)

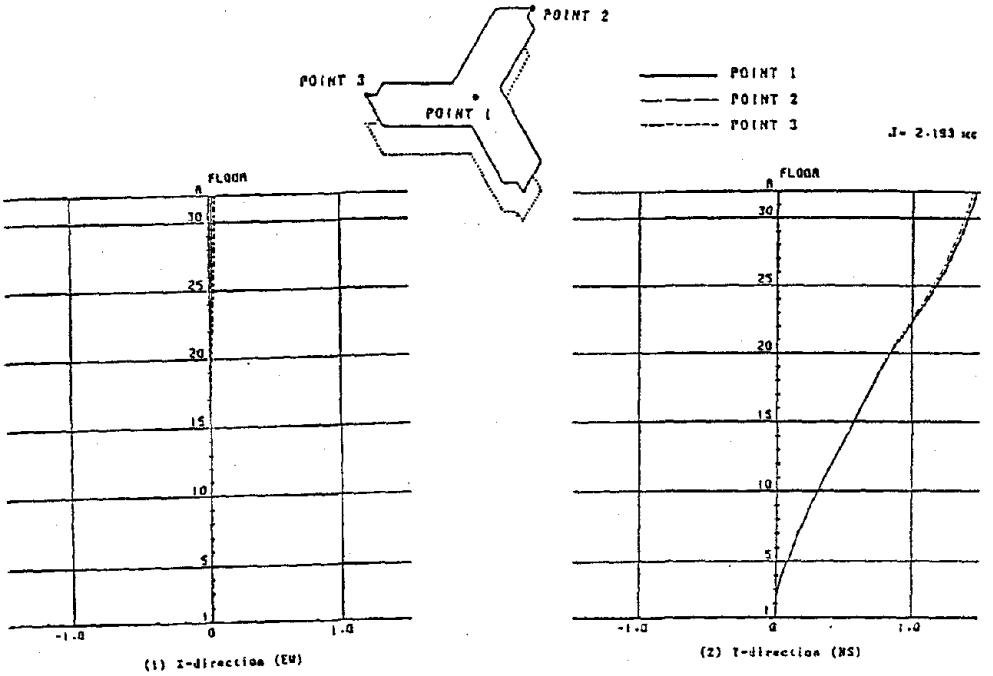

Figure 4.61 - 1st vibration mode (T=2.19 sec)

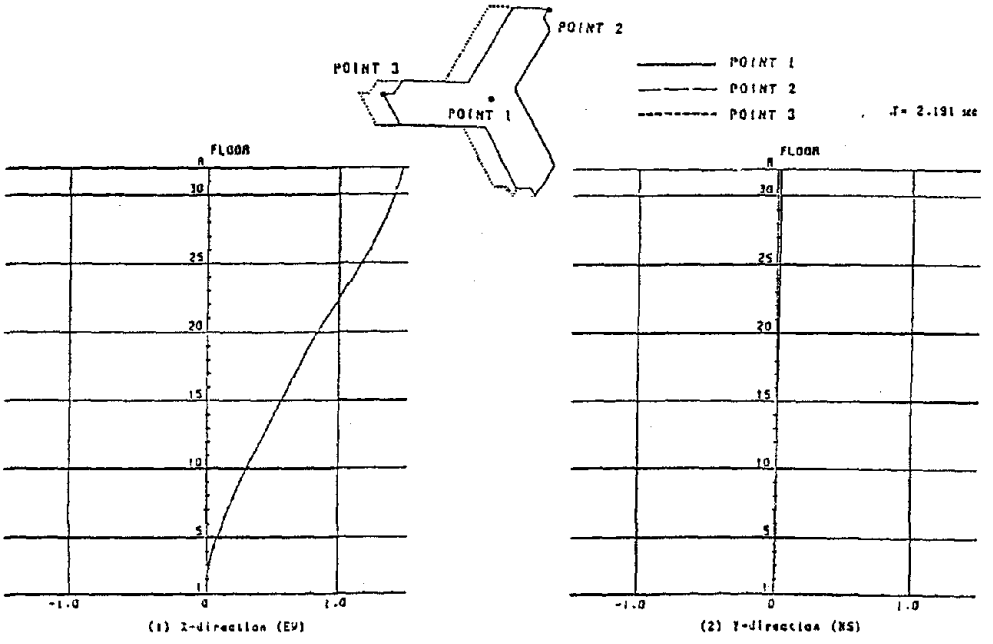

Figure 4.62 - 2nd vibration mode (T=2.29 sec)

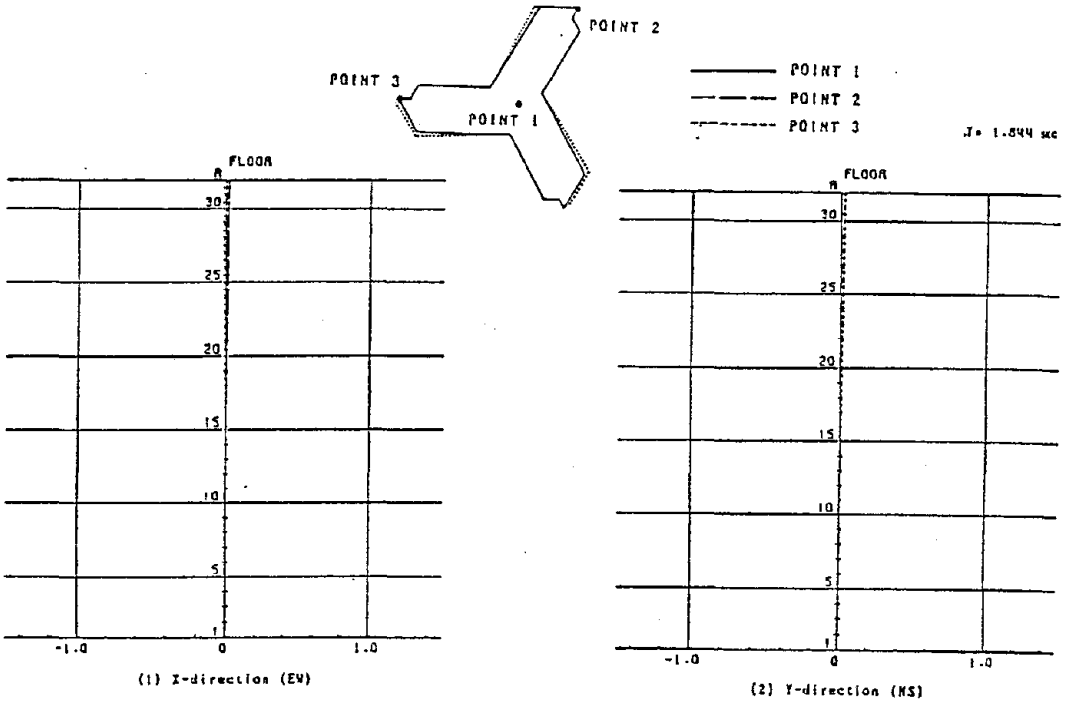

Figure 4.63 - 3rd vibration mode (T=1.84 sec)

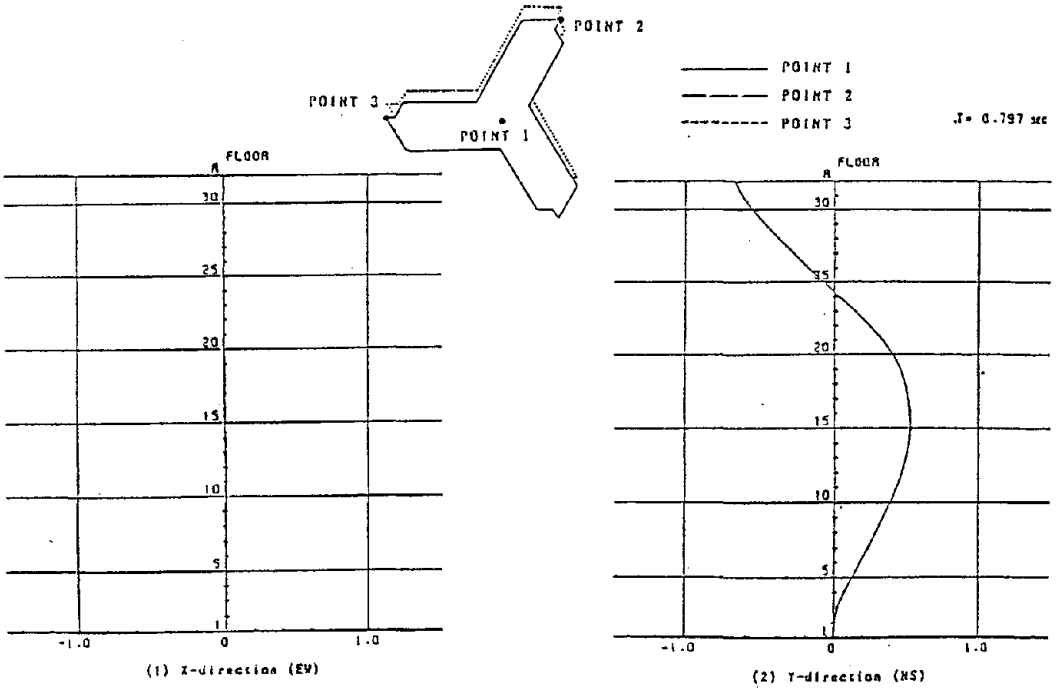

Figure 4.64 - 4th vibration mode (T=0.80 sec)

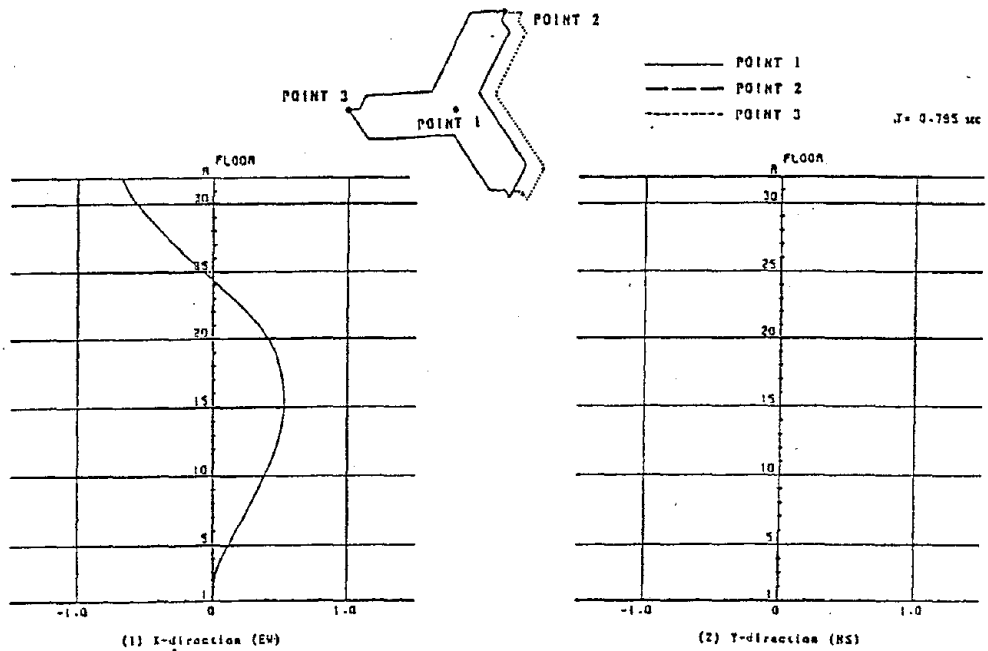

Figure 4.65 - 5th vibration mode (T=0.80 sec)

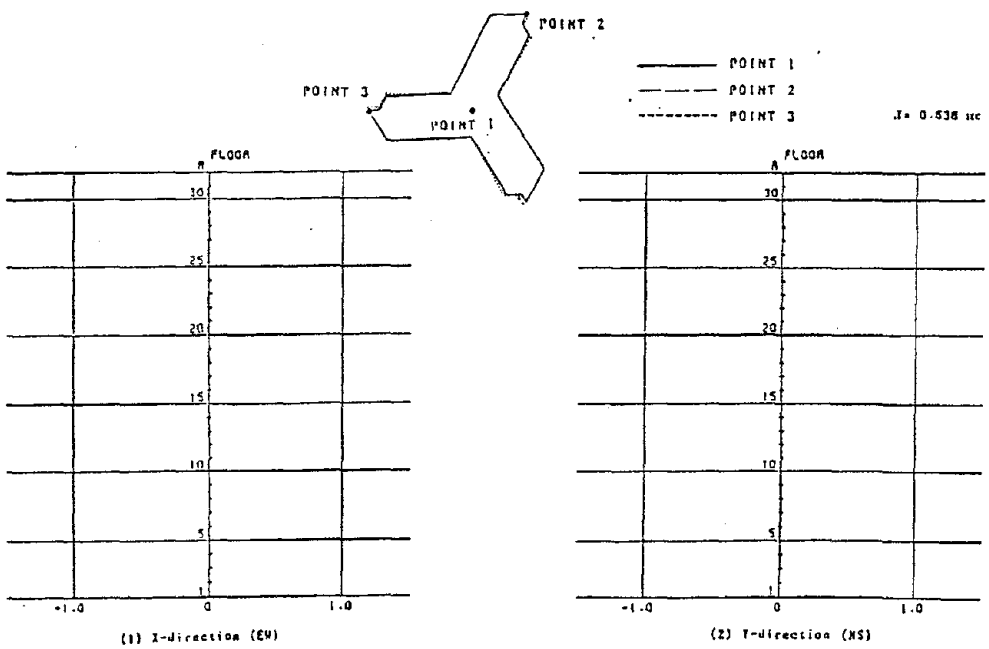

Figure 4.66 - 6th vibration mode (T=0.64 sec)

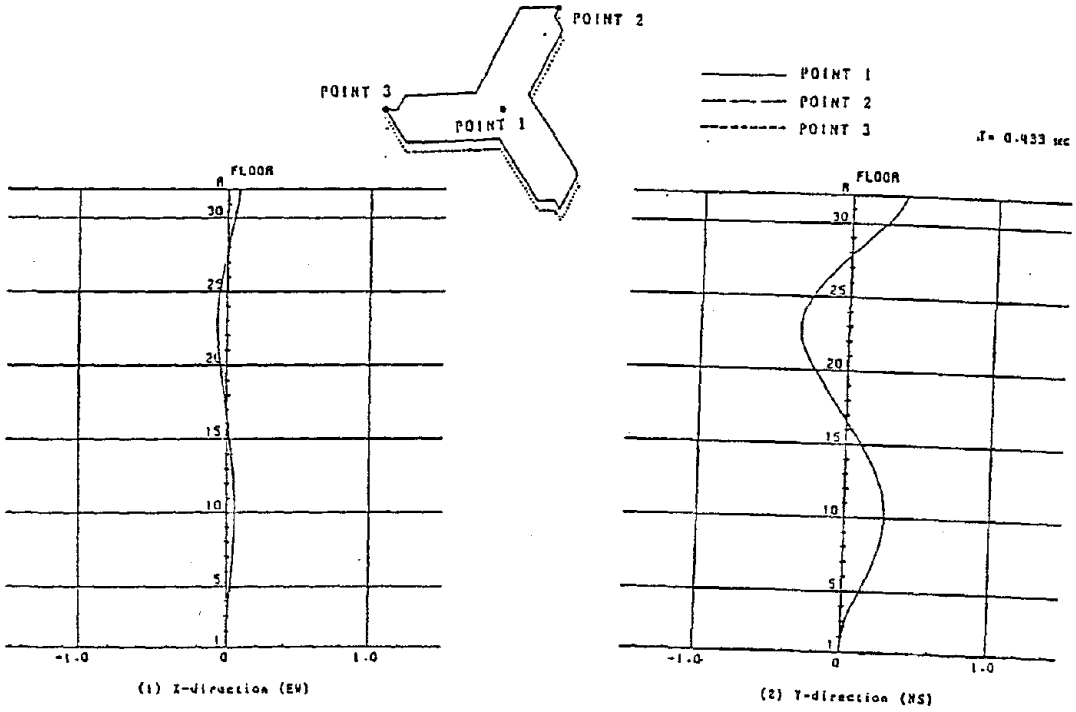

Figure 4.67 - 7th vibration mode (T=0.43 sec)

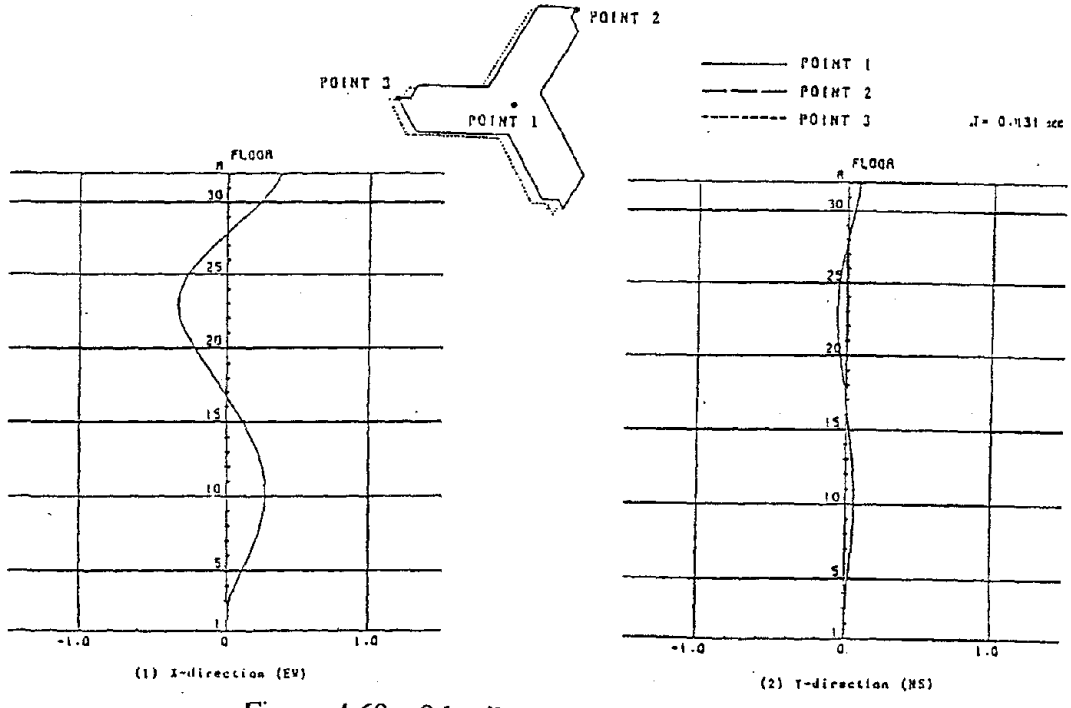

Figure 4.68 - 8th vibration mode (T=0.43 sec)

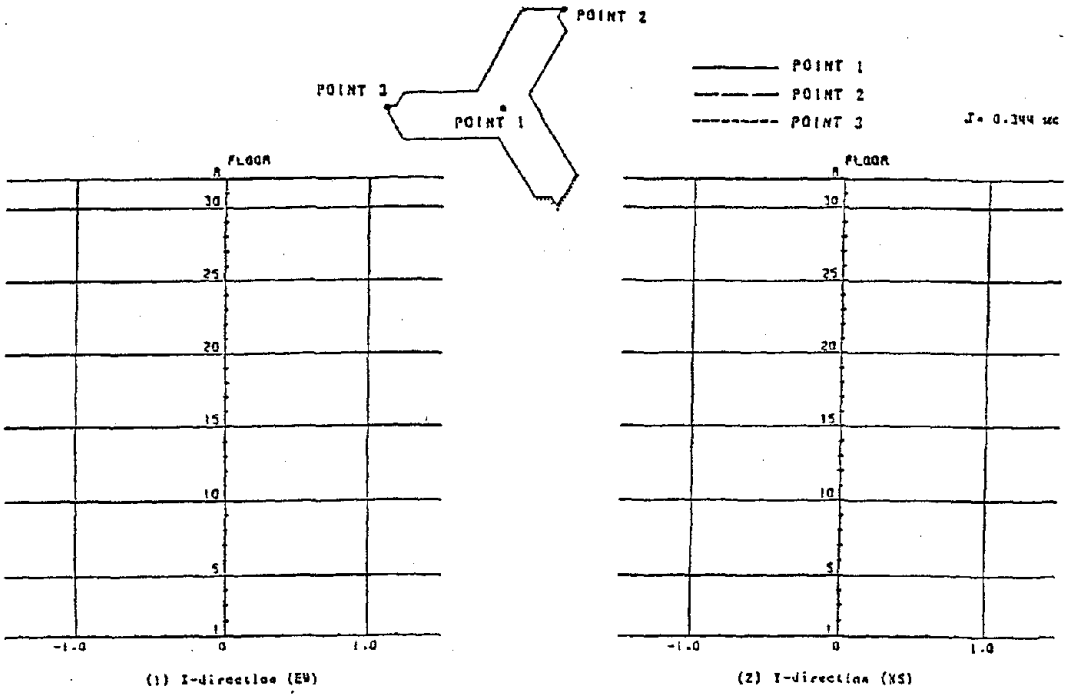

Figure 4.69 - 9th vibration mode (T=0.34 sec)

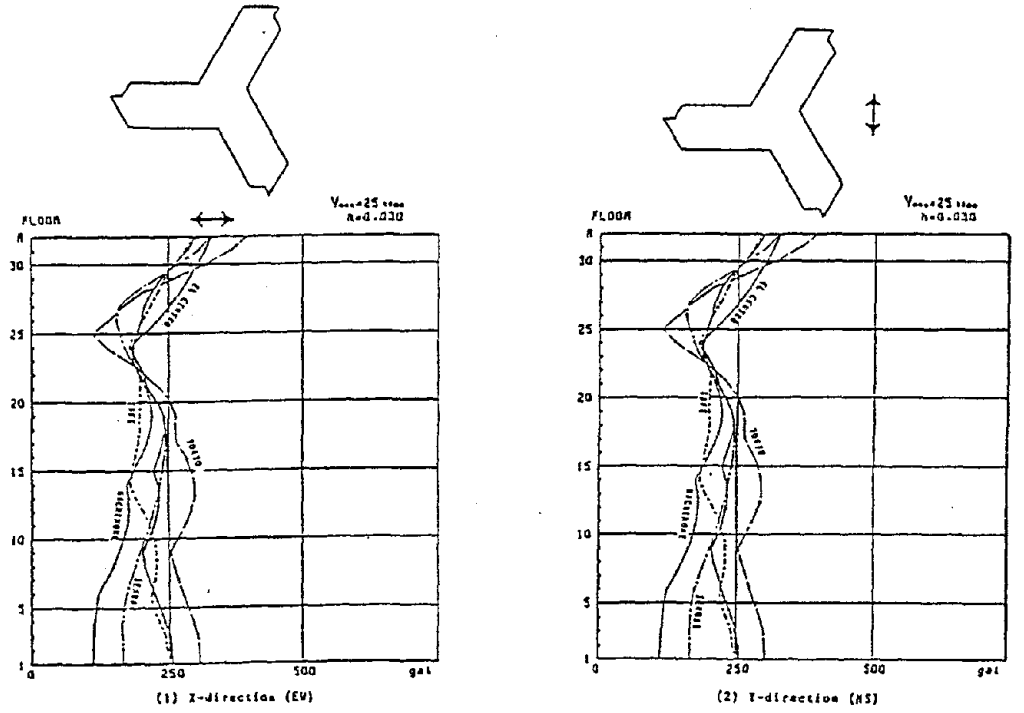

Figure 4.70 - Maximum floor acceleration (input 25 cm/sec normalized, elastic)

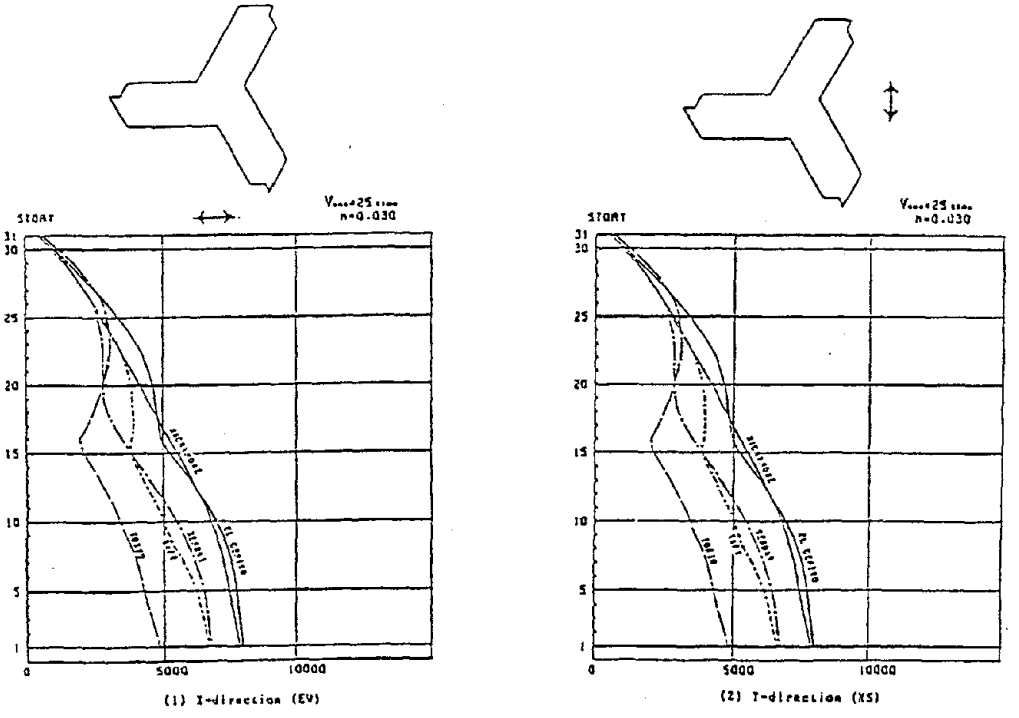

Figure 4.71 - Maximum shear force (input 24 cm/sec normalized, elastic)

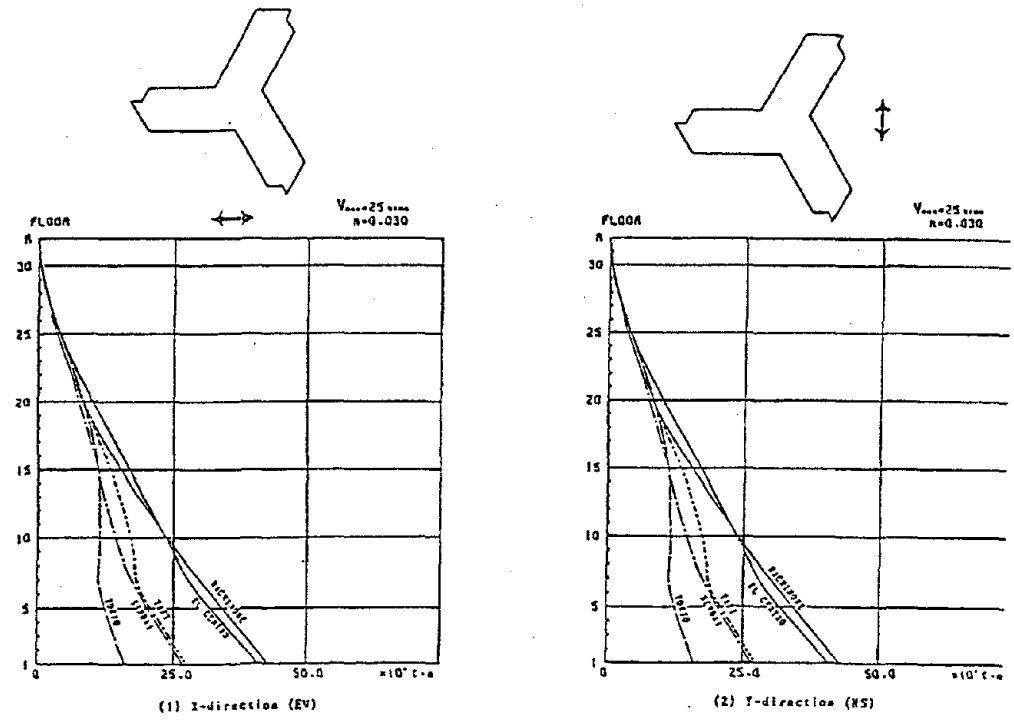

Figure 4.72 - Maximum overturning moment (input 25 cm/sec normalized, elastic)

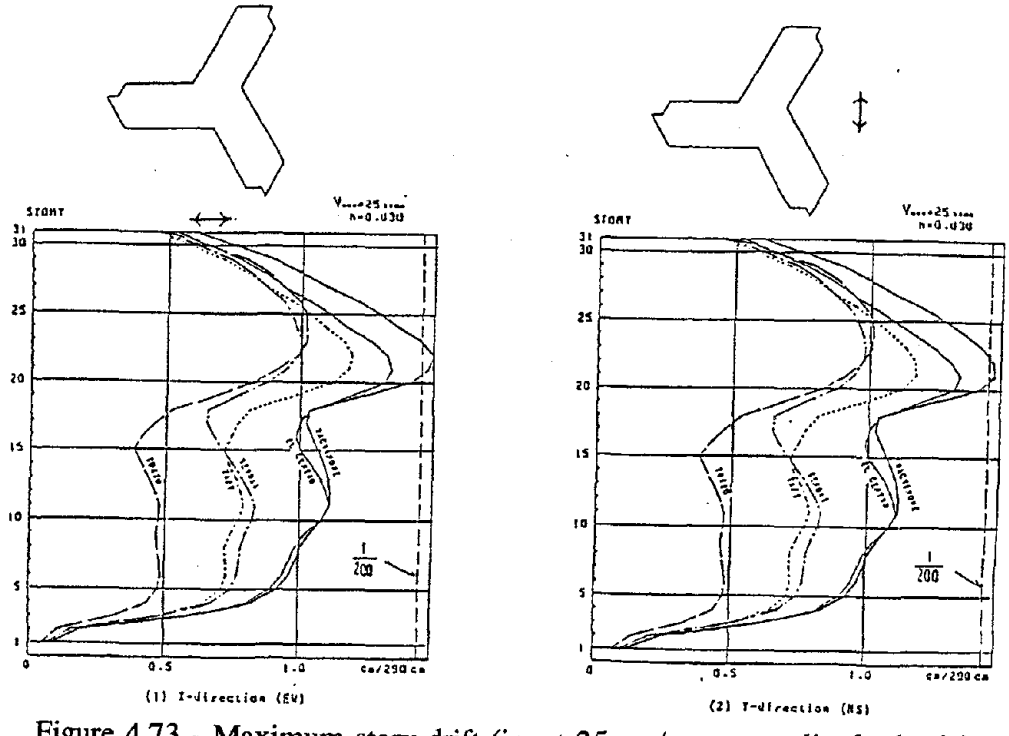

Figure 4.73 - Maximum story drift (input 25 cm/sec, normalized, elastic)

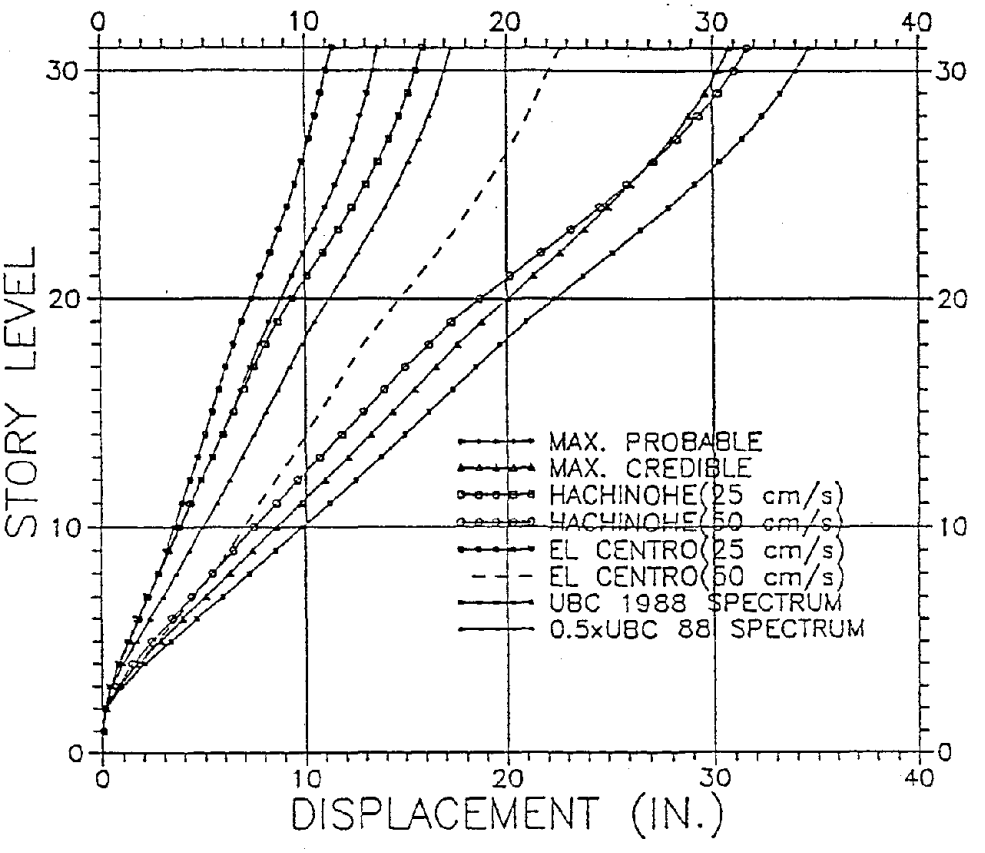

Figure 4.74 - Maximum floor displacement, U.S. vs. Japanese practice

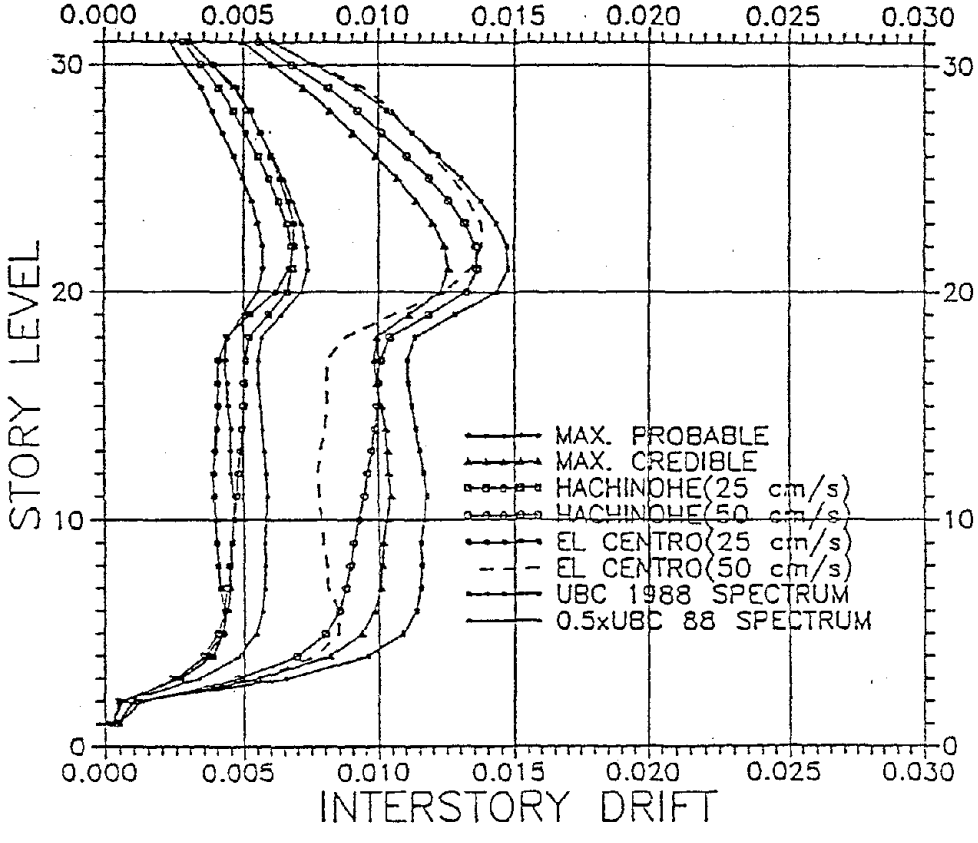

Figure 4.75 - Maximum drift index, U.S. vs. Japanese practice

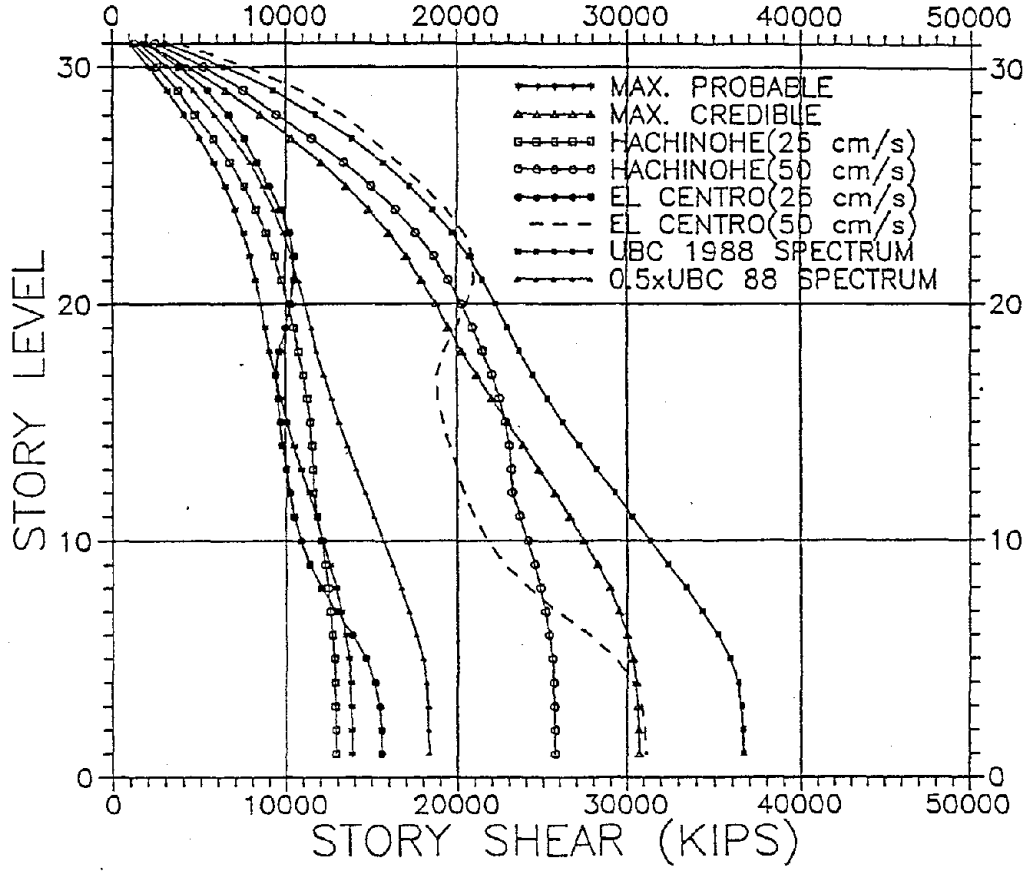

Figure 4.76 - Maximum story shear, U.S. vs. Japanese practice

Appendix 4.1 - 3-D Frame Analysis Method

(1) 3-Dimensional Rigorous Frame Analysis Method "FAPP-IV" [31]

Computer program "FAPP-Ⅳ" is used for analyses of the building structure, which is the three-dimensional general-purpose frame analysis computer program for high rise building structures developed by the Muto Institute.

While "FAPP-Ⅰ", "FAPP-Ⅱ" and "FAPP-Ⅲ" have been used for the buildings with ordinary-shaped floor plan, "FAPP-Ⅳ" was developed and used rather for the building which had irregular-shaped floor plan. For example, the Z-shaped Keio Plaza Hotel with 47 stories and the V-shaped Akasaka Prince Hotel with 37 stories were designed through the repetitive applications of the "FAPP-Ⅳ".

The outline of "FAPP-Ⅳ" is described below;

As shown in FIG.Ⅲ.1, "FAPP-Ⅳ" assumes the framework to consist of four kinds of elements of column (including wall) beam, bracing and joint panel between column and beam. Member's stiffness matrix is prepared considering bending, shearing and axial deformation for a column, bending and shearing deformation for a beam, axial deformation for a bracing, and shearing deformation for a joint panel

It is assumed here that two joint panels crossing perpendicularly to each other at a nodal point are set in the two principal directions of column's cross section, and have the same center. And their rotation and shearing deformations in the two principal directions are independent of each other. Relative horizontal deformation of the slab is neglected, i.e., the slab is assumed to be rigid in the horizontal plane.

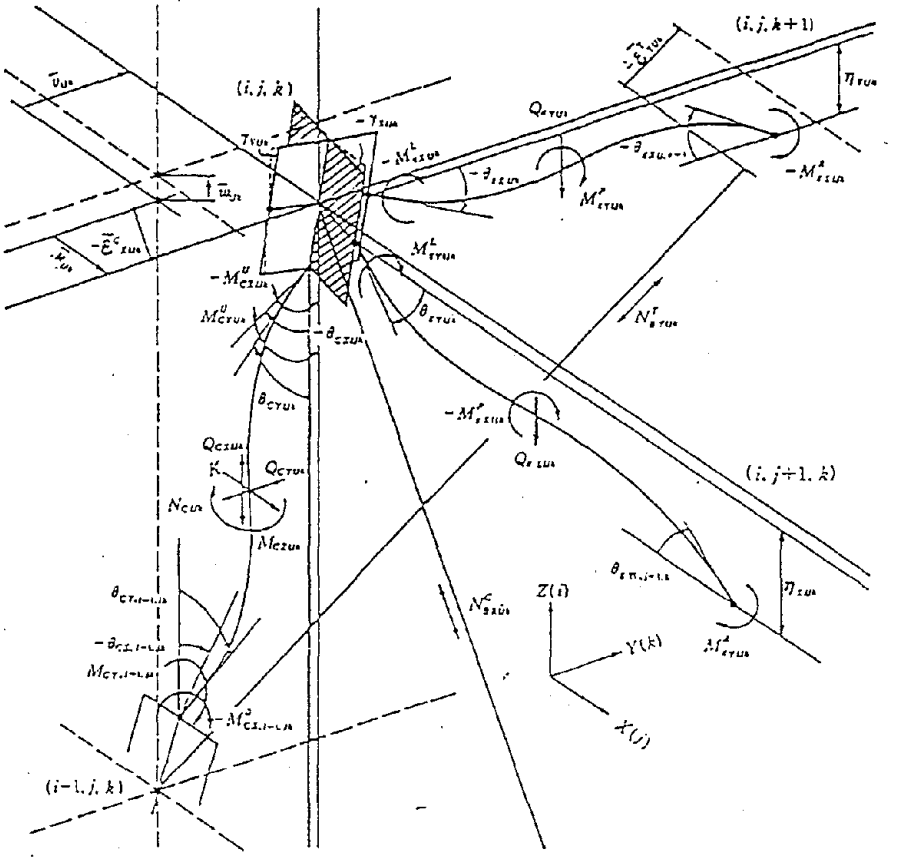

FIG. Ⅲ.1. STRESSES AND DEFORMATIONS
OF THE ELEMENTS OF FRAMEWORK

Equilibrium equation of each member element in its local coordinate system is as follows, using the symbols in FIG.Ⅲ.1.

a) Column

$$\begin{Bmatrix} {}_zM_U^c \\ {}_zM_D^c \\ {}_yM_U^c \\ {}_yM_D^c \\ {}_zQ^c \\ {}_yQ^c \\ N^c \\ M_T^c \end{Bmatrix}_{i,j,k} = \begin{bmatrix} {}_za^c & {}_zb^c & 0 & 0 & {}_zc^c & 0 & 0 & 0 \\ {}_zb^c & {}_za^c & 0 & 0 & {}_zc^c & 0 & 0 & 0 \\ 0 & 0 & {}_ya^c & {}_yb^c & 0 & {}_yc^c & 0 & 0 \\ 0 & 0 & {}_yb^c & {}_ya^c & 0 & {}_yc^c & 0 & 0 \\ {}_zc^c & {}_zc^c & 0 & 0 & {}_zd^c & 0 & 0 & 0 \\ 0 & 0 & {}_yc^c & {}_yc^c & 0 & {}_yd^c & 0 & 0 \\ 0 & 0 & 0 & 0 & 0 & 0 & e^c & 0 \\ 0 & 0 & 0 & 0 & 0 & 0 & 0 & f^c \end{bmatrix}_{i,j,k} \cdot \begin{Bmatrix} {}_z\theta_i{}^c \\ {}_z\theta_{i+1}{}^c \\ {}_y\theta_i{}^c \\ {}_y\theta_{i+1}{}^c \\ \overline{u_i} \\ \overline{v_i} \\ \overline{w_i} \\ \phi_i{}^c \end{Bmatrix}_{jk} \quad \text{---(Ⅲ-1)}$$

b) Beam

$$\begin{Bmatrix} {}_zM_L^g \\ {}_zM_R^g \\ {}_zQ^g \\ {}_zM_T^g \end{Bmatrix}_{i,j,k} = \begin{bmatrix} {}_za^g & {}_zb^g & {}_zc^g & 0 \\ {}_zb^g & {}_za^g & {}_zc^g & 0 \\ {}_zc^g & {}_zc^g & {}_zd^g & 0 \\ 0 & 0 & 0 & {}_zf^g \end{bmatrix}_{i,j,k} \cdot \begin{Bmatrix} {}_z\theta_j^g \\ {}_z\theta_{j+1}{}^g \\ {}_z\overline{\lambda}_j \\ {}_z\phi_j \end{Bmatrix}_{ik}$$

$$\begin{Bmatrix} {}_yM_L^g \\ {}_yM_R^g \\ {}_yQ^g \\ {}_yM_T^g \end{Bmatrix}_{i,j,k} = \begin{bmatrix} {}_ya^g & {}_yb^g & {}_yc^g & 0 \\ {}_yb^g & {}_ya^g & {}_yc^g & 0 \\ {}_yc^g & {}_yc^g & {}_yd^g & 0 \\ 0 & 0 & 0 & {}_yf^g \end{bmatrix}_{i,j,k} \cdot \begin{Bmatrix} {}_y\theta_k^g \\ {}_y\theta_{k+1}{}^g \\ {}_y\overline{\lambda}_k \\ {}_y\phi_k \end{Bmatrix}_{ij} \quad \text{--------(Ⅲ-2)}$$

c) Joint panel

$$\begin{aligned} \{{}_zM^P\}_{i,j,k} &= [{}_zG^P]_{i,j,k} \cdot \{{}_z\gamma\}_{i,j,k} \\ \{{}_yM^P\}_{i,j,k} &= [{}_yG^P]_{i,j,k} \cdot \{{}_y\gamma\}_{i,j,k} \end{aligned} \quad \text{----------(Ⅲ-3)}$$

d) Bracing

$$\begin{aligned} \{{}_zP\}_{i,j,k} &= [{}_zS^B]_{i,j,k} \cdot \{{}_z\eta\}_{i,j,k} \\ \{{}_yP\}_{i,j,k} &= [{}_yS^B]_{i,j,k} \cdot \{{}_y\eta\}_{i,j,k} \end{aligned} \quad \text{----------(Ⅲ-4)}$$

In the generalized coordinate system, displacements in Eqs. (Ⅲ-1)-(Ⅲ-4) are expressed as

$$
\begin{cases}
{}_{x(y)}\theta^{c}_{i,j,k} = {}_{x(y)}\theta_{i,j,k} - \dfrac{1}{2}\,{}_{x(y)}\gamma_{i,j,k} \\
{}_{x(y)}\theta^{g}_{i,j,k} = {}_{x(y)}\theta_{i,j,k} + \dfrac{1}{2}\,{}_{x(y)}\gamma_{i,j,k} \\
\overline{u}_{i,j,k} = (-u_{jk} - {}_{x}D_{jk}\cdot{}_{z}\theta^{g}_{jk})_{i} - (-u_{jk} + {}_{x}D_{jk}\cdot{}_{z}\theta^{g}_{jk})_{i+1} \\
\overline{v}_{i,j,k} = (v_{jk} - {}_{y}D_{jk}\cdot{}_{y}\theta^{g}_{jk})_{i} - (v_{jk} + {}_{y}D_{jk}\cdot{}_{y}\theta^{g}_{jk})_{i+1} \\
\overline{w}_{i,j,k} = w_{i+1,j,k} - w_{i,j,k} \\
{}_{x}\overline{\lambda}_{i,j,k} = (-w - {}_{z}B\cdot{}_{z}\theta^{c})_{i,j+1,k} - (-w + {}_{x}B\cdot{}_{z}\theta^{c})_{i,j,k} \\
{}_{y}\overline{\lambda}_{i,j,k} = (w - {}_{y}B\cdot{}_{y}\theta^{c})_{i,j,k+1} - (w + {}_{y}B\cdot{}_{y}\theta^{c})_{i,j,k} \\
{}_{z}\overline{\eta}_{i,j,k} = (w_{i,j,k} - w_{i+1,j+1,k})\,h_{i}/l^{B}_{i,j,k} + (u_{i,j,k} - u_{i+1,j+1,k})\,{}_{z}l^{B}_{i,j,k}/l^{B}_{i,j,k}
\end{cases}
\qquad \text{----------(Ⅲ-5)}
$$

where xθijk, yθijk: rotational angles of joint panel
xγijk, yγijk: shearing deformation angles of joint panel
uijk , vijk : horizontal displacements at center of joint panel
wijk : vertical displacement at center of joint panel

The rigid floor assumption allows the i-th floor displacement to be represented as three degrees of freedom; horizontal displacements U_i, V_i and torsional rotation angle Φ_i at the center of gravity of its floor. Consequently, horizontal displacements u_{ijk}, v_{ijk} at each joint panel are expressed as Eq.(Ⅲ-6), using the coordinates of center of gravity ($_xe$, $_ye$) and those of each nodal point ($_xL$, $_yL$) in the generalized coordinate system. Torsional deformation angles of each element in the local coordinate system are expressed as Eq.(Ⅲ-7). (see FIG.Ⅲ.2)

$$
\begin{cases}
u_{i,j,k} = U_i - ({}_{y}L_{k} - {}_{y}e_{i})\Phi_{i} \\
v_{i,j,k} = V_i + ({}_{z}L_{j} - {}_{x}e_{i})\Phi_{i}
\end{cases}
\qquad \text{----------(Ⅲ-6)}
$$

$$
\begin{cases}
\phi^{c}_{ijk} = \Phi_{i} - \Phi_{i+1} \\
{}_{x}\phi_{ijk} = {}_{y}\theta_{ijk} - {}_{y}\theta_{i,j+1,k} \\
{}_{y}\phi_{ijk} = {}_{z}\theta_{ijk} - {}_{z}\theta_{i,j,k+1}
\end{cases}
\qquad \text{----------(Ⅲ-7)}
$$

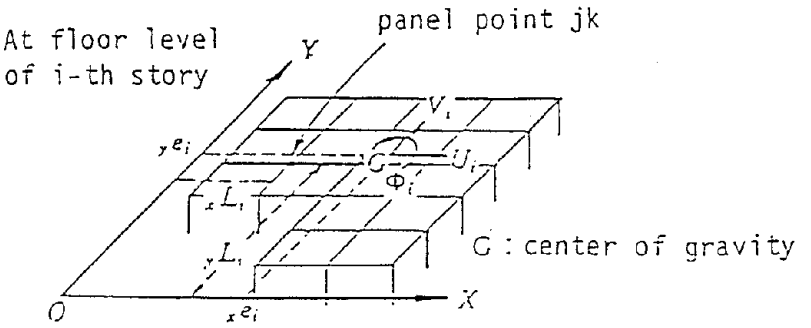

FIG.Ⅲ.2. GENERALIZED COORDINATE SYSTEM

After composing stiffness matrix at each story segment by using the transformation matrix expressed as Eq.(Ⅲ-5)-(Ⅲ-7), equilibrium equation between forces and displacements of the whole building structure can be obtained as Eq.(Ⅲ-8) due to displacement continuity condition of each story.

$$\begin{Bmatrix} R_1 \\ R_2 \\ \vdots \\ R_i \\ \vdots \\ R_N \\ \hline R_{xyz} \end{Bmatrix} = \left[\begin{array}{cccccc|c} K_1 & C_1 & & & & & E_1 \\ C_1^T & K_2 & C_2 & & & & E_2 \\ & \ddots & \ddots & \ddots & & & \vdots \\ & & C_{i-1}^T & K_i & C_i & & E_i \\ & & & \ddots & \ddots & \ddots & \vdots \\ & & & & C_{N-1}^T & K_N & E_N \\ \hline E_1^T & E_2^T & \cdots & E_i^T & \cdots & E_N^T & F_1 \end{array}\right] \begin{Bmatrix} \tau_1 \\ \tau_2 \\ \vdots \\ \tau_i \\ \vdots \\ \tau_N \\ \hline \tau_{xyz} \end{Bmatrix} \qquad \text{----------(Ⅲ-8)}$$

where $\tau_i = |{}_x\theta_i, {}_x\gamma_i, {}_y\theta_i, {}_y\gamma_i, w_i|^T_{jk}$, $j=1\sim s$, $k=1\sim t$

$\tau_{xyz} = |U_i, V_i, \Phi_i|^T$, $i=1\sim N$

t : number of columns along x-direction
s : number of columns along y-direction
N : number of stories

Stiffness matrix at the center of gravity can be obtained by reducing the displacements of Eq.(Ⅲ-8) to r_{xyz}.

In order to conduct the statical frame analysis against specified external forces, $\{R\}$, Eq.(Ⅲ-8) shall be first solved. Then, through the backward calculation using the other equations, member stresses and deformations are finally obtained.

For the Eigen-value analysis in order to obtain natural periods and vibration modes, Eq.(Ⅲ-8) must be changed into dynamic equillibrium equation by replacing $\{R\}$ to inertia forces $-[M]\{\ddot{r}_{xyz}\}$.

Dynamic response analysis is also conducted after substituting damping forces $\gamma[K]\{\dot{r}_{xyz}\}$ and excitation forces $\alpha[M]$, where γ and α are viscous damping coefficient and input ground acceleration respectively.

(2) Frame Analysis Method by Symplified Procedure"FASP"

Against severe and worst earthquakes, non-linear dynamic analyses are excecuted by Frame Analysis Method by Simplified Procedure, "FASP". In this method, bending-shearing elements are substituted for the plane frames which compose the building structure. In substituting bending-shearing elements, the total deflections which are obtained by the aforementioned FAPP method are divided into the bending deflections of the whole building structure due to the axial deformation of columns and the shearing deflections due to each own deformation of framing members, as shown in FIG.Ⅲ.3. Depending on the results of the division, the bending and shearing stiffnesses are evaluated.

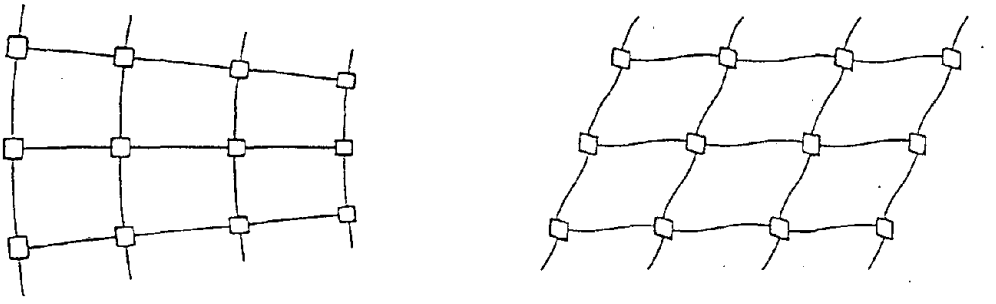

FIG.Ⅲ.3 DIVISION INTO BENDING AND SHEARING DEFORMATION

The relationship of the j-th bending-shearing element between external force and displacement at the i-th story is indicated in the following equation.

$$\begin{Bmatrix} M_{ij} \\ P_{ij} \\ M_{i+1j} \\ P_{i+1j} \end{Bmatrix} = \begin{bmatrix} a_{ij} & c_{ij} & b_{ij}-c_{ij} \\ c_{ij} & d_{ij} & c_{ij}-d_{ij} \\ b_{ij} & c_{ij} & a_{ij}-c_{ij} \\ -c_{ij} & -d_{ij} & -c_{ij} \quad d_{ij} \end{bmatrix} \begin{Bmatrix} \theta_{ij} \\ u_i \\ \theta_{i+1j} \\ \theta_{i+1j} \end{Bmatrix} \quad \cdots\cdots(\mathrm{III}-9)$$

where, M_{ij} : bending moment at the i-th story of the j-th element
P_{ij} : lateral force at the i-th story of the j-th element
θ_{ij} : rotation angle at the i-th story of the j-th element
u_i : horizontal displacement at the j-th story

$$\left.\begin{aligned} a_{ij} &= \frac{2EI_{ij}}{l_{ij}} \cdot \frac{2+\beta_{ij}}{1+2\beta_{ij}}, \quad b_{ij} = \frac{2EI_{ij}}{l_{ij}} \cdot \frac{1-\beta_{ij}}{1+2\beta_{ij}} \\ c_{ij} &= -\frac{a_{ij}+b_{ij}}{l_{ij}}, \quad d_{ij} = -\frac{2c_{ij}}{l_{ij}} \\ \beta_{ij} &= \frac{6EI_{ij}}{GA_{ij}l_{ij}^2} \end{aligned}\right\} \cdots\cdots (\text{III}-10)$$

E : Young's modulus
I_{ij} : geometrical moment of inertia at the i-th story of the j-th element
G : shear modulus of elasticity
A_{ij} : effective shear area at the i-th story of the j-th element

When m pieces of bending-shearing element are connected by rigid floor slabs in their plane as a whole, the equilibrium equation of the i-th floor segment is as follows;

$$\begin{Bmatrix} M_{i1} \\ \vdots \\ M_{ij} \\ \vdots \\ M_{im} \\ P_i \\ M_{i+1\,1} \\ \vdots \\ M_{i+1\,j} \\ \vdots \\ M_{im} \\ P_{i+1} \end{Bmatrix} = \begin{bmatrix} a_{i1} & & 0 & & c_{i1} & b_{i1} & & 0 & & -c_{i1} \\ & \ddots & & & \vdots & & \ddots & & & \vdots \\ & & a_{ij} & & c_{ij} & & & b_{ij} & & -c_{ij} \\ 0 & & & \ddots & \vdots & 0 & & & \ddots & \vdots \\ & & & a_{im} & c_{im} & & & & b_{im} & -c_{im} \\ c_{i1} & \cdots & c_{ij} & \cdots & e_i & c_{i1} & \cdots & c_{ij} & \cdots & -e_i \\ b_{i1} & & & & c_{i1} & a_{i1} & & & & -c_{i1} \\ & \ddots & & 0 & \vdots & & \ddots & & 0 & \vdots \\ & & b_{ij} & & c_{ij} & & & a_{ij} & & -c_{ij} \\ 0 & & & \ddots & \vdots & 0 & & & \ddots & \vdots \\ & & & b_{im} & c_{im} & & & & a_{im} & -c_{im} \\ -c_{i1} & \cdots & -c_{ij} & \cdots & -e_i & -c_{i1} & \cdots & -c_{ij} & \cdots & e_i \end{bmatrix} \begin{Bmatrix} \theta_{i1} \\ \theta_{ij} \\ \theta_{im} \\ u_i \\ \theta_{i+1\,1} \\ \theta_{i+1\,j} \\ \theta_{i+1\,m} \\ u_{i+1} \end{Bmatrix} \cdots\cdots (\text{III}-11)$$

Where, $e_i = \sum_{j=1}^{m} d_{ij}$

Eq.(Ⅲ-11) is expressed simply in the following equation.

$$\begin{Bmatrix} \overline{R_i} \\ \overline{R_{i+1}} \end{Bmatrix} = \begin{bmatrix} K_i & C_i \\ C_i^T & K_i' \end{bmatrix} \begin{Bmatrix} r_i \\ r_{i+1} \end{Bmatrix} \quad \cdots\cdots (Ⅲ-12)$$

Consequently, the equilibrium equation of the whole building structure is expressed followingly from the continuity of the story displacement.

$$\begin{Bmatrix} R_1 \\ R_2 \\ \vdots \\ R_i \\ \vdots \\ R_{N-1} \\ R_N \end{Bmatrix} = \begin{bmatrix} K_1 & C_1 & & & & \\ C_1^T & K_1'+K_2 & C_2 & & & \\ & C_{i-1}^T & K_{i-1}'+K_i & C_i & & \\ & & C_{N-2}^T & K_{N-2}'+K_{N-1} & C_{N-1} & \\ & & & C_{N-1}^T & K_{N-1}'+K_N & \end{bmatrix} \begin{Bmatrix} r_1 \\ r_2 \\ \vdots \\ r_i \\ \vdots \\ r_{N-1} \\ r_N \end{Bmatrix} \quad \cdots\cdots (Ⅲ-13)$$

Shear stiffness GA_{ij} is assumed to have nonlinear degrading property. Bending deformation is smaller, and the bending stiffness EI_{ij} is assumed to remain elastic. Since, in the nonlinear earthquake response analysis, coefficients a_{ij}, b_{ij}, c_{ij}, d_{ij} and β_{ij} in Eq.(Ⅲ-10) vary from time to time, the stiffness matrix of the whole building structure in Eq.(Ⅲ-13) is directly used without reduction.

5. SEISMIC RESISTANCE CAPACITY AND SEISMIC DEMANDS

5.1 IMPORTANCE OF PREDICTING SEISMIC RESISTANCE CAPACITY

From the results obtained in the evaluation of the seismic performance of the Y Building using the linear elastic analyses described in the previous chapter, the following observations became apparent:

1. When the linear elastic analytical models of the building were subjected to what are considered as moderate earthquake ground motions, service or functionality level, such as the motions recorded at or near the building during the Loma Prieta earthquake and the five records (normalized to a peak velocity of 25 cm/sec) considered by the Kajima team, the building may develop some yielding of the steel reinforcement. This observation is arrived at by comparing the values of the response parameters, maximum acceleration, displacement, interstory drift and story shear, obtained from these records with those that resulted from the modal spectral analyses using the MPDS and the ACI strength method.

2. When the linear elastic models of the building are subjected to earthquake ground motions representative of the safety or survival limit state, the values obtained for the primary response parameters exceed those obtained from the MPDS (supposed to induce first significant yield) by more than 100%. These ground motions are either those which have already been recorded on similar site conditions in the U.S. (Hollister and James Road) or which are considered as typical for this level

of ground motion in Japanese practice (the five records of Table 4.4 normalized to a maximum velocity of 50 cm/sec).

In view of the above results, the building could sustain significant yielding and large interstory drift during ground motions that are representative of the maximum credible (safety or survival) earthquake. This poses the following three questions which must be answered: first, what is the actual resistance capacity (maximum strength and deformation that the structure can sustain without collapse) of the building? Second, what are the maximum strength and deformations that can be demanded by the most severe earthquake ground motions that can occur at the foundation of the building? Third, will the existing (designed and constructed) building safely resist the demanded responses under the predicted extreme earthquake motion at its foundation?

To answer the above questions it is important first to estimate the actual lateral load versus deformation relationship of the building up to its collapse and then, according to this relationship, to predict its nonlinear (inelastic) behavior when subjected to what is considered to be the critical, credible earthquake ground motions that might occur at the site during the life of the structure.

5.2 PREDICTION OF THE SEISMIC RESISTANCE CAPACITY

In Ref. 43, one of the authors has emphasized that a building's strength and deformation capacity cannot be predicted solely on the basis of the building's mechanical characteristics. The spatial distribution (shape function) of the forces and deformations and their variation with time, from which the strength and deformation characteristics of

the building are to be determined, must be established. Estimating the probable critical excitation is one of the most difficult problems and involves perhaps one of the largest uncertainties [44].

At present the following two procedures are commonly used to predict the seismic resistance capacity of a structure: (1) static analysis and (2) dynamic response spectrum analysis. A detailed discussion of the two procedures is given in Ref. 43.

Although the procedure based on static analysis is significantly less time consuming, its application to an irregular building like the Y Building is a tremendous task if a realistic 3-D model of such a building is used. Thus even in the case of the static analysis procedure, approximate methods are often used in practice. One such approximate method has been used by the Kajima team. A 3-D equivalent model for nonlinear dynamic response analysis based on the results obtained from the static nonlinear analysis was developed and will be illustrated in a later section (5.4).

On the basis of the results obtained from preliminary investigations of possible nonlinear behavior of the building, which will be described in the next section, it is concluded that due to the irregular geometry of the building and some areas of increased demands that have been identified in computing the stress ratios, it is desirable to develop a 3-D model and conduct a detailed 3-D analysis. It is believed that an approximate 3-D analysis is now possible and that a detailed nonlinear finite element analysis of this case study building will be feasible in the near future.

5.3 APPROXIMATE DETERMINATION OF THE RESISTANCE CAPACITY, SELECTION OF CRITICAL GROUND MOTIONS AND ESTIMATION OF BUILDING RESPONSE.

5.3.1 Resistance Capacity. A lower bound of the strength capacity can be obtained by computing the lateral resistance at first yielding. To recognize when this occurs, it is convenient to compute the capacity ratio which is defined as the ratio between the internal forces (flexural moment for the beams and interaction of axial and flexural forces for the columns and shear walls) that results from 80% of the MPDS at each critical section and the yielding capacity of that section. The results obtained are presented in Figs. 5.1 through 5.9.

The maximum capacity ratios (positive or negative) for the beams in column line 1 in the west wing (W1) are summarized in Fig. 5.1. Here it can be seen that the largest value occurs at the fifth floor level with all of the floors above the 2nd having demands above or near the calculated capacity. The column capacity ratios for column line W1 are shown in Fig. 5.2 where it can be seen that all column demands are less than the calculated capacity. These data are further summarized in Fig. 5.3 which shows the distribution of the maximum beam and column capacity ratios over the height. Here the increased demand of the beams at the fifth level can be clearly seen.

The capacity ratios for the beams of column line 2 in the west wing (W2) are summarized in Fig. 5.4. Here it can be seen that in the lower floors, the ratios are either close to or just above unity. In the upper floors, however, there is a significant increase in the capacity ratios in the exterior beams. That the largest values of the capacity ratios are

at the exterior beams is not surprising: it is primarily due to the reduced clear span of these members which causes them to attract larger bending moments. The capacity ratios for the columns which are summarized in Fig. 5.5 indicate that the demand on all of these members is below the nominal capacity.

The distribution of the maximum capacity ratios over the height of frame W2 is shown in Fig. 5.6, where the increased demand in the beams at the 22nd level is readily apparent. Analysis of these results presented in Figs. 5.1 through 5.6 reveals that the structure, as far as its strength is concerned, has a region of increased demand at the 22nd story level, particularly when it is subjected to motions in the E-W (X) direction. The main reason for this increase is the existence of the already mentioned relatively short beams at each end of the interior frame along column line 2 which for the west wing is denoted as W2. These end beams, which are between column lines A'B and EF (see Fig. 2.2), have clear spans of 12.5 feet and 14.3 feet, respectively while the interior ones have practically twice the clear span length (26 feet). Because all the beams along column line 2 have the same cross section, it is obvious that the stiffness of the two exterior beams will be practically twice that of the interior beams and consequently will attract significantly larger moments when the frame is subjected to lateral deformations. Furthermore, because there is a significant decrease in the reinforcement provided to this beam at the 22nd story level, the ratio of demand to capacity has its peak value (1.51) at this location (see Fig. 5.6). Because the beam is under-reinforced in flexure (ρ=1.7%), and because it is doubly reinforced and well confined [#4 ties at 4 in. (=d/5)], and in addition the maximum nominal shear stress that can be developed corresponds to approximately 2.5 $\sqrt{f'_c}$, it is clear that this beam can develop significant rotation ductility

without any decrease in its flexural capacity. In other words, although the observed increase in demand could result in yielding of the reinforcement, this will not impair the lateral capacity of the frame and therefore of the whole structure.

The capacity ratios for the beams of a transverse frame on column line C in the north wing (NC) are summarized in Fig. 5.7. Here it can be seen that all demands are less than the nominal capacities, however, it is of interest to note that the maximum demands occur at the 28th and 22nd floor levels. Values for the column capacity ratios for this frame are summarized in Fig. 5.8, where it can be seen that all demands are less than nominal capacity. Here it is also of interest to note that the maximum demands (0.98) are in the columns just above the shear wall (3rd level) and at the 22nd level. This can be readily seen from the distribution of maximum capacity ratio over the height, which is presented in Fig. 5.9.

From the above discussion it is clear that the first yielding will occur at the 22nd story level when the corresponding base shear reaches a value of 0.8(13,900/1.51) = 7364 kips rather than at the design base shear of 11,120 kips determined from 80% of the MPDS. These values correspond to seismic yield coefficients of 7364/134,050 = 0.055 and 11,120/134,050 = 0.083.

Analysis of the results shown in Figs. 5.1 through 5.9 together with an approximate analysis of the shear strength of the 22nd story indicates that yielding of the structure will not commence until the seismic base shear coefficient reaches a value that can vary from 0.14 to 0.17 depending on the type of ground motion or, in other words, on how the

inertia forces are distributed over the height of the structure during its dynamic response to each of the different ground motions that can occur at the foundation. The development of the above range of values for seismic base shear coefficients has been confirmed by the results obtained from the approximate method used by the Kajima research team which is discussed in section 5.4.

It should be noted that, depending on the type of ground motion, the local ductility that will be demanded in the exterior short-length beams in the 22nd story of the frame can be very large, on the order of at least twice the global ductility demand. It should also be noted that in order to obtain reliable estimates of the local ductility it is necessary to conduct 3-D nonlinear analyses on a 3-D finite element model. The authors are conducting this work at present. A direct estimate of local ductility cannot be obtained from the use of a stick (cantilever) model, such as the one used in the analysis discussed in Chapter 4, or a combination of stick (cantilever) models as will be discussed later in this chapter.

5.3.2 Selection of Critical Ground Motions. As has been pointed out previously, the dynamic load capacity of a building depends on the type of excitation. From the discussion offered in References 1, 45 and 46, it has been concluded that in order to select the critical ground motions for evaluating the nonlinear response it is necessary to analyze not only the elastic and inelastic spectra of the different maximum credible ground motions for strength but also for their energy input, E_I , and particularly for their hysteretic energy, E_H , (cumulative ductility and number of yielding reversals). These analyses are required to identify among all the earthquake motions that have been

recorded on similar soil conditions, the ones that could be critical for the building under study. Initially the authors considered the records used in the linear elastic analyses reported in Chapter 4 which are summarized in Table 4.4 and Figs. 4.49 and 4.50. Furthermore, they also considered some of the records that were studied in References 1, 45 and 46.

5.3.2.1 Critical Ground Motions Used in the Linear Elastic Analyses. A total of eight recorded ground motion time-histories was considered in these analyses; five by the Kajima team (Hachinohe, El Centro, Taft, Sendai and Tokyo) and five by the CUREe team (Emeryville, Hollister, James Road, El Centro and Hachinohe). From analyses of the Linear Elastic Response Spectra (LERS), Inelastic Response Spectra (IRS or C_y spectra for different ductilities), E_I and E_H spectra of the actual records (not normalized to other peak ground response) the most critical record for this building seems to be the James Road record. Its E_I and C_y spectra are shown in Figs. 5.10 and 5.11. From analyses of the E_I, E_H and C_y of all the recorded motions analyzed by the authors for soft-soil sites [46], the most critical recorded ground motion for this building is the motion recorded during the 1985 Mexico City earthquake at the SCT station. The E_I and C_y spectra for this record are shown in Figs. 5.10, 5.12 and 5.13, respectively.

5.3.3 Estimation of Building Response. An estimate of the expected global ductility demand for the building when subjected to the critical ground motions identified above can be obtained directly from the C_y spectra that have previously been obtained for SDOF systems subjected to such ground motions (Figs. 5.11 and 5.13) using the estimated values of the yielding capacities of the structure: 0.14 to 0.17 g. Results shown in Fig. 5.11

indicate that for a period of 2.6 seconds and a C_y of 0.14, the required global ductility could be about 3.5. For a C_y of 0.17, the required global ductility is reduced to about 2.8. The estimated maximum displacement at the roof for a C_y of 0.17 is $(3/2)(2.6/2\pi)^2(g)(2.8)\doteq 47$ inches. Similar results are obtained from Fig. 5.13. Note that if it is assumed that the inelastic deformations are equal to those obtained assuming elastic behavior, then, from Fig. 4.51, the displacement at the roof when subjected to the James Road recorded ground motion is about 50 inches.

5.4 NONLINEAR ANALYSES CONDUCTED BY THE KAJIMA RESEARCHERS

As discussed in section 4.4, the Kajima research team initially developed a 3-D linear elastic model of the Y Building for conducting linear elastic analyses of the response of the building when subjected to what the Japanese consider as service level earthquake ground motions (Table 4.4). They also developed a simplified 3-D nonlinear model following the step-by-step procedure illustrated in the flow chart of Fig. 4.58 and discussed in section 4.4.3. A brief description of this simplified nonlinear model follows.

5.4.1 Kajima 3-D Nonlinear Model. As described in section 4.4.3 of this report, on the basis of the results of static analyses the simplified equivalent bending-shearing cantilever model was established and its natural periods and vibration modes were calibrated with those of the 3-D linear elastic model (Fig. 4.58). In the development of the 3-D nonlinear model the following simplifying assumptions were made:

1. The whole superstructure system was modeled by the five shearing elements and the three bending-shearing elements shown in Fig. 5.14. These eight elements

were linked at each floor level by a rigid floor slab as shown in Fig 5.15. The resulting 3-D nonlinear model consisted of a 31 lumped mass model, which was assumed to be fixed at the ground level, having three degrees of freedom at each story level.

2. In the development of the bending-shearing elements the total deflections of the basic original 3-D elastic model were divided as illustrated in the sketches shown in Fig. 5.16 into the bending deflections of the whole structure due to the axial deformation of the columns and shearing deformation resulting from the deformation of each of the framing members. Using the results from this division, the bending and shearing stiffness of the simplified 3-D nonlinear model elements were evaluated. A detailed description of the 3-D frame analysis methodology is presented in Appendix 4.1.

5.4.1.1 Restoring Force Characteristics of the 3-D Nonlinear Model. These characteristics were derived following the procedure illustrated in Fig. 4.58. This procedure consists of the following main steps:

1. **3-D nonlinear static step-by-step analyses.** Considering each of the elements of Figs. 5.14 and 5.15, the flexural cracking moment (M_{cr}) and the yielding moment (M_y) for each element (columns and beams) were calculated, assuming no effect of axial force on the beams and the effect of constant axial force on the columns. Then, the simplified trilinear relationship between moment and rotation angle was assumed for each column and beam as shown in Fig. 5.17 (a). The seismic

lateral load which corresponded to the base shear coefficient of 0.10 was determined. This was based on the vertical distribution coefficient (A_i) of story shear force which is defined in the Japanese Building Standard Law Enforcement Ordinance [47]. The 3-D nonlinear static step-by-step analysis was conducted by gradually increasing the intensity of this distributed load. Data for the building, including the design lateral seismic load corresponding to the base shear coefficient of 0.10 are shown in Table 4.3.

2. **Determination of the skeleton curve of the bending-shearing element.** The relationship between the story shear force and the story shear drift was obtained from the static analysis above. Following this, the equivalent trilinear skeleton curve of each shearing element was established. In Fig. 5.17 (b), the elastic shear stiffness is S, the shear forces at the 1st and 2nd yielding points are Q_1 and Q_2, the stiffness reduction ratio at the 2nd yielding point is α_1 and the 3rd shear stiffness is $\alpha_2 \times S$. Examples of the skeleton curves are shown in Figs. 5.18 and Fig. 5.19. For each shearing element the values of α_1 and α_2 were estimated as 0.4 to 0.5 and 0.1 to 0.2, respectively. The relationship between moment and rotation angle was assumed to be linear elastic.

3. **Selection of the hysteresis loop for the shearing element.** The degrading trilinear loop shown in Fig. 5.20 was assumed for the restoring force characteristic of the skeleton curve.

4. **Determination of the ductility factor.** In order to evaluate the safety of this building a ductility factor μ was defined as given below and illustrated in Fig. 5.21.

$$\mu = \frac{\delta_r}{\delta_2} \qquad (5.1)$$

where δ_r is the maximum story shear drift and δ_2 is the story shear drift at the 2nd yielding point, Q_2.

5.4.2 Results from the Nonlinear Analyses. The response of the 3-D nonlinear model to the five earthquake ground motion records of Table 4.4, normalized to result in a maximum velocity of 50 cm/sec, were analyzed. The results obtained are summarized by the plots of Figs. 5.22 through 5.32 and by the values given in Tables 5.1 to 5.3.

5.4.3 Evaluation of the Results Obtained. As is illustrated by the results given in Table 5.2 and the plots of Fig. 5.25 the maximum values of the interstory drift indices (story drift angle) in the upper stories (19 to 27) exceed 1% when the building is subjected to the normalized El Centro and Hachinohe records. According to Japanese practice, interstory drift indices under these ground motions should be limited to values equal to or smaller than 1%. Thus, the design of the Y Building does not satisfy the interstory drift or shear drift angle criteria of Japanese seismic design practice.

Analysis of the results obtained for the maximum values of the displacement ductility factors given in Table 5.3 and illustrated by the plots of Figs. 5.26 to 5.31 indicates that the model of the Y Building can undergo significant yielding of its reinforcement (2nd

yielding point of the restoring force versus displacement relationship) when subjected to any one of the five normalized earthquake ground motions. Although the largest ductility demand is by the Tokyo 101 record, $\mu = 3.41$ at the 27th story, the most severe motions demanding the formation of larger numbers of plastic hinges are the normalized El Centro and Hachinohe records. Although plastic hinges are formed in the 3rd up to the 15th stories, the most severe ductility ratio demands are developed in the upper stories.

According to Japanese practice the displacement ductility factor, μ, for RC buildings should be less than one when subjected to earthquake ground motions having a peak velocity of 50 cm/sec. Therefore, according to these analyses, the Y Building as designed does not satisfy the requirements of Japanese practice regarding the maximum acceptable values for the displacement ductility factors and interstory drift indices.

Analysis of the values given in Table 5.1 and the plots of Fig. 5.23 indicates that the maximum total base shears varied, depending on the ground motion and its direction, from 6,172 tons (13,607 kips) to 9,069 tons (19,994 kips) when the 3-D nonlinear model of the building was subjected to the 50 cm/sec records of Table 4.4 applied in the E-W (X) direction. In the N-S (Y) direction the variation in total base shear was from 7,667 tons (16,903 kips) to 10,080 tons (22,222 kips). The largest base shear was demanded by the normalized Taft record and the next most severe was due to the normalized El Centro record. The 10,080 tons (22,222 kips) correspond to a seismic base shear coefficient of about 0.17. When this coefficient is compared with the coefficient for which the building was designed, 0.08, it becomes clear that the building has an overstrength of more than 100%.

5.5 COMPARISON WITH ELASTIC ANALYSES

The maximum values of the capacity ratios over the height of the building which are summarized in Figs. 5.3 and 5.6 show a similar trend to that of the ductility demands obtained by the Kajima researchers using the simplified inelastic model [Fig. 5.28(1)]. Recall that the capacity ratios are for the individual elements, whereas, the ductilities are average values for the story segment. Also, the capacity ratios were calculated for 80% of the MPDS whereas the ductilities were calculated for normalized time-histories. Both studies indicate that there is an area of increased demand in the 4th-5th levels and that the maximum demand occurs at the 22nd-23rd levels. In a similar manner, the capacity ratios summarized in Fig. 5.9 can be compared with the ductility ratios shown in Fig. 5.27(1). As mentioned previously, the ductility demand for a critical element may be more than twice the average demand of the story to which such an element belongs. For this reason, the authors feel it is essential to conduct a more refined 3-D inelastic analysis of the structure.

The interstory drift indices obtained from the elastic and inelastic studies also show a very similar pattern. The results shown in Fig. 4.75 for the elastic analysis and Fig. 5.25 for the inelastic analysis both indicate a bulge in the IDI that begins at the 18th floor and reaches its maximum value at the 22nd and 23rd floor levels. For the elastic case this value is 0.0135 and for the inelastic case it is 0.015 in the X direction [see Table 5.2 and Fig. 5.25(1)]. In the Y direction it is 1/65 = 0.0154. In both cases, the IDI obtained from the analyses in this region are above those used in Japanese practice and are approaching what is considered an upper limit in U.S. practice (0.015).

It is also of interest to compare the story shears presented in Fig. 4.77 with those of Fig. 5.23. Considering the shears due to the normalized El Centro ground motion which is common to both figures, it can be seen that the maximum elastic base shear is 31,000 kips and the maximum inelastic base shear is approximately 19,100 kips (see Table 5.1 - 8672 tons x 2.2 kips/ton). This reduced base shear in the inelastic case is representative of inelastic response (plastic redistribution of internal forces) where the inelastic behavior of critical members limits the amount of lateral force that can be developed by the structure. In this case the substantial decrease in base shear indicates that there is a significant amount of inelastic behavior under the El Centro ground motion normalized to 50 cm/sec. This is confirmed by the high interstory ductility factors, 2.53 and 2.19 at the 23rd and 5th stories, respectively, that were computed by the Kajima team (see Table 5.3).

Table 5.1 - Maximum Shear Force and Base Shear Coefficient
(input 50cm/s normalized, h=0.03, Non-linear)

Earthquake	X-direction		Y-direction	
	Shear Force	Base Shear Coef.	Shear Force	Base Shear Coef.
EL CENTRO	8672 ton	0.144	9522 ton	0.158
TAFT	9069 ton	0.151	10080 ton	0.168
TOKYO 101	7759 ton	0.129	8857 ton	0.147
SENDAI TH038	6172 ton	0.103	7667 ton	0.127
HACHINOHE	6860 ton	0.114	8692 ton	0.145

Table 5.2 - Maximum Story Drift and Drift Angle
(input 50cm/s normalized, h=0.03, Non-linear)

Earthquake	X-direction		Y-direction	
	Drift Angle (Drift)	Story	Drift Angle (Drift)	Story
EL CENTRO	1/68 (4.23 cm)	23	1/70 (4.13 cm)	23
TAFT	1/112 (2.59 cm)	20	1/110 (2.63 cm)	20
TOKYO 101	1/90 (3.23 cm)	28	1/93 (3.11 cm)	28
SENDAI TH038	1/123 (2.35 cm)	13	1/138 (2.11 cm)	13
HACHINOHE	1/74 (3.93 cm)	23	1/65 (4.43 cm)	22

Table 5.3 - Maximum Ductility Factor
(input 50cm/s normalized, h=0.03, Non-linear)

Earthquake	X-direction			Y-direction		
	Ductitity	Frame	Story	Ductility	Frame	Story
EL CENTRO	2.53	S-L	23	2.19	W-T	5
TAFT	2.48	N-T	5	1.59	W-T	5
TOKYO 101	3.41	N-T	27	1.75	C-Y	27
SENDAI TH038	1.91	N-T	10	1.49	W-T	5
HACHINOHE	2.76	N-T	27	2.33	W-T	27

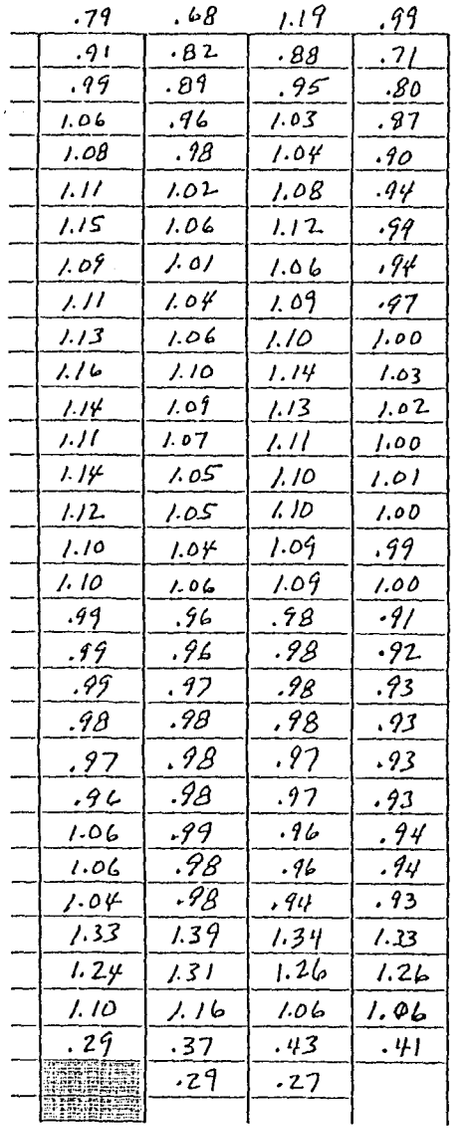

.79	.68	1.19	.99
.91	.82	.88	.71
.99	.89	.95	.80
1.06	.96	1.03	.87
1.08	.98	1.04	.90
1.11	1.02	1.08	.94
1.15	1.06	1.12	.99
1.09	1.01	1.06	.94
1.11	1.04	1.09	.97
1.13	1.06	1.10	1.00
1.16	1.10	1.14	1.03
1.14	1.09	1.13	1.02
1.11	1.07	1.11	1.00
1.14	1.05	1.10	1.01
1.12	1.05	1.10	1.00
1.10	1.04	1.09	.99
1.10	1.06	1.09	1.00
.99	.96	.98	.91
.99	.96	.98	.92
.99	.97	.98	.93
.98	.98	.98	.93
.97	.98	.97	.93
.96	.98	.97	.93
1.06	.99	.96	.94
1.06	.98	.96	.94
1.04	.98	.94	.93
1.33	1.39	1.34	1.33
1.24	1.31	1.26	1.26
1.10	1.16	1.06	1.06
.29	.37	.43	.41
	.29	.27	

Figure 5.1 - Girder capacity ratios, column line W1 (0.8 MPDS)

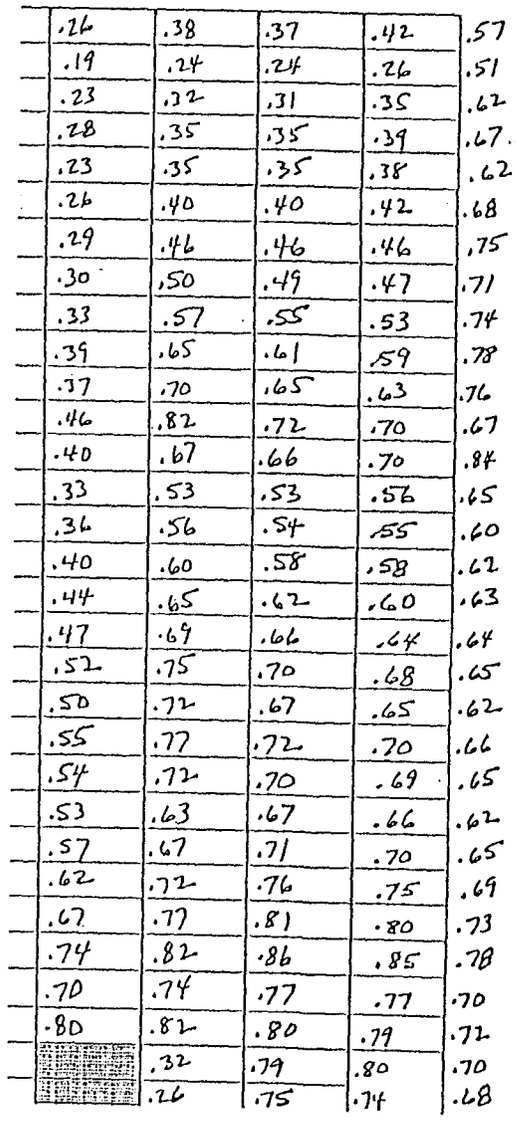

.26	.38	.37	.42	.57
.19	.24	.24	.26	.51
.23	.32	.31	.35	.62
.28	.35	.35	.39	.67
.23	.35	.35	.38	.62
.26	.40	.40	.42	.68
.29	.46	.46	.46	.75
.30	.50	.49	.47	.71
.33	.57	.55	.53	.74
.39	.65	.61	.59	.78
.37	.70	.65	.63	.76
.46	.82	.72	.70	.67
.40	.67	.66	.70	.84
.33	.53	.53	.56	.65
.36	.56	.54	.55	.60
.40	.60	.58	.58	.62
.44	.65	.62	.60	.63
.47	.69	.66	.64	.64
.52	.75	.70	.68	.65
.50	.72	.67	.65	.62
.55	.77	.72	.70	.66
.54	.72	.70	.69	.65
.53	.63	.67	.66	.62
.57	.67	.71	.70	.65
.62	.72	.76	.75	.69
.67	.77	.81	.80	.73
.74	.82	.86	.85	.78
.70	.74	.77	.77	.70
.80	.82	.80	.79	.72
	.32	.79	.80	.70
	.26	.75	.74	.68

Figure 5.2 - Column line capacity ratios, W1 (0.8 MPDS)

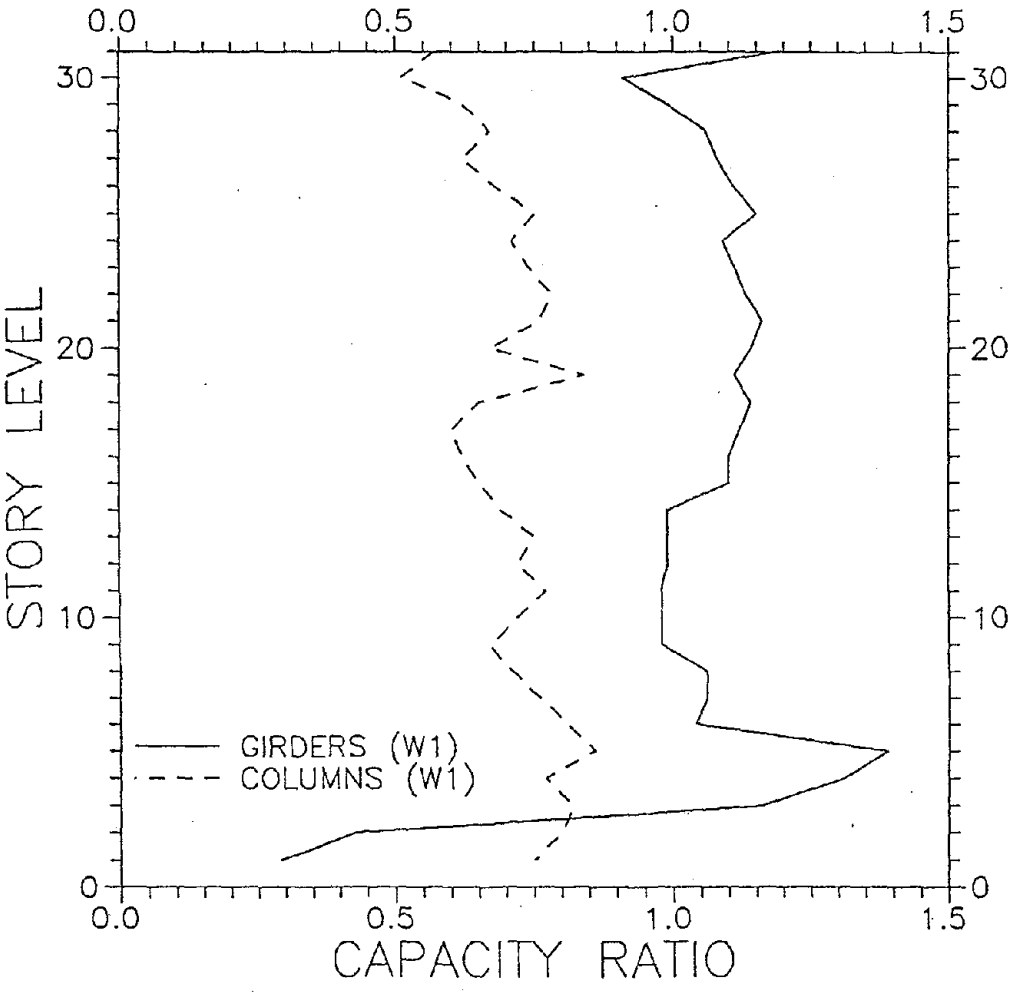

Figure 5.3 - Maximum capacity ratios, column line W1, 0.8, MPDS.

1.12	.77	.59	.69	.70	
1.10	.83	.70	.80	.91	
1.24	.91	.78	.87	1.11	
1.40	.99	.88	.97	1.32	
1.22	.95	.85	.92	.99	
1.28	1.00	.90	.97	1.06	
1.35	1.03	.94	1.02	1.13	
1.41	.98	.90	.97	1.24	
1.47	1.00	.93	.99	1.30	
1.51	1.03	.95	1.01	1.34	
1.17	.95	.89	.94	1.10	
1.17	.97	.91	.96	1.12	
1.10	.96	.90	.96	1.09	
.92	.92	.84	.91	1.01	
.86	.90	.83	.90	.96	
.86	.90	.83	.89	.97	
.88	.90	.84	.89	1.00	
.91	.90	.85	.89	1.03	
.93	.90	.85	.89	1.07	
.96	.89	.86	.89	1.10	
.67	.89	.86	.89	.95	
.69	.88	.87	.88	.95	
.70	.88	.88	.89	.92	
.73	.88	.88	.89	.98	
.77	.86	.88	.88	.99	
.80	.85	.88	.87	.99	
.83	.82	.87	.84	.98	
.81	.76	.82	.79	.92	
.74	.66	.72	.67	.75	
.79	.20	.32	.37	.35	
.07	[illegible]	.22	.18		
	[illegible]				

Figure 5.4 - Girder capacity ratios, column line W2 (0.8 MPDS)

.54	.77	.66	.60	.66	.43
.44	.70	.58	.54	.68	.50
.44	.83	.70	.67	.81	.44
.39	.91	.76	.72	.87	.35
.30	.82	.68	.66	.81	.33
.34	.86	.71	.70	.84	.38
.37	.89	.75	.75	.88	.40
.35	.79	.76	.76	.91	.40
.39	.82	.82	.82	.94	.43
.44	.83	.85	.85	.96	.48
.50	.71	.75	.74	.76	.52
.63	.66	.75	.74	.71	.65
.62	.78	.82	.81	.82	.89
.41	.57	.65	.64	.74	.55
.42	.54	.62	.61	.71	.54
.44	.54	.63	.63	.72	.55
.47	.55	.65	.64	.74	.58
.49	.56	.67	.67	.76	.61
.52	.58	.70	.70	.78	.63
.51	.52	.66	.66	.72	.62
.55	.52	.68	.68	.72	.67
.58	.49	.65	.65	.68	.68
.61	.46	.62	.62	.62	.69
.65	.48	.65	.66	.64	.72
.72	.49	.69	.69	.66	.75
.66	.51	.68	.72	.69	.71
.73	.53	.72	.75	.72	.73
.81	.48	.64	.66	.85	.60
1.01	.76	.86	.66	.67	.68
.89	[illegible]	.17	.67	.61	.63
.67	[illegible]	.22	.69	.62	.63

Figure 5.5 - Column capacity ratios, column line W2 (0.8 MPDS)

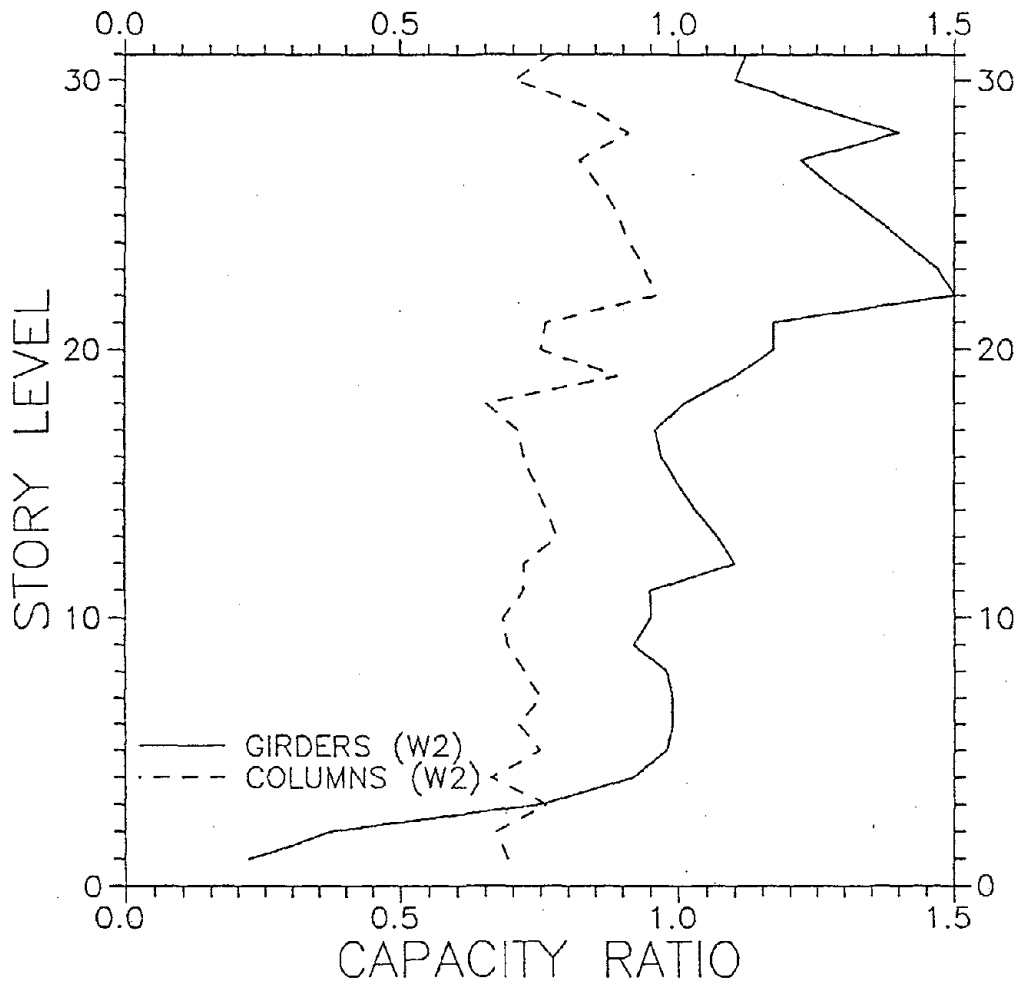

Figure 5.6 - Maximum capacity ratios, column line W2, MPDS.

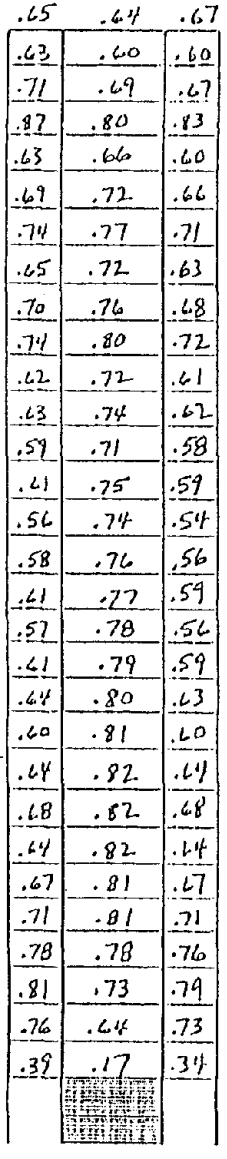

.65	.64	.67
.63	.60	.60
.71	.69	.67
.87	.80	.83
.63	.66	.60
.69	.72	.66
.74	.77	.71
.65	.72	.63
.70	.76	.68
.74	.80	.72
.62	.72	.61
.63	.74	.62
.59	.71	.58
.61	.75	.59
.56	.74	.54
.58	.76	.56
.61	.77	.59
.57	.78	.56
.61	.79	.59
.64	.80	.63
.60	.81	.60
.64	.82	.64
.68	.82	.68
.64	.82	.64
.67	.81	.67
.71	.81	.71
.78	.78	.76
.81	.73	.79
.76	.64	.73
.39	.17	.34

Figure 5.7 - Girder capacity ratios, column line NC (0.8 MPDS)

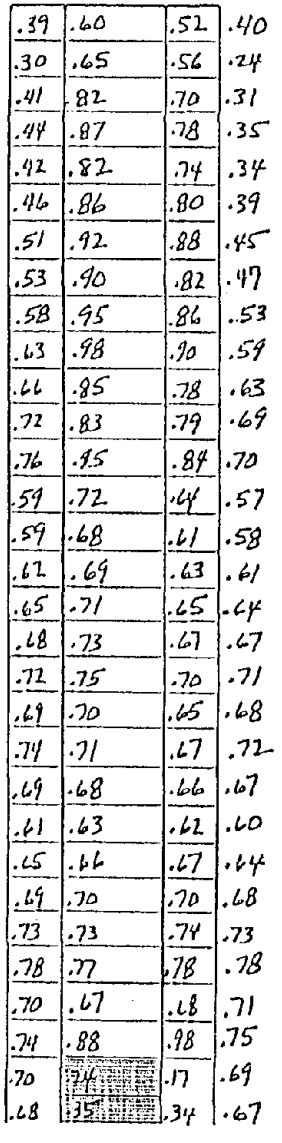

.39	.60	.52	.40
.30	.65	.56	.24
.41	.82	.70	.31
.44	.87	.78	.35
.42	.82	.74	.34
.46	.86	.80	.39
.51	.92	.88	.45
.53	.90	.82	.47
.58	.95	.86	.53
.63	.98	.90	.59
.66	.85	.78	.63
.72	.83	.79	.69
.76	.85	.84	.70
.59	.72	.64	.57
.59	.68	.61	.58
.62	.69	.63	.61
.65	.71	.65	.64
.68	.73	.67	.67
.72	.75	.70	.71
.69	.70	.65	.68
.74	.71	.67	.72
.69	.68	.66	.67
.61	.63	.62	.60
.65	.66	.67	.64
.69	.70	.70	.68
.73	.73	.74	.73
.78	.77	.78	.78
.70	.67	.68	.71
.74	.88	.98	.75
.70	.74	.17	.69
.68	.35	.34	.67

Figure 5.8 - Column capacity ratios, column line NC (0.8 MPDS)

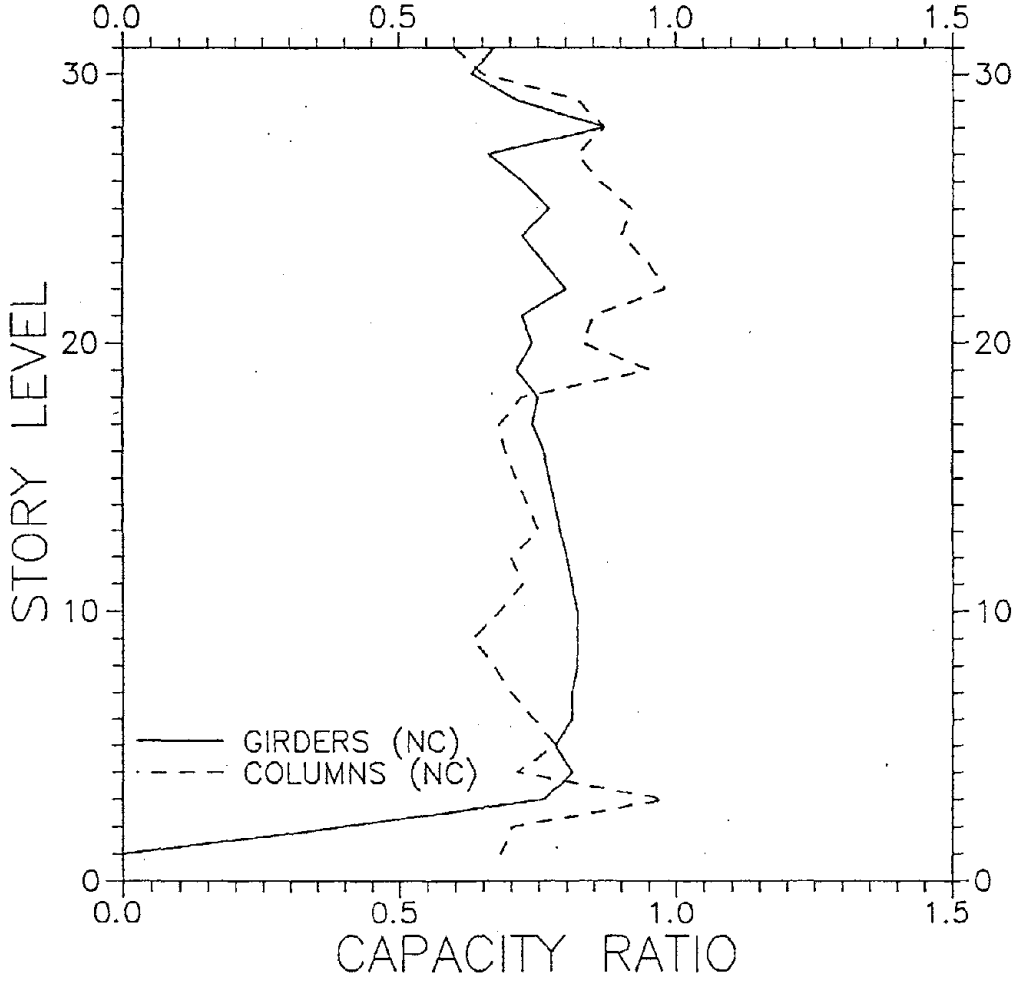

Figure 5.9 - Maximum capacity ratios, column line NC, MPDS.

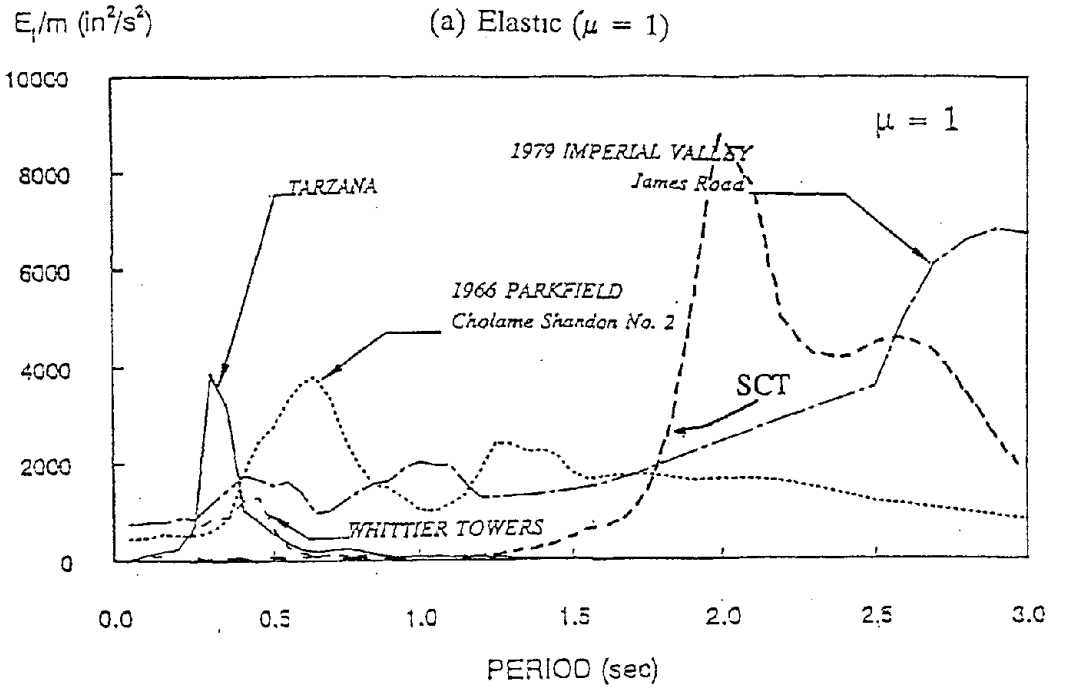

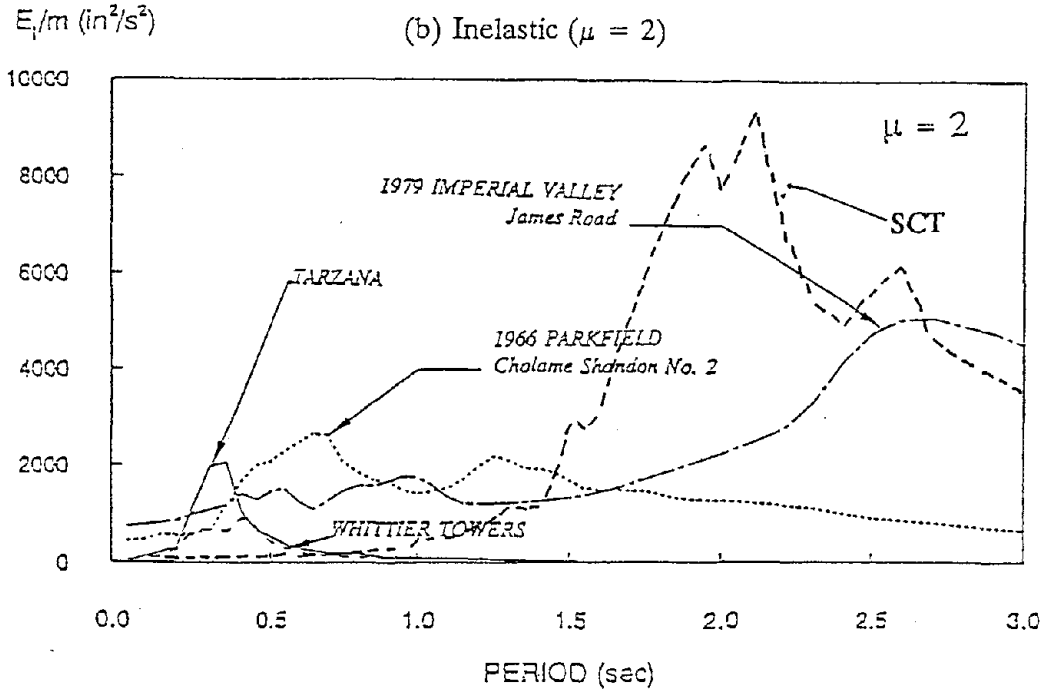

Figure 5.10 - Input energy spectra.

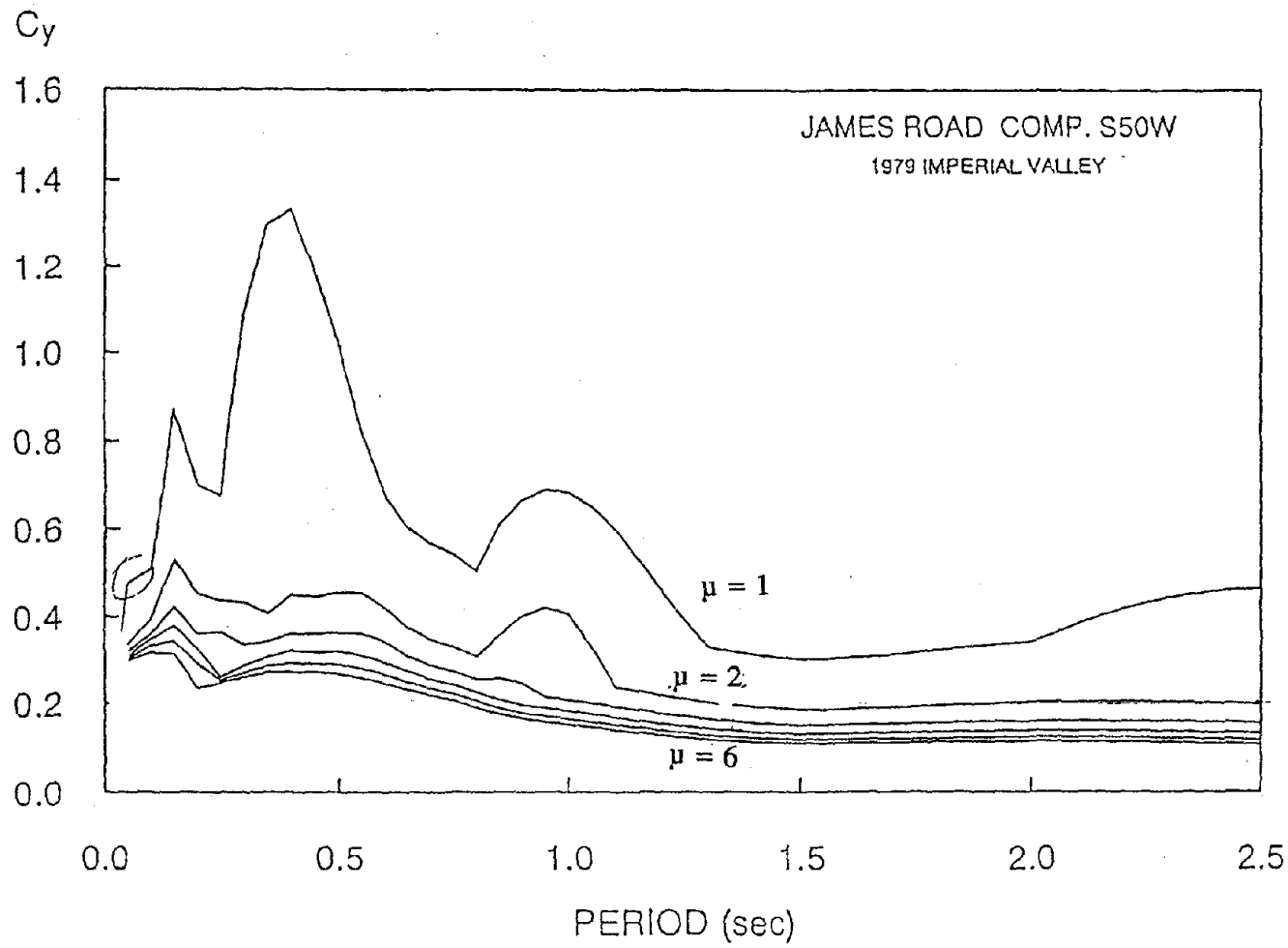

Figure 5.11 - Inelastic response spectra, James Road S50W.

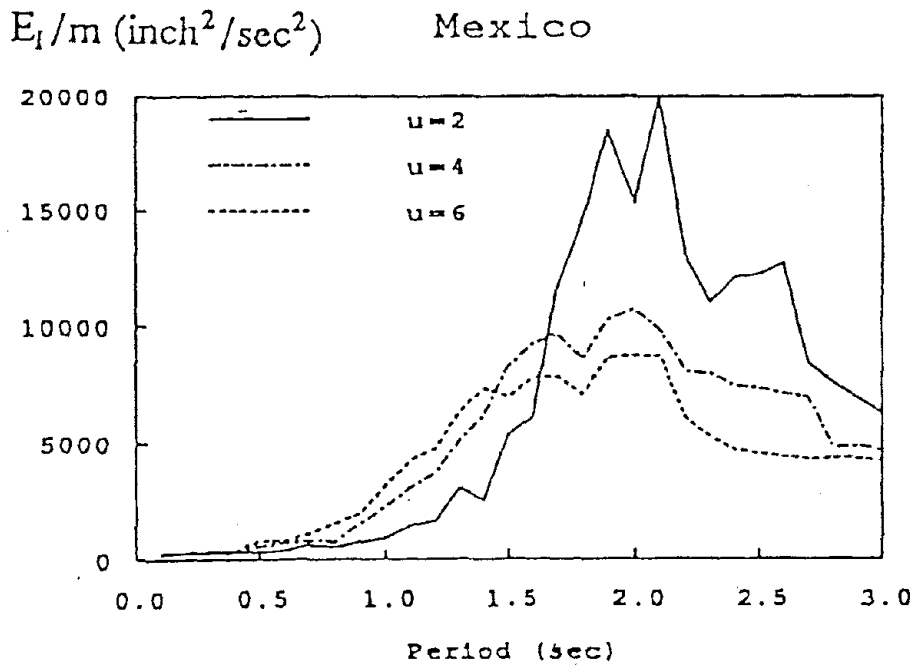

Figure 5.12 - Input energy spectra, Mexico City, SCT, 1985.

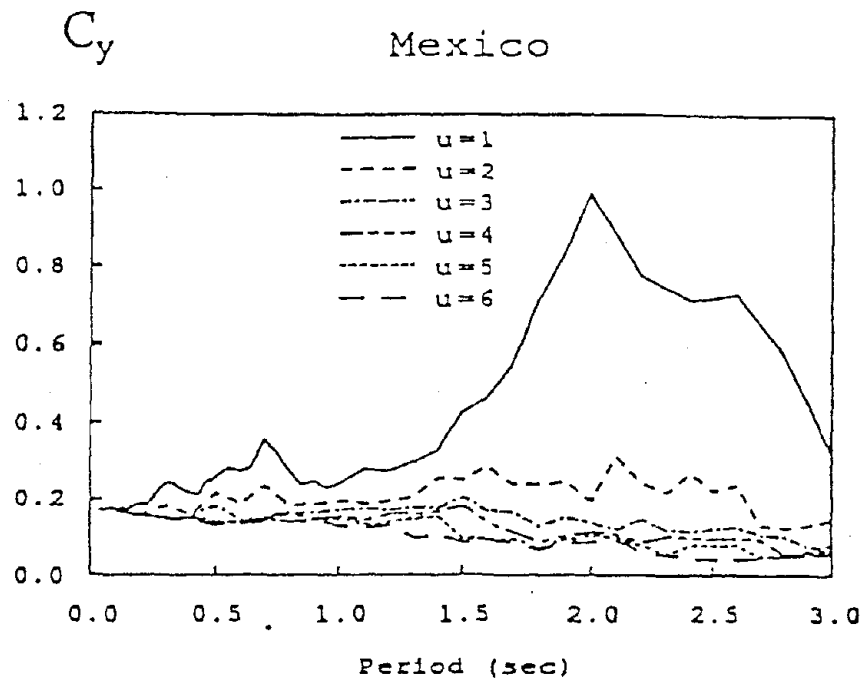

Figure 5.13 - Resistance coefficient spectra, Mexico City, SCT, 1985.

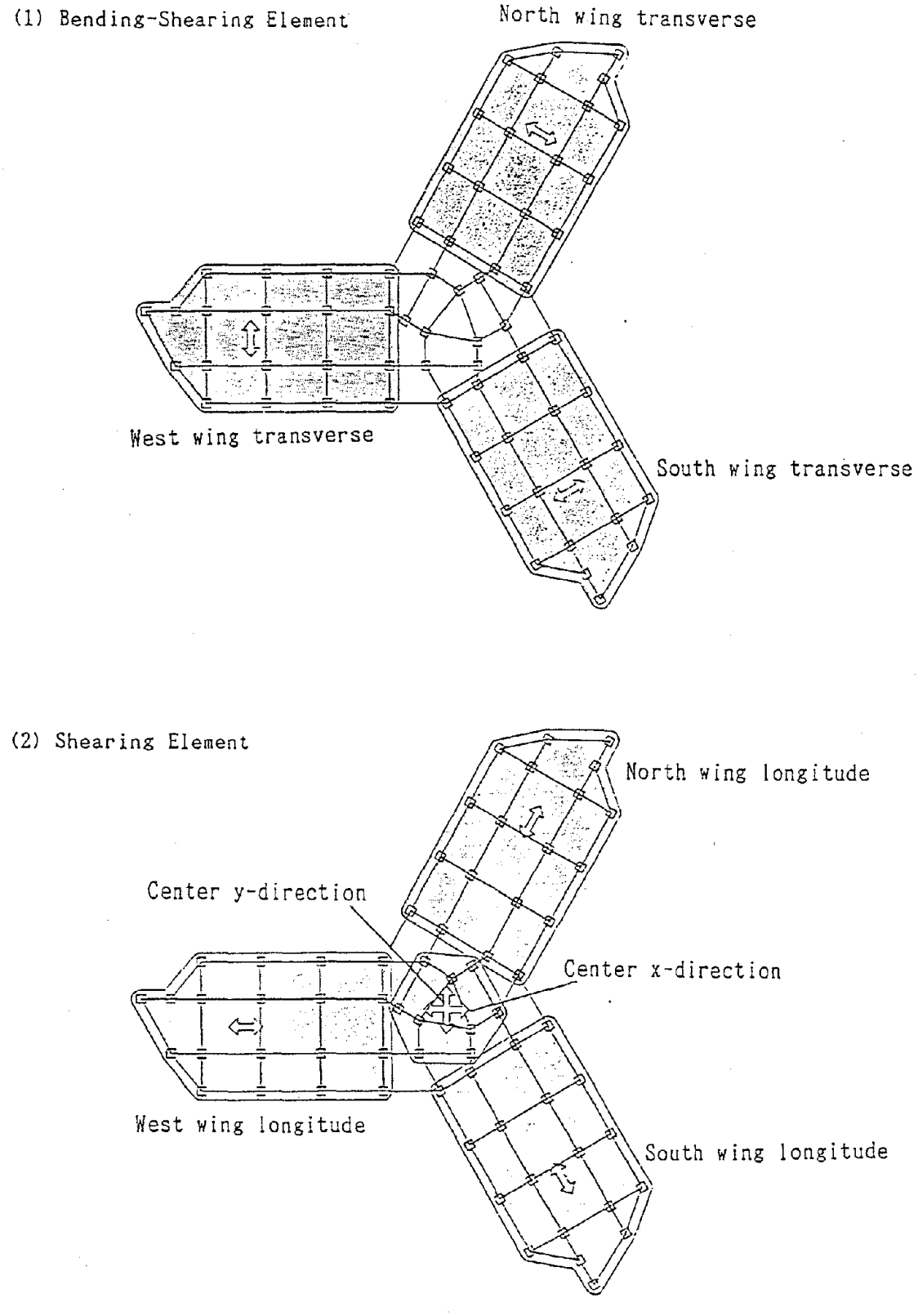

Figure 5.14 - Discretization of Y Building for nonlinear analysis.

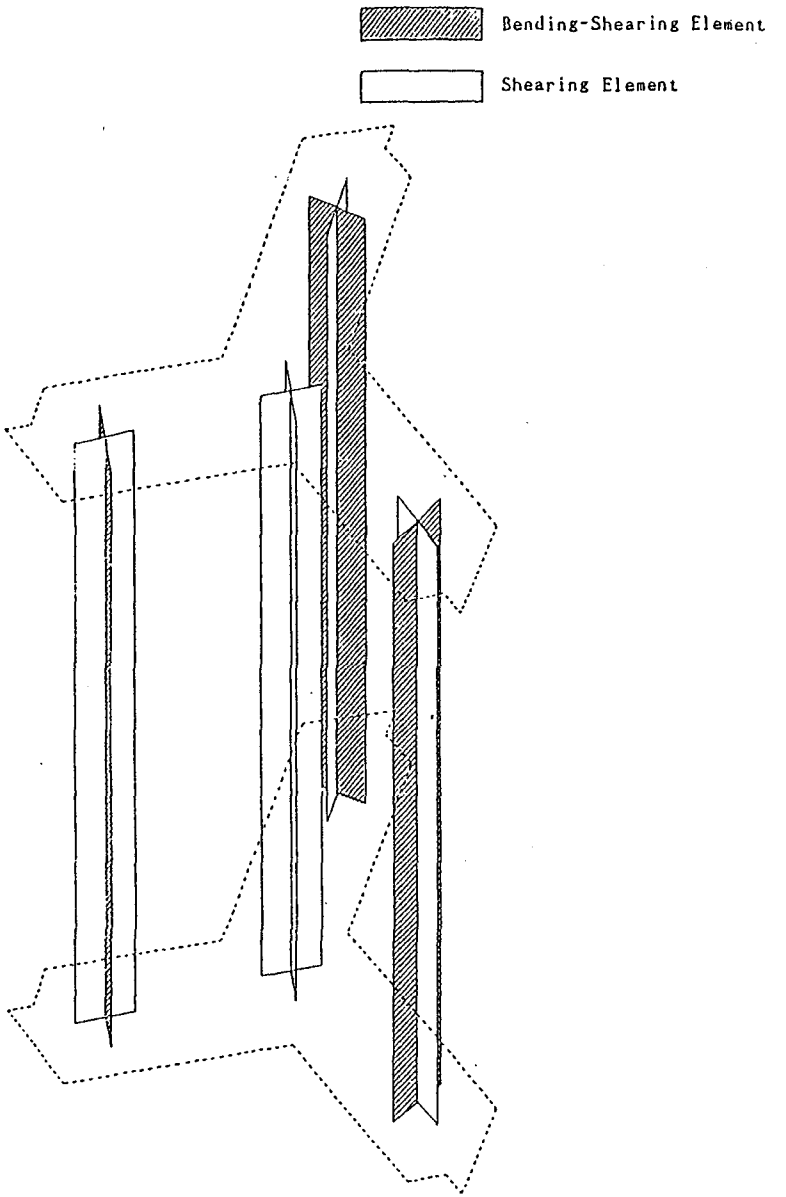

Figure 5.15 - Simplified 3-D nonlinear model.

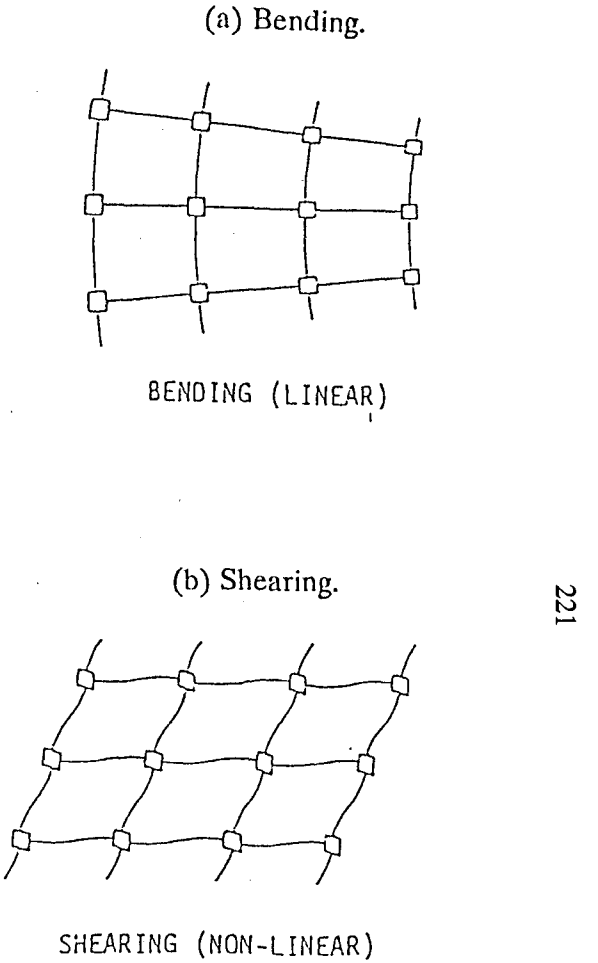

Figure 5.16 - Discretized building deformation patterns.

(a) Perform Non-linear Step-by-step Analysis

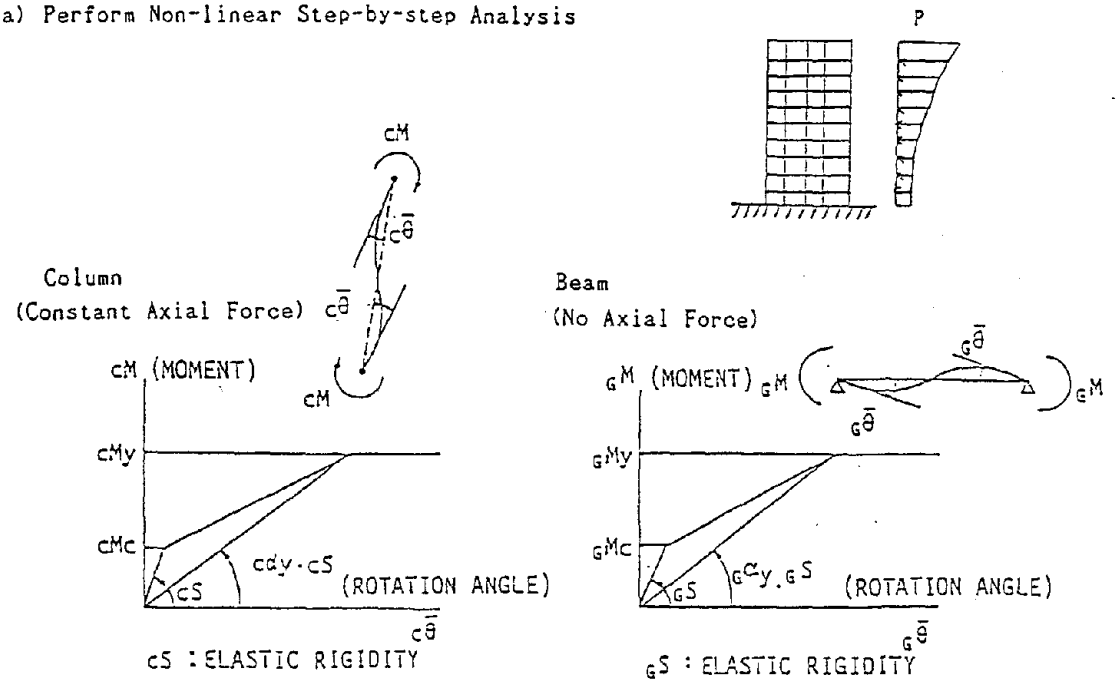

(b) Define Skeleton Curve of Bending-Shearing Element

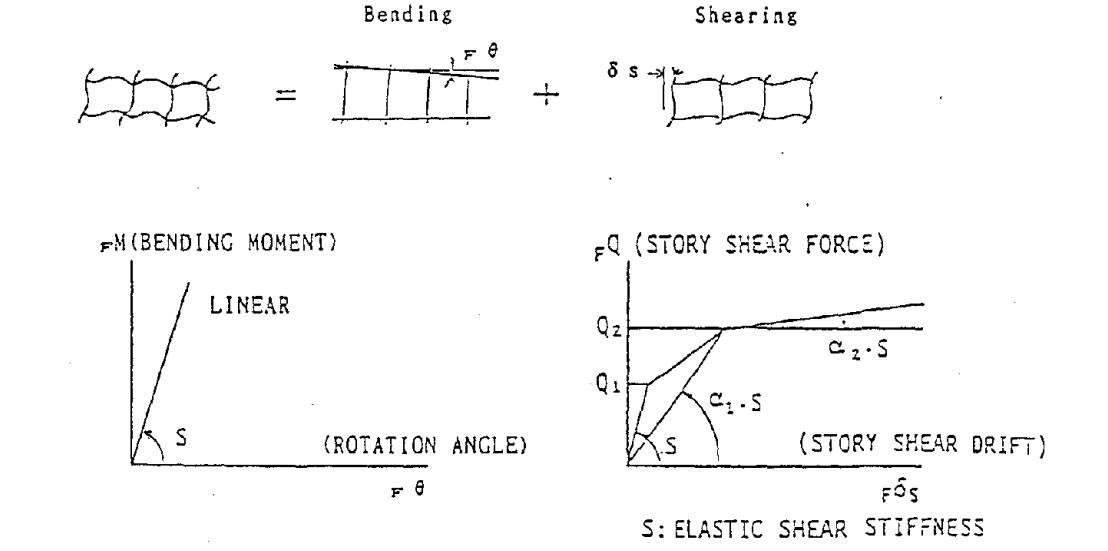

Figure 5.17 - Restoring force characteristics.

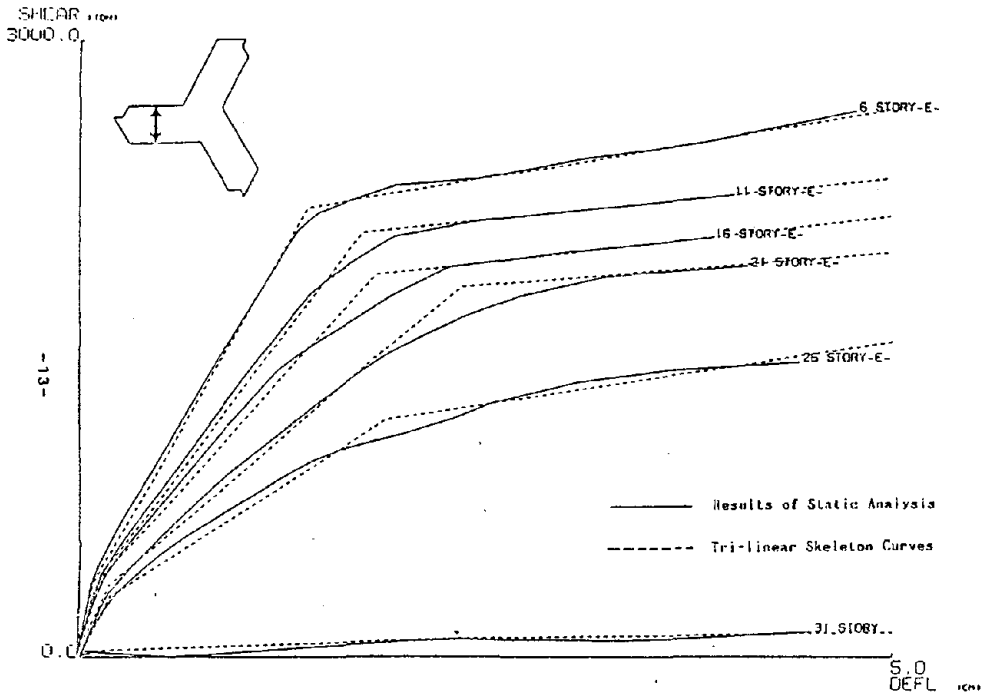

Figure 5.18 - Comparison of skeleton curve, west wing transverse.

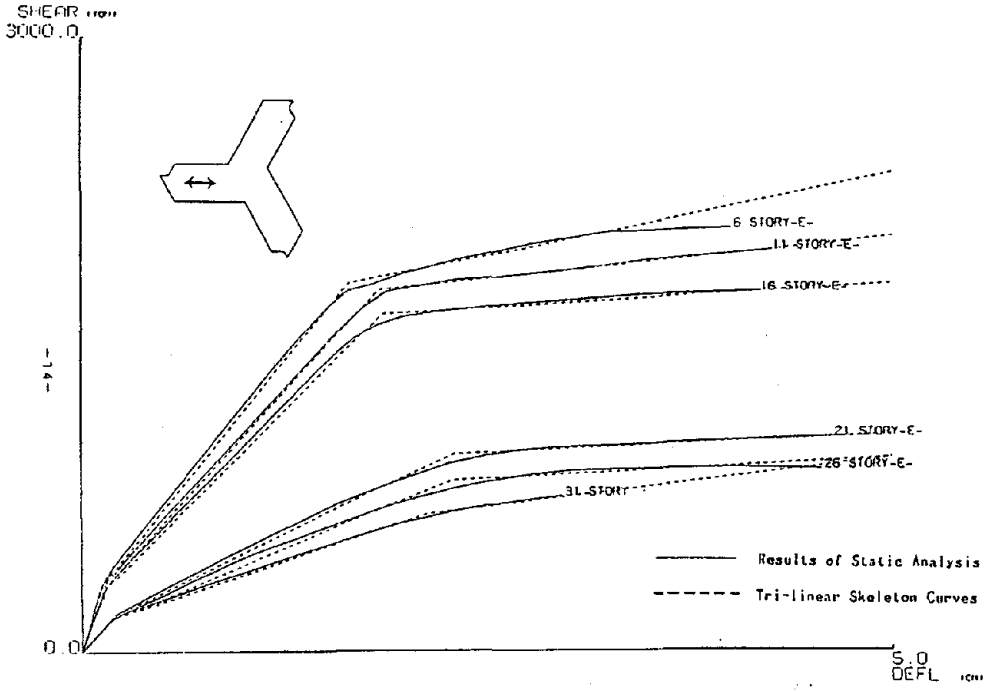

Figure 5.19 - Comparison of skeleton curve, west wing longitudinal.

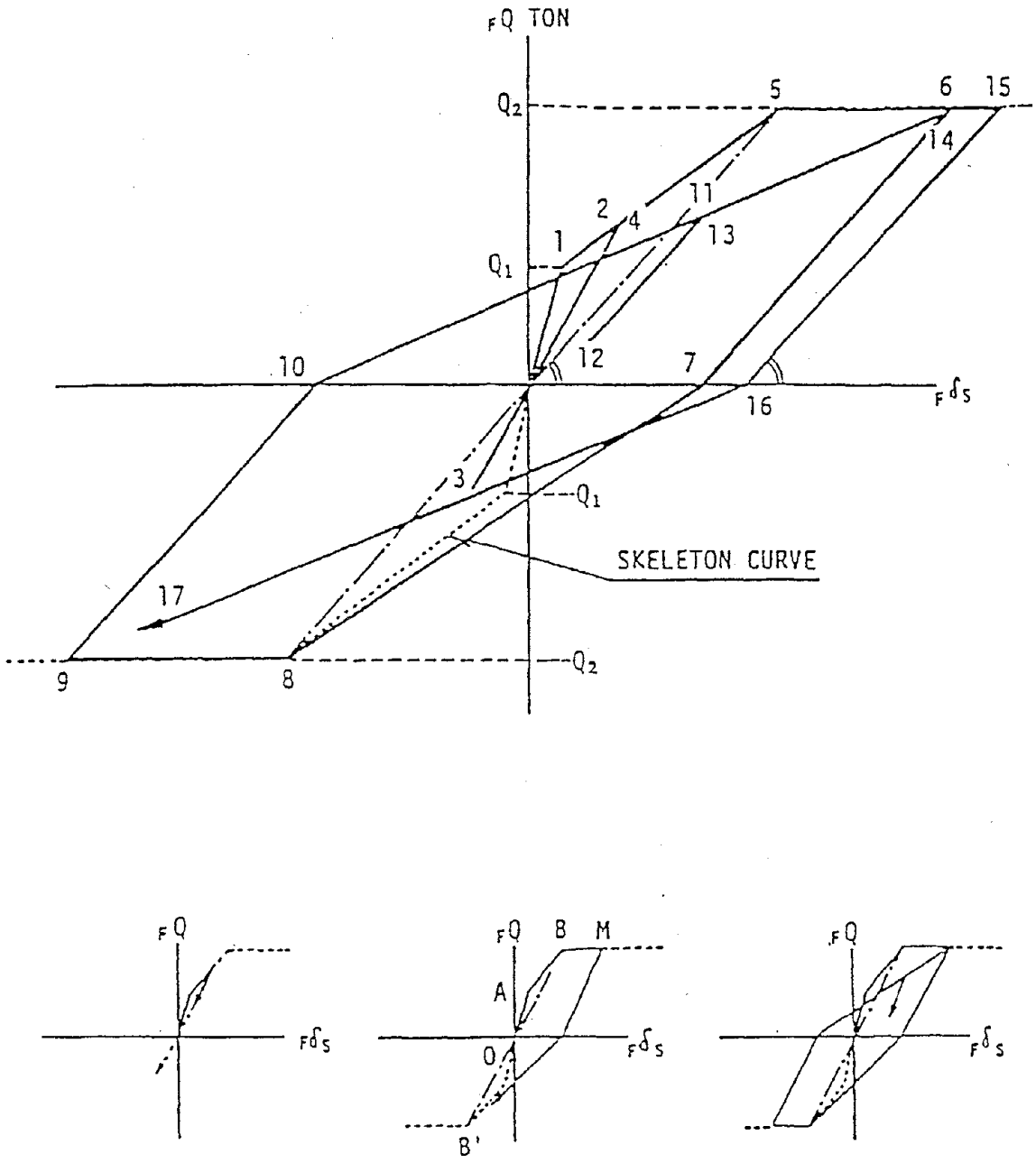

Figure 5.20 - Hysteretic behavior of shearing element.

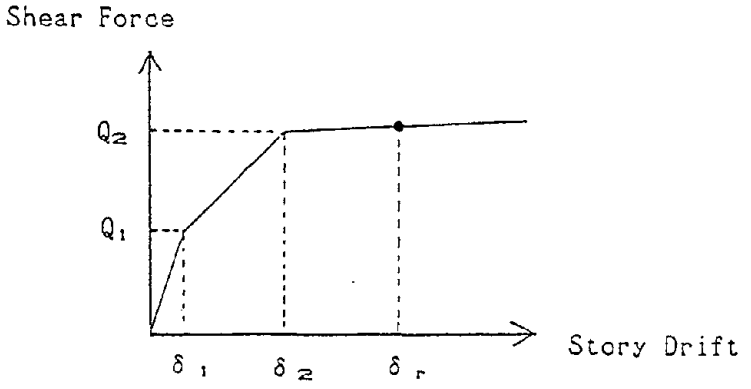

Figure 5.21 - Idealized story shear vs. displacement.

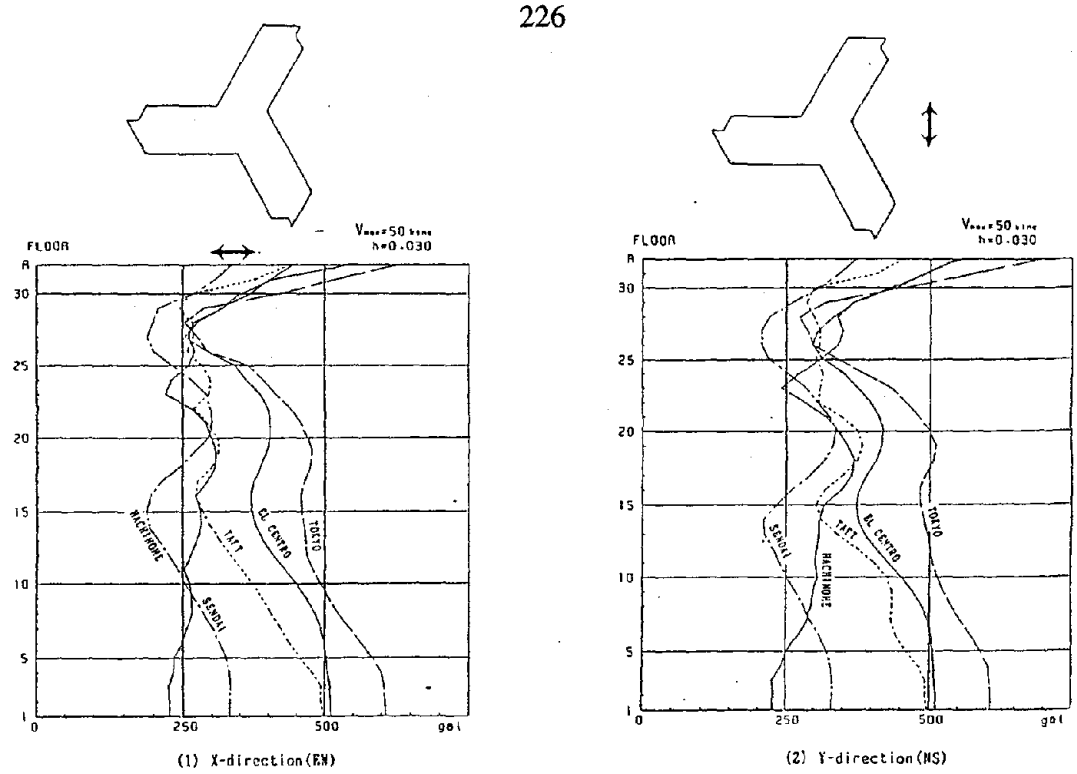

Figure 5.22 - Maximum acceleration (50 cm/sec., h = 0.03, nonlinear).

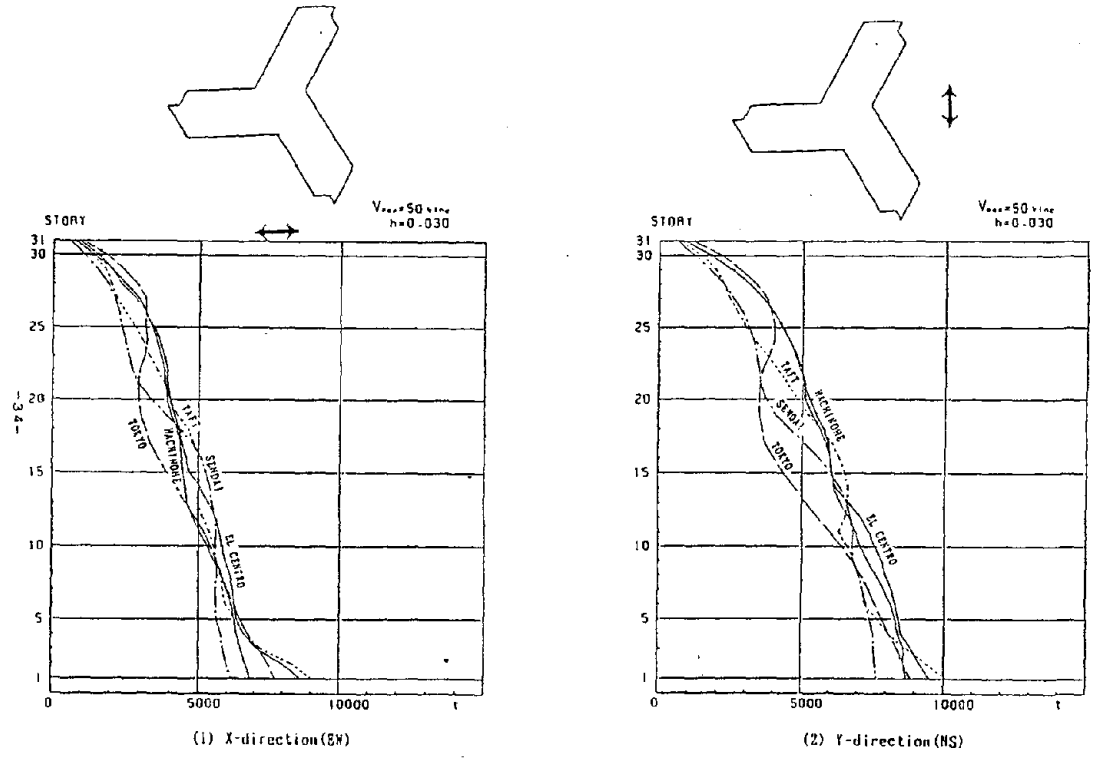

Figure 5.23 - Maximum shear force (50 cm/sec., h = 0.03, nonlinear).

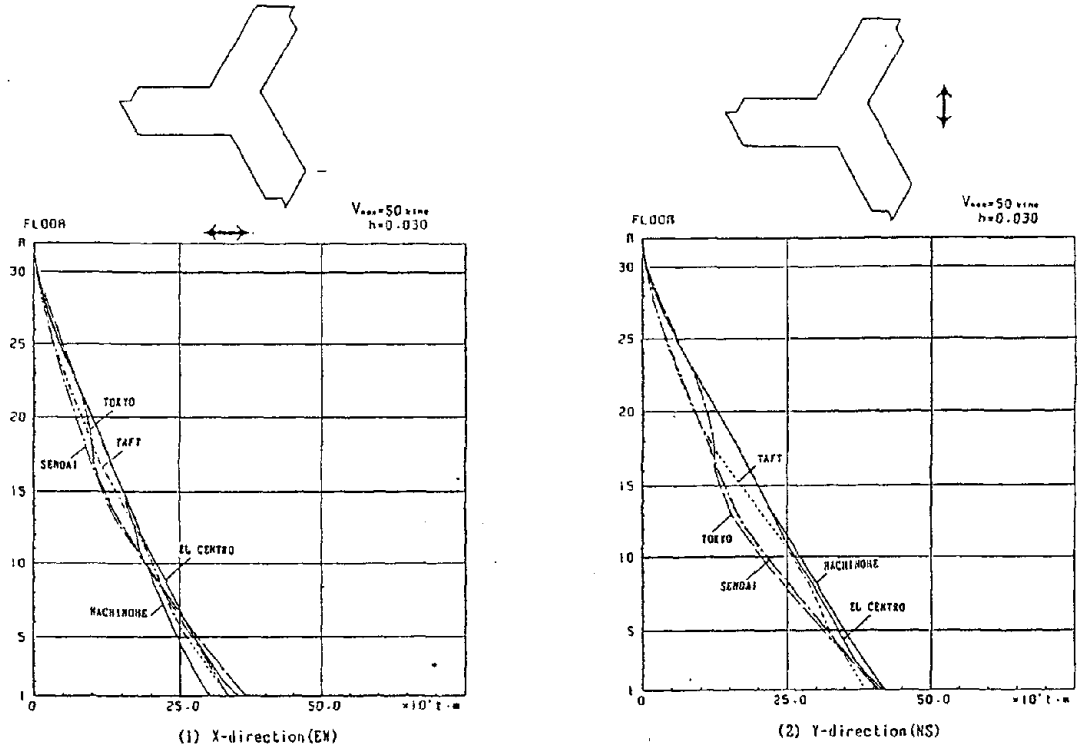

Figure 5.24 - Maximum overturning moment (50cm/sec., h = 0.03, nonlinear).

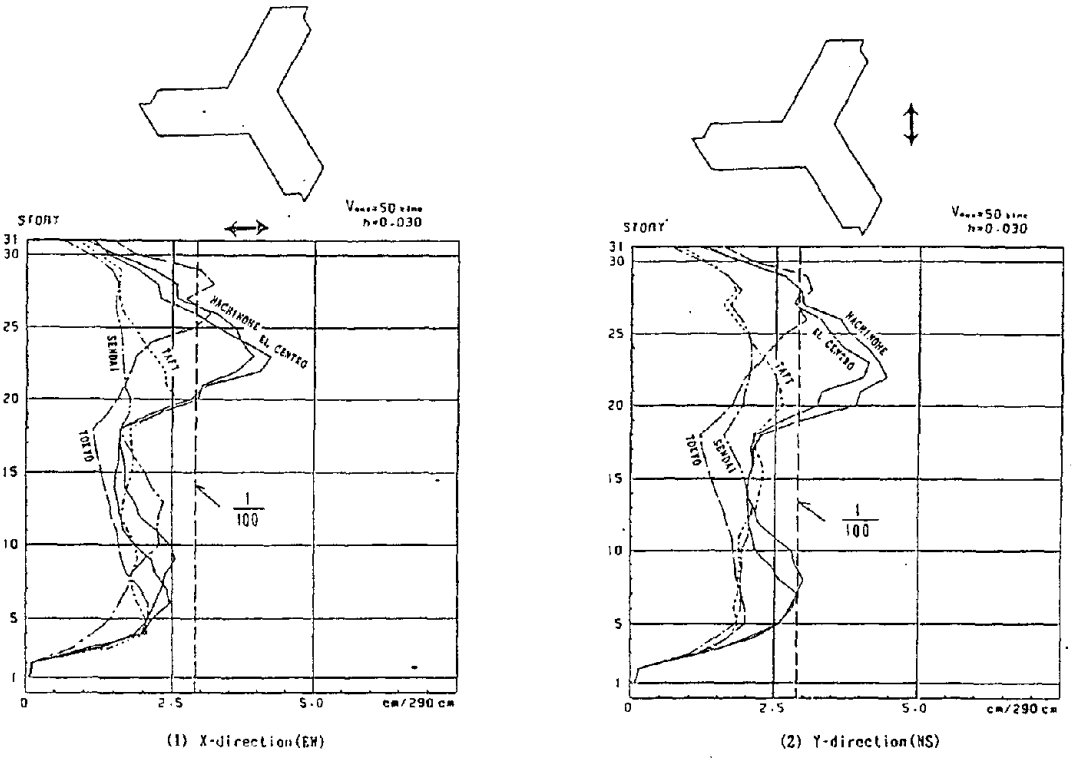

Figure 5.25 - Maximum story drift (50 cm/sec., h = 0.03, nonlinear).

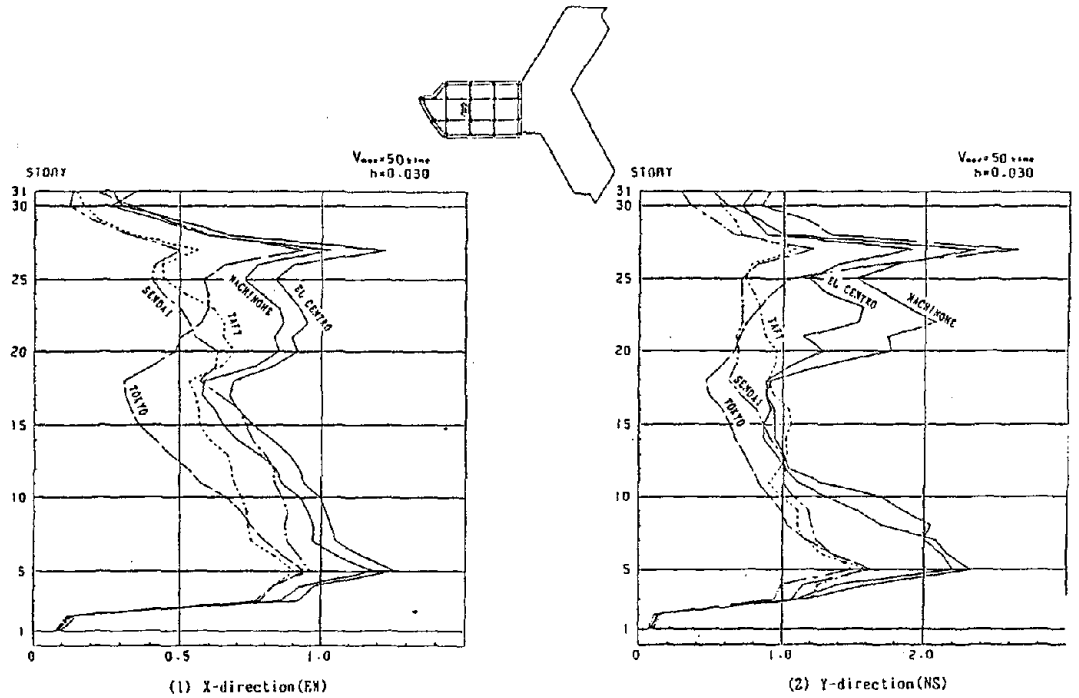

Figure 5.26 - Maximum story ductility, west wing transverse (50 cm/sec., h = 0.03, nonlinear).

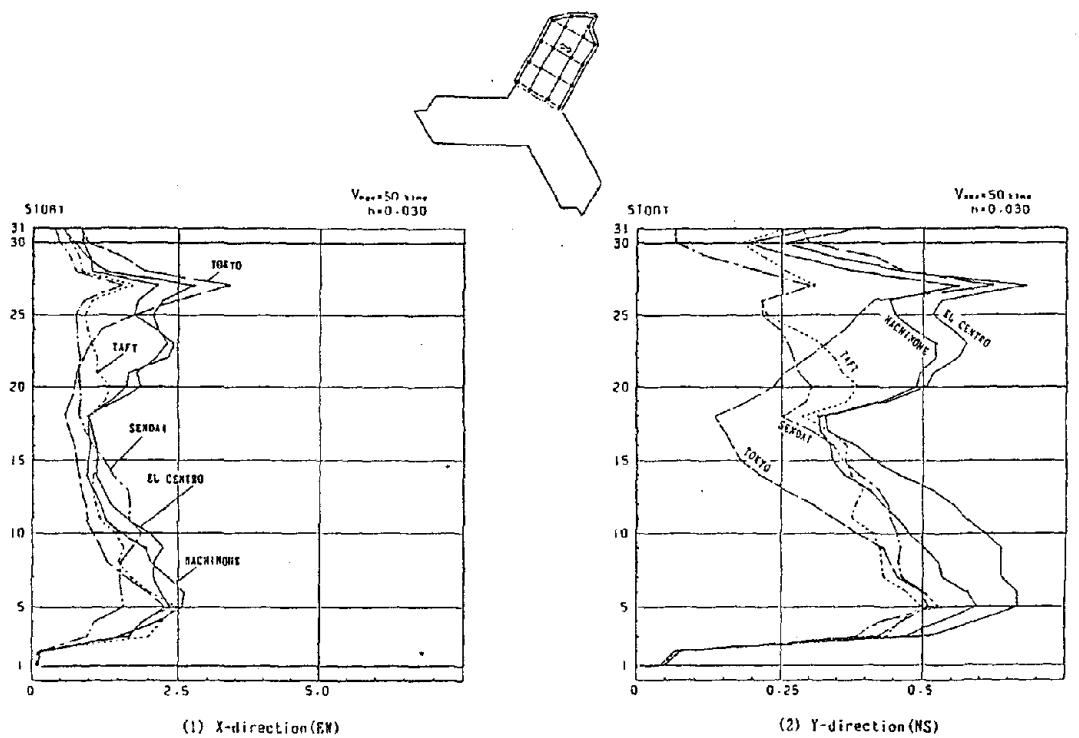

Figure 5.27 - Maximum story ductility, north wing transverse (50 cm/sec., h = 0.03, nonlinear).

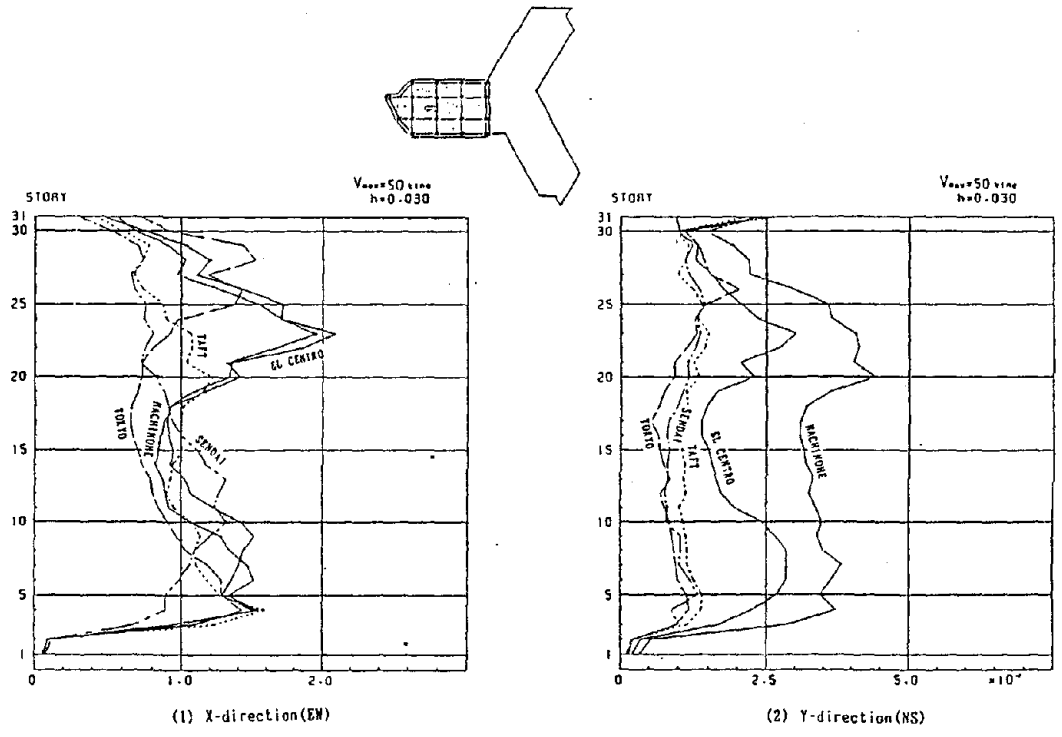

Figure 5.28 - Maximum story ductility, west wing transverse (50 cm/sec., h = 0.03, nonlinear).

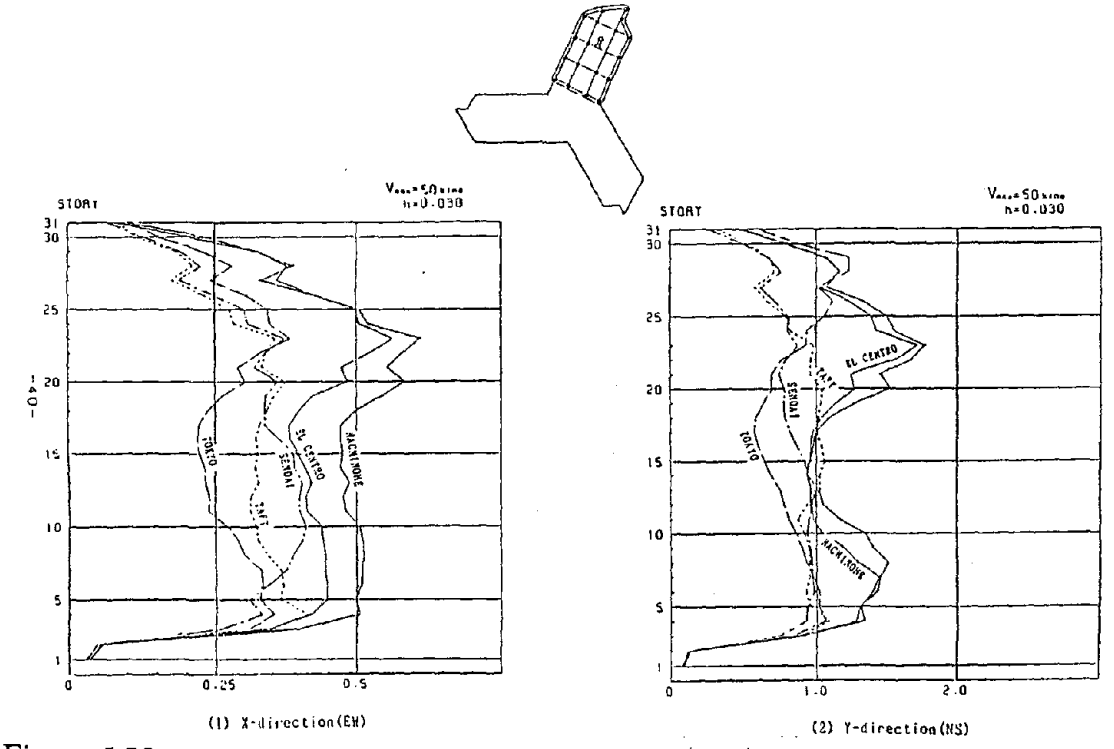

Figure 5.29 - maximum story ductility, north wing longitudinal (50 cm/sec., h = 0.03, nonlinear).

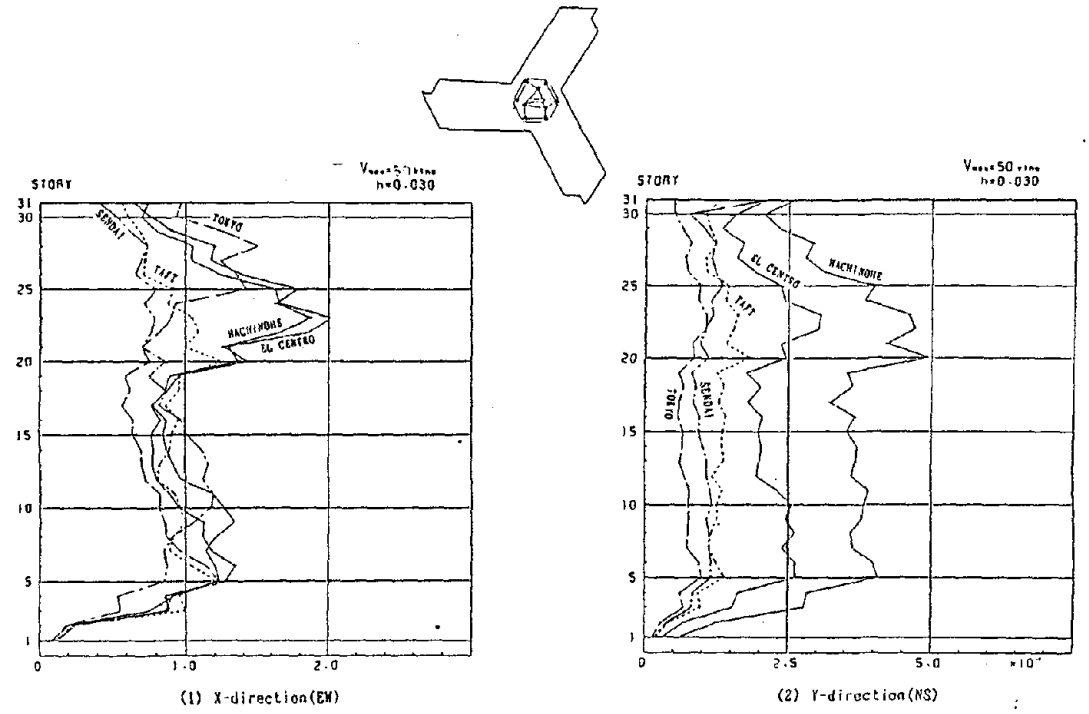

Figure 5.30 - Maximum story ductility, center east-west (50 cm/sec., h = 0.03, nonlinear).

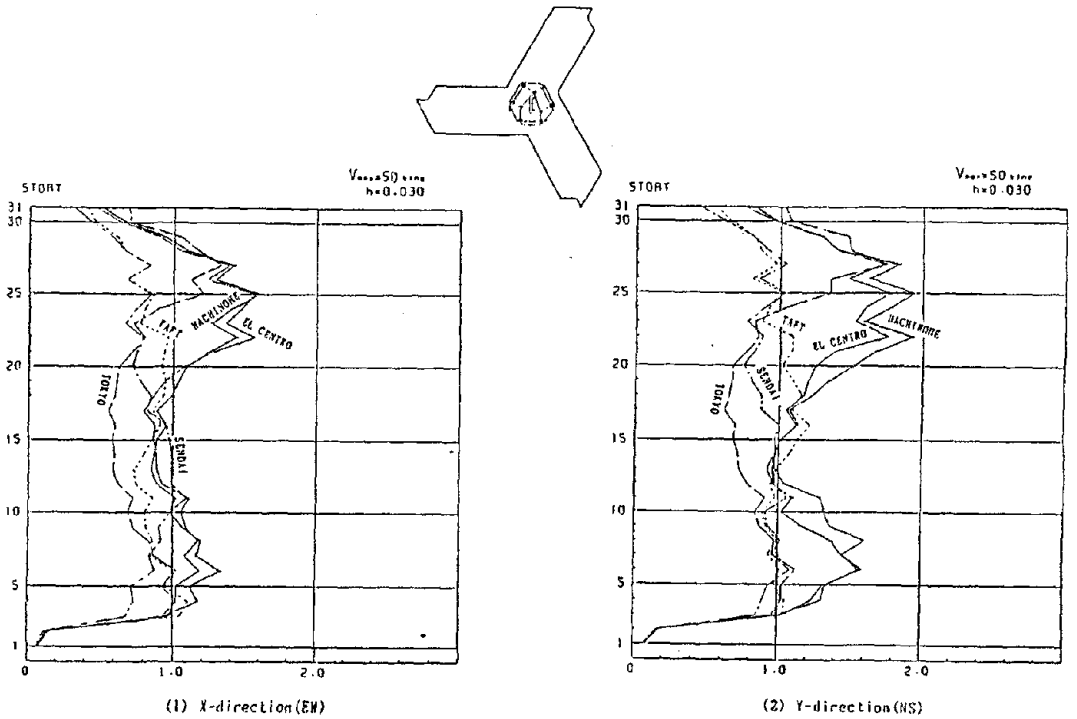

Figure 5.31 - Maximum story ductility, center north south (50 cm/sec., h = 0.03, nonlinear).

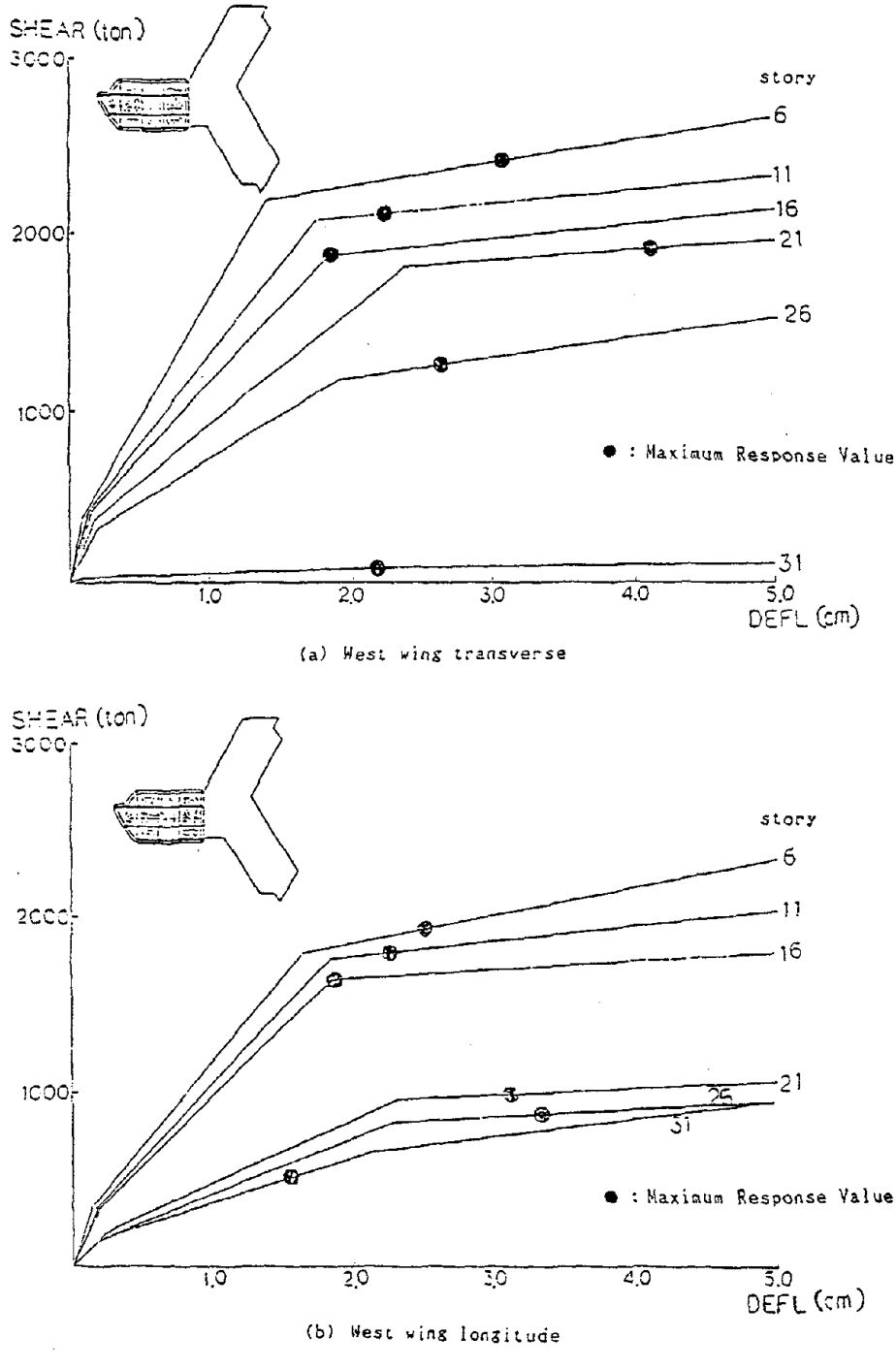

Figure 5.32 - Maximum response value on skeleton curve (50 cm/s, h=0.03, nonlinear)

6. SUMMARY, CONCLUSIONS AND RECOMMENDATIONS

6.1 SUMMARY AND CONCLUSIONS

This study has performed a detailed analysis of a 30 story reinforced concrete moment frame which in plan has three equally spaced wings in the shape of a Y. The building contains 583 condominium units and was completed in 1983. The building code used for the design was the 1979 UBC. However, for the seismic design the designers decided to supplement these requirements with site specific response spectra representative of maximum probable and maximum credible earthquakes. Ambient and forced vibration tests were conducted on the structure in 1983 near the end of construction. The building was instrumented with 21 strong motion accelerometers at the time of the 1989 Loma Prieta earthquake and recorded peak accelerations which ranged from 0.26g at the base to 0.47g at the roof. This caused only limited damage to nonstructural components and no visible damage to the structural system.

System identification techniques were used on the recorded data to identify the vibration mode shapes and periods. Moving window Fourier analyses were performed to investigate changes in the period of vibration during the earthquake. The response effects of torsion, rocking and soil-structure interaction were also evaluated using the recorded data. This information was then used to construct a simplified model of the building which could be used for parametric studies and code evaluations. Expanding on the identification studies and the response analyses conducted with the simplified model, a detailed, elastic finite element model of the building was developed, using the SAP90 program, which contained 6,816 degrees of freedom. Using this general model, seven

different mathematical models were developed to investigate various modeling considerations for reinforced concrete structures. These models were evaluated by making critical comparisons with the recorded earthquake response and with the results of the earlier ambient and forced vibration tests. One of the models was selected for detailed comparisons which included floor acceleration time history, floor displacement time history and floor response spectra. This model was also used to investigate the response of the building to other ground motions that have been recorded during recent earthquakes.

For the analysis of the soundness (adequacy) of the designed structure, a detailed finite element model similar to the one used with the SAP90 program was developed and used with the ETABS program and validated against the SAP90 model. This model was then used to make critical comparisons between lateral code loads, site spectra and recorded ground motions considering design parameters such as maximum lateral displacement, maximum interstory drift index (story drift angle) and maximum story shear. Effects of modal combination, P-Δ, and 2-D versus 3-D modeling were also investigated.

Working independently from the same database, the Kajima research team developed a 3-D elastic model of the building and investigated the design relative to current Japanese design practice. Critical comparisons were then made between U.S. and Japanese seismic design requirements.

In order to evaluate the damage potential of the building, the authors performed a detailed capacity check of the individual members of certain critical frames using the maximum

probable design spectrum. At the same time the Kajima researchers used the results from their 3-D elastic model to develop a simplified 3-D inelastic model. The damage potential of the building was then evaluated by analyzing the results obtained from these two distinct approaches.

Based on these extensive studies, the following general observations (conclusions) are presented:

1. Comparison of the dynamic characteristics of the building identified following the earthquake with those obtained from ambient and forced vibration tests at the end of construction indicated that the fundamental period of vibration had increased by as much as 57%. However, this change is not considered unreasonable on the basis of changes reported in other RC buildings.

2. Moving-window Fourier analyses indicated that there were no significant changes in the dynamic characteristics of the building during the earthquake.

3. Analyses of the recorded data indicate that there was very little torsional movement in the building and that soil-structure interaction and rocking effects were small.

4. If the dynamic properties are available or if the results of a detailed analytical model are available, a simplified model can be constructed which will produce

good estimates of the response and can be used for parametric sensitivity studies and overall response evaluations.

5. Detailed 3-D finite element models can be used to obtain an accurate estimate of the dynamic response prior to yielding of the reinforcing steel, however, owing to cracking, RC structures actually become weakly nonlinear systems at low lateral force levels representative of the service loads. For this reason, it may be necessary for the designer to consider more than one analytical model when evaluating the dynamic response. There is a need to consider the range (bounds) for the value of the fundamental period, and not just a single deterministic value.

6. Calculation of the elastic energy input to the structure by the recorded base motions indicates that the input in the E-W direction is 2.5 times that in the N-S direction, although the fault rupture was predominately in the N-S direction. A further study of input energy indicates that the recorded motion at the base of the structure was not a very severe test for this structural system. The ground motion recorded at Hollister, which is much closer to the epicenter of the Loma Prieta earthquake, resulted in an input energy that was 5.6 times that of the recorded base motion. Using the ground motion recorded at James Road during the 1979 Imperial Valley earthquake resulted in an input energy that was 22 times larger than the recorded base motion.

7. This building was designed to remain elastic (no yielding of the reinforcing steel) for lateral forces obtained by using 80% of the MPDS. These lateral forces

resulted in a base shear which was almost 2.2 times the base shear due to the lateral force requirements of the 1979 UBC. Results of the analyses show that had the building been designed for these minimal code loads, the damage resulting from this earthquake would have been much more substantial.

8. Acceleration spectra for the recorded base motion and the motion recorded at Hollister indicate that both records have a strong acceleration content in the period range of 0.9 to 1.2 seconds, which includes the 4th and 5th modes of the building (2nd mode E-W and 2nd mode N-S). Because these spectral accelerations were not included in the relatively narrow band site design spectra, MPDS, the lateral forces in the upper half of the building due to the recorded time histories are as much as 50% higher than those predicted by the MPDS.

9. For this structure, use of the CQC modal combination method with the MPDS resulted in story shears that were more than 17% higher than those obtained using the SRSS method. Even larger variation was obtained for the MCDS.

10. The interaction of axial load with the lateral frame displacement, i.e., P-Δ effects, does not cause a significant increase in the total lateral displacement, even for the James Road ground motions, which produce interstory drift angles of more than 2% at certain levels.

11. The lateral base shear coefficient for this building based on the 1979 UBC requirements is 0.04. The base shear coefficient obtained from the MPDS is 0.08,

whereas the value specified in the Japanese code (BSL) is 0.10. Since the lateral force requirements of the 1988 UBC are similar to the 1979 UBC, it can be concluded that for a building of this type, the minimum Japanese lateral force requirements would be 2.5 times greater than those of the United States.

12. The two levels of earthquake ground motion (normalized to peak velocities of 25 cm/sec and 50 cm/sec) used in Japanese practice are similar to the concept of the maximum probable and maximum credible spectra used in the design of this building. However, owing to the deficiencies in the frequency content of the site spectra discussed above, the normalized time histories give a better estimation of the actual response. Japanese practice also requires that the displacement ductility of the structure under both motions be less than 1.0. On the basis of the results of their studies, the Kajima researchers conclude that the upper stories of this building are not adequate when compared with Japanese practice.

13. Use of the 1988 UBC response spectrum for soft-soil sites and a structural system factor, R_w, equal to unity results in response envelopes which are similar to those obtained following Japanese design practice.

14. Capacity ratios calculated by the authors show a good correlation over the height of the building when compared with the ductility ratios calculated by the Kajima researchers using their simplified 3-D nonlinear model. However, evaluation of the capacity ratios indicates that the ductility demand of certain critical members of the frame may be considerably higher than the average ductility demand

reported by the Kajima study. Therefore the authors believe that the only reliable way to quantify this demand is to perform a detailed 3-D nonlinear analysis.

15. Evaluation of the capacity ratios and the nonlinear response analyses indicates that the yielding seismic resistance coefficient for this structure is approximately 0.17, indicating that the building has an inherent overstrength of more than 100%.

16. The structural system factor specified by the 1988 UBC for a moment-resistant reinforced concrete frame is assigned a value of 12. This value appears to be excessively high based on the results of this study. Although the design of this building was based on a particular site spectrum and ultimate strength, an equivalent R_w can be estimated from the data developed as part of this study if it is assumed that the design for 80% of the MPDS is acceptable. It has been shown previously that the base shear obtained by using 80% of the MPDS is almost 2.2 times that obtained using the code values, based on $R_w = 12$. If this value of 2.2 is reduced by 1.4 to reflect the effect of the ultimate strength design that was used with 0.80 MPDS, the resulting value for R_w becomes $12(2.2/1.4) = 7.6$. Considering that the estimated nonlinear response of the design based on the 0.80 MPDS, when subjected to possible critical severe earthquake ground motions, resulted in values of interstory drift as high as 1.5% and story displacement ductility as high as 3.41, then it is clear that the above reduction factor of 7.6 may still be too high. Note that if it is considered that the design based on 0.80 MPDS resulted in an overstrength of $(0.17 - 0.08)/0.08 = 1.1$, the reduction factor due to ductility is approximately $7.6/2.1 = 3.6$.

6.2 RECOMMENDATIONS

Considering the results obtained in the studies reported herein and the general observations presented above, the following recommendations are made.

1. A 3-D nonlinear finite element model of the building should be developed considering the present mechanical (dynamic) characteristics. This model and a reliable 3-D nonlinear analysis program should be used to evaluate the strength, deformation and energy dissipation capacities of the constructed building considering different possible critical earthquake ground motions that can occur in the future. Critical comparisons should then be made between this analysis and those obtained using either a 3-D linear elastic model or a simplified nonlinear model. The results should then be evaluated to determine whether it is possible to estimate the strength, global and local ductility ratios, maximum deformation and energy dissipation capacities using these less complex analysis methods.

2. Care should be exercised when selecting a design spectrum for a soft-soil site, because of uncertainties in estimating both the soil period and the building period. A spectrum covering a wide band of periods on either side of the estimated soil period should be used. Use of a narrow band spectrum may underestimate the frequency content of the base motions and result in a reduced estimate of the structural response.

3. A range of periods should be considered for the aseismic design of reinforced concrete structures owing to the reduction in stiffness resulting from cracking and

cumulative damages that occur under service loads. Results of this study and observations from previous earthquakes indicate that the period may lengthen by as much as 50%.

4. The CQC method of modal combination should be used for the dynamic response spectrum analysis of three-dimensional systems, particularly those with closely spaced modes.

5. Further studies should be conducted to define the concepts of building lateral force capacity and structural system factor better. Current values of the structural system factor may be unconservatively high.

REFERENCES

1. Bertero, V.V., Anderson, J., Krawinkler, H. and Miranda, E., "Design Guidelines for Ductility and Drift Limits: Review of the State-of-the Practice and of-the-Art on Ductility and Drift-Based Earthquake Resistant Design of Buildings," CUREe-Kajima Research Project Task #1, *Report No. UCB/EERC-91/15*, Earthquake Engineering Research Center, University of California at Berkeley, July 1991.

2. 1990 World Almanac, Pharos Books, New York, New York, 1990.

3. Miranda, E., and Bertero, V.V., "Evaluation of Seismic Performance and Estimation of Potential Damage - Case Study: A Ten-Story RC Building," CUREe-Kajima Research Project Tasks #3-5, 88 pp., Earthquake Engineering Research Center, University of California at Berkeley, July 1991.

4. Tai, J.C., Yang, Y.C., and Lin, T.Y., "Design and Construction of a Thirty-Story Concrete Ductile Framed Structure Emeryville-East San Francisco Bay," *Proceedings of the 8th World Conference on Earthquake Engineering*, Vol. V, pp. 371-379, San Francisco, 1984.

5. Maley, R., Acosta, A., Ellis, F., Etheredge, E., Foote, L., Johnson, D., Porcella, R., Salsman, M., and Switzer, J., "U.S. Geological Survey Strong-Motion Records from the Northern California (Loma Prieta) Earthquake of October 17, 1989," *Open-File Report 89-568*, Department of the Interior, United States Geological Survey, October 1989.

6. Governor's Board of Inquiry on the October 17, 1989 Loma Prieta Earthquake, "*Competing Against Time*," State of California, May 1990.

7. Hudson, D.E., "Reading and Interpreting Strong-Motion Accelerograms," Earthquake Engineering Research Institute, Special Monograph, Berkeley, California, 1979.

8. Trifunac, M.D., "Zero Base Line Correction of Strong-Motion Accelerograms," *Bulletin of the Seismological Society of America*, Vol. 64, No. 4, pp. 1209-1219, August 1979.

9. Trifunac, M.D., and Lee, V.W., "A Note on the Accuracy of Computed Ground Displacements from Strong-Motion Accelerograms," *Bulletin of the Seismological Society of America*, Vol. 65, No. 3, pp. 581-626, June 1975.

10. Nigam, N.C., and Jennings, P.C., "Calculation of Response Spectra from Strong-Motion Earthquake Records," *Bulletin of the Seismological Society of America*, Vol. 59, No. 2, pp 909-922, 1969.

11. Hart, G.C., and Yao, J.T.P., "System Identification in Structural Dynamics," *Journal of Engineering Mechanics*, ASCE, Vol. 103, No. EM6, pp. 1089-1104, 1976.

12. McVerry, G.H., "Frequency Domain Identification of Structural Models from Earthquake Records," *Report EERL 79-02*, Earthquake Engineering Research Laboratory, Caltech, Pasadena, California, 1979.

13. Torkamani, M.A., and Hart, G.C., "Building System Identifications Using Earthquake Data," *Report No. UCLA-Eng-7507*, University of California at Los Angeles, California, 1975.

14. Udwadia, F.E., and Shah, P.C., "Identification of Structures Through Records Obtained during Strong Earthquake Ground Motions," *Journal of Engineering for Industry*, ASME, Vol. 98, pp. 1347-1362, 1975.

15. Cooley, J.W., and Tukey, J.W., "An Algorithm for the Machine Computation of Complex Fourier Series," *Math. Comput.*, pp. 297-301, 1965.

16. Bloomfield P., Fourier Analysis of Time Series: An Introduction, John Wiley & Sons, New York, 1976.

17. Becker, R.R., Chamber J.M., *S: An Interactive Environment for Data Analysis and Graphics*, Wadworth Statistics/Probability Series, New York, 1984.

18. Tukey, J.W., Exploratory Data Analysis, Addison Wesley, 1973.

19. Skinner, A.J., Handbook for Earthquake Generated Forces and Moments in Tall Buildings, Dominion Physics Laboratory, New Zealand, 1960.

    Also: Rogers, G.L. Dynamics of Framed Structures, John Wiley & Sons, 1959.

20. Clough, R.W., and Penzien, J., Dynamics of Structures, McGraw-Hill, 1975.

21. Stagner, J.R., and Hart, G.C., "Damping Estimation and Digital Filtering Applied to Structural Motions," *Report No. UCLA-ENG 7181*, Earthquake Engineering and Structures Laboratory, University of California at Los Angeles, California, December 1971.

22. Stephen, R.M., Wilson, E.L., Stander N., "Dynamic Properties of a Thirty-Story Condominium Tower Building," *Report No. UCB/EERC-85/03*, Earthquake Engineering Research Center, University of California at Berkeley, April 1985.

23. Del Valle, E., and Prince, J., "Analytical and Experimental Studies of Vibration in Two Buildings," *Proceedings of the Third World Conference on Earthquake Engineering*, Vol II, pp. 578-662, New Zealand, 1965.

24. NOAA/EERI, Murphy, L.M., Editor, "San Fernando, California Earthquake of February 9, 1971," NOAA, U.S. Department of Commerce, Vols. I, II and III, 1973.

25. Pardoen, G.C., "Imperial County Services Building, Ambient Vibration Test Results," *Report No. 79/14*, Civil Engineering Department, University of Canterbury, New Zealand, 1979.

26. Rojahn, C., and Mork, P.N., "An Analysis of Strong-Motion Data from a Severely Damaged Structure - The Imperial County Services Building, El Centro, California, in the Imperial Valley , California, Earthquake of October 15, 1979," Geological Survey, *Professional Paper 1254*, Washington, D.C., 1982.

27. Nagaya, M., Akita, K., Kitagawa, Y., Osawa, Y., "Vibration Tests of a 29-Story Frame Type Building," *Proceedings of the 9th World Conference on Earthquake Engineering*, Vol. V, pp. 601-606, Tokyo, Japan, 1988.

28. Haviland, R., Biggs, J.M., and Vanmarcke, E.H., "A Study of the Uncertainties in the Fundamental Translational Periods and Damping Values for Real Buildings," *Publication No. R76-12*, Massachusetts Institute of Technology, February 1976.

29. Bertero, V.V., Earthquake Hazard Reduction: Technical Capability - U.S. Perspective," *Proceedings of the 2nd U.S. - Japan Workshop on Urban Earthquake Hazards Reduction*, pp. 10-51, Shimizu, Japan, July 27-29, 1988.

30. Tanaka, T., Yoshizawa, S. Osawa, Y., and Morishita, T., "Period and Damping of Vibration in Actual Buildings During Earthquakes," *Bulletin of the Earthquake Research Institute*, University of Tokyo, Vol. 47, pp. 1073-1092, Japan, 1969.

31. Okamoto, S., Wight. J., Nakata, S., Yoshimura, M., and Kaminosoma, T., "Testing, Repair and Strengthening, and Retesting of a Full-Scale Seven-Story Reinforced Concrete Building," *Publication SP-84*, Earthquake Effects on Reinforced Concrete Structures, U.S. - Japan Research, American Concrete Institute, pp. 133-161, Detroit, Michigan, 1985.

32. Bertero, V.V., Aktan, A.E., Charney, F.A., and Sause, R., "U.S. - Japan Cooperative Earthquake Research Program: Earthquake Simulation Tests and Associated Studies of a 1/5th Scale Model of a 7-Story Reinforced Concrete Test Structure," *Report No. UCB/EERC-84/05*, Earthquake Engineering Research Center, University of California at Berkeley, June 1984.

33. Foutch, D.A., Goel, S.C., Roeder, C.W., "Preliminary Report on Testing of a Full-Scale Six-Story Steel Building," *Structural Research Series No. 527*, University of Illinois, Urbana-Champaign, November, 1986.

34. Uang, C.-M., and Bertero, V.V., "Earthquake Simulation Tests and Associated Studies of a 0.3-Scale Model of a 6-Story Concentrically Braced Steel Structure," *Report No. UCB/EERC-86/10*, Earthquake Engineering Research Center, University of California at Berkeley, December 1986.

35. Whittaker, A. S., Uang, C.-M., and Bertero, V.V., "Earthquake Simulation Tests and Associated Studies of a 0.3-Scale Model of a 6-Story Eccentrically Braced Steel Structure," *Report No. UCB/EERC-87/02*, Earthquake Engineering Research Center, University of California at Berkeley, July 1987.

36. Shahrooz, B.M., and Moehle, J.P, "Experimental Study of Seismic Response of Reinforced Concrete Setback Buildings," *Report No. UCB/EERC-87/16*, University of California at Berkeley, October 1987.

37. Udwadia, F.E., and Trifunac, M.D., "Time and Amplitude Dependent Response of Structures," *Earthquake Engineering and Structural Dynamics*, Vol. 2, pp. 359-378, 1974.

38. Wilson, E.L., and Habibullah, A., SAP90 A Series of Computer Programs for the Static and Dynamic Finite Element Analysis of Structures: User's Manual, Computers and Structures, Inc., Berkeley, California, 1989.

39. American Concrete Institute, "Building Code Requirements for Structural Plain Concrete," pp. 318-389, Detroit, Michigan, 1989.

40. Building Officials Conference, "Uniform Building Code," 1979, 1982, 1985, and 1988 Editions, Whittier, California.

41. Wilson, E.L., and Habibullah, A., ETABS, A User's Manual, Computers and Structures, Inc., Berkeley, California, 1989.

42. Wilson, E.L., Der Kiureghian, A., and Bayo, E.P., " A Replacement for the SRSS Method in Seismic Analysis," *Earthquake Engineering and Structural Dynamics*, Vol. 9, No. 2, pp. 187-194, March/April 1981.

43. Bertero, V.V., "Strength and Deformation Capacities of Buildings under Extreme Environments," Structural Engineering and Structural Mechanics, Pister, K.S., ed., pp. 188-237, Prentice-Hall Inc., Englewood Cliffs, New Jersey, 1980.

44. Anderson, J.C., and Bertero, V.V., "Uncertainties in Establishing Design Earthquakes," *Journal of the Structural Division*, ASCE, vol. 113, No. 8, August 1987.

45. Krawinkler, H., Nasser, A., and Rahnama, N., "Evaluation of Damage Potential of Recorded Ground Motions," CUREe-Kajima Research Report, Stanford University, Stanford, California, June 1991.

46. Bertero, V.V. and Miranda, E., "Evaluation of Damage Potential of Recorded Ground Motions and its Implications for Design of Structures," A CUREe-Kajima Research Report, 52 pp., August 1991.

47. International Association for Earthquake Engineering, "Japan Building Standard Law," pp. 579-681, Earthquake Resistant Regulations: A World List - 1988, Gakujutsu Bunken Fukyu-Kai, Oh Okayama 12-1, Meguroko, Tokyo 152, Japan, July 1988.

EARTHQUAKE ENGINEERING RESEARCH CENTER REPORT SERIES

EERC reports are available from the National Information Service for Earthquake Engineering(NISEE) and from the National Technical Information Service(NTIS). Numbers in parentheses are Accession Numbers assigned by the National Technical Information Service; these are followed by a price code. Contact NTIS, 5285 Port Royal Road, Springfield Virginia, 22161 for more information. Reports without Accession Numbers were not available from NTIS at the time of printing. For a current complete list of EERC reports (from EERC 67-1) and availability information, please contact University of California, EERC, NISEE, 1301 South 46th Street, Richmond, California 94804.

UCB/EERC-81/01 "Control of Seismic Response of Piping Systems and Other Structures by Base Isolation," by Kelly, J.M., January 1981, (PB81 200 735)A05.

UCB/EERC-81/02 "OPTNSR- An Interactive Software System for Optimal Design of Statically and Dynamically Loaded Structures with Nonlinear Response," by Bhatti, M.A., Ciampi, V. and Pister, K.S., January 1981, (PB81 218 851)A09.

UCB/EERC-81/03 "Analysis of Local Variations in Free Field Seismic Ground Motions," by Chen, J.-C., Lysmer, J. and Seed, H.B., January 1981, (AD-A099508)A13.

UCB/EERC-81/04 "Inelastic Structural Modeling of Braced Offshore Platforms for Seismic Loading," by Zayas, V.A., Shing, P.-S.B., Mahin, S.A. and Popov, E.P., January 1981, INEL4, (PB82 138 777)A07.

UCB/EERC-81/05 "Dynamic Response of Light Equipment in Structures," by Der Kiureghian, A., Sackman, J.L. and Nour-Omid, B., April 1981, (PB81 218 497)A04.

UCB/EERC-81/06 "Preliminary Experimental Investigation of a Broad Base Liquid Storage Tank," by Bouwkamp, J.G., Kollegger, J.P. and Stephen, R.M., May 1981, (PB82 140 385)A03.

UCB/EERC-81/07 "The Seismic Resistant Design of Reinforced Concrete Coupled Structural Walls," by Aktan, A.E. and Bertero, V.V., June 1981, (PB82 113 358)A11.

UCB/EERC-81/08 "Unassigned," by Unassigned, 1981.

UCB/EERC-81/09 "Experimental Behavior of a Spatial Piping System with Steel Energy Absorbers Subjected to a Simulated Differential Seismic Input," by Stiemer, S.F., Godden, W.G. and Kelly, J.M., July 1981, (PB82 201 898)A04.

UCB/EERC-81/10 "Evaluation of Seismic Design Provisions for Masonry in the United States," by Sveinsson, B.I., Mayes, R.L. and McNiven, H.D., August 1981, (PB82 166 075)A08.

UCB/EERC-81/11 "Two-Dimensional Hybrid Modelling of Soil-Structure Interaction," by Tzong, T.-J., Gupta, S. and Penzien, J., August 1981, (PB82 142 118)A04.

UCB/EERC-81/12 "Studies on Effects of Infills in Seismic Resistant R/C Construction," by Brokken, S. and Bertero, V.V., October 1981, (PB82 166 190)A09.

UCB/EERC-81/13 "Linear Models to Predict the Nonlinear Seismic Behavior of a One-Story Steel Frame," by Valdimarsson, H., Shah, A.H. and McNiven, H.D., September 1981, (PB82 138 793)A07.

UCB/EERC-81/14 "TLUSH: A Computer Program for the Three-Dimensional Dynamic Analysis of Earth Dams," by Kagawa, T., Mejia, L.H., Seed, H.B. and Lysmer, J., September 1981, (PB82 139 940)A06.

UCB/EERC-81/15 "Three Dimensional Dynamic Response Analysis of Earth Dams," by Mejia, L.H. and Seed, H.B., September 1981, (PB82 137 274)A12.

UCB/EERC-81/16 "Experimental Study of Lead and Elastomeric Dampers for Base Isolation Systems," by Kelly, J.M. and Hodder, S.B., October 1981, (PB82 166 182)A05.

UCB/EERC-81/17 "The Influence of Base Isolation on the Seismic Response of Light Secondary Equipment," by Kelly, J.M., April 1981, (PB82 255 266)A04.

UCB/EERC-81/18 "Studies on Evaluation of Shaking Table Response Analysis Procedures," by Blondet, J. M., November 1981, (PB82 197 278)A10.

UCB/EERC-81/19 "DELIGHT.STRUCT: A Computer-Aided Design Environment for Structural Engineering," by Balling, R.J., Pister, K.S. and Polak, E., December 1981, (PB82 218 496)A07.

UCB/EERC-81/20 "Optimal Design of Seismic-Resistant Planar Steel Frames," by Balling, R.J., Ciampi, V. and Pister, K.S., December 1981, (PB82 220 179)A07.

UCB/EERC-82/01 "Dynamic Behavior of Ground for Seismic Analysis of Lifeline Systems," by Sato, T. and Der Kiureghian, A., January 1982, (PB82 218 926)A05.

UCB/EERC-82/02 "Shaking Table Tests of a Tubular Steel Frame Model," by Ghanaat, Y. and Clough, R.W., January 1982, (PB82 220 161)A07.

UCB/EERC-82/03 "Behavior of a Piping System under Seismic Excitation: Experimental Investigations of a Spatial Piping System supported by Mechanical Shock Arrestors," by Schneider, S., Lee, H.-M. and Godden, W. G., May 1982, (PB83 172 544)A09.

UCB/EERC-82/04 "New Approaches for the Dynamic Analysis of Large Structural Systems," by Wilson, E.L., June 1982, (PB83 148 080)A05.

UCB/EERC-82/05 "Model Study of Effects of Damage on the Vibration Properties of Steel Offshore Platforms," by Shahrivar, F. and Bouwkamp, J.G., June 1982, (PB83 148 742)A10.

UCB/EERC-82/06 "States of the Art and Pratice in the Optimum Seismic Design and Analytical Response Prediction of R/C Frame Wall Structures," by Aktan, A.E. and Bertero, V.V., July 1982, (PB83 147 736)A05.

UCB/EERC-82/07 "Further Study of the Earthquake Response of a Broad Cylindrical Liquid-Storage Tank Model," by Manos, G.C. and Clough, R.W., July 1982, (PB83 147 744)A11.

UCB/EERC-82/08 "An Evaluation of the Design and Analytical Seismic Response of a Seven Story Reinforced Concrete Frame," by Charney, F.A. and Bertero, V.V., July 1982, (PB83 157 628)A09.

UCB/EERC-82/09 "Fluid-Structure Interactions: Added Mass Computations for Incompressible Fluid," by Kuo, J.S.-H., August 1982, (PB83 156 281)A07.

UCB/EERC-82/10 "Joint-Opening Nonlinear Mechanism: Interface Smeared Crack Model," by Kuo, J.S.-H., August 1982, (PB83 149 195)A05.

UCB/EERC-82/11 "Dynamic Response Analysis of Techi Dam," by Clough, R.W., Stephen, R.M. and Kuo, J.S.-H., August 1982, (PB83 147 496)A06.

UCB/EERC-82/12 "Prediction of the Seismic Response of R/C Frame-Coupled Wall Structures," by Aktan, A.E., Bertero, V.V. and Piazzo, M., August 1982, (PB83 149 203)A09.

UCB/EERC-82/13 "Preliminary Report on the Smart 1 Strong Motion Array in Taiwan," by Bolt, B.A., Loh, C.H., Penzien, J. and Tsai, Y.B., August 1982, (PB83 159 400)A10.

UCB/EERC-82/14 "Seismic Behavior of an Eccentrically X-Braced Steel Structure," by Yang, M.S., September 1982, (PB83 260 778)A12.

UCB/EERC-82/15 "The Performance of Stairways in Earthquakes," by Roha, C., Axley, J.W. and Bertero, V.V., September 1982, (PB83 157 693)A07.

UCB/EERC-82/16 "The Behavior of Submerged Multiple Bodies in Earthquakes," by Liao, W.-G., September 1982, (PB83 158 709)A07.

UCB/EERC-82/17 "Effects of Concrete Types and Loading Conditions on Local Bond-Slip Relationships," by Cowell, A.D., Popov, E.P. and Bertero, V.V., September 1982, (PB83 153 577)A04.

UCB/EERC-82/18 "Mechanical Behavior of Shear Wall Vertical Boundary Members: An Experimental Investigation," by Wagner, M.T. and Bertero, V.V., October 1982, (PB83 159 764)A05.

UCB/EERC-82/19 "Experimental Studies of Multi-support Seismic Loading on Piping Systems," by Kelly, J.M. and Cowell, A.D., November 1982, (PB90 262 684)A07.

UCB/EERC-82/20 "Generalized Plastic Hinge Concepts for 3D Beam-Column Elements," by Chen, P. F.-S. and Powell, G.H., November 1982, (PB83 247 981)A13.

UCB/EERC-82/21 "ANSR-II: General Computer Program for Nonlinear Structural Analysis," by Oughourlian, C.V. and Powell, G.H., November 1982, (PB83 251 330)A12.

UCB/EERC-82/22 "Solution Strategies for Statically Loaded Nonlinear Structures," by Simons, J.W. and Powell, G.H., November 1982, (PB83 197 970)A06.

UCB/EERC-82/23 "Analytical Model of Deformed Bar Anchorages under Generalized Excitations," by Ciampi, V., Eligehausen, R., Bertero, V.V. and Popov, E.P., November 1982, (PB83 169 532)A06.

UCB/EERC-82/24 "A Mathematical Model for the Response of Masonry Walls to Dynamic Excitations," by Sucuoglu, H., Mengi, Y. and McNiven, H.D., November 1982, (PB83 169 011)A07.

UCB/EERC-82/25 "Earthquake Response Considerations of Broad Liquid Storage Tanks," by Cambra, F.J., November 1982, (PB83 251 215)A09.

UCB/EERC-82/26 "Computational Models for Cyclic Plasticity, Rate Dependence and Creep," by Mosaddad, B. and Powell, G.H., November 1982, (PB83 245 829)A08.

UCB/EERC-82/27 "Inelastic Analysis of Piping and Tubular Structures," by Mahasuverachai, M. and Powell, G.H., November 1982, (PB83 249 987)A07.

UCB/EERC-83/01 "The Economic Feasibility of Seismic Rehabilitation of Buildings by Base Isolation," by Kelly, J.M., January 1983, (PB83 197 988)A05.

UCB/EERC-83/02 "Seismic Moment Connections for Moment-Resisting Steel Frames.," by Popov, E.P., January 1983, (PB83 195 412)A04.

UCB/EERC-83/03 "Design of Links and Beam-to-Column Connections for Eccentrically Braced Steel Frames," by Popov, E.P. and Malley, J.O., January 1983, (PB83 194 811)A04.

UCB/EERC-83/04 "Numerical Techniques for the Evaluation of Soil-Structure Interaction Effects in the Time Domain," by Bayo, E. and Wilson, E.L., February 1983, (PB83 245 605)A09.

UCB/EERC-83/05 "A Transducer for Measuring the Internal Forces in the Columns of a Frame-Wall Reinforced Concrete Structure," by Sause, R. and Bertero, V.V., May 1983, (PB84 119 494)A06.

UCB/EERC-83/06 "Dynamic Interactions Between Floating Ice and Offshore Structures," by Croteau, P., May 1983, (PB84 119 486)A16.

UCB/EERC-83/07 "Dynamic Analysis of Multiply Tuned and Arbitrarily Supported Secondary Systems," by Igusa, T. and Der Kiureghian, A., July 1983, (PB84 118 272)A11.

UCB/EERC-83/08 "A Laboratory Study of Submerged Multi-body Systems in Earthquakes," by Ansari, G.R., June 1983, (PB83 261 842)A17.

UCB/EERC-83/09 "Effects of Transient Foundation Uplift on Earthquake Response of Structures," by Yim, C.-S. and Chopra, A.K., June 1983, (PB83 261 396)A07.

UCB/EERC-83/10 "Optimal Design of Friction-Braced Frames under Seismic Loading," by Austin, M.A. and Pister, K.S., June 1983, (PB84 119 288)A06.

UCB/EERC-83/11 "Shaking Table Study of Single-Story Masonry Houses: Dynamic Performance under Three Component Seismic Input and Recommendations," by Manos, G.C., Clough, R.W. and Mayes, R.L., July 1983, (UCB/EERC-83/11)A08.

UCB/EERC-83/12 "Experimental Error Propagation in Pseudodynamic Testing," by Shiing, P.B. and Mahin, S.A., June 1983, (PB84 119 270)A09.

UCB/EERC-83/13 "Experimental and Analytical Predictions of the Mechanical Characteristics of a 1/5-scale Model of a 7-story R/C Frame-Wall Building Structure," by Aktan, A.E., Bertero, V.V., Chowdhury, A.A. and Nagashima, T., June 1983, (PB84 119 213)A07.

UCB/EERC-83/14 "Shaking Table Tests of Large-Panel Precast Concrete Building System Assemblages," by Oliva, M.G. and Clough, R.W., June 1983, (PB86 110 210/AS)A11.

UCB/EERC-83/15 "Seismic Behavior of Active Beam Links in Eccentrically Braced Frames," by Hjelmstad, K.D. and Popov, E.P., July 1983, (PB84 119 676)A09.

UCB/EERC-83/16 "System Identification of Structures with Joint Rotation," by Dimsdale, J.S., July 1983, (PB84 192 210)A06.

UCB/EERC-83/17 "Construction of Inelastic Response Spectra for Single-Degree-of-Freedom Systems," by Mahin, S. and Lin, J., June 1983, (PB84 208 834)A05.

UCB/EERC-83/18 "Interactive Computer Analysis Methods for Predicting the Inelastic Cyclic Behaviour of Structural Sections," by Kaba, S. and Mahin, S., July 1983, (PB84 192 012)A06.

UCB/EERC-83/19 "Effects of Bond Deterioration on Hysteretic Behavior of Reinforced Concrete Joints," by Filippou, F.C., Popov, E.P. and Bertero, V.V., August 1983, (PB84 192 020)A10.

UCB/EERC-83/20 "Correlation of Analytical and Experimental Responses of Large-Panel Precast Building Systems," by Oliva, M.G., Clough, R.W., Velkov, M. and Gavrilovic, P., May 1988, (PB90 262 692)A06.

UCB/EERC-83/21 "Mechanical Characteristics of Materials Used in a 1/5 Scale Model of a 7-Story Reinforced Concrete Test Structure," by Bertero, V.V., Aktan, A.E., Harris, H.G. and Chowdhury, A.A., October 1983, (PB84 193 697)A05.

UCB/EERC-83/22 "Hybrid Modelling of Soil-Structure Interaction in Layered Media," by Tzong, T.-J. and Penzien, J., October 1983, (PB84 192 178)A08.

UCB/EERC-83/23 "Local Bond Stress-Slip Relationships of Deformed Bars under Generalized Excitations," by Eligehausen, R., Popov, E.P. and Bertero, V.V., October 1983, (PB84 192 848)A09.

UCB/EERC-83/24 "Design Considerations for Shear Links in Eccentrically Braced Frames," by Malley, J.O. and Popov, E.P., November 1983, (PB84 192 186)A07.

UCB/EERC-84/01 "Pseudodynamic Test Method for Seismic Performance Evaluation: Theory and Implementation," by Shing, P.-S.B. and Mahin, S.A., January 1984, (PB84 190 644)A08.

UCB/EERC-84/02 "Dynamic Response Behavior of Kiang Hong Dian Dam," by Clough, R.W., Chang, K.-T., Chen, H.-Q. and Stephen, R.M., April 1984, (PB84 209 402)A08.

UCB/EERC-84/03 "Refined Modelling of Reinforced Concrete Columns for Seismic Analysis," by Kaba, S.A. and Mahin, S.A., April 1984, (PB84 234 384)A06.

UCB/EERC-84/04 "A New Floor Response Spectrum Method for Seismic Analysis of Multiply Supported Secondary Systems," by Asfura, A. and Der Kiureghian, A., June 1984, (PB84 239 417)A06.

UCB/EERC-84/05 "Earthquake Simulation Tests and Associated Studies of a 1/5th-scale Model of a 7-Story R/C Frame-Wall Test Structure," by Bertero, V.V., Aktan, A.E., Charney, F.A. and Sause, R., June 1984, (PB84 239 409)A09.

UCB/EERC-84/06 "Unassigned," by Unassigned, 1984.

UCB/EERC-84/07 "Behavior of Interior and Exterior Flat-Plate Connections subjected to Inelastic Load Reversals," by Zee, H.L. and Moehle, J.P., August 1984, (PB86 117 629/AS)A07.

UCB/EERC-84/08 "Experimental Study of the Seismic Behavior of a Two-Story Flat-Plate Structure," by Moehle, J.P. and Diebold, J.W., August 1984, (PB86 122 553/AS)A12.

UCB/EERC-84/09 "Phenomenological Modeling of Steel Braces under Cyclic Loading," by Ikeda, K., Mahin, S.A. and Dermitzakis, S.N., May 1984, (PB86 132 198/AS)A08.

UCB/EERC-84/10 "Earthquake Analysis and Response of Concrete Gravity Dams," by Fenves, G. and Chopra, A.K., August 1984, (PB85 193 902/AS)A11.

UCB/EERC-84/11 "EAGD-84: A Computer Program for Earthquake Analysis of Concrete Gravity Dams," by Fenves, G. and Chopra, A.K., August 1984, (PB85 193 613/AS)A05.

UCB/EERC-84/12 "A Refined Physical Theory Model for Predicting the Seismic Behavior of Braced Steel Frames," by Ikeda, K. and Mahin, S.A., July 1984, (PB85 191 450/AS)A09.

UCB/EERC-84/13 "Earthquake Engineering Research at Berkeley - 1984," by EERC, August 1984, (PB85 197 341/AS)A10.

UCB/EERC-84/14 "Moduli and Damping Factors for Dynamic Analyses of Cohesionless Soils," by Seed, H.B., Wong, R.T., Idriss, I.M. and Tokimatsu, K., September 1984, (PB85 191 468/AS)A04.

UCB/EERC-84/15 "The Influence of SPT Procedures in Soil Liquefaction Resistance Evaluations," by Seed, H.B., Tokimatsu, K., Harder, L.F. and Chung, R.M., October 1984, (PB85 191 732/AS)A04.

UCB/EERC-84/16 "Simplified Procedures for the Evaluation of Settlements in Sands Due to Earthquake Shaking," by Tokimatsu, K. and Seed, H.B., October 1984, (PB85 197 887/AS)A03.

UCB/EERC-84/17 "Evaluation of Energy Absorption Characteristics of Highway Bridges Under Seismic Conditions - Volume I (PB90 262 627)A16 and Volume II (Appendices) (PB90 262 635)A13," by Imbsen, R.A. and Penzien, J., September 1986.

UCB/EERC-84/18 "Structure-Foundation Interactions under Dynamic Loads," by Liu, W.D. and Penzien, J., November 1984, (PB87 124 889/AS)A11.

UCB/EERC-84/19 "Seismic Modelling of Deep Foundations," by Chen, C.-H. and Penzien, J., November 1984, (PB87 124 798/AS)A07.

UCB/EERC-84/20 "Dynamic Response Behavior of Quan Shui Dam," by Clough, R.W., Chang, K.-T., Chen, H.-Q., Stephen, R.M., Ghanaat, Y. and Qi, J.-H., November 1984, (PB86 115177/AS)A07.

UCB/EERC-85/01 "Simplified Methods of Analysis for Earthquake Resistant Design of Buildings," by Cruz, E.F. and Chopra, A.K., February 1985, (PB86 112299/AS)A12.

UCB/EERC-85/02 "Estimation of Seismic Wave Coherency and Rupture Velocity using the SMART 1 Strong-Motion Array Recordings," by Abrahamson, N.A., March 1985, (PB86 214 343)A07.

UCB/EERC-85/03 "Dynamic Properties of a Thirty Story Condominium Tower Building," by Stephen, R.M., Wilson, E.L. and Stander, N., April 1985, (PB86 118965/AS)A06.

UCB/EERC-85/04 "Development of Substructuring Techniques for On-Line Computer Controlled Seismic Performance Testing," by Dermitzakis, S. and Mahin, S., February 1985, (PB86 132941/AS)A08.

UCB/EERC-85/05 "A Simple Model for Reinforcing Bar Anchorages under Cyclic Excitations," by Filippou, F.C., March 1985, (PB86 112 919/AS)A05.

UCB/EERC-85/06 "Racking Behavior of Wood-framed Gypsum Panels under Dynamic Load," by Oliva, M.G., June 1985, (PB90 262 643)A04.

UCB/EERC-85/07 "Earthquake Analysis and Response of Concrete Arch Dams," by Fok, K.-L. and Chopra, A.K., June 1985, (PB86 139672/AS)A10.

UCB/EERC-85/08 "Effect of Inelastic Behavior on the Analysis and Design of Earthquake Resistant Structures," by Lin, J.P. and Mahin, S.A., June 1985, (PB86 135340/AS)A08.

UCB/EERC-85/09 "Earthquake Simulator Testing of a Base-Isolated Bridge Deck," by Kelly, J.M., Buckle, I.G. and Tsai, H.-C., January 1986, (PB87 124 152/AS)A06.

UCB/EERC-85/10 "Simplified Analysis for Earthquake Resistant Design of Concrete Gravity Dams," by Fenves, G. and Chopra, A.K., June 1986, (PB87 124 160/AS)A08.

UCB/EERC-85/11 "Dynamic Interaction Effects in Arch Dams," by Clough, R.W., Chang, K.-T., Chen, H.-Q. and Ghanaat, Y., October 1985, (PB86 135027/AS)A05.

UCB/EERC-85/12 "Dynamic Response of Long Valley Dam in the Mammoth Lake Earthquake Series of May 25-27, 1980," by Lai, S. and Seed, H.B., November 1985, (PB86 142304/AS)A05.

UCB/EERC-85/13 "A Methodology for Computer-Aided Design of Earthquake-Resistant Steel Structures," by Austin, M.A., Pister, K.S. and Mahin, S.A., December 1985, (PB86 159480/AS)A10 .

UCB/EERC-85/14 "Response of Tension-Leg Platforms to Vertical Seismic Excitations," by Liou, G.-S., Penzien, J. and Yeung, R.W., December 1985, (PB87 124 871/AS)A08.

UCB/EERC-85/15 "Cyclic Loading Tests of Masonry Single Piers: Volume 4 - Additional Tests with Height to Width Ratio of 1," by Sveinsson, B., McNiven, H.D. and Sucuoglu, H., December 1985.

UCB/EERC-85/16 "An Experimental Program for Studying the Dynamic Response of a Steel Frame with a Variety of Infill Partitions," by Yanev, B. and McNiven, H.D., December 1985, (PB90 262 676)A05.

UCB/EERC-86/01 "A Study of Seismically Resistant Eccentrically Braced Steel Frame Systems," by Kasai, K. and Popov, E.P., January 1986, (PB87 124 178/AS)A14.

UCB/EERC-86/02 "Design Problems in Soil Liquefaction," by Seed, H.B., February 1986, (PB87 124 186/AS)A03.

UCB/EERC-86/03 "Implications of Recent Earthquakes and Research on Earthquake-Resistant Design and Construction of Buildings," by Bertero, V.V., March 1986, (PB87 124 194/AS)A05.

UCB/EERC-86/04 "The Use of Load Dependent Vectors for Dynamic and Earthquake Analyses," by Leger, P., Wilson, E.L. and Clough, R.W., March 1986, (PB87 124 202/AS)A12.

UCB/EERC-86/05 "Two Beam-To-Column Web Connections," by Tsai, K.-C. and Popov, E.P., April 1986, (PB87 124 301/AS)A04.

UCB/EERC-86/06 "Determination of Penetration Resistance for Coarse-Grained Soils using the Becker Hammer Drill," by Harder, L.F. and Seed, H.B., May 1986, (PB87 124 210/AS)A07.

UCB/EERC-86/07 "A Mathematical Model for Predicting the Nonlinear Response of Unreinforced Masonry Walls to In-Plane Earthquake Excitations," by Mengi, Y. and McNiven, H.D., May 1986, (PB87 124 780/AS)A06.

UCB/EERC-86/08 "The 19 September 1985 Mexico Earthquake: Building Behavior," by Bertero, V.V., July 1986.

UCB/EERC-86/09 "EACD-3D: A Computer Program for Three-Dimensional Earthquake Analysis of Concrete Dams," by Fok, K.-L., Hall, J.F. and Chopra, A.K., July 1986, (PB87 124 228/AS)A08.

UCB/EERC-86/10 "Earthquake Simulation Tests and Associated Studies of a 0.3-Scale Model of a Six-Story Concentrically Braced Steel Structure," by Uang, C.-M. and Bertero, V.V., December 1986, (PB87 163 564/AS)A17.

UCB/EERC-86/11 "Mechanical Characteristics of Base Isolation Bearings for a Bridge Deck Model Test," by Kelly, J.M., Buckle, I.G. and Koh, C.-G., November 1987, (PB90 262 668)A04.

UCB/EERC-86/12 "Effects of Axial Load on Elastomeric Isolation Bearings," by Koh, C.-G. and Kelly, J.M., November 1987.

UCB/EERC-87/01 "The FPS Earthquake Resisting System: Experimental Report," by Zayas, V.A., Low, S.S. and Mahin, S.A., June 1987.

UCB/EERC-87/02 "Earthquake Simulator Tests and Associated Studies of a 0.3-Scale Model of a Six-Story Eccentrically Braced Steel Structure," by Whittaker, A., Uang, C.-M. and Bertero, V.V., July 1987.

UCB/EERC-87/03 "A Displacement Control and Uplift Restraint Device for Base-Isolated Structures," by Kelly, J.M., Griffith, M.C. and Aiken, I.D., April 1987.

UCB/EERC-87/04 "Earthquake Simulator Testing of a Combined Sliding Bearing and Rubber Bearing Isolation System," by Kelly, J.M. and Chalhoub, M.S., 1987.

UCB/EERC-87/05 "Three-Dimensional Inelastic Analysis of Reinforced Concrete Frame-Wall Structures," by Moazzami, S. and Bertero, V.V., May 1987.

UCB/EERC-87/06 "Experiments on Eccentrically Braced Frames with Composite Floors," by Ricles, J. and Popov, E., June 1987.

UCB/EERC-87/07 "Dynamic Analysis of Seismically Resistant Eccentrically Braced Frames," by Ricles, J. and Popov, E., June 1987.

UCB/EERC-87/08 "Undrained Cyclic Triaxial Testing of Gravels-The Effect of Membrane Compliance," by Evans, M.D. and Seed, H.B., July 1987.

UCB/EERC-87/09 "Hybrid Solution Techniques for Generalized Pseudo-Dynamic Testing," by Thewalt, C. and Mahin, S.A., July 1987.

UCB/EERC-87/10 "Ultimate Behavior of Butt Welded Splices in Heavy Rolled Steel Sections," by Bruneau, M., Mahin, S.A. and Popov, E.P., September 1987.

UCB/EERC-87/11 "Residual Strength of Sand from Dam Failures in the Chilean Earthquake of March 3, 1985," by De Alba, P., Seed, H.B., Retamal, E. and Seed, R.B., September 1987.

UCB/EERC-87/12 "Inelastic Seismic Response of Structures with Mass or Stiffness Eccentricities in Plan," by Bruneau, M. and Mahin, S.A., September 1987, (PB90 262 650)A14.

UCB/EERC-87/13 "CSTRUCT: An Interactive Computer Environment for the Design and Analysis of Earthquake Resistant Steel Structures," by Austin, M.A., Mahin, S.A. and Pister, K.S., September 1987.

UCB/EERC-87/14 "Experimental Study of Reinforced Concrete Columns Subjected to Multi-Axial Loading," by Low, S.S. and Mochle, J.P., September 1987.

UCB/EERC-87/15 "Relationships between Soil Conditions and Earthquake Ground Motions in Mexico City in the Earthquake of Sept. 19, 1985," by Seed, H.B., Romo, M.P., Sun, J., Jaime, A. and Lysmer, J., October 1987.

UCB/EERC-87/16 "Experimental Study of Seismic Response of R. C. Setback Buildings," by Shahrooz, B.M. and Moehle, J.P., October 1987.

UCB/EERC-87/17 "The Effect of Slabs on the Flexural Behavior of Beams," by Pantazopoulou, S.J. and Moehle, J.P., October 1987, (PB90 262 700)A07.

UCB/EERC-87/18 "Design Procedure for R-FBI Bearings," by Mostaghel, N. and Kelly, J.M., November 1987, (PB90 262 718)A04.

UCB/EERC-87/19 "Analytical Models for Predicting the Lateral Response of R C Shear Walls: Evaluation of their Reliability," by Vulcano, A. and Bertero, V.V., November 1987.

UCB/EERC-87/20 "Earthquake Response of Torsionally-Coupled Buildings," by Hejal, R. and Chopra, A.K., December 1987.

UCB/EERC-87/21 "Dynamic Reservoir Interaction with Monticello Dam," by Clough, R.W., Ghanaat, Y. and Qiu, X-F., December 1987.

UCB/EERC-87/22 "Strength Evaluation of Coarse-Grained Soils," by Siddiqi, F.H., Seed, R.B., Chan, C.K., Seed, H.B. and Pyke, R.M., December 1987.

UCB/EERC-88/01 "Seismic Behavior of Concentrically Braced Steel Frames," by Khatib, I., Mahin, S.A. and Pister, K.S., January 1988.

UCB/EERC-88/02 "Experimental Evaluation of Seismic Isolation of Medium-Rise Structures Subject to Uplift," by Griffith, M.C., Kelly, J.M., Coveney, V.A. and Koh, C.G., January 1988.

UCB/EERC-88/03 "Cyclic Behavior of Steel Double Angle Connections," by Astaneh-Asl, A. and Nader, M.N., January 1988.

UCB/EERC-88/04 "Re-evaluation of the Slide in the Lower San Fernando Dam in the Earthquake of Feb. 9, 1971," by Seed, H.B., Seed, R.B., Harder, L.F. and Jong, H.-L., April 1988.

UCB/EERC-88/05 "Experimental Evaluation of Seismic Isolation of a Nine-Story Braced Steel Frame Subject to Uplift," by Griffith, M.C., Kelly, J.M. and Aiken, I.D., May 1988.

UCB/EERC-88/06 "DRAIN-2DX User Guide.," by Allahabadi, R. and Powell, G.H., March 1988.

UCB/EERC-88/07 "Theoretical and Experimental Studies of Cylindrical Water Tanks in Base-Isolated Structures," by Chalhoub, M.S. and Kelly, J.M., April 1988.

UCB/EERC-88/08 "Analysis of Near-Source Waves: Separation of Wave Types using Strong Motion Array Recordings," by Darragh, R.B., June 1988.

UCB/EERC-88/09 "Alternatives to Standard Mode Superposition for Analysis of Non-Classically Damped Systems," by Kusainov, A.A. and Clough, R.W., June 1988.

UCB/EERC-88/10 "The Landslide at the Port of Nice on October 16, 1979," by Seed, H.B., Seed, R.B., Schlosser, F., Blondeau, F. and Juran, I., June 1988.

UCB/EERC-88/11 "Liquefaction Potential of Sand Deposits Under Low Levels of Excitation," by Carter, D.P. and Seed, H.B., August 1988.

UCB/EERC-88/12 "Nonlinear Analysis of Reinforced Concrete Frames Under Cyclic Load Reversals," by Filippou, F.C. and Issa, A., September 1988.

UCB/EERC-88/13 "Implications of Recorded Earthquake Ground Motions on Seismic Design of Building Structures," by Uang, C.-M. and Bertero, V.V., November 1988.

UCB/EERC-88/14 "An Experimental Study of the Behavior of Dual Steel Systems," by Whittaker, A.S. , Uang, C.-M. and Bertero, V.V., September 1988.

UCB/EERC-88/15 "Dynamic Moduli and Damping Ratios for Cohesive Soils," by Sun, J.I., Golesorkhi, R. and Seed, H.B., August 1988.

UCB/EERC-88/16 "Reinforced Concrete Flat Plates Under Lateral Load: An Experimental Study Including Biaxial Effects," by Pan, A. and Moehle, J., October 1988.

UCB/EERC-88/17 "Earthquake Engineering Research at Berkeley - 1988," by EERC, November 1988.

UCB/EERC-88/18 "Use of Energy as a Design Criterion in Earthquake-Resistant Design," by Uang, C.-M. and Bertero, V.V., November 1988.

UCB/EERC-88/19 "Steel Beam-Column Joints in Seismic Moment Resisting Frames," by Tsai, K.-C. and Popov, E.P., November 1988.

UCB/EERC-88/20 "Base Isolation in Japan, 1988," by Kelly, J.M., December 1988.

UCB/EERC-89/01 "Behavior of Long Links in Eccentrically Braced Frames," by Engelhardt, M.D. and Popov, E.P., January 1989.

UCB/EERC-89/02 "Earthquake Simulator Testing of Steel Plate Added Damping and Stiffness Elements," by Whittaker, A., Bertero, V.V., Alonso, J. and Thompson, C., January 1989.

UCB/EERC-89/03 "Implications of Site Effects in the Mexico City Earthquake of Sept. 19, 1985 for Earthquake-Resistant Design Criteria in the San Francisco Bay Area of California," by Seed, H.B. and Sun, J.I., March 1989.

UCB/EERC-89/04 "Earthquake Analysis and Response of Intake-Outlet Towers," by Goyal, A. and Chopra, A.K., July 1989.

UCB/EERC-89/05 "The 1985 Chile Earthquake: An Evaluation of Structural Requirements for Bearing Wall Buildings," by Wallace, J.W. and Moehle, J.P., July 1989.

UCB/EERC-89/06 "Effects of Spatial Variation of Ground Motions on Large Multiply-Supported Structures," by Hao, H., July 1989.

UCB/EERC-89/07 "EADAP - Enhanced Arch Dam Analysis Program: Users's Manual," by Ghanaat, Y. and Clough, R.W., August 1989.

UCB/EERC-89/08 "Seismic Performance of Steel Moment Frames Plastically Designed by Least Squares Stress Fields," by Ohi, K. and Mahin, S.A., August 1989.

UCB/EERC-89/09 "Feasibility and Performance Studies on Improving the Earthquake Resistance of New and Existing Buildings Using the Friction Pendulum System," by Zayas, V., Low, S., Mahin, S.A. and Bozzo, L., July 1989.

UCB/EERC-89/10 "Measurement and Elimination of Membrane Compliance Effects in Undrained Triaxial Testing," by Nicholson, P.G., Seed, R.B. and Anwar, H., September 1989.

UCB/EERC-89/11 "Static Tilt Behavior of Unanchored Cylindrical Tanks," by Lau, D.T. and Clough, R.W., September 1989.

UCB/EERC-89/12 "ADAP-88: A Computer Program for Nonlinear Earthquake Analysis of Concrete Arch Dams," by Fenves, G.L., Mojtahedi, S. and Reimer, R.B., September 1989.

UCB/EERC-89/13 "Mechanics of Low Shape Factor Elastomeric Seismic Isolation Bearings," by Aiken, I.D., Kelly, J.M. and Tajirian, F.F., November 1989.

UCB/EERC-89/14 "Preliminary Report on the Seismological and Engineering Aspects of the October 17, 1989 Santa Cruz (Loma Prieta) Earthquake," by EERC, October 1989.

UCB/EERC-89/15 "Experimental Studies of a Single Story Steel Structure Tested with Fixed, Semi-Rigid and Flexible Connections," by Nader, M.N. and Astaneh-Asl, A., August 1989, (PB91 229 211/AS)A10.

UCB/EERC-89/16 "Collapse of the Cypress Street Viaduct as a Result of the Loma Prieta Earthquake," by Nims, D.K., Miranda, E., Aiken, I.D., Whittaker, A.S. and Bertero, V.V., November 1989, (PB91 217 935/AS)A05.

UCB/EERC-90/01 "Mechanics of High-Shape Factor Elastomeric Seismic Isolation Bearings," by Kelly, J.M., Aiken, I.D. and Tajirian, F.F., March 1990.

UCB/EERC-90/02 "Javid's Paradox: The Influence of Preform on the Modes of Vibrating Beams," by Kelly, J.M., Sackman, J.L. and Javid, A., May 1990, (PB91 217 943/AS)A03.

UCB/EERC-90/03 "Earthquake Simulator Testing and Analytical Studies of Two Energy-Absorbing Systems for Multistory Structures," by Aiken, I.D. and Kelly, J.M., October 1990.

UCB/EERC-90/04 "Damage to the San Francisco-Oakland Bay Bridge During the October 17, 1989 Earthquake," by Astaneh, A., June 1990.

UCB/EERC-90/05 "Preliminary Report on the Principal Geotechnical Aspects of the October 17, 1989 Loma Prieta Earthquake," by Seed, R.B., Dickenson, S.E., Riemer, M.F., Bray, J.D., Sitar, N., Mitchell, J.K., Idriss, I.M., Kayen, R.E., Kropp, A., Harder, L.F., Jr. and Power, M.S., April 1990.

UCB/EERC-90/06 "Models of Critical Regions in Reinforced Concrete Frames Under Seismic Excitations," by Zulfiqar, N. and Filippou, F., May 1990.

UCB/EERC-90/07 "A Unified Earthquake-Resistant Design Method for Steel Frames Using ARMA Models," by Takewaki, I., Conte, J.P., Mahin, S.A. and Pister, K.S., June 1990.

UCB/EERC-90/08 "Soil Conditions and Earthquake Hazard Mitigation in the Marina District of San Francisco," by Mitchell, J.K., Masood, T., Kayen, R.E. and Seed, R.B., May 1990.

UCB/EERC-90/09 "Influence of the Earthquake Ground Motion Process and Structural Properties on Response Characteristics of Simple Structures," by Conte, J.P., Pister, K.S. and Mahin, S.A., July 1990.

UCB/EERC-90/10 "Experimental Testing of the Resilient-Friction Base Isolation System," by Clark, P.W. and Kelly, J.M., July 1990.

UCB/EERC-90/11 "Seismic Hazard Analysis: Improved Models, Uncertainties and Sensitivities," by Araya, R. and Der Kiureghian, A., March 1988.

UCB/EERC-90/12 "Effects of Torsion on the Linear and Nonlinear Seismic Response of Structures," by Sedarat, H. and Bertero, V.V., September 1989.

UCB/EERC-90/13 "The Effects of Tectonic Movements on Stresses and Deformations in Earth Embankments," by Bray, J. D., Seed, R. B. and Seed, H. B., September 1989.

UCB/EERC-90/14 "Inelastic Seismic Response of One-Story, Asymmetric-Plan Systems," by Goel, R.K. and Chopra, A.K., October 1990.

UCB/EERC-90/15 "Dynamic Crack Propagation: A Model for Near-Field Ground Motion.," by Seyyedian, H. and Kelly, J.M., 1990.

UCB/EERC-90/16 "Sensitivity of Long-Period Response Spectra to System Initial Conditions," by Blasquez, R., Ventura, C. and Kelly, J.M., 1990.

UCB/EERC-90/17 "Behavior of Peak Values and Spectral Ordinates of Near-Source Strong Ground-Motion over a Dense Array," by Niazi, M., June 1990.

UCB/EERC-90/18 "Material Characterization of Elastomers used in Earthquake Base Isolation," by Papoulia, K.D. and Kelly, J.M., 1990.

UCB/EERC-90/19 "Cyclic Behavior of Steel Top-and-Bottom Plate Moment Connections," by Harriott, J.D. and Astaneh, A., August 1990, (PB91 229 260/AS)A05.

UCB/EERC-90/20 "Seismic Response Evaluation of an Instrumented Six Story Steel Building," by Shen, J.-H. and Astaneh, A., December 1990.

UCB/EERC-90/21 "Observations and Implications of Tests on the Cypress Street Viaduct Test Structure," by Bollo, M., Mahin, S.A., Moehle, J.P., Stephen, R.M. and Qi, X., December 1990.

UCB/EERC-91/01 "Experimental Evaluation of Nitinol for Energy Dissipation in Structures," by Nims, D.K., Sasaki, K.K. and Kelly, J.M., 1991.

UCB/EERC-91/02 "Displacement Design Approach for Reinforced Concrete Structures Subjected to Earthquakes," by Qi, X. and Moehle, J.P., January 1991.

UCB/EERC-91/03 "Shake Table Tests of Long Period Isolation System for Nuclear Facilities at Soft Soil Sites," by Kelly, J.M., March 1991.

UCB/EERC-91/04 "Dynamic and Failure Characteristics of Bridgestone Isolation Bearings," by Kelly, J.M., April 1991.

UCB/EERC-91/05 "Base Sliding Response of Concrete Gravity Dams to Earthquakes," by Chopra, A.K. and Zhang, L., May 1991.

UCB/EERC-91/06 "Computation of Spatially Varying Ground Motion and Foundation-Rock Impedance Matrices for Seismic Analysis of Arch Dams," by Zhang, L. and Chopra, A.K., May 1991.

UCB/EERC-91/07 "Estimation of Seismic Source Processes Using Strong Motion Array Data," by Chiou, S.-J., July 1991.

UCB/EERC-91/08 "A Response Spectrum Method for Multiple-Support Seismic Excitations," by Der Kiureghian, A. and Neuenhofer, A., August 1991.

UCB/EERC-91/09 "A Preliminary Study on Energy Dissipating Cladding-to-Frame Connection," by Cohen, J.M. and Powell, G.H., September 1991.

UCB/EERC-91/10 "Evaluation of Seismic Performance of a Ten-Story RC Building During the Whittier Narrows Earthquake," by Miranda, E. and Bertero, V.V., October 1991.

UCB/EERC-91/11 "Seismic Performance of an Instrumented Six Story Steel Building," by Anderson, J.C. and Bertero, V.V., November 1991.

UCB/EERC-91/12 "Performance of Improved Ground During the Loma Prieta Earthquake," by Mitchell, J.K. and Wentz, Jr., F.J., October 1991.

UCB/EERC-91/13 "Shaking Table - Structure Interaction," by Rinawi, A.M. and Clough, R.W., October 1991.

UCB/EERC-91/14 "Cyclic Response of RC Beam-Column Knee Joints: Test and Retrofit," by Mazzoni, S., Moehle, J.P. and Thewalt, C.R., October 1991.

UCB/EERC-91/15 "Design Guidelines for Ductility and Drift Limits: Review of State-of-the-Practice and State-of-the-Art in Ductility and Drift-Based Earthquake-Resistant Design of Buildings," by Bertero, V.V., Anderson, J.C., Krawinkler, H., Miranda, E. and The CUREe and The Kajima Research Teams, July 1991.

UCB/EERC-91/16 "Evaluation of Seismic Performance of a Thirty-Story RC Building," by Anderson, J.C., Miranda, E., Bertero, V.V. and The Kajima Project Research Team, July 1991.